Mechanism of Wet Anisotropic Etching of Silicon for Nano-Scale Applications

Irina Stateikina

A Thesis

in

The Department

of

Electrical and Computer Engineering

Presented in Partial Fulfillment of the Requirements
for the Degree of Doctor of Philosophy at
Concordia University
Montreal, Quebec, Canada

April 11, 2007

Your file Votre référence
ISBN: 978-0-494-30139-5
Our file Notre référence
ISBN: 978-0-494-30139-5

ABSTRACT

Mechanism of Wet Anisotropic Etching of Silicon for Nano-Scale Applications

Irina Stateikina
Concordia University, 2006

The fabrication processes of recent MEMS devices require the use of anisotropic etching and variety of concave structures.

Analysis of these structures uncovered phenomenon in the etch rates of surfaces exposed by anisotropic etchant. This phenomenon could not be explained without consideration of the composition of these surfaces on atomic level.

My study raised the step-based modeling of these planes, their relative interactions, and dependence on the etching environment. Control of this environment and better understanding of the different factors that influence the etch rates of these surfaces is the main theme of my work.

To help with the analysis of the studied surfaces a set of the experiments was done using a wagon-wheel pattern that provided the necessary assortment of concave structures for the purpose of this research. A mathematical model was built to help understand the processes that are responsible for anomalies in the etch rates and profiles of surfaces exposed on sidewalls of spokes in the wagon-wheel experiment.

Detailed examination of the profiles of the surfaces and their relative location within the same concave structure suggested the possibility of application of these surfaces in creation of different patterns for nano-applications. The major concern is the control of etch rates of these planes in order do achieve the necessary precision for the application on such scale. Light illumination of the etched surfaces is analyzed as a possible component in providing the necessary level of control.

Influence of the light intensity and different wavelengths is studied with the thought of application of the respective parameters in order to achieve a satisfactory control over the etch rates of illuminated surfaces.

ACKNOWLEDGEMENTS

I would like to express my deepest gratitude to my supervisors Dr. Leslie M. Landsberger and Dr. Mojtaba Kahrizi. This work would not be possible without their constant support and guidance along the way.

I also want to thank the members of my examination committee for their wonderful comments on my work.

And finally, very special thanks to my son Maksim for his encouragement and understanding during the years of my study.

Table of Contents

List of Figures

List of Tables

List of Abbreviations

3D - Three Dimensional

AFM - Atomic Force Microscopy

CMOS - Complementary Metal-Oxide-Semiconductor

EDP - Ethylene Diamine Pyrocatechol

EPA - Effective Plane Advancement

EPW - Diamine-Pyrocatechol-Water

ER - Etch Rate

FCC - Face Centered Cube

FR - Removal Frequency

IC - Integrated Circuit

KOH - Potassium Hydroxide

LiOH - Lithium Hydroxide

MI - Miller Indices

MEMS- Micro-Electro-Mechanical Systems

NaOH - Sodium Hydroxide

OPC - Open Circuit Potential

PBC - Periodic Bond Chain

SCE - Saturated Calomel Electrodes

SCR - Space Charge Region

SE - Step-Edge

STM - Scanning Tunnelling Microscopy

TMAH- Tetra-Methyl Ammonia Hydroxide

TW - Terrace Width

UER - Under Etch Rate

USW - Unit-Step Width

VLSI -Very Large Scale Integration

List of Symbols

E_c - an energy of the bottom of the conduction band, (eV)

E_F - Fermi energy, (eV)

E_{Fi} - an intrinsic Fermi energy, (eV)

E_v - an energy of the top of the valence band, (eV)

$EPA_{\{100\}}$ - Effective Plane Advancement of a plane with {100}-oriented terraces, (Å)

$EPA_{\{110\}}$ - Effective Plane Advancement of a plane with {110}-oriented terraces, (Å)

$EPA_{\{111\}}(\theta)$ - Effective Plane Advancement of a plane with {111}-oriented terraces, (Å)

$EPA_P(35.26°)$ - Effective Plane Advancement of a {110} plane, (Å)

ER - Etch Rate, (μm/h)

ER_{CC} - Etch Rate value taken from canonical curve, (μm/h)

Q - the charge, (coul)

SE_1 - a step-edge of the first or top-most out of two adjacent facets

SE_1-1 - a "first" step-edge on the first/top-most facet

T - a temperature, (K or C)

$TW_{\{111\}}$ - a terrace width, {111}-oriented, (Å)

TW_{min} - a terrace width at the crossover, {100}- or {110}-oriented, (Å)

U - a potential difference, (V)

USW - Unit-Step Width, (Å)

$USW_{\{111\}}$ - Unit-Step Width representing how far the edge of the step will advance on {111}-oriented terrace, (Å)

V_{bi} - a built-in potential, (V)

a - a lattice constant, (Å)

a_1, a_2, a_3 - vector components

b_1, b_2, b_3 - vector components

c - a speed of light in vacuum, (cm/s)

d_1 - a distance travelled by the SE on the plane with defined etch rate, (Å)

h - Plank's constant, (eV-s or J-s)

$h_{\{100\}}$ - a height of a step on K-based plane with {100} oriented terraces, (Å)

$h_{\{110\}}$ - a height of a step on P-based plane with {110} oriented terraces, (Å)

$h_{\{111\}}$ - a height of a step on a plane with {111} oriented terraces, (Å)

k - Boltzmann's constant, (eV/K or J/K)

s_1, s_2 - a step-spacing on the first and second analysed facet, respectively, (Å)

$s_{\{100\}}$ - a step spacing on a K-based plane with {100}-oriented terraces, (Å)

$s_{\{110\}}$ - a step spacing on a P-based plane with {110}-oriented terraces, (Å)

$s_{\{111\}}$ - a step spacing on a plane with {111}-oriented terraces, (Å)

v - a step-edge velocity in the direction perpendicular to the edge of the step, (μm/h)

$v\|_1$ - a step-edge (SE) velocity on the first facet with respect to the boundary between two adjacent facets, (μm/h)

$w_{\{100\}}$ - a width of {100}-oriented terrace, (Å)

$w_{\{110\}}$ - a width of {110}-oriented terrace, (Å)

$w_{\{111\}}$ - a width of {111}-oriented terrace, (Å)

α - an inclination angle, (degrees)

γ - an angle that the PBCs or K-rows at step-edges make with a reference line - line perpendicular to the boundary between two facets, (degrees)

δ - a deviation angle, (degrees)

ε_0 - a permittivity of free space, (F/cm^2)

ε_r - a dielectric constant

ξ - an angle between {110} oriented terrace and P-based plane with $\{hhl\}$ Miller Indices, (degrees or rad)

θ - an angle between {111} oriented terrace and K- or P-based plane, (degrees or rad)

θ_P, θ_K - angles of a plane with respect to {111} oriented surface for P-based and K-based planes, respectively, (degrees or rad)

λ - a wavelength, (nm)

v - an angle between {100} oriented terrace and K-based plane with $\{hll\}$ Miller Indices, (degrees or rad)

"The greater danger for most of us lies not in setting our aim too high and falling short; but in setting our aim too low, and achieving our mark"

Michelangelo Buonarroti
1475-1564

1. Introduction

The world of science undergoes constant changes. The main stream of knowledge was split into separate paths: physics, chemistry, biology. With new discoveries, which become pronounced in the last century, new divisions were developed. Demands of the recent years concentrate on few main criteria: faster, smaller, more efficient, and less costly. Thus miniaturisation enters every branch and division of sciences binding them together once again in the "magical" nanoscale dimension. This statement follows the famous empirical Moore's law[1] outcome of which according to consensual agreement must end in approximately 2012 with minimum dimensions of 35nm, [1]. Nowadays, medical instruments are fabricated using the same technology as for construction of AFM probe tip, mechanical engineers study mechanical properties of proteins, biochemist's creation, with a help of nano-probes, electrical engineers, in collaboration with biologists grow circuits on silicon substrate, [2].

Following this trend, this work addresses wet anisotropic etching of silicon, more specifically, wet-chemical anisotropic etching of concave structures in a silicon crystal and phenomena and anomalies that come along with this process.

This first Chapter will introduce the subject of anisotropic etching as an important aspect of fabrication of 3D structures in micromachining technology and will touch upon the terminology that can be useful in reading the subsequent chapters.

[1] Gordon Moore, in 1965, observed that the number of transistors per square inch on integrated circuits had doubled every year since the integrated circuit was invented. In subsequent years, the pace slowed down a bit, but data density has doubled approximately every 18 months, and this is the current definition of Moore's Law, [3].

1.1. Silicon

Understanding of the structure of silicon becomes more important in the fabrication of micro components of any integrated circuit (IC) with their respective size reduction.

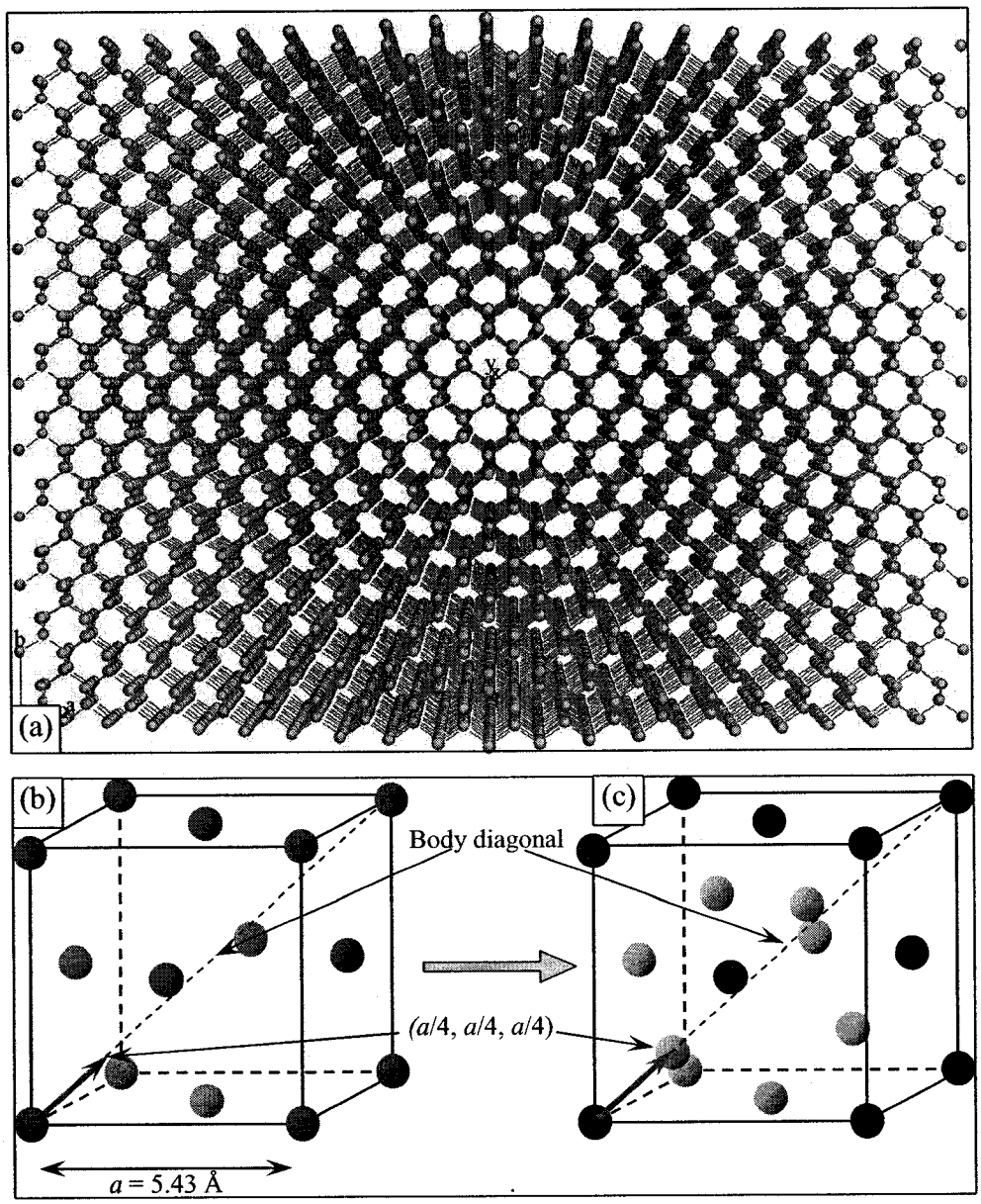

Figure 1-1: (a) An atomic reconstruction of a diamond structure of silicon crystal, (b) Face Centred Cube (FCC)[2] with the indication of the body diagonal, and (c) Unit-Cell Cube as a building block of a diamond silicon lattice.

[2] FCC is a cube with an atom at each corner and an additional atom at each face/side of this cube.

Especially, in fabrication of 3D structures, such as sensors, actuators, micro-mirror switches, etc. - fairly new but already well established field of Micro-Electro-Mechanical Systems (MEMS). These structures, following the Moore's law, are reaching dimensions in the nano-meter range, i.e. the atom-size scale, and, therefore, affected largely by the atomic structure of the material they are made of. In other words, the performance of these components is affected by the properties and atomic structure of silicon

The crystal structure of silicon is represented by a diamond lattice in Figure 1-1 (a). The lattice in this figure is shown as a view from a point, in the direction of a so-called honey comb view, i.e. a view of silicon crystal from a <110>, direction.

This lattice configuration can be achieved by the advancement of a Face Centered Cubic Lattice (FCC) with respect to another FCC along the Cube's body diagonal one quarter of its length, see Figure 1-1(b).

The Unit-Cell Cube, shown in Figure 1-1(c), is considered a building block of a silicon crystal lattice (lattice constant[3] a = 5.43Å), and helps to illustrate a number of basic parameters in the silicon structure.

1.2. Basic Planes in Silicon Crystal

With the fundamental understanding of silicon lattice and its building block, Unit-Cell Cube, three basic orientations of silicon crystal can be demonstrated. Figure 1-2 illustrates these orientations as three basic planes with {100}, {110} and {111} Miller

[3] Defines distance between atoms in unit-cell cube; measure of structural compatibility between various crystals.

Indices[4]. These planes represent surfaces with distinct atomic features and are utilized as main orientations for silicon wafers used in micro-fabrication technology.

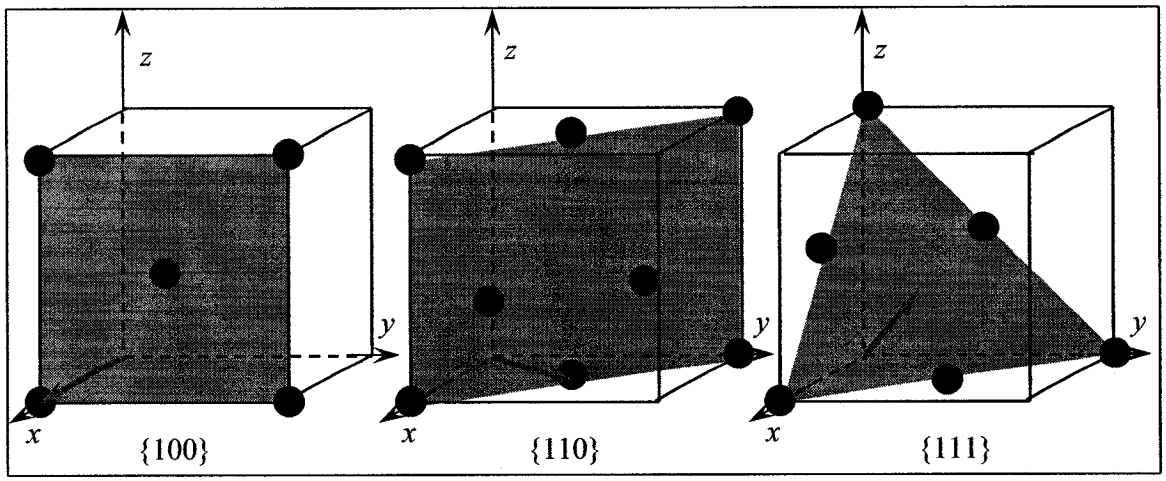

Figure 1-2: Schematic representation of 3 basic orientation of the silicon crystal based on the planes within the Unit-Cell Cube (only atoms present on the surface of indicated planes are shown).

Silicon wafers with {100} and {111} orientations have been commonly used for a majority of applications. More recently, with the development of micromachining technology (MEMS), {110}-oriented wafers are the focus of more study as a background for a larger variety of 3D structures.

1.3. Etching

In the context of this work the etching is referred to as a wet-chemical etching for the purpose of pattern/template transfer on a silicon wafer of specified {100}, {110}, or {111} orientation, and further formation of concave structures based on the imposed template.

Two major types of wet-chemical etching can be identified:

Isotropic – having physical properties that do not vary with direction and

[4] The Miller indices are defined as the smallest possible integers, which have the same ratios as the inverse of the intersections of a given plane with a set of axis defined by the unit vectors of that crystal, [4].

Anisotropic[5] – with physical properties that vary with the change of orientation, [6].

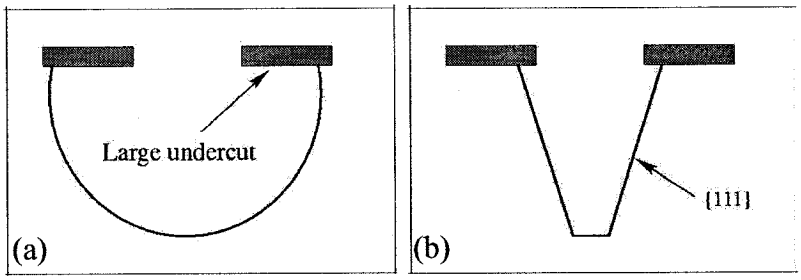

Figure 1-3: Schematic representation of a cross-section of a cavity etched (a) in isotropic, and (b) in anisotropic etchant.

Isotropic etching, therefore, is significant in removing exposed matter with the same rate in all directions, whereas anisotropic etching process is selective depending on crystal orientation, (see Figure 1-3).

For any concave structure, the anisotropic etchant is going to selectively expose planes with the slowest etch rate, such as {111} oriented surface, which considered globally the one with the slowest etch rate, [7]-[12].

Smaller undercut and reasonable predictability of features in concave structures, achieved by anisotropic etching in silicon crystal, makes this type of etching the choice of preference.

Due to its popularity, the wet-chemical anisotropic etching of silicon caught my attention, and developed into extensive work presented here.

1.4. Wagon-Wheel Pattern

Analysis of concave structures created by wet-chemical anisotropic etching of bulk silicon suggested the need for a "universal pattern" to enable such study using planar silicon process technology[6].

---

[5] Anisotropy, from Greek, is a combination of words "iso" (ισο), meaning "the same" and "tropos" (τροπος), meaning "direction" with the negating prefix making the whole word to be translated as "not the same in all directions", [7].

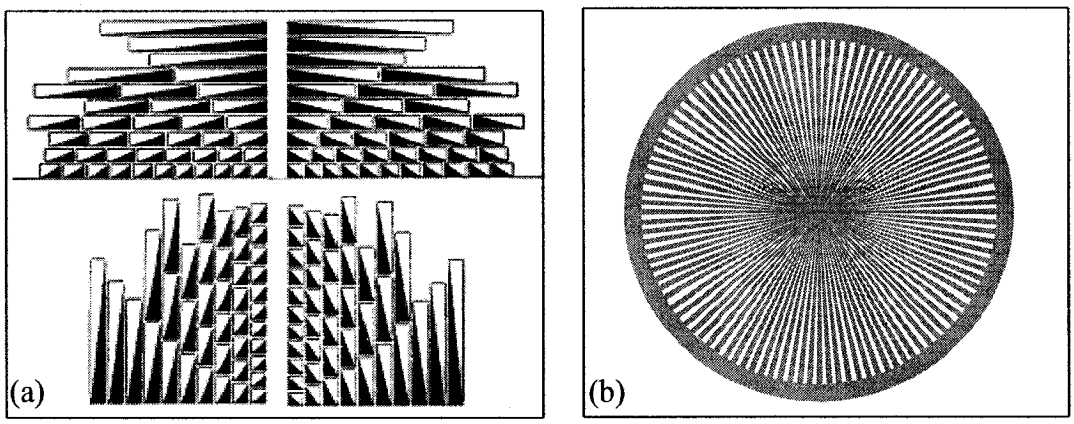

Figure 1-4: Schematic representation of (a) the mask pattern made out of right-angled triangles, with angles varying from 5° to 45° in intervals of 1 degree, Figure from [8], and (b) a typical wagon-wheel pattern, Figure from [9].

Different patterns were used over the years of research in this field. An example of one of these patterns is presented in Figure 1-4(a), [8]. The mask adopted for the purpose of this study is a wagon-wheel pattern, a simplified example of which is schematically illustrated in Figure 1-4(b), [9].

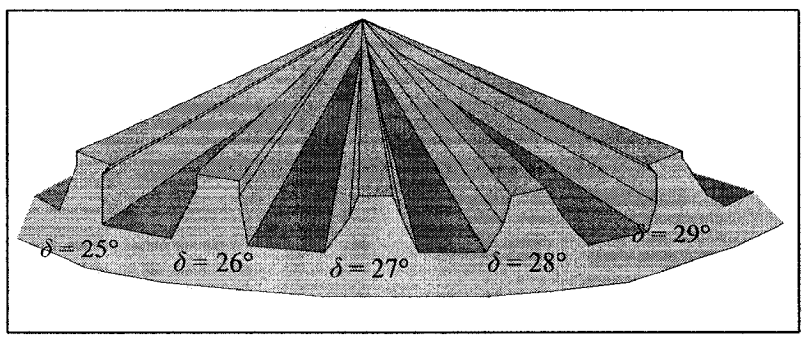

Figure 1-5: The schematic representation of a segment of wafer with the multifaceted walls of the spokes etched using a typical wagon-wheel pattern, Figure from [9].

The advantage of the wagon-wheel mask is in providing a variety of repeatable concave structures - spokes, sidewalls of which present the wide spectrum of surfaces used in this study, see Figure 1-5.

[6] Pattern transfer is done using a photolithography, see Appendix I.

The experimental results of etching of a wagon-wheel pattern for two types of silicon wafer orientations, {100} and {110}, respectively, are schematically depicted in Figure 1-6, [9]. Planes specified in this figure are not only those of the wafer surface orientation but also those that appear on sidewalls of etched spokes, (dark color indicating the masked regions and light – anisotropically etched areas).

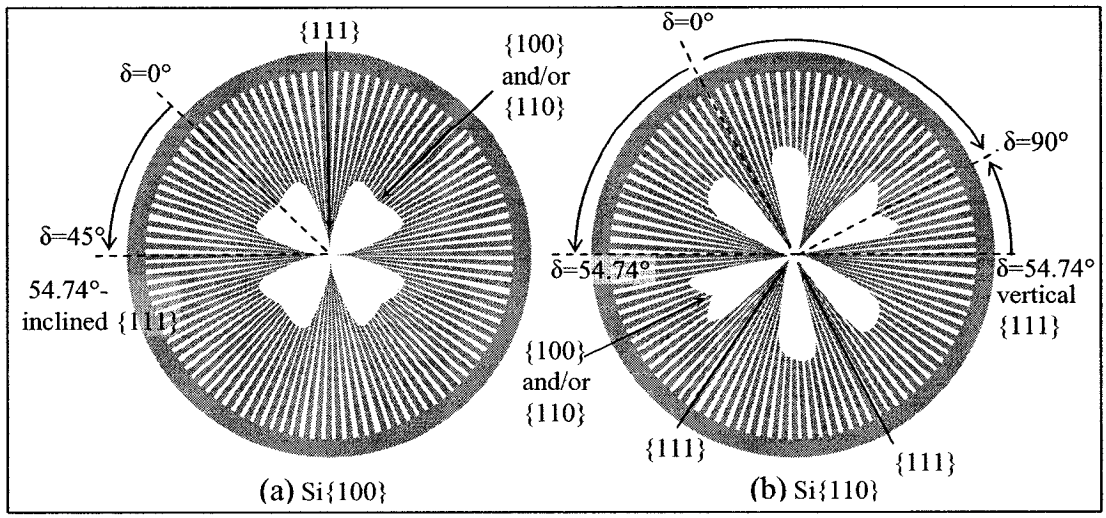

Figure 1-6: Top view of the wagon-wheel profile etched anisotropically for (a) on the silicon wafer of {100} orientation and (b) on silicon wafer of {110} orientation, (dark color indicating the masked regions and light – anisotropically etched areas). Specified planes are side-wall planes of etched cavities, figure from [9].

1.5. Etch Rates

From the first study of anisotropically etched wagon-wheel profiles illustrated in Figure 1-6 it can be seen that areas where {111}-oriented planes appear on side-walls of spokes, the etching process is significantly slower compared to other areas (minimum under-etch). This signifies that {111}-oriented surfaces, globally considered atomically flat, have the slowest etch rates, compared to other orientations, in any anisotropic etchant. It was shown, [7], [10], that the precise etch rate of {111} planes is not easy to measure due to many factors, i.e. imprecision in mask alignment, error margin in optical measurements, or simply due to a human error. It is generally agreed, that the {111}

oriented surface, due to its crystallographic profile and globally slowest etch rate, may be considered an atomically flat surface, [7], [11]-[12].

However, under various circumstances, other two of the basic planes were observed to have locally slowest etch rates. Si{100} and Si{110}, as can be seen in Figure 1-6, appear to have local minima in overall etch rates and under some conditions may be considered "flat", [19].

Etch rates, among an assortment of factors, depend on the type of anisotropic etchant used, temperature and the etchant concentration.

1.6. Choice of the Etchant

Alkali – a water-soluble chemical that reacts with acid to form salts; bases include oxides and hydroxides of metals and ammonia, [6].

Variety of alkaline solutions, such as potassium hydroxide (KOH), sodium hydroxide (NaOH), lithium hydroxide (LiOH), ethylene diamine pyrocatechol (EDP), tetra-methyl ammonia hydroxide (TMAH), etc., are used as anisotropic etchants of silicon.

Hydroxide ions (OH^-), common for the majority of anisotropic etching solutions, largely considered to be responsible for the etching anisotropy, [11]-[13]. But given the variation of the experimental etch rate data, cations (K^+, Na^+) are believed to influence the etching outcome as well.

Number of reasons may be listed in order for any of selected anisotropic etchants to be considered better than others.

KOH is the anisotropic etchant used, largely, in studies involving wet-chemical anisotropic etching of bulk silicon. It offers a very good anisotropy, according to some sources: {111}:{110}:{100} → 1:600:400. But it is also a very corrosive etchant with

low selectivity with respect to the masking material, SiO_2. Moreover, potassium hydroxide is not compatible with CMOS[7] process technology – due to alkali ion contamination.

EDP, also known as ethylene diamine-pyrocatechol-water (EPW), is another common etchant used in fabrication where the anisotropy is required ($\{111\}:\{100\} \rightarrow 1:35$). But being highly corrosive (must be used only in a fume collecting bench and will rust any metallic surface in vicinity) its application is limited, in particular due to incompatibility with CMOS process technology.

TMAH was proposed in 1976 by Asano *et al,* [14], to be used as a cleaning and etching solution for silicon surfaces. Detailed characterization of the $(CH_3)_4NOH$, (chemical molecular formulae of TMAH) was reported in 1991, [15]-[16].

TMAH possesses a number of properties that are more suitable for a university research laboratory, or any less sophisticated fabrication facility:

- easily obtained (has been used in VLSI (Very Large Scale Integration) microelectronics processes, as developer for positive photoresist)
- compatible with CMOS process technology (no alkali metals)
- simplicity of handling and low toxicity
- high etching rates of silicon
- suitable anisotropy (etch rate ratio $\{100\}:\{111\} \rightarrow$ up to 50)
- smooth etched surfaces for high etchant concentrations (25%)
- excellent selectivity to masking material (low etch rates of SiO_2 and Si_3N_4), [9].

[7] CMOS – Complementary Metal-Oxide-Semiconductor.

1.7. Experimental Setup Used in this Work

The experimental setup for wet anisotropic etching is fairly simple and may be described as a "reflux system" (schematic illustration of such system is show in Figure 1-7). Chosen anisotropic etchant, TMAH, is heated in a Pyrex beaker to the temperature of 80°C.

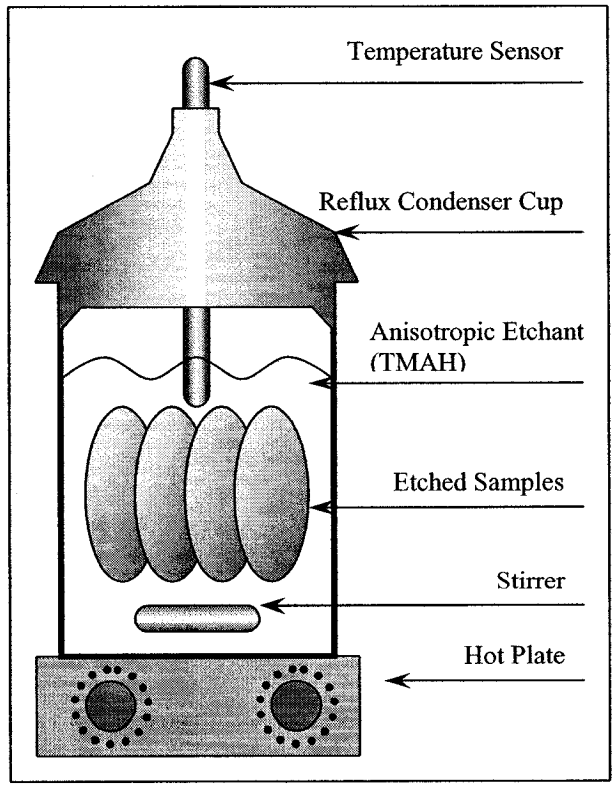

Figure 1-7: Experimental setup for wet chemical anisotropic etching of bulk silicon.

During the etching process, escaping vapor alters the required etchant concentration, which is maintained constant with the help of a water-cooled Reflux Condenser Cup. This represents a simplified picture of the majority of setups for the wet chemical anisotropic etching of silicon.

There are a variety of additional factors that play an important role in the etch rates and their control. Discussion on this subject will continue throughout this work.

1.8. Motivation and Outline

A main goal of this work is to build a fundamental theory of modelling and behaviour of planes exposed on the side-walls of concave structures anisotropically etched in bulk silicon crystal.

In short, this work endeavours to provide an explanation to some of the phenomena and anomalies met in the study of experimental data obtained from wagon-wheel under-etch experiments.

The use of concave shapes has already proven to be useful in a variety of micro-mechanical structures: under-etch cavities for cantilevers, V-grooves, micro-fluidic channels, [17], etc. With the development of optical structures, silicon fell back due to its unsatisfactory optical properties. However, it was shown that in quantum confinement model, silicon exhibits properties suitable for optical applications. The quantum confinement of silicon is mostly achieved by electro-chemical etching and results in the porous silicon samples, [18]. However, the quantum confinement, i.e. structures with nano-sized dimensions, may be achieved by wet-chemical anisotropic etching, given that a precision control of the etching process is achieved.

Thus, the final part of this work is devoted to the exploration of the etch control techniques, concentrating on one from the variety of available options.

The following chapters will address these subjects in order:

Chapter 1, Introduction, establishes a general outline of this work, facilitating the understanding of pages to follow with the definitions of some basic terms.

Chapter 2, Geometric Properties of Step-based Planes, addresses all geometric properties of surfaces that appear as facets on sidewalls of concave structures/spokes obtained in

under-etch wagon-wheel experiments. These surfaces/facets will be defined in a manner useful for further understanding of the material, and establish a background for their analysis.

Chapter 3, Step Spacing Determination, details the parameters that would, contribute to the mathematical model of anisotropically etched concave structures.

Chapter 4, Removal Frequency and Etch Rates, connects the etch rate of any given facet to the actual plane geometry. Geometric structure was already discussed in great detail in couple of previous chapters and, therefore, application of this concept should follow flawlessly.

Chapter 5, Step-Edge Velocity, will show additional outlook on actions on the facet surfaces and, finally will concentrate on their interactions.

Chapter 6, Atomic Level Analysis of Step-based Silicon Surfaces, will narrow down the analysis of a specific boundary between facets, from the atomic point of view. It shows an application of all information available up to this point (as discussed in previous chapters) to the detailed analysis of interactions between adjacent facets in concave structures.

Chapter 7, Etch Rate Control: Introduction of the Light Illumination to Wagon-Wheel Under-Etch Experiment, will address the final portion of this study – control over the etch rates of surfaces in concave structures. It addresses, specifically, the influence of light illumination on the under-etch/etch rates of these surfaces. Experiments and experimental results are presented and relevant conclusions are made.

Chapter 8, the Summary and Conclusion, summarises the outcome of this study, listing contributions and suggesting trends for the future work.

2. Geometric Properties of Step-Based Planes

2.1. Background Information

Silicon surfaces that are not of the three basic orientations ({111}, {110}, and {100}, see paragraph 2) are often described by a step-based model. The model assumes that vicinal planes, i.e. planes near atomically flat surfaces, such as {111}-oriented surface, (), are composed of flat terraces separated by steps. A step-based profile is schematically illustrated in Figure 2-1. The steps height, ideally, is equal to the thickness of one atomic layer and the steps are evenly spaced over the given surface.

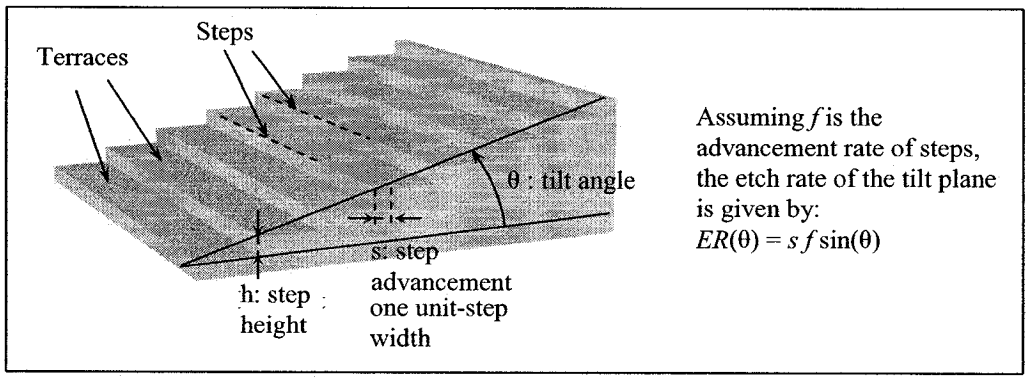

Figure 2-1: Schematic representation of a step-based plane and its advancement as the etching proceeds, Figure from [9].

The step-based model of vicinal planes was established and well developed with an advance of study in the area of wet-chemical anisotropic etching by number of researchers, [7], [10]-[16], [19]-[30]. Allongue *at al.* [20], among others, provided one of

the first evidences of the actual steps on silicon surfaces. Planes vicinal to {111}-orientation (tilted 0.7° from basic {111} orientation) were etched in sodium hydroxide NaOH at room temperature. Steps, spaced approximately 360 Å, were identified using Scanning Tunnelling Microscopy (STM). The model assumes that vicinal planes (in the vicinity of {111}), are composed of flat terraces separated by steps, height of which is ideally equal to one atomic layer. Etching of planes in the vicinity of atomically "flat" surface is believed to occur predominantly at the edge of these steps. Close observations of silicon surfaces, etched in typical wet anisotropic etchant such as TMAH, support the construction of a step-based model which describes the etching of silicon by the advancement of steps along flat {111}-oriented planes, [9], [11].

Further work in support of the step-based model was done by Hines *et al.* [30].

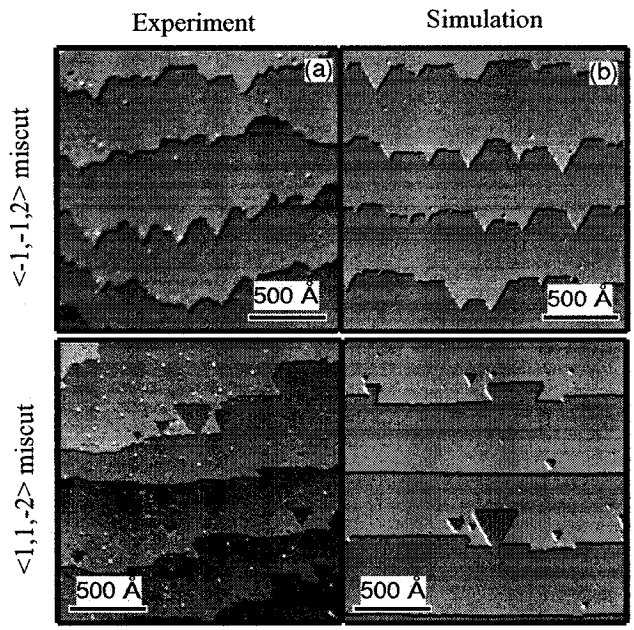

Figure 2-2: Experimental results and simulated morphologies of Si{111} etched in 0.02% IPA-doped NH_4F, Figure from [30].

This research group augmented the results from the experiments (H-terminated surfaces in vicinity of {111}-oriented plane, pre-cut to $\{1\bar{1}2\}$ and $\{\bar{1}\bar{1}2\}$ orientations, etched in 0.02% IPA-doped NH_4F) with kinetic Monte Carlo simulations.

The large scale (10^6 atoms) chemically realistic computer simulations based on the probability of removal of atoms from the edges of the steps, provided the possibility of direct comparison to the STM micrographs. Results of these simulations and their similarity to the experimental data are presented in Figure 2-2, upholding the step-based model as a more realistic representation of vicinal planes.

The combination of these observations support the assumption of the principal importance of the crystal features presented to the etchant in determining the etch rate. Research in several laboratories has shown that the step-based model is important in the study of the atomic mechanisms of anisotropic etching of silicon, [9]-[12], [31]-[39].

However, experimental work by Elalamy *et al* [9] shows that a model of wet anisotropic etching of silicon must not be solely based on the crystal features presented to the etchant; the boundaries of under-etched facets, and step interaction at those boundaries, are also likely to play an important role in determining etch rates, [33]-[35]. But in order to be able to analyse these interactions, clear understanding of the surface geometry is needed.

2.2. Introduction

In the experimental work completed in this laboratory, oxide-covered {100} and {110} silicon samples, wagon-wheel patterned, were etched in 19wt.% and 25wt.% TMAH, heavily stirred with a constant temperature of 80°C.

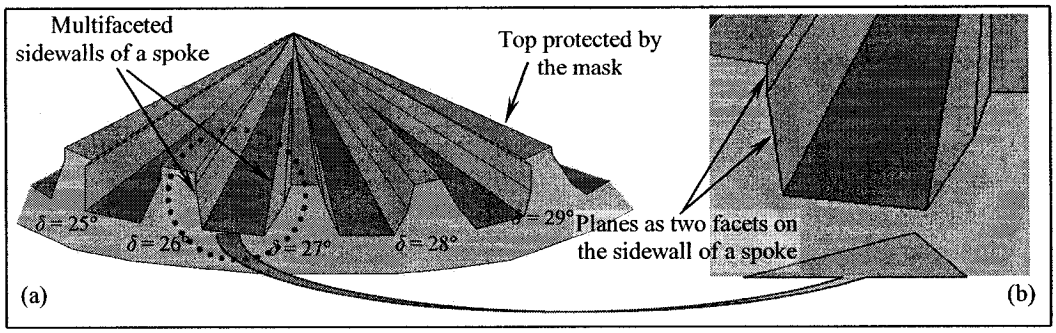

Figure 2-3: (a) Schematic representation of a segment of a sample used in under-etch wagon-wheel experiment and (b) close view on a cross-section of one of the spokes with the sidewalls composed of two facets.

Optical and scanning electron microscopy was used to study the under-etch behaviour of the wagon-wheel spokes, and to investigate the morphology, inclination angles, and roughness patterns, of the cavity sidewall facets in detail, Figure 2-3.

Meticulous analysis of the experimental results by Z. Elalamy, [9] and A. Pandy, [31], identified all planes present on sidewalls of spokes from the wagon-wheel under-etch experiment and grouped them into two families of planes. The basic principles of the model would suggest that finding the etch rates of the two families of planes would be sufficient to understand the etching of concave structures. However, the experimental results vary substantially from ideal etched rates predicted by the model. It was found that planes of the same crystal orientation etched at different rates depending on their relative location.

A number of conclusions arose from the experimental work. It was hypothesized that, at least, the following factors may contribute to the etching of silicon by influencing interactions between adjacent facets: facet size, step intersection angle at facet boundaries, relative direction of step propagation on adjacent facets (same or opposite), and relative deviation of angles of steps with respect to the inter-facet boundary.

In light of these findings, an analysis of the phenomena relevant to combinations of two adjacent interacting facets is introduced in this work:

- identification of the possible combinations existing between two adjacent facets in the under etch experiment,
- determination of the specific Miller Indices, (MI), of each interacting plane,
- establishing of plane profiles,
- terrace width and step removal frequency calculation, etc.

A substantial portion of basic experimental data was collected by Z. Elalamy *et al,* [9], such as experimental measurements (with optical and electron microscope). Analysis of the facet size influence as well as the possibility of the facets interaction at the boundary was commenced.

My work is a continuation and expansion from the vast amount of data available. Details of specific contribution on my part will be listed throughout this work in order to help to distinguish it from the previous study.

In the subsequent pages a number of parameters, identified by Z. Elalamy are listed up to the identification of specific Miller Indices for analysed surfaces, (section 2.5). From this point, my work in this chapter consisted in further development of fundamental factors that will help in better understanding of successive study.

2.3. Definition of Basic Parameters

In order to simplify the understanding of the subsequent discussion, it may be important to define the following parameters.

The common angles that are used in this text are:

- Deviation angle, δ, is the angle between two lines, *both on the wafer surface*, representing the position of the mask-edge with respect to a crystallographic reference:
  - for Si{100} the crystallographic reference is a line 45° deviated from the wafer flat as shown in Figure 2-4, left. Note that this crystallographic reference represents the intersection of a vertical {100} and 45°-inclined {110} planes with respect to {100}-oriented wafer surface;
  - for Si{110}, the crystallographic reference is a line 54.74° deviated from the wafer flat as shown in Figure 2-4, right. This crystallographic reference represents the intersection of a vertical {100} and 35.26°-inlined {111} planes with respect to {110}-oriented wafer surface.

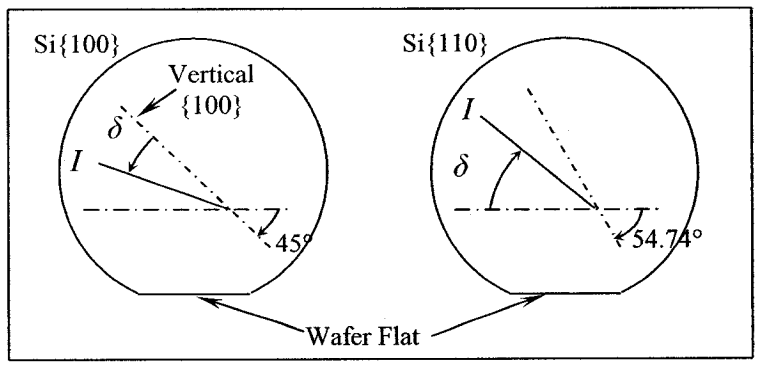

Figure 2-4: Schematic representation of the mask-edge *I* located at the deviation angle δ from the wafer flat for the Si{100} and Si{110} wafers respectively, figure adopted from [9].

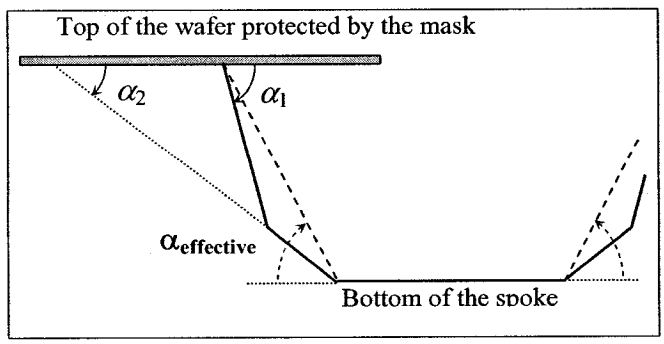

Figure 2-5: Schematic cross-section of an under-etched spoke with the indication of inclination angles α of the side-wall facets.

- Inclination angle, α, is the angle between a facet on side-walls of a spoke in the under-etch experiment with respect to the (horizontal) wafer surface, see Figure 2-5.
- Inverted planes – planes with the inclination angle $\alpha > 90°$. (Appear only as a top-most facet).
- Vertical planes – planes with the inclination angle $\alpha = 90°$.
- Angle of rotation from a {111}-oriented plane, θ, emphasizes the nature of two families of planes and helps to position each of these planes with respect to the nearest {111} oriented plane, see Figure 2-6.

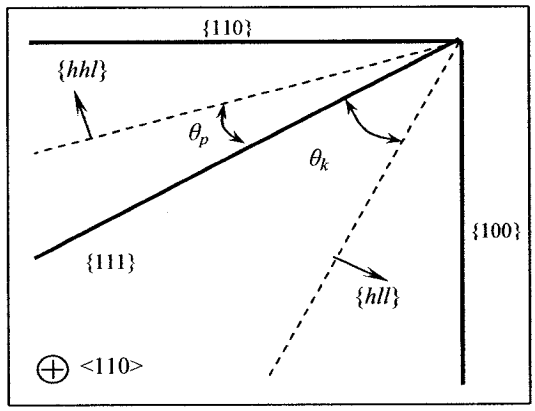

Figure 2-6: Schematic view of Si planes from <110> direction[8], figure adopted from [32].

- The braces "{", "}" are used to represent a family of planes having identical atomic features, such as $\{hll\}$[9].
- (hll) represents a plane with the specific Miller Indices
- $<hll>$ represents the direction or orientation of certain feature, point of view, etc.

[8] θ_p and θ_k stand for angles of a plane with respect to {111} plane for P-based and K-based planes, respectively.
[9] Here *"l"* stands for the low-numbered index and *"h"* – high-numbered index.

2.4. Two Families of Planes

Two identified types of planes are represented by distinct atomic features: one, bounded by rows of kinks, K-based planes and another - by zigzag periodic bond chains (PBC's), P-based planes, [9], [33]-[35]. In other words, the etched planes are assumed to be built of terraces, separated by steps, the edges of which are defined by PBC-s or rows of kinks, see Figure 2-7.

As the etching proceeds, the removal of a chain/row that defines the step-edge in the step-based model is considered to be instantaneous, compared to nucleation of new single-atom defects on an intact step-edge. Therefore, the step-edge is said to be "moving" in a direction perpendicular to its length, and this is defined as "step propagation" (see Figure 2-1).

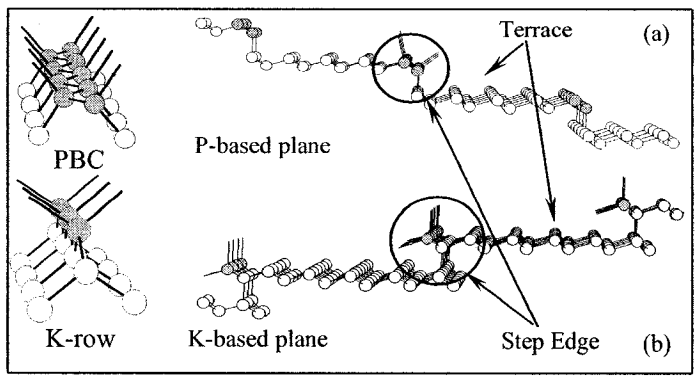

Figure 2-7: Crystallographic model of (a) Periodic Bond Chain, PBC, and a P-based plane, and (b) row of kinks, type 2, and K-based plane, figure from [9].

In this work, this rapid (pseudo-instantaneous) removal of step atoms is referred to as "zipping" and it applies to PBC-s as well as to rows of kinks. Chabal *et al,* [37], found only kinks of the type shown in Figure 2-7(b). Accordingly, this work assumes that the K-based step edges are only composed of kinks of that type, and that zipping of a row of kinks removes all atoms until the next row of the same type is exposed.

In some literature sources, the terraces of the planes in the step-based etching model terraces are defined as any "flat" surfaces in the crystal. According to some studies, [38], for silicon, the terrace may be {111}-oriented surface (globally considered as a plane with the slowest etch rate, hence atomically flat), but under certain condition {100}- or {110}-oriented surfaces can be regarded as atomically "flat" and, therefore, might be regarded as terrace orientations in the appropriate setting, [21]. This statement will be explored in greater detail in following chapters.

Thus two families of planes may be represented by three basic terrace orientations {111}, globally accepted and {110} and {100} - under certain conditions, with the two distinct types of step-edges: PBC and K-row.

2.5. Miller Indices Determination

The first step to the detailed analysis of the step-based surfaces is identification of theoretical inclination angles of all possible planes, which could appear in the under-etch experiment on side-walls of spokes. This data was collected and summarised in Figure 2-8 and Figure 2-9, [9], [31].

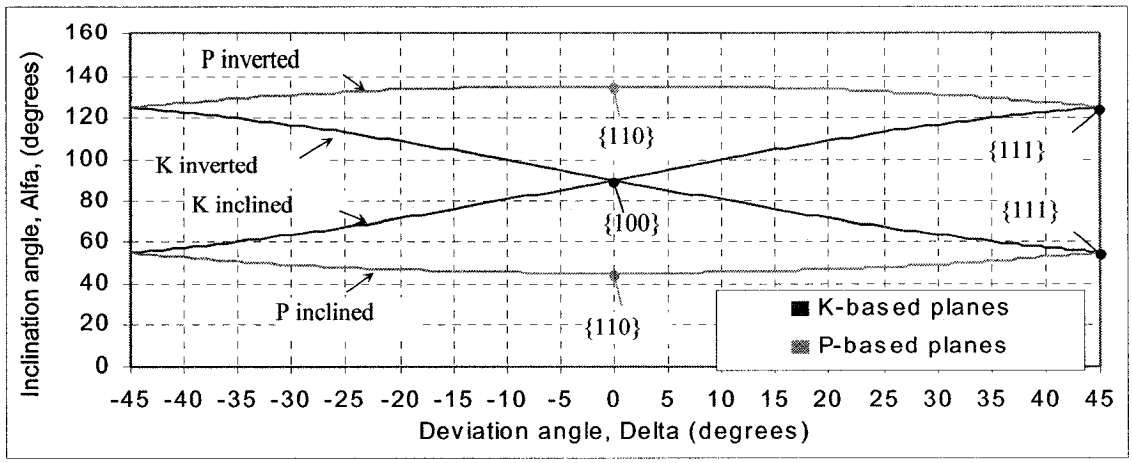

Figure 2-8: Ideal curves (calculated from a model based on only {111} terraces and <110> directed step edges), representing the positions of all possible inclination angles of the facets on the side-walls of a spoke with respect to the mask-edge deviation angle, δ, on Si{100}, figure from [9].

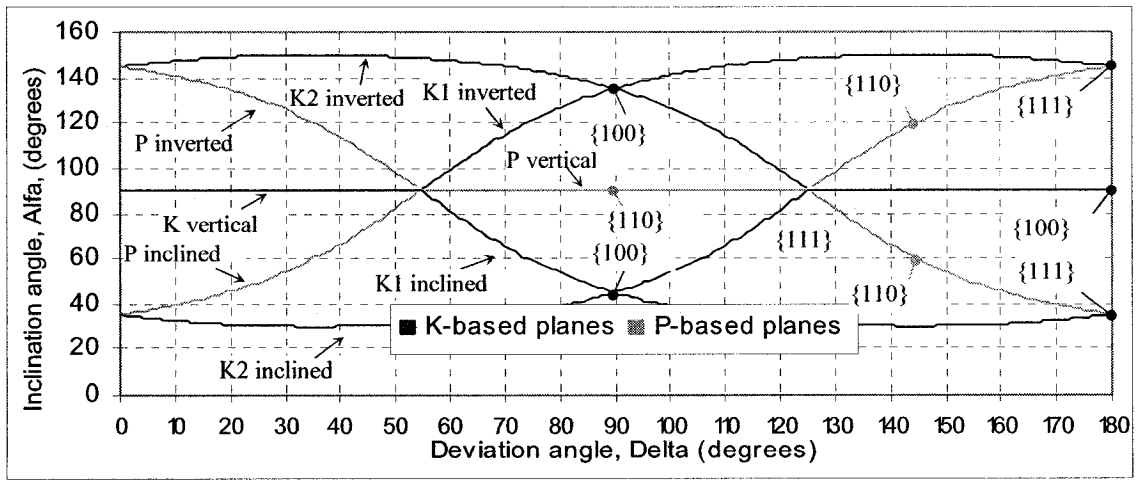

Figure 2-9: Ideal curves (calculated from a model based on only {111} terraces and <110> directed step edges), representing the positions of all possible inclination angles of the facets on the side-walls of a spoke with respect to the mask-edge deviation angle, δ, on Si{110}, figure from [9].

Calculations of Miller Indices for series of planes shown in Figure 2-8 and Figure 2-9 that may appear in wagon-wheel under-etch experiments on Si{100} and Si{110}, respectively, are presented below.

2.5.1. Si{100}: K-based Family of Planes

As a basis for illustration of these calculations the Unit–Cell Cube is used. For a silicon wafer having specific Miller Indices (001), top face of the cube, Figure 2-10 demonstrates the position of all possible K-based inclined planes[10] that may be found on side-walls of spokes for the deviation angle ranging $0 < \delta < 45°$ and inclination angles $54.74°$((111)-plane) $< \alpha < 90°$(vertical (010) plane).

These planes may be obtained by the rotation of (010) → (*lhl*) → (111) along the rotational axis *AB*, (Figure 2-10).

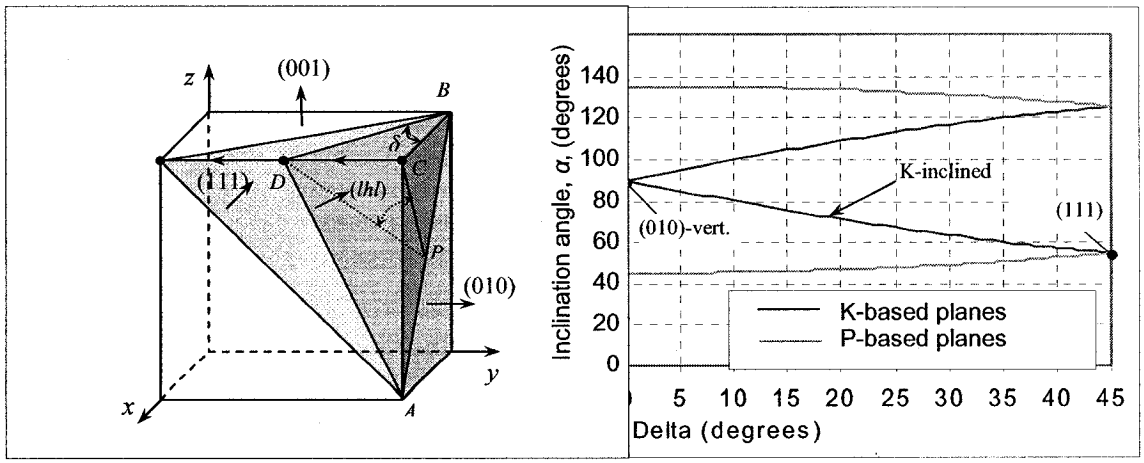

Figure 2-10: Schematic representation of rotation from specific (010) plane to (111), as a base for calculation related to K-based family of inclined planes with the input of theoretical inclination angles from the half of Figure 2-8.

It is possible to determine Miller Indices of this family of planes from the basic geometry. From Figure 2-10, *ABC* is a (010) plane, *ABD* is a K-based plane obtained by the rotation of *ABC* with respect to *AB* – axes of rotation.

[10] Inclination angles $\alpha < 90°$.

In order to obtain Miller Indices of *ABD* plane, which represents a K-inclined plane, we have to know intercepts with *x*, *y* and *z* axis. This may be easily determined by the following calculations:

$$\frac{CD}{BD} = \sin\delta, \quad \frac{BC}{BD} = \cos\delta \tag{2.1}$$

We know that *BC* is a side of a Unit-Cell Cube and its length is 1, so

$$\frac{1}{BD} = \cos\delta \Rightarrow BD = \frac{1}{\cos\delta} \tag{2.2}$$

$$CD = BD\sin\delta = \frac{\sin\delta}{\cos\delta} = \tan\delta \tag{2.3}$$

Intercepts for K-based inclined plane are (tan δ, 1, tan δ), and Miller Indices may be expressed as reciprocals of the intercepts, or (1, 1/tan δ, 1).

To check these calculations, from Figure 2-10:

$$\angle DPC = \arcsin\frac{DC}{DP} = \arccos\frac{CP}{DP} = \arctan\frac{DC}{CP}$$

$$\frac{CP}{CB} = \sin 45^\circ \Rightarrow CP = \frac{1}{\sqrt{2}}$$

$$\angle DPC = \arctan\frac{DC}{CP} = \arctan\left(\sqrt{2}\cdot DC\right) = \arctan\left(\sqrt{2}\cdot\tan\delta\right)$$

This angle can also be expressed as the dot product between (010) and (*lhl*) planes.

$$\angle DPC = \arccos\left(\frac{a_1b_1 + a_2b_2 + a_3b_3}{\left|\vec{a}\right|\left|\vec{b}\right|}\right) \tag{2.4}$$

Similar approach may be used to determine the Miller Indices (MI) for the family of K-based inverted planes.

These planes may be obtained by the following rotation: $(010) \rightarrow (lh\bar{l}) \rightarrow (11\bar{1})$, see Figure 2-8.

From the analysis of the summary of theoretical calculations, crystal geometry, and the experimental data, inverted planes happen to be from the same family of planes as a respective inclined facet of the K-based group.

Example 2.1: Position of K-inclined facet on the sidewall of a spoke in the under-etch experiment at the deviation angle $\delta = 5°$, (Figure 2-11).

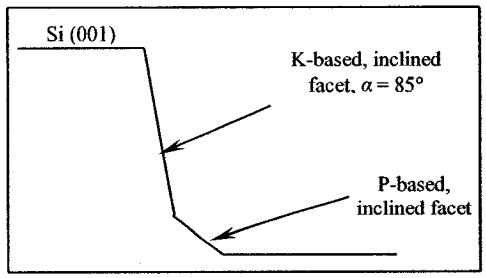

Figure 2-11: Schematic view of a cross-section profile of a spoke in wagon-wheel experiment on Si{100} at $\delta = 5°$ composed of two inclined facets.

The Miller Indices of K-inclined plane that appears on the side wall of a spoke at $\delta = 5°$ will be $(\tan 5°, 1, \tan 5°) \rightarrow \left(1, \frac{1}{\tan 5°}, 1\right) \rightarrow (1, 11.43, 1)$. For $\delta = 5°$

$\angle DPC = \arctan\left(\sqrt{2} \cdot \tan 5°\right) = 7.0532°$, and the dot product:

$$\angle DPC = \arccos\left(\frac{a_1 b_1 + a_2 b_2 + a_3 b_3}{|\vec{a}||\vec{b}|}\right) = \arccos\left(\frac{11.43}{\sqrt{1}\sqrt{11.43^2 + 1 + 1}}\right) = 7.053°$$

If a K-inverted facet were detected in the under-etch experiment at $\delta = 5°$, its MI would be $(1\ 11.43\ \bar{1})$.

2.5.2. Si{100}: P-based Family of Planes

The family of P-based inclined planes on silicon wafer with specific Mille Indices (001), see Figure 2-12, may be obtained by the following rotation: (011) → (*lhh*) → (111).

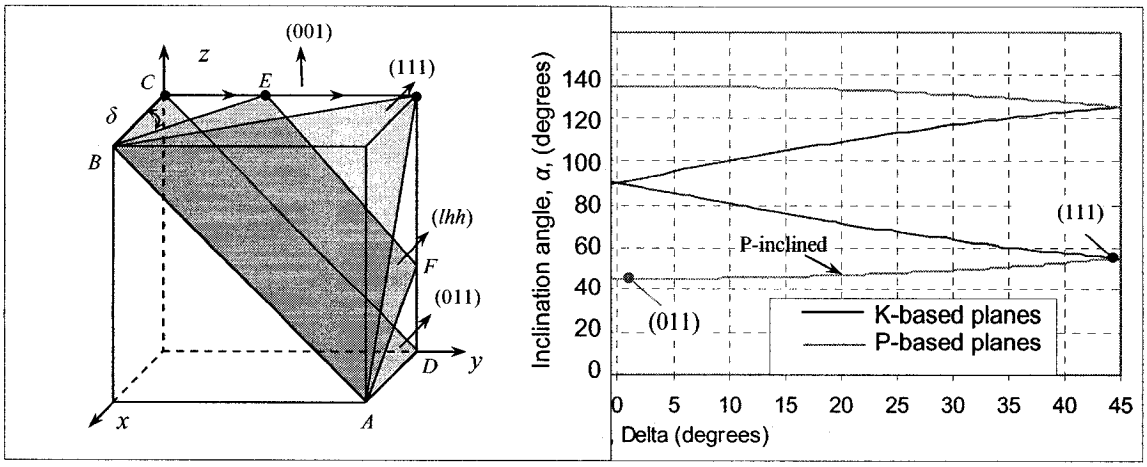

Figure 2-12: Schematic representation of rotation of (011) plane as a base for the family of P-based inclined planes with the input of theoretical inclination angles from the half of Figure 2-8.

Similarly to the above discussion, calculation of MI for P-inclined plane may be done as follows: from Figure 2-12, *ABCD* is a (011) plane, *ABEF* is a P-based plane obtained by the rotation of *ABCD* around axes of rotation *AB*.

In order to obtain MI of *ABEF* plane, we have to know the intercepts with *x*, *y* and *z*.

$$\frac{CE}{BE} = \sin\delta, \quad \frac{BC}{BE} = \cos\delta \tag{2.5}$$

We know that BC = 1, so

$$\frac{1}{BE} = \cos\delta \Rightarrow BE = \frac{1}{\cos\delta} \tag{2.6}$$

$$CE = BE\sin\delta = \frac{\sin\delta}{\cos\delta} = \tan\delta \tag{2.7}$$

Therefore, the intercepts for the P-based inclined plane may be expressed as (tanδ, 1, 1) and MI as reciprocals of intercepts – (1, 1/tanδ, 1/tanδ)

Similarly to the K-inverted planes, same approach may be used to determine MI for the family of P-based inverted planes.

This family can be obtained by the rotation of $(01\bar{1}) \rightarrow (lh\bar{h}) \rightarrow (11\bar{1})$.

Example 2.2: P-inclined facet on the side-wall of a spoke in the under-etch experiment at the deviation angle $\delta = 5°$ appears as a second facet, (Figure 2-11).

MI of P-inclined facet: $(\tan 5°, 1, 1) \rightarrow \left(1, \frac{1}{\tan 5°}, \frac{1}{\tan 5°}\right) \rightarrow (1, 11.43, 11.43)$

If a P-inverted facet were detected on a side-wall of a spoke in the under-etch experiment at $\delta = 5°$, its MI are $(1\ 11.43\ \overline{11.43})$.

The Table 2.1 below is an extract of the finalized calculations of MI for P- and K-based facets on Si{100} based on the experimental data. Please note, that the Miller Indices for P-inverted facets are present as theoretical values only, since it was not detected in the experimental measurements of the samples etched at 25wt.% TMAH at 80°C.

Table 2.1: Summary of calculated Miller Indices for planes appearing as facets on side-walls of spokes in Si{100} etched in 25wt.% TMAH at 80°C for $0° \leq \delta \leq 5°$ and $15° \leq \delta \leq 20°$.

Delta	α - 1st facet	α - 2nd facet	α - 3rd facet	K-inverted			K-inclined			P-inverted			P-inclined		
0	90	45		0	1	0	0	1	0	0	1	1	0	1	1
1	89	45.004		1	57.3	-1	1	57.3	1	1	57.3	-57.3	1	57.3	57.3
2	88.001	45.017		1	28.6	-1	1	28.6	1	1	28.6	-28.6	1	28.6	28.6
3	87.004	45.039		1	19.1	-1	1	19.1	1	1	19.1	-19.1	1	19.1	19.1
4	86.01	45.07		1	14.3	-1	1	14.3	1	1	14.3	-14.3	1	14.3	14.3
5	85.019	45.109		1	11.4	-1	1	11.4	1	1	11.4	-11.4	1	11.4	11.4
⋮															⋮
15	75.489	45.993		1	3.73	-1	1	3.73	1	1	3.73	-3.73	1	3.73	3.73
16	105.41	73.703	46.132	1	3.49	-1	1	3.49	1	1	3.49	-3.49	1	3.49	3.49
17	106.3	72.828	46.28	1	3.27	-1	1	3.27	1	1	3.27	-3.27	1	3.27	3.27
18	107.17	71.966	46.437	1	3.08	-1	1	3.08	1	1	3.08	-3.08	1	3.08	3.08
19	108.03	71.118	46.604	1	2.9	-1	1	2.9	1	1	2.9	-2.9	1	2.9	2.9
20	108.88	70.284	46.781	1	2.75	-1	1	2.75	1	1	2.75	-2.75	1	2.75	2.75

2.5.3. Si{110}: K-based Family of Planes

Data from the under-etch experiment on Si{110} provides larger variety of facets that appear on side-walls of spokes, compared to Si{100}, (Figure 2-8 and Figure 2-9). K-based planes may appear as two different types of inclined facets (in this text referred to as K1-inclined and K2-inclined based on their relative position with respect to each other), vertical facet – K-vertical, and two types of inverted facets (K1-inverted and K2-inverted), see Figure 2-9.

Different approach to calculations of MI is used for Si{110} wafer since the geometrical calculations proved to be somewhat complicated. For simplicity, MI determination was done for the inclined facets first.

The family of K2-inclined planes, inclination angles $\alpha < 45°$, is to be found as the bottom most facets on the side-wall of a spoke, (Figure 2-9). On silicon wafer with specific Miller Indices (011) this group of planes may be obtained by the following rotation: (111) → (*llh*) → (001).

Examining indices of this K-based plane, (*llh*), it may be assumed that in the geometry of a Unit-Cell Cube these indices may be written as (1,1,x), where $x > 1$.

Applying vector calculus[11], let $\bar{a} = (011)$ *and* $\bar{b} = (11x)$. And from a dot product, $\bar{a} \bullet \bar{b}$, a quadratic equation with one unknown may be written:

$$x^2\left(2\cos^2\alpha - 1\right) + 2x + \left(4\cos^2\alpha - 1\right) = 0, \qquad \textbf{(2.8)}$$

where α is the facet inclination angle.

[11] Vector calculus is a field of mathematics concerned with multivariate real analysis of vectors in two or more dimensions. It consists of a suite of formulas and problem solving techniques very useful for engineering and physics, [40].

Roots of the equation (2.8) can be determined by the simple formulae:

$$x_{K2-inclined} = \frac{-1 \pm \sqrt{1-1\left(2\cos^2\alpha - 1\right)\left(4\cos^2\alpha - 1\right)}}{2\cos^2\alpha - 1} \qquad \textbf{(2.9)}$$

Respectively, K2-inverted plane (if present appears as the top-most facet, see Figure 2-9) that is formed by the rotation $(1\bar{1}\bar{1}) \rightarrow (l\bar{h}\bar{l}) \rightarrow (0\bar{1}0)$ comes from the same family of planes as a K2-inclined at the same deviation angle.

Example 2.3: At δ = 5° on Si{110}, the experimental data shows only one facet present – K2-inclined, Figure 2-13.

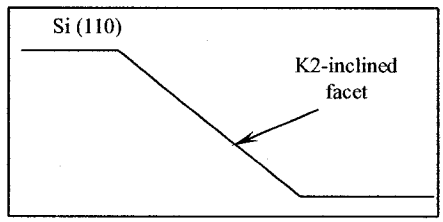

Figure 2-13: Schematic view of a cross-section profile of a spoke in wagon-wheel experiment on Si{110} at δ = 5° with the sidewall composed of one K2-inclined facet.

$$x_{K2-inclined} = \frac{-1 \pm \sqrt{1-\left(1-2\cos(32.36636)\right)\left(1-4\cos(32.36636)\right)}}{1-2\cos(32.36636)} = 1.02221624$$

Therefore, the Miller Indices of K2-inclined plane are at δ = 5° (1, 1, 1.02).

If a K2-inverted facet were present in under-etch experiment at δ = 5° on Si{110}, its MI would be $(1\ \overline{1.02}\ \bar{1})$.

On silicon wafer with specific Miller Indices (011) K1-inclined plane, inclination angle $35.26° < \alpha < 90°$ (Figure 2-9), is obtained by the rotation $(1\bar{1}1) \rightarrow (l\bar{l}h) \rightarrow (001)$.

MI calculations for this group of planes will look as follows:

Using $\bar{a} = (011)$ *and* $\bar{b} = (1\bar{1}x)$, where $x > 1$, and a dot product:

$$x_{K1-inclined} = \frac{1 \pm \sqrt{1-\left(1-2\cos^2\alpha\right)\left(1-4\cos^2\alpha\right)}}{1-2\cos^2\alpha}. \qquad \textbf{(2.10)}$$

Respectively, the K1-inverted plane - the rotation $(1\bar{1}1) \rightarrow (l\bar{h}l) \rightarrow (0\bar{1}0)$ - belongs to the same family of planes as a K1-inclined at the same deviation angle.

Example 2.4: If both, K1-inclined and K1-inverted planes were present at the deviation angle $\delta = 70°$ on Si{110}, respective inclination angles $\alpha = 64.12°$ and $\alpha = 115.88°$ MI may be written as $\left(1,\bar{1},2.7565\right)$ for K1-inclined and $\left(1,\overline{2.7565},1\right)$ for K1-inverted.

K-vertical plane, inclination angle $\alpha = 90°$ (Figure 2-9), is observed at deviation angles $0° \leq \delta \leq 55°$ and obtained by the rotation $(100) \rightarrow (h\bar{l}l) \rightarrow (1\bar{1}1)$. MI calculations are reduced to the following formulae:

$$x_{K-vertical} = \frac{2 \pm \sqrt{4 - \left(3\cos^2 \xi - 1\right)\left(6\cos^2 \xi - 4\right)}}{3\cos^2 \xi - 1}, \tag{2.11}$$

where ξ is the angle between K-vertical plane and a specific $(1\bar{1}1)$ plane, determined as $(54.73561° - \delta)$ and $x > 1$.

2.5.4. Si{110}: P-based Family of Planes

P-based group of planes on Si{110} may appear as P-inclined, P-vertical, or P-inverted facet, see Figure 2-9. MI for the P-inclined plane that appears on spokes side-walls for the specific (011) wafer surface, may be obtained by the rotation of $(111) \rightarrow (hlh) \rightarrow (101) \rightarrow (h\bar{l}h) \rightarrow (1\bar{1}1)$. Similarly, to the computation for K-based group:

$$x_{P-inclined} = \frac{-1 \pm \sqrt{1 - \left(2\cos^2 \alpha - 1\right)\left(4\cos^2 \alpha - 1\right)}}{4\cos^2 \alpha - 1}, \tag{2.12}$$

where α is the facet inclination angle.

P-inverted surfaces: rotation of $(1\bar{1}\bar{1}) \rightarrow (h\bar{h}\bar{l}) \rightarrow (1\bar{1}0) \rightarrow (h\bar{h}l) \rightarrow (1\bar{1}1)$. MI can be determined the same way as for the P-inclined family of planes on Si{100}, (see Section 2.5.2).

P-vertical planes obtained by the rotation: $(1\bar{1}1) \rightarrow (l\bar{h}h) \rightarrow (0\bar{1}1)$

$$x_{P-vertical} = \sqrt{\frac{-\cos^2 \xi}{2(\cos^2 \xi - 1)}}, \tag{2.13}$$

where ξ – is the angle between P-vertical plane and a specific $(1\bar{1}l)$ plane, determined as $(54.73561° - \delta)$ and $x > 1$.

Table 2.2: Summary of the Miller Indices calculations of planes appearing as facets on sidewalls of a spoke in Si{110} etched in 25wt.% TMAH at 80°C $30° \leq \delta \leq 32°$ and $53° \leq \delta \leq 56°$

δ	α - 1st Facet	α - 2nd Facet	α - 3rd Facet	K2-inc, (11x)	K1-inc, (1-1x)	K-vert, (x-11)	K1-inv, (1x1)	K2-inv, (1x-1)	P-inc, (x1x)	P-vert, (1-x x)	P-inv, (x-x -1)
0	34.97			1.02				-1	1.02		1.02
⋮											⋮
30	90	54.07	30.1	1.82		2.45		-1.8	5.45		5.45
31	90	55.12	30.07	1.85		2.35		-1.8	6.66		6.66
32	90	56.2	30.04	1.88		2.26		-1.9	8.6		8.6
⋮											⋮
54	90			2.95		1.03		-2.9	1.06		1.06
55	90			3.02	1.02	1.01	-1	-3	0	1.01	0
56	90			3.1	1.07		-1.1	-3.1		1.05	

The Table 2.2 is an extract of the finalized calculations of MI for P- and K-based facets on Si{110} based on the experimental data for the samples etched at 25wt.% TMAH at 80°C.

2.6. Atomic Construction of Step-Based Planes

Now, that the Miller Indices of both families of planes detected in our under-etch experiment are known, it is useful for further analysis to determine and illustrate plane profiles.

Such construction may be described (below) by using an example.

From the experimental data for Si{100} etched at 25wt.% TMAH, two facets appear on the sidewall of a spoke at δ = 5°: K-inclined as a top-most facet and P-inclined as a second one, Figure 2-14.

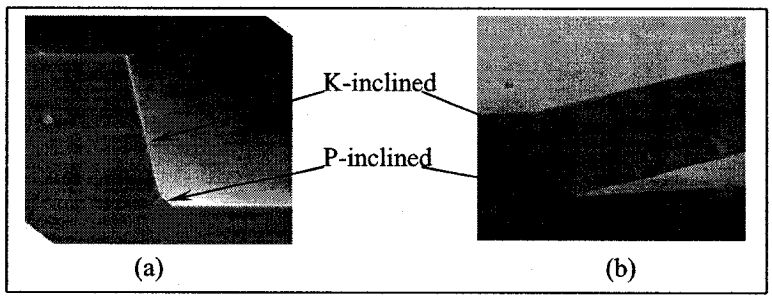

Figure 2-14: SEM picture of (a) cross-section and (b) side view of the side wall of a spoke at δ = 5° on Si{100} etched in 25wt% TMAH, figure from [9].

As it was shown earlier, the MI of the K-inclined and the P-inclined planes at this deviation angle are (1, 11.43, 1) and (1, 11.43, 11.43) respectively, (see Example 2.1 and Example 2.2 above).

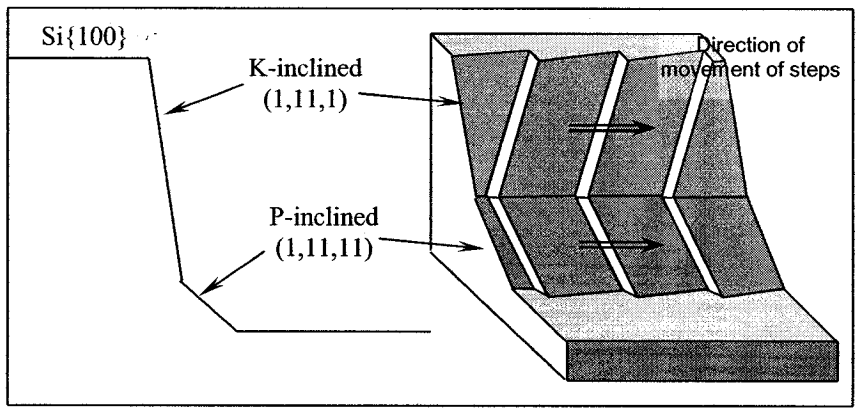

Figure 2-15: Schematic representation of a sidewall of a spoke on Si{100} etched in 25% TMAH for 1.5 hours at δ = 5° (a) cross-section view, (b) side view.

It is known, that the precision of the alignment in our samples might contain an error of ±0.5°. Therefore, to simplify the analyses the following approximation will be used: at the exact deviation angle δ = 5.194°, MI are (1, 11, 1) and (1, 11, 11) for K-based and P-based facets, respectively. Their relative position is illustrated in a schematic diagram of

Figure 2-15(a) and (b). Diagrams like this Figure 2-15 are used to visualize the etched surfaces and the relative movement of steps on those etched surfaces.

This approximation allows the use of software to create a crystallographic reconstruction of these planes, see Figure 2-16(a) and (b).

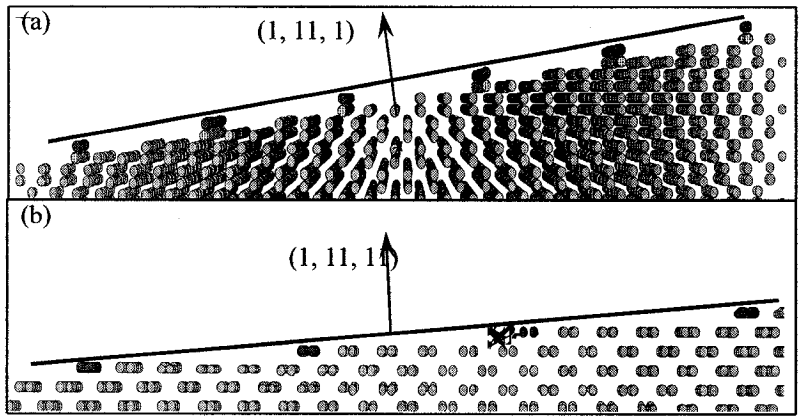

Figure 2-16: Crystallographic construction of (a) K-based (1, 11, 1) and (b) P-based (1, 11, 11) plane profiles[12].

Similarly, the profile of any plane that appears as a facet on sidewalls of spokes may be constructed, allowing general analyses of these planes.

2.7. Summary and Contributions

The purpose of this Chapter is to define the geometric properties of surfaces available for analysis in wagon-wheel under-etch experiment. A large portion of these parameters was described by Z. Elalamy *et al.*, [9]. However, as a part of the research group, I contributed to a majority of this study.

My particular share of the work included detailed calculations of Miller Indices of all planes appearing on sidewalls of spokes and the crystallographic reconstruction of said surfaces. Even though this Chapter does not provide any explicit explanation to the phenomena of wet-chemical anisotropic etching, it is necessary for a fundamental

[12] Created with the help of CaRIne software.

understanding of silicon surface geometry and a large part of subsequent study is based on this understanding.

3. Step Spacing Determination

3.1. Introduction

As it was identified earlier, the step-based etching model suggests that two families of planes (P-based and K-based planes) compose most of facets in under-etched structures, where each facet is assumed to be built of "flat" terraces, separated by steps, the edge of which is defined by periodic bond chains (PBC-s), or rows of kinks, respectively, [9], [12], [30]-[31], [33]-[38].

Note that the presence of a preponderance of such P-based and K-based surfaces on etched silicon confirms that the atoms on the edges of the terraces (the step atoms) must be removed as highly correlated groups. This is likely to be due to a relatively low probability of removal of an atom from the intact chain of atoms on a step-edge, compared to the probability of removal of an atom on a step-edge after its neighbouring atom is already removed.

Flat terraces in the step-based model are assumed to be {111}-oriented surfaces. However, under various types of circumstances, other planes are also observed to be (to varying extent) flat or locally slowest-etching, or both. Note that a local minimum in etch rate may be consistent with the presence of a flat plane (at the local minimum), along with step-based etching for other planes deviated by small angles. For example, {100} and {110} planes have been observed to be flat under various conditions and have been studied as the basis for step movement, [13], [34], [38].

In this section, the step spacing determination is done for two families of planes typically detected in wagon-wheel under-etch experiments. The step-based model with

terraces as {111}-oriented planes is taken as the basis of these calculations, and is augmented by the step-spacing determination of planes with {110}- and {100}-oriented terraces where appropriate.

3.2. General Assumption – {111}-oriented Terrace

3.2.1. K-based Family of Planes

In order to facilitate these calculations, a honey-comb view of the crystal lattice is introduced, i.e. view of the silicon lattice in a <110> direction. This achieves a cross-sectional view of the plane in a direction perpendicular to the step orientation. Schematic construction of a cross-section of a K-based plane with Miller Indices {*llh*} that appears as a facet on the sidewall of a spoke is shown in Figure 3-1.

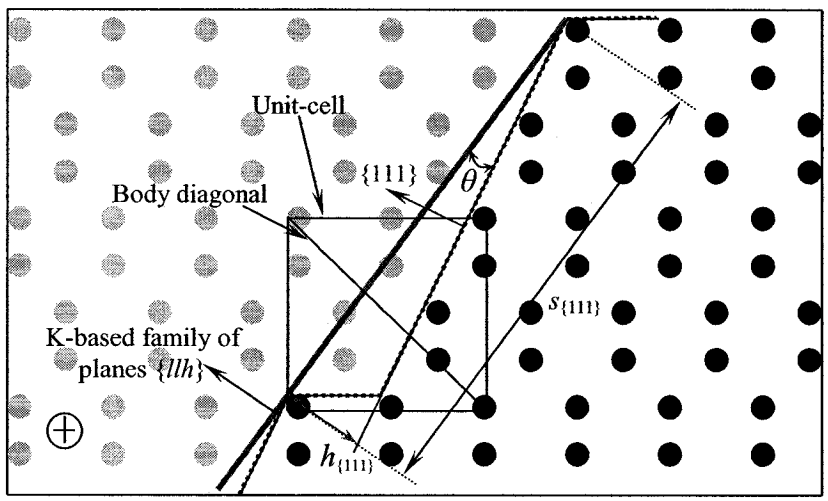

Figure 3-1: Schematic representation of a K-based plane for step height calculations based on {111}-oriented terrace viewed from <110> direction – honey-comb view[13].

Light gray and black circles in this figure indicate atoms that compose the crystal lattice viewed from a <110> direction, creating a honey-comb profile. Black atoms indicate the simplified construction of a cross-section of this plane, whereas light gray atoms just

[13] Note that the presence of an atom on the body diagonal is only due to the imperfection of the figure.

indicate the positions of atoms that are already removed by the etchant in order to achieve the K-based plane in question.

From the basic geometry, the step height of a K-based plane with {111}-oriented surface as a terrace can be determined as a distance between two {111} planes, Figure 3-1. This distance is a ⅓ of body diagonal of a Unit-Cell Cube with its side of 5.43Å, see Figure 3-2, and calculations are reduced to the following:

$$h_{(111)} = \frac{5.43\sqrt{3}}{3} = 3.135012 \times 10^{-10} m, \tag{3.1}$$

where $h_{(111)}$ is the step height on the K-based plane with {111}-oriented terrace, and 5.43Å is the lattice constant.

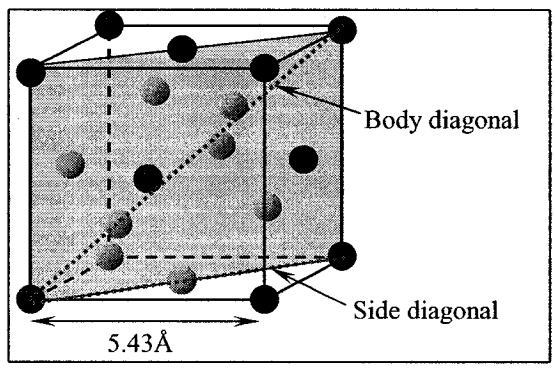

Figure 3-2: Unit-Cell Cube of a diamond silicon lattice.

The step spacing, or the distance between two step-edges, can be determined as:

$$s_{\{111\}} = \frac{h_{\{111\}}}{\sin\theta}, \tag{3.2}$$

where $s_{\{111\}}$ is the step spacing on a plane with {111}-oriented terraces, (Figure 3-1).

θ is the angle between K-based plane and the terrace, {111}-oriented surface, (Figure 3-1).

3.2.2. P-based Family of Planes

Similarly, the step height of P-based plane with {111}-oriented terraces can be calculated as a distance between two {111} planes, (Figure 3-2 and Figure 3-3). Similarly to the K-based planes, the step height for P-based planes with {111}-oriented terraces is $h_{(111)} = 3.135\,\mathring{A}$ and the step spacing can be determined from the following:

$$s_{\{111\}} = \frac{h_{\{111\}}}{\sin\theta}, \tag{3.3}$$

where θ is the angle between P-based plane and the {111}-oriented terrace, Figure 3-3.

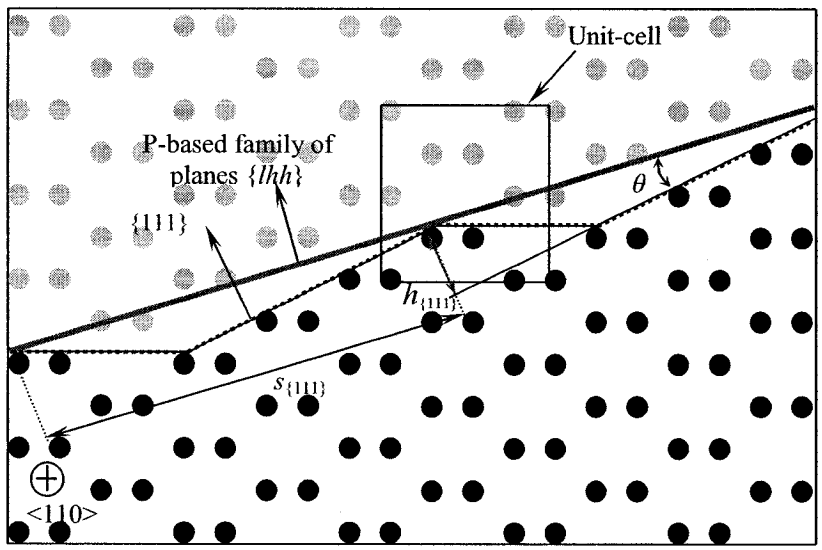

Figure 3-3: Schematic representation of a P-based plane for step height calculations based on {111}-oriented terrace viewed from <110> direction – honey-comb view.

3.3. General Assumption – {100}-oriented Terrace

3.3.1. K-based Family of Planes in Vicinity of Basic {100} Surface

As it was indicated earlier, terraces in the step-based model under certain conditions may be represented by {100}- or {110}-oriented planes. This assumption comes from the idea that in the vicinity of {100} plane it might be reasonable to regard a K-based plane in the step-based model with {100}-oriented surface as a terrace, [38].

From the basic geometry, the step height of a K-based plane with {100} terrace can be calculated as distance between two {100} planes, (Figure 3-4).

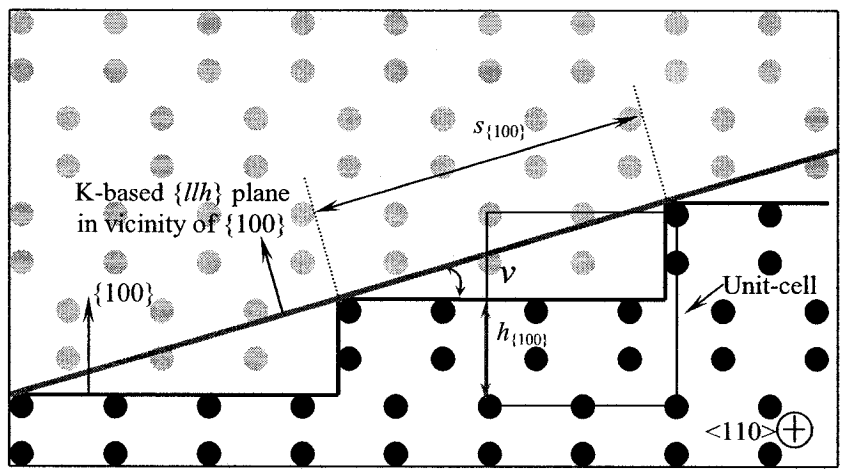

Figure 3-4: Schematic representation of a K-based plane in vicinity of {100} plane for step height calculations based on {100}-oriented terrace viewed from <110> direction – honey-comb view.

This distance is ½ of a side of the Unit-Cell Cube, or a half of lattice constant, (Figure 3-2 and Figure 3-4).

$$h_{(100)} = \frac{5.43}{2} = 2.715 \times 10^{-10} m, \tag{3.4}$$

where $h_{(100)}$ – is the step height for K-based plane with {100} terrace and

5.43Å is the lattice constant.

The step spacing can be determined as:

$$s_{\{100\}} = \frac{h_{\{100\}}}{\sin \nu}, \tag{3.5}$$

where $s_{\{100\}}$ is the step spacing on a plane with {100}-oriented terraces

ν is the angle between K-inclined plane and {100}-oriented terrace.

3.4. General Assumption – {110}-oriented Terrace

3.4.1. P-based Family of Planes in Vicinity of Basic {110} Surface

Similarly, to the K-based surfaces considered in the previous section, same argument may be used in the step spacing determination on P-based planes in vicinity of {110} plane. For the step-based etching model, P-based planes with the small deviation from the basic {110} surface are to be formed of {110}-oriented terraces and steps aligned with PBC-s. The step height in this plane is a distance between two {110} planes, (Figure 3-5).

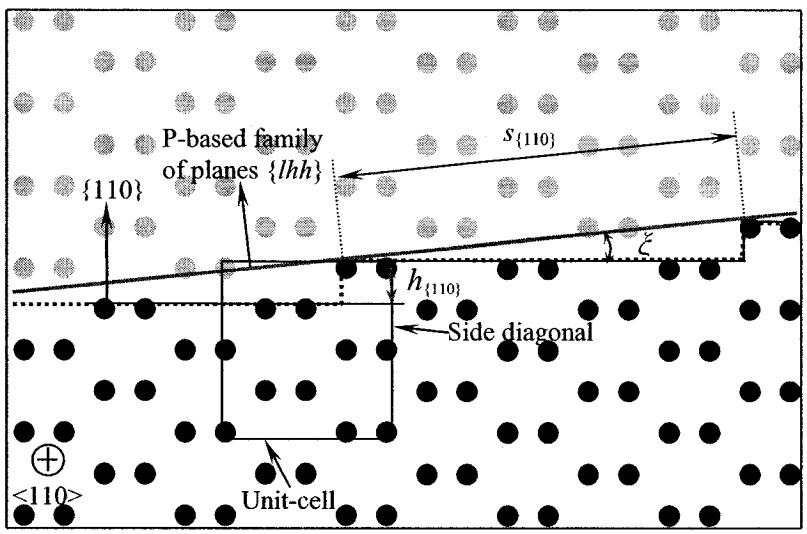

Figure 3-5: Schematic representation of a P-based plane in vicinity of {110} plane for step height calculations based on {110}-oriented terrace viewed from <110> direction – honey-comb view.

This distance is as a ¼ side diagonal of Unit-Cell Cube, (Figure 3-2 and Figure 3-5).

$$h_{(110)} = \frac{5.43 \cdot \sqrt{2}}{4} = 1.919794911 \times 10^{-10} m, \tag{3.6}$$

where $h_{(110)}$ – is the step height for {110} terrace and

5.43Å is the lattice constant, (Figure 3-5).

The step spacing, or distance between two step-edges, can be expressed as:

$$s_{\{110\}} = \frac{h_{\{110\}}}{\sin\xi}, \tag{3.7}$$

where $s_{\{110\}}$ is the step spacing on a plane with {110}-oriented terraces and

ξ is the angle between P-inclined plane and the {110}-oriented terrace.

3.5. Ideal Step Spacing Determined for Surfaces with {111}-, {110}- and {100}-oriented Terraces

Using the information from preceding sections, the ideal step-spacing was calculated for two families of planes.

Figure 3-6 provides the summary of calculated ideal step spacing for planes detected in the wagon-wheel under-etch experiment on Si{100} etched in 25wt.% TMAH, (the general etching model assumption that the terraces are {111}-oriented surfaces).

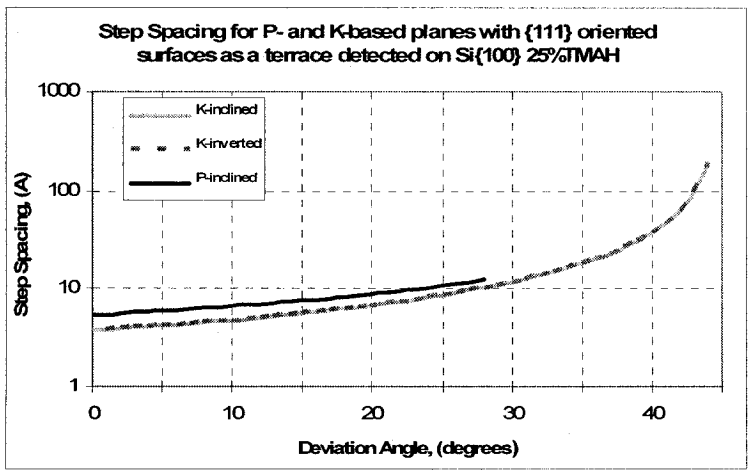

Figure 3-6: Graphic representation of summarized calculations of the step spacing of all planes that were detected on sidewalls of spokes in the wagon-wheel under-etch experiment on Si{100} etched in 25wt.% TMAH, (based on the general etching model with {111}-oriented terraces).

Similar summaries were done for Si{110} etched in 25wt.% TMAH and Si{100}and Si{110} etched in 19wt.% TMAH.

Figure 3-7 represents a summary of step spacing calculations for planes detected in the wagon-wheel under-etch experiment on Si{100} etched in 25wt.% TMAH, (with the assumption that the terraces may be {100}- and {110}-oriented surfaces for P-based and K-based planes, respectively).

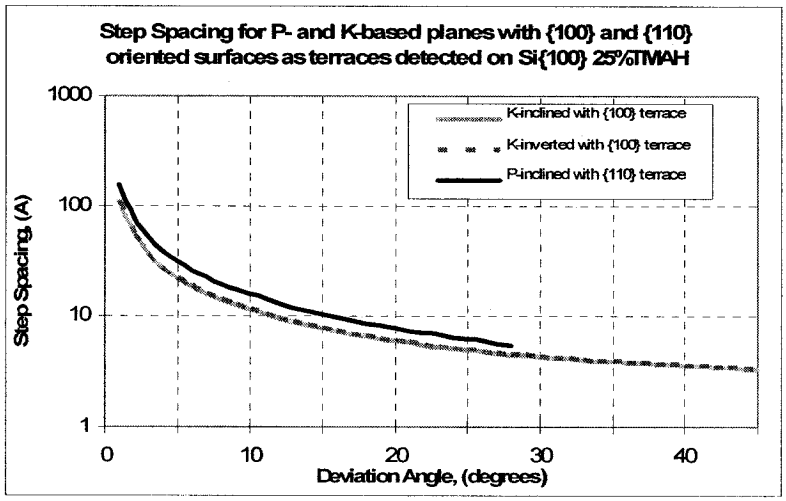

Figure 3-7: Graphic representation of summarized calculations for the step spacing of all planes detected on sidewalls of spokes in the wagon-wheel under-etch experiment on Si{100} etched in 25wt.% TMAH, (assuming that in the vicinity of the {100} and {110} planes they may appear as terraces in the step-based model).

Similar summaries were done for Si{110} etched in 25wt.% TMAH and Si{100}and Si{110} etched in 19wt.% TMAH.

Further analysis proved useful to determine the additional parameter – terrace width. Therefore, based on the basic geometry of K- and P-based planes, the following can be calculated:

$$w_{\{111\}} = h_{\{111\}} / \tan\theta \tag{3.8}$$

$$w_{\{110\}} = h_{\{110\}} / \tan\xi \tag{3.9}$$

$$w_{\{100\}} = h_{\{100\}} / \tan\nu \qquad (3.10)$$

where $w_{\{111\}}$ is the width of {111}-oriented terrace,

$w_{\{110\}}$ is the width of {110}-oriented terrace,

$w_{\{100\}}$ is the width of {100}-oriented terrace.

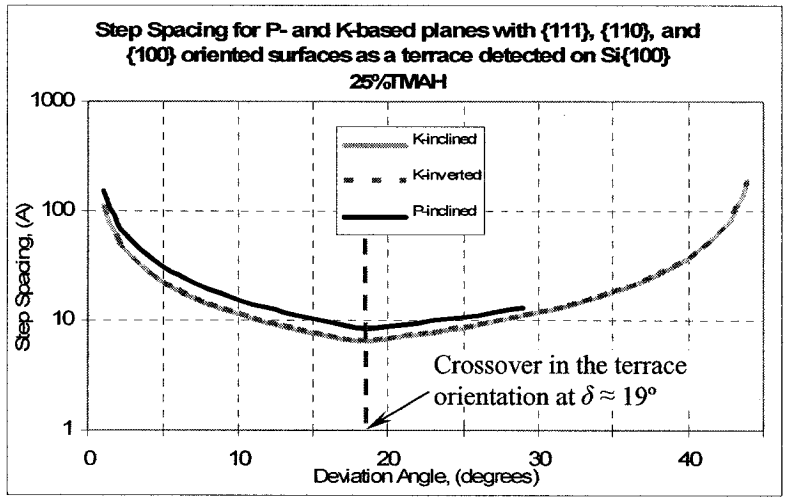

Figure 3-8: Graphic representation of summarized calculations for the step spacing of all planes detected on sidewalls of spokes in the wagon-wheel under-etch experiment on Si{100} etched in 25wt.% TMAH, taking into account the crossover in the terrace orientation.

Figure 3-8 represents the summary of the step-spacing of all surfaces detected on Si{100} etched in 25wt.% TMAH. The significance of this graph is in visual representation of the location of the change in the orientation of terraces, or crossover in the terrace orientation (appears at the deviation angle of approximately 19° for both types of planes on Si{100}).

Further analysis of the relation between the features of the etch rate curve and the terrace-width crossover is provided in the next section.

3.6. Silicon Wet Etch Anisotropy: Analysis of the Effect of {111}, {110}, {100} Terrace Widths, [19]

A step-based model of wet anisotropic etching of silicon is examined in conjunction with observations from wagon-wheel under-etch experiments of Si{100} and Si{110} in tetra-methyl ammonium hydroxide (TMAH) at 25 wt% at 80°C. Stepped surfaces may be composed of flat {111} terraces, and/or flat {100} or {110} terraces. Transitions (crossovers) between terrace orientations are theoretically analyzed and found to be approximately {331} and {311} planes, respectively. These crossover planes occur at several deviation angles and under-etched facets. The theoretical crossovers are compared to experimental observations regarding transitions in facet configuration, roughness, and etch-rate. These crossovers may significantly influence the complexity of etch rate variation and facet appearance or disappearance in an under-etch experiment.

In the study of wet anisotropic etching of silicon, etch models involve the movement of steps on "flat" crystallographic planes on the surface of the silicon, [12], [20], [21]. The most obvious such planes are the {111}-family planes, which are also globally the slowest-etching planes in silicon. The steps are modeled as being the edges of small areas of the "flat" plane (called "terraces"). The average terrace width is a maximum (theoretically infinite, for an ideal flat surface) at {111} planes, and the average terrace width decreases for planes deviated away from {111}.

However, under various types of circumstances, other planes are also observed to be (to varying extent) "flat", or locally slowest-etching, or both. Note that a local minimum in etch rate may be consistent with the presence of a "flat" plane (at the local minimum), along with step-based etching for other planes deviated by small angles from

that "flat" plane. For example, {100} and {110} planes have been observed to be flat under certain conditions, [12]-[13], and have been studied as the basis for step movement, [12]-[13], [34].

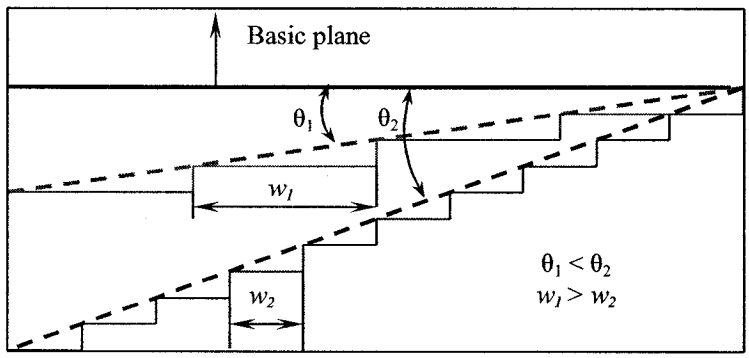

Figure 3-9: Steps and terraces for two different planes deviated at angles theta, ($\theta_1 < \theta_2$) from the "flat" plane. w_1 and w_2 are the terrace widths.

Figure 3-9 illustrates steps and terraces for two different deviation angles away from the (unspecified) flat plane. If the flat plane is in the {111} family, the terraces are {111} facets, and the step edges are typically periodic bond chains or rows of kinks. For example, for the specific (111) plane these step edges move in $<1\bar{1}2>$ or $<\bar{1}\bar{1}2>$ directions, respectively.

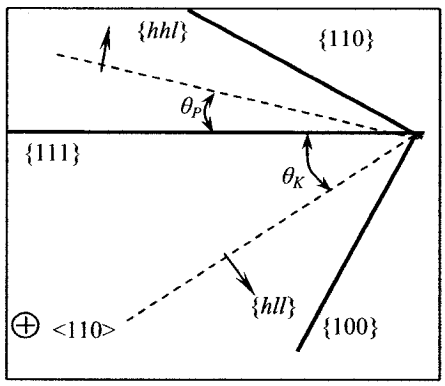

Figure 3-10: Schematic view of Si surfaces viewed from a <110> direction, [32].

Figure 3-10 shows the general rotation angle of a plane away from {111}. The angle θ_P, describes rotation from {111} to {110}, while θ_K describes rotation from {111} to {100}. Consequently, two types of planes may be identified: one, bounded by rows of kinks, features characteristic of the planes between (100) and (111) surfaces, and another, by

periodic zigzag bond chains (PBC-s), for planes between (111) and (110) surfaces, [9], [34], [41]. In other words, the etched planes are assumed to be built of terraces, separated by steps, the edges of which are defined by PBC-s or rows of kinks, as depicted in Figure 3-11.

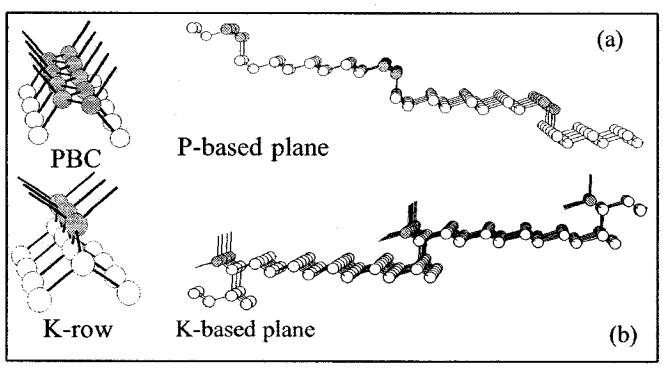

Figure 3-11: Crystallographic model of (a) Periodic Bond Chain, PBC, and a P-based plane, and (b) row of kinks, type 2, and K-based plane, [9].

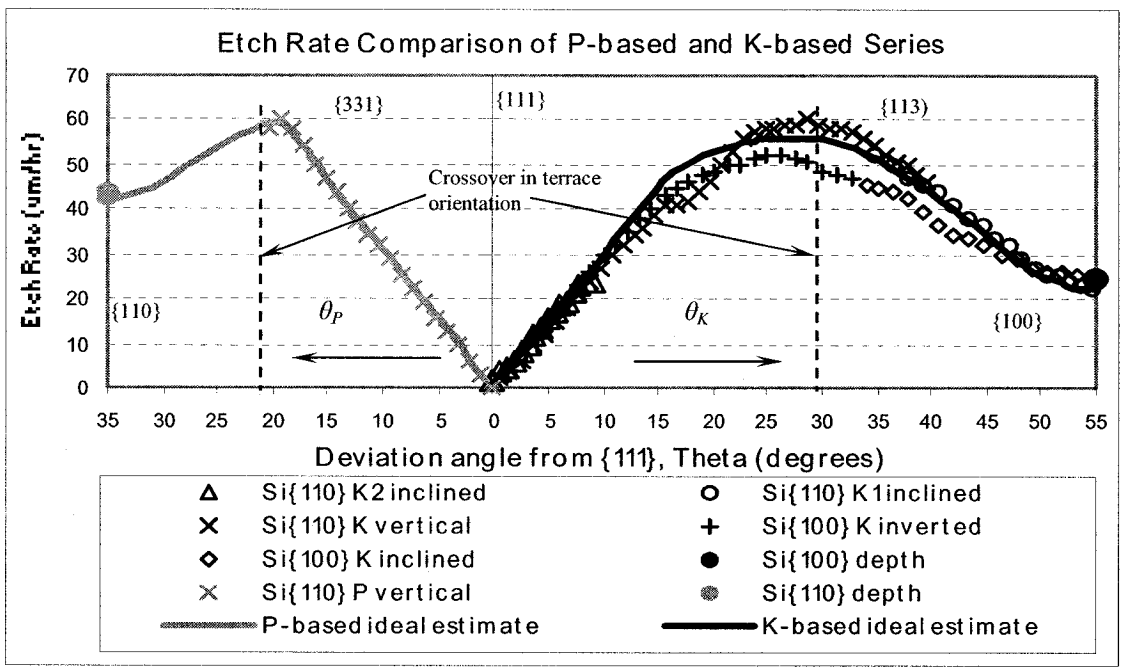

Figure 3-12: Experimental results and analysis of Si{110} 25wt% TMAH : P-based and K-based series comparison, [34].

Figure 3-12 shows canonical curves, [34], from experimental etches in TMAH 25wt.%, where the silicon etch rate is plotted as a function of θ_P and θ_K. These results are based on the experimental work executed previously in the same laboratory where oxide-covered

{100} and {110} silicon samples, wagon-wheel patterned, were etched in 25wt.% TMAH, heavily stirred with a constant temperature of 80°C, [9]. This wagon-wheel experiment, [11], aims to analyze the under-etch behaviour of concave structures, specifically the profiles of the sidewalls of the etched spokes. Detailed investigation of the morphology, inclination angles, and roughness patterns of the cavity sidewall facets identified all planes appearing on the sidewalls of spokes from the wagon-wheel experiment and grouped them into two families of planes: K-based (located between (100) and (111) surfaces in the crystal structure) and P-based (located between (111) and (110) surfaces). Etching time and measured parameters, such as inclination angles of the exposed sidewall facets, as well as their size, allowed accurate determination of the etch rates of all exposed surfaces, summary of which is illustrated in Figure 3-12. Refs [9] and [34] discussed the findings that the same crystallographic features were found to etch at different rates (e.g. for θ_K between 15° and 45°), and hypothesized that these differences were due to facet boundary effects. Obviously the {111} plane is the slowest etching, but two other local minima are present at {100} and {110}.

In this work, the theoretical terrace widths are calculated and analyzed for planes hypothetically having {111}-, {100}-, and {110}-terraces, [41]. The analyses are done as a function of deviation angle away from the {111}, {100} and {110} planes, which are treated as being hypothetically flat for the purposes of this analysis.

Step height for {111} oriented terraces: $h_{(111)} = \frac{5.43\sqrt{3}}{3} = 3.135\,\text{Å}$ and the terrace width can be determined as: $w_{\{111\}} = \frac{h_{\{111\}}}{\tan\theta}$.

Similarly, for {100} oriented terraces $h_{(100)} = \frac{5.43}{2} = 2.715\,\text{Å}$ and $w_{\{100\}} = \frac{h_{\{100\}}}{\tan\nu}$.

And for {110} oriented terraces: $h_{(110)} = \frac{5.43 \cdot \sqrt{2}}{4} = 1.92\,\text{Å}$ and $w_{\{110\}} = \frac{h_{\{110\}}}{\tan\xi}$.

Where θ, ν, and ξ are the angles between the plane in question and {111}, {100} or {110} oriented terrace, respectively, and 5.43 Å is the lattice constant.

From such calculations, the theoretical terrace widths can be compared at each deviation angle, in Figure 3-13. Note that the terrace widths would be infinite at ideally-flat {110}, {111} and {100} planes, and as such these are not shown explicitly in the figure.

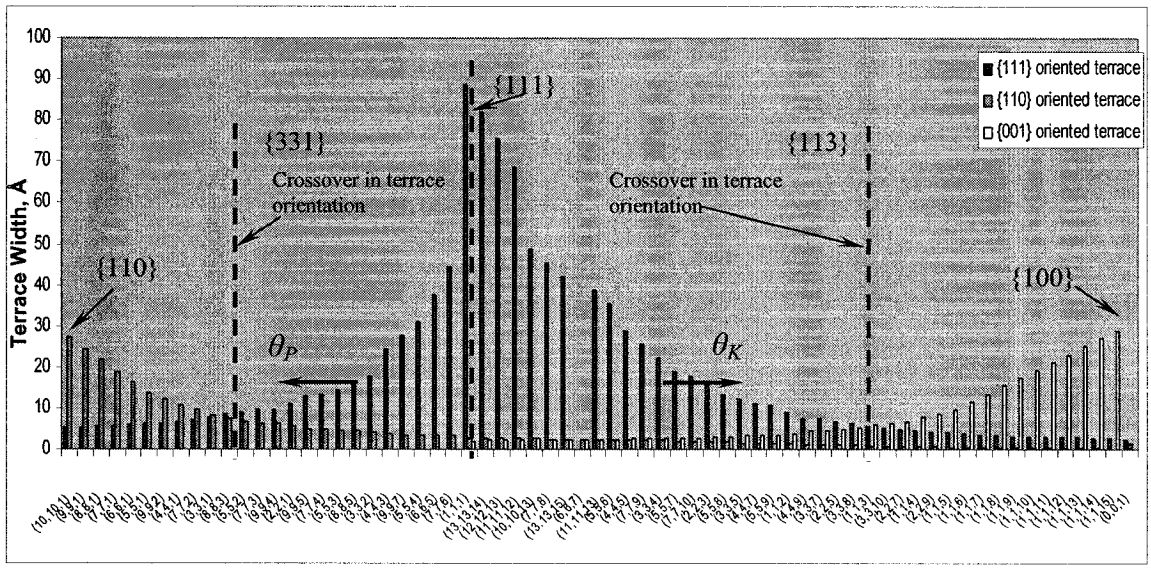

Figure 3-13: Relative terrace width variation for different terrace orientations.

As Figure 3-13 shows, the terrace widths decrease from the respective flat planes, leading to crossovers in the theoretical terrace widths, very close to {331} (for P-based planes, θ_P = 21.62°, about 14° rotated from the {110} plane, and the exact Miller Indices would be {2.913 2.913 1}), and very close to {113} (for K-based planes θ_K = 29.05°, about 26° rotated from the {100} plane, and the exact Miller Indices would be {1 1 2.940}). At the

crossovers, the theoretical terrace width for K-based planes is 6.5Å, and for P-based planes is 8.57Å.

The calculated crossovers in terrace widths occur close to the local maxima in etch rates of P-based and K-based planes seen in Figure 3-12. Between {111} and {331}, the etch rate increases rapidly, as one would expect for a step-based model based on (111) terraces, increasing monotonically as a function of deviation angle, θ_P. Between {331} and {110}, as theta increases the etch rate decreases, which would be consistent with step movement being based on {110} planes instead of {111}. For K-based planes, the etch rate increases rapidly between {111} and {113}, again as one would expect for a step-based model based on {111} terraces, increasing monotonically as a function of θ_K. For θ_K greater than this, (closer to {100}), the etch rate may be consistent with a step-based model based on {100} planes, consistent with Ref [12]. At the crossovers, the etched surface is expected to be rough, with both types of terraces, and the etch rates are expected to be elevated or maximal.

3.6.1. Under-etch Experiments on Si{100}

The above approach was used to analyze the step spacing of the facets on sidewalls of spokes found in wagon-wheel under-etch experiments, as a function of mask-edge deviation angle. When the crossover rotation angles (θ_P and θ_K) are transformed into the {100} coordinate system, they both fall at approximately $\delta \approx 19^\circ$ deviated from the intersection of the {111} plane with the {100} wafer surface (about 26 degrees deviated from intersections with the wafer surface of under-etched {100} plane and {110} plane). Figure 3-14 shows these locations overlaid on the summary of facets found in under-etch experiments on Si{100} in 25wt% TMAH at 80°C. This deviation angle corresponds to a

zone of 3-faceted under-etched surfaces. For P-based facets this crossover is theoretically at $\delta = 18.945°$, while for K-based facets theoretically it is at $\delta = 18.784°$. It is remarkable that the crossovers in both P- based and K-based facets occur close to the same deviation angle in the {100} under-etch experiment (note that this is not the case for {110} under-etch experiments – see below).

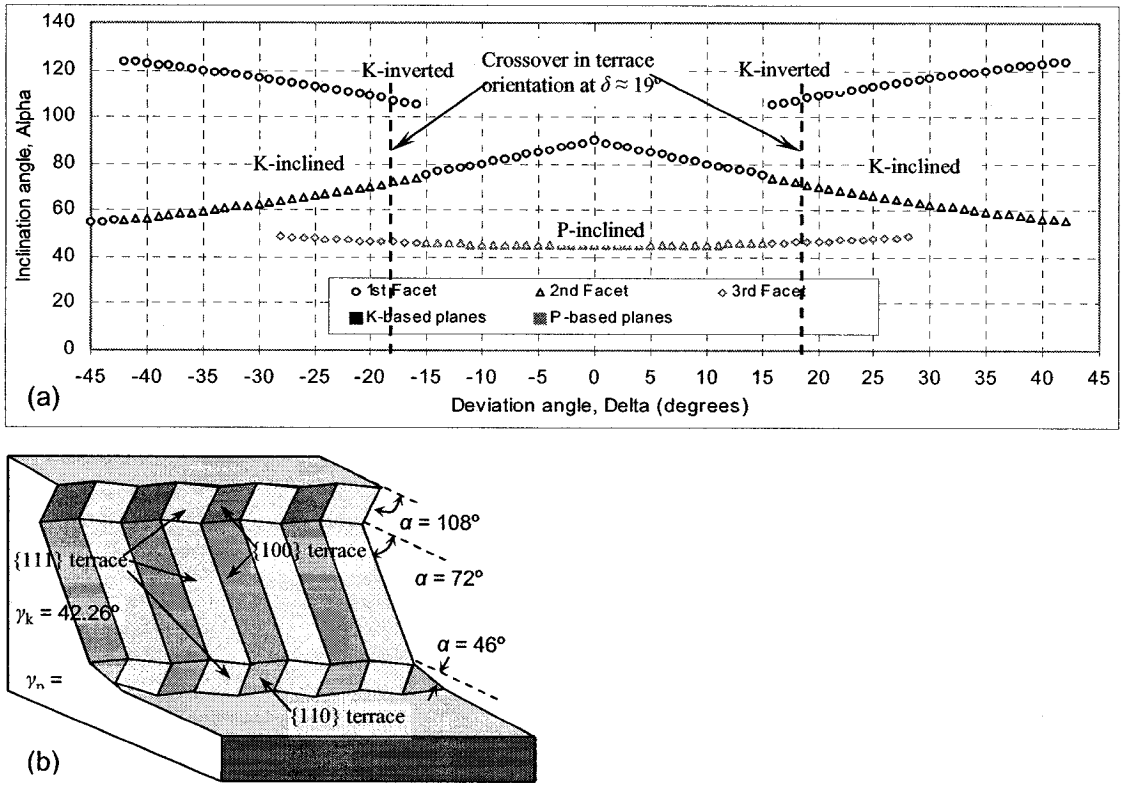

Figure 3-14: (a) Summary of the experimental data representing relative position of the inclination angles of the facets on the side-walls of a spoke with respect to the deviation angle on Si{100} etched in 25% TMAH with the indication of the crossover in the terrace orientation, (Figure from [9]), and (b) schematic representation of the step-based etching surfaces at deviation angle $\delta \approx 19°$ indicated in (a).

At $\delta \approx 19°$, in the ideal very close to both crossovers, the step edges may be continuous (see Figure 3-14(b)) from the upper silicon surface to the bottom of the cavity, beginning with 6.5 Å -wide terraces of both {111} and {100} on the uppermost inverted K-based plane having inclination angle ≈108°, crossing the facet boundary to the K-based plane having inclination angle ≈72°, and the same ideal terrace widths, further crossing the next

facet boundary to the P-based plane having inclination angle ≈46°, where the ideal terrace widths switch to 8.57 Å, for both {111} and {110} terraces.

Figure 3-15 shows a SEM of an under-etched sidewall at $\delta \approx 20°$, roughly corresponding to the crossovers. A very small K-inverted facet is visible at the top, and an even smaller P-inclined facet is visible at the bottom. The large K-inclined facet in between has evident striations aligned parallel to the ideal crystallographic steps depicted in Figure 3-14(b).

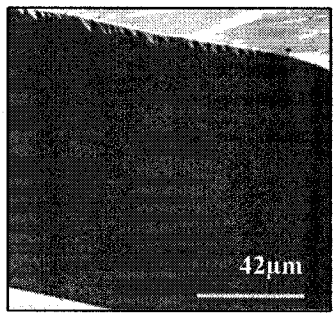

Figure 3-15: SEM of sidewall of a spoke on Si{100} wafer etched in 25% TMAH at $\delta \approx 20°$, 5 hours etching time.

3.6.2. Under-etch Experiments on Si{110}

The same approach was used to analyze the case of Si{110} wafers etched in 25wt% TMAH. However, since the situation is more complex in the Si{110} system, Figure 3-16 summarizes all of the theoretically-available terrace-width crossovers on each of the available facets that could appear in an under-etch experiment. Real under-etch experiments will feature only a subset of the available facets, and therefore only a subset of the available crossovers.

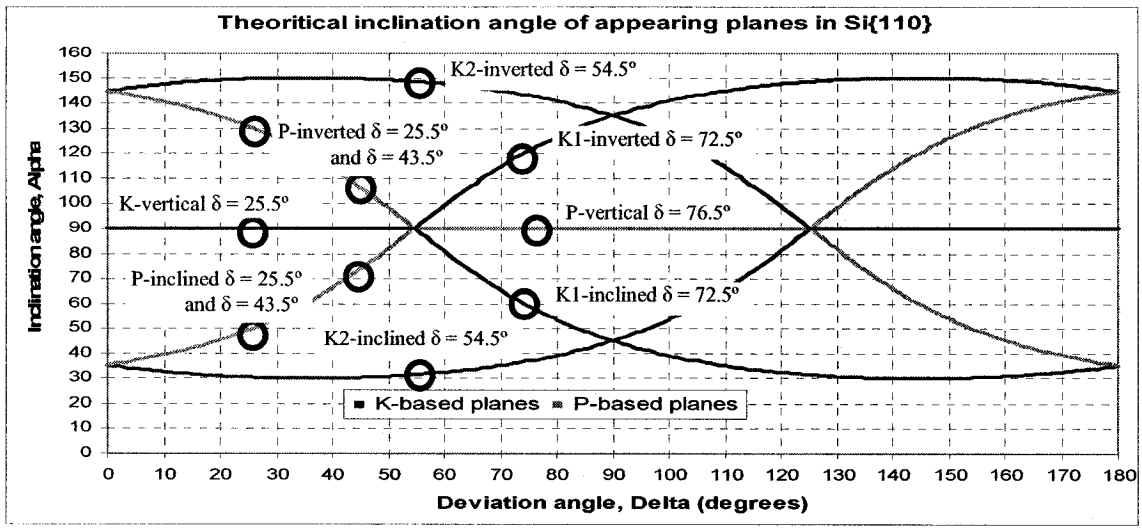

Figure 3-16: Theoretical inclination angle of planes that may appear on the sidewalls of spokes in the under-etch wagon-wheel experiment.

Figure 3-17 shows the real under-etch data for Si{110} etched in 25wt% TMAH. The crossover on K-vertical is present at $\delta \approx 25°$ (to be exact $\delta = 25.6875°$).

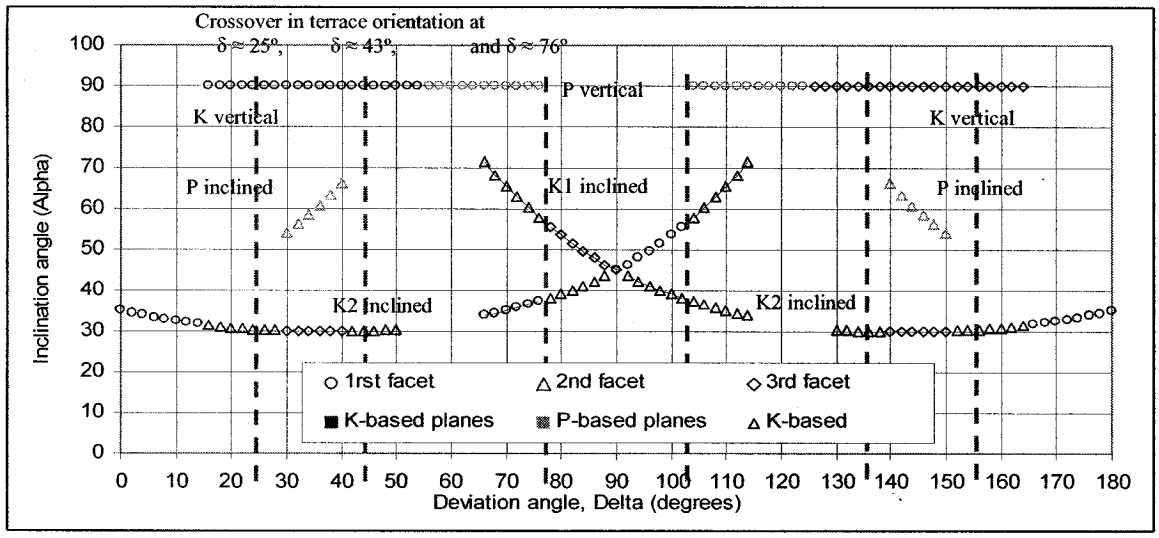

Figure 3-17: Summary of the experimental data representing relative position of the inclination angles of the facets on the side-walls of a spoke with respect to the deviation angle on Si{110} etched in 25% TMAH with the indication of the crossover in the terrace orientation, (Figure from [9]).

Other crossovers on P-inclined at $\delta \approx 43°$ ($\delta = 43.522°$), and on P-vertical at $\delta \approx 76°$, ($\delta = 76.357°$) are also potentially relevant and are examined below.

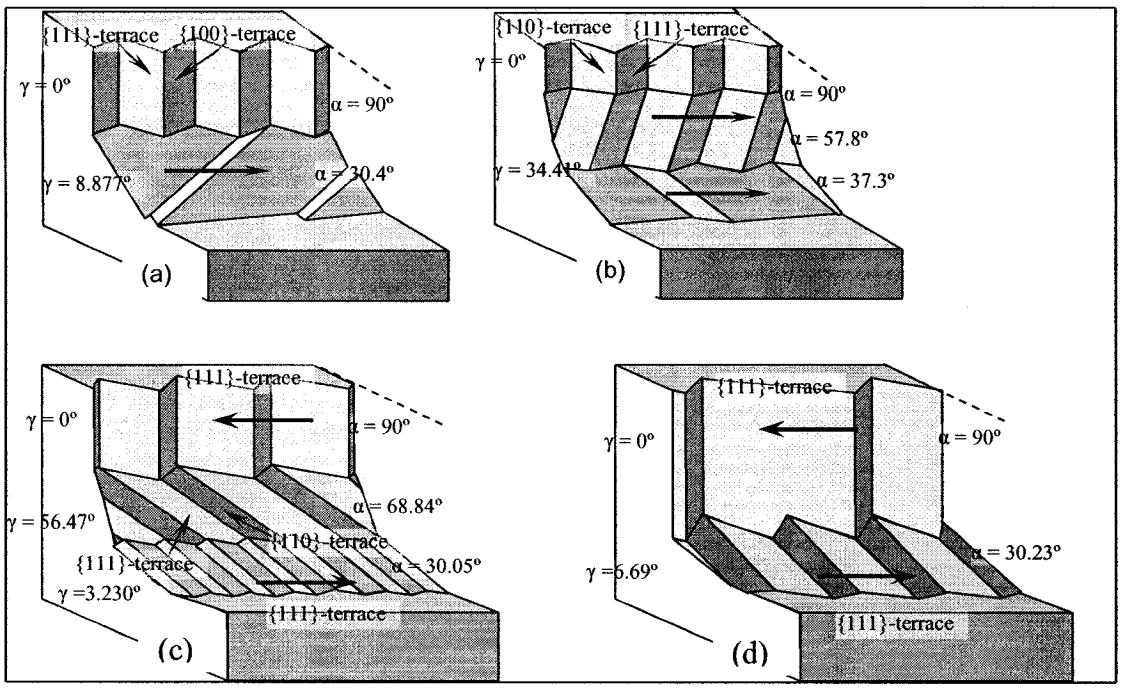

Figure 3-18: Schematic representation of the step-based etching surfaces showing relative movement of steps based on {111} oriented terraces at (a) $\delta \approx 25°$, (b) $\delta \approx 76°$, (c) $30° < \delta < 43°$, and (d) $\delta \geq 43°$ ($\delta = 43°$)

Figure 3-18 shows schematic representations of the step-based etching surfaces showing relative movement of steps, where appropriate. Unlike in the experiment on Si{100}, the deviation angles at which the crossovers occur are not located at the same point. In two out of three cases the crossover planes appear as a topmost facet.

3.6.2.1. Deviation angle $\delta \approx 25°$ (Figure 3-18a):

Two facets are present on the sidewall of a spoke: K-vertical - crossover plane, and K2-inclined - {111}-oriented terrace.

At $\delta \approx 25°$, the terrace edges on the lower, K-based, facet have a two-to-one correspondence with the terrace edges on the upper (crossover) facet.

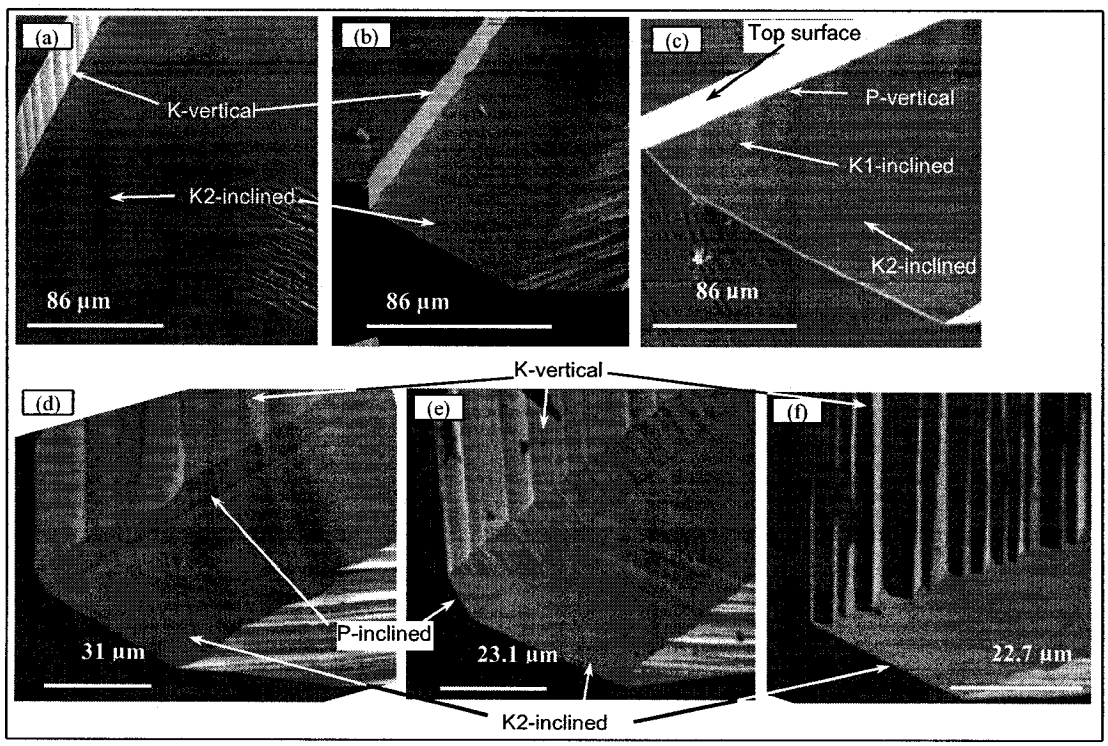

Figure 3-19: SEM of sidewalls of spokes in wagon-wheel under-etch experiment etched in 25% TMAH at (a) $\delta \approx 23.5°$, etching time 1h 30 min, (b) $\delta \approx 23.8°$, etching time 3 hours, (c) $\delta \approx 75.8°$, etching time 3 hours, (d) $\delta \approx 38.8°$, etching time 1h 30 min, (e) $\delta \approx 39.8°$, etching time 1h 30 min, (f) $\delta \approx 43°$, etching time 1h 30 min.

Figure 3-19 (a,b) shows the etched surfaces at $\delta \approx 24°$ (near 25°). The top-most (K-vertical) facet has significant undulation (roughness).

3.6.2.2. Deviation angle at or near $\delta \approx 43°$:

The experimental data in Figure 3-17 shows a transition from three sidewall facets to two sidewall facets.

- For $30° < \delta < 43°$ there are three facets: K-vertical - {111}-oriented terrace, a P-inclined crossover plane, and a K2-inclined {111}-oriented terrace.
- For $\delta \geq 43°$ there are two facets: K-vertical - {111}-oriented terrace, and a K2-inclined {111}-oriented terrace (*there is no crossover plane present*).

The step-spacing correspondence also may be separated into two areas:

- for $30° < \delta < 43°$, with three facets present, the step correspondence at $\delta = 42°$, for example, is 1.32 : 1 between P-inclined and K-vertical facets, and around 1:2.33 between P-inclined and K2-inclined, see Figure 3-18(c).
- for $\delta \geq 43°$, with only two facets present, the step correspondence at $\delta = 43°$, for example, is approximately 1:2 between K-vertical and K2-inclined, (1 : 1.94), see Figure 3-18(d).

Figure 3-19(d) and Figure 3-19 (e), showing spokes at δ = 39-40° and δ = 41-42° respectively, (the under-etched surfaces on opposite sides of a spoke are deviated by 1°), show the presence of the P-inclined facet, followed by its abrupt disappearance for $\delta \geq$ 43° (Figure 3-19 (f)). Figure 3-19 (g) demonstrates the abrupt disappearance, between the right side of the spoke at δ = 41-42° and the left side of the spoke at δ = 43-44°.

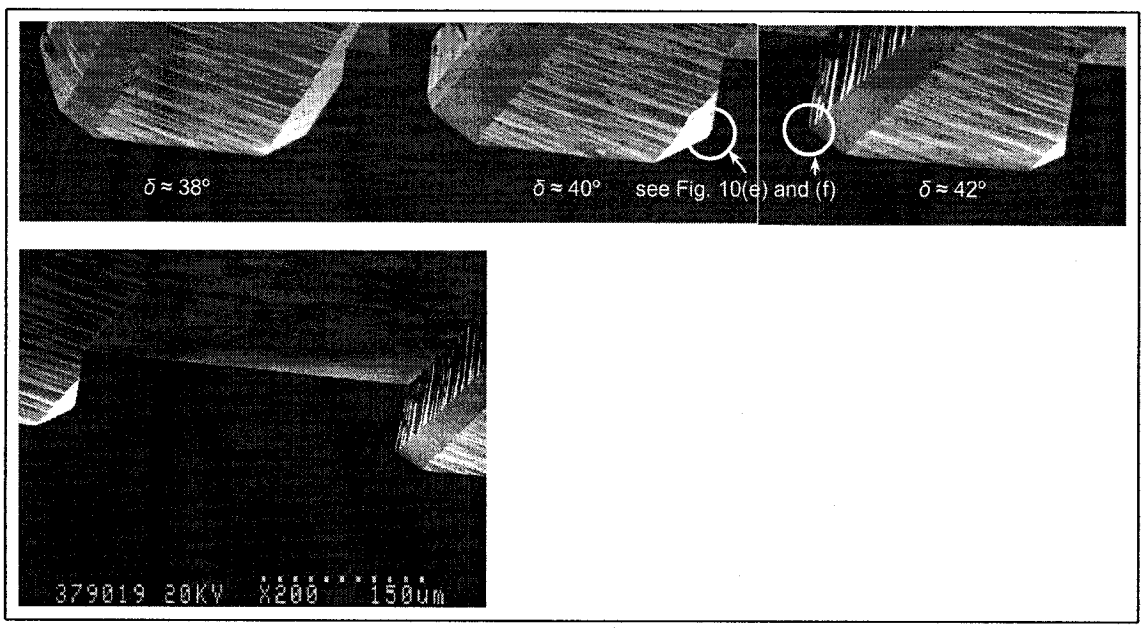

Figure 3-20: SEM of a panoramic view of spokes in wagon-wheel under-etch experiment etched for 1h 30 min in 25% TMAH in vicinity of $\delta \approx 43°$.

This case is also demonstrated in a panoramic view of the cross-section of Si{110} sample in vicinity of $\delta \approx 43°$, see Figure 3-20.

Note that the micrographs of the P-based inclined facet in the vicinity of the deviation angle $\delta \approx 43°$ show silicon surfaces after an etching time of 1 hour 30 minutes. As it was shown in previous works [9], the etch rates and facets exposed in the wagon-wheel under-etch experiment vary with time. The exact deviation angle at which the P-inclined facet disappears was found to vary slightly (± 2°).

The P-inclined facet with the crossover in the terrace orientation at $\delta \approx 43°$ appears as a second facet. In the under-etch curve of Figure 3-21 it can be seen that it may correspond to more-complex behaviour in the under-etch rate. This crossover facet may influence the etch rates of adjacent facets through effects operating at the boundaries with adjacent facets.

3.6.2.3. Deviation angle at or near $\delta \approx 76°$:

The experimental data in Figure 3-17 also shows a transition from three sidewall facets to two sidewall facets.

- For $65° < \delta < 76°$ there are three facets: P-vertical crossover plane, K1-inclined {100}-oriented terrace, and K2-inclined {100}-oriented terrace.
- For $\delta \geq 76°$ there are two facets: K1-inclined {100}-oriented terrace, and a K2-inclined {111}-oriented terrace (*there is no crossover plane present*).

At $\delta \approx 76°$, the P-vertical and adjacent to it K1-inclined facet have a correspondence of (1 : 1.19) between the terrace edges Figure 3-19(c) shows the etched surfaces at $\delta = 75.8°$ (near 76°). The top-most (P-vertical) facet is very small, as indicated in the figure.

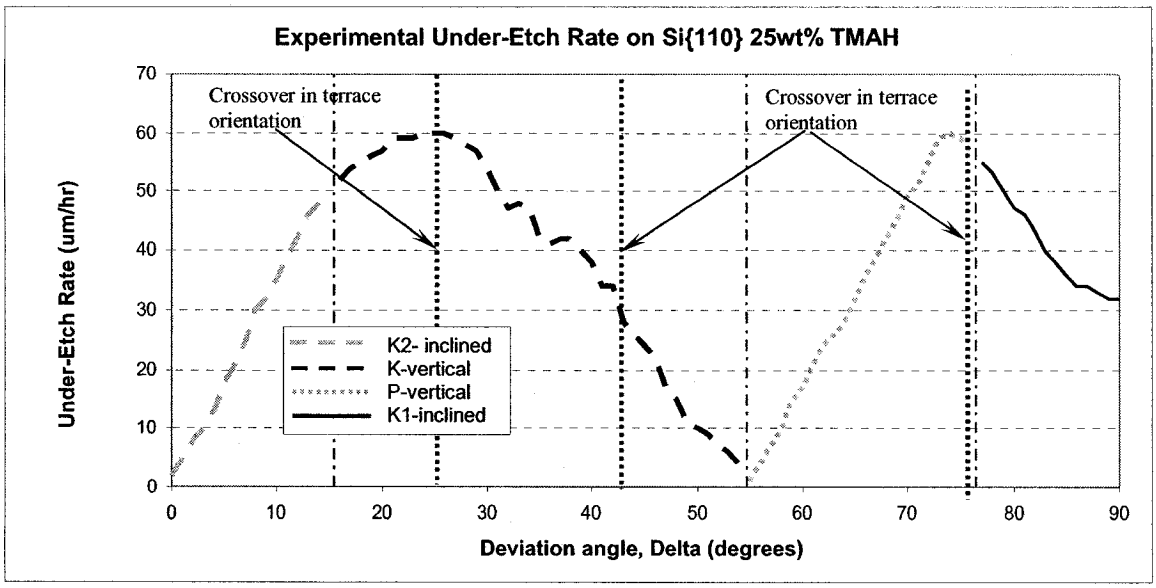

Figure 3-21: Experimental Under-Etch data with respect to deviation angle in the wagon wheel under-etch experiment on Si{110} etched in 25wt.% TMAH, Figure from [9].

Figure 3-21 compares these crossover planes with the under-etch rates. The crossovers in the upper facets correspond roughly to etch rate maxima, for the K-vertical facet at $\delta \approx 25°$, plane with etch rate $\approx$ 60 μm/h, and for the P-vertical facet at $\delta \approx 76°$, plane with the etch rate $\approx$ 57μm/h.

Looking again at the theoretically available crossovers in Figure 3-16, and comparing globally to the actual under-etch data in Figure 3-17; it is possible that the crossovers significantly influence the presence or absence of certain facets. Notably:

- the presence of the P-inclined facet only between its two crossovers at $\delta \approx 25°$, and $\delta \approx 43°$.
- the presence of the P-vertical facet only at deviation angles below its crossover at $\delta < 76°$.

Further work is in progress to explore and analyze the correspondence of experiment with theory, and the potential impact of such crossovers on under-etch experiments.

3.7. Contributions

- This chapter expands the general analysis of two families of planes that were typically observed in the under-etch wagon-wheel experiment. As an important parameter fundamental to subsequent discussions, step spacings on P- and K-based planes were calculated. The basis for these calculations was a traditional Step-Based Model of P- and K-based planes with terraces composed of {111}-oriented surfaces. However, this model was extended to include planes in the vicinity of two basic orientations, {100} and {110}, as being composed of steps and terraces of {100} and {110} orientation, respectively.
- The concept of "cross-over" in terrace orientation for planes rotated from {111} towards {100} or {110} oriented surfaces was introduced and analyzed.
- The notion of a crossover deviation angle at which the width of {111} terrace is equal to the width of {100}- of {110}-oriented terraces, and the determination that this crossover occurs at $\delta \approx 19^{\circ}$ for both families of planes on Si{100}, where the under-etched facets are observed to be composed of 3 facets, and there is the potential for quasi continuous terrace edges across all three facets.
- Si{110} wafers provide larger variety of facets on sidewalls of spokes and, consequently the crossover in terrace orientation can be listed for the respective facets as follows, see Figure 3-16:

  - K2-inclined, K2-inverted — $\delta \approx 54.5^{\circ}$
  - K1-inclined, K1-inverted — $\delta \approx 72.5^{\circ}$
  - K-vertical — $\delta \approx 25.5^{\circ}$
  - P-vertical — $\delta \approx 76.5^{\circ}$

- P-inclined, P-inverted - $\delta \approx 25.5°$ and $\delta \approx 43.5°$

- K2-inclined, K2-inverted - $\delta \approx 25°$

- When the top-most facet in a wagon-wheel under-etch experiment is a crossover facet, this often corresponds to a local or global maximum in under-etch rate, for both Si{100} (at $\delta \approx 19°$) and Si{110} under-etch experiments, (at $\delta \approx 25°$ and $\delta \approx 76°$).
- Crossovers may significantly influence the complexity of etch rate variation and facet appearance or disappearance in an under-etch experiment

4. Removal Frequency and the Etch Rate

4.1. Background Information

Detailed analysis of step-based surface geometry attempted, in the previous chapter, provided an overview of these surfaces. However, this work predominantly concentrates on the wet-chemical anisotropic etching and, consequently, etch rates of these surfaces. A perfect match of inclination angles of the under-etched plane to the values on the theoretical curve points to the fundamental connection of frequency of removal of chains/rows on the step-based surface to their respective etch rates, [32]. Hence, there is a clear relation between the geometry of a step-based surface and its etch rate via chain/row removal frequency (FR). The frequency of removal corresponds to how many K-rows or Periodic Bond Chains (PBC-s) have to be removed from the edge of the step per unit time in order for the plane to advance according to the etch rate data (Figure 4-1).

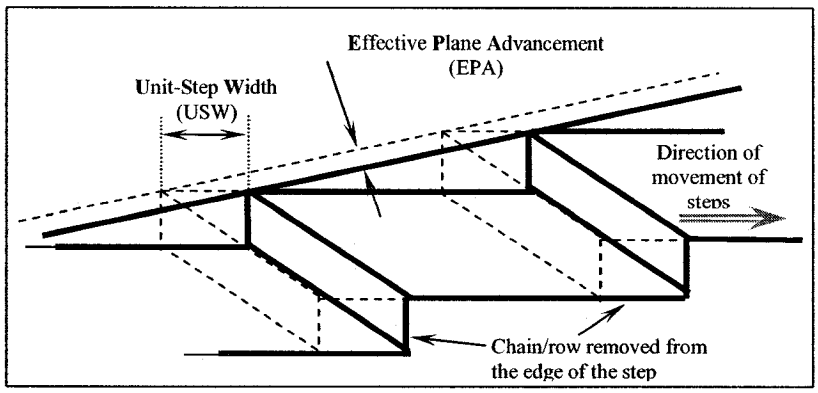

Figure 4-1: Schematic representation of the plane advancement due to the removal of chain/rows from edges of steps in the step-based plane model.

4.2. Introduction

In order to facilitate removal frequency calculations the further parameter needs to be defined – Effective Plane Advancement, (EPA). EPA identifies how far a plane will advance in the direction perpendicular to its surface if one chain/row is removed

simultaneously from the each step-edge of this plane, Figure 4-1. That is, if every step-edge (SE) will move a distance referred to as Unit-Step Width (USW), (Figure 4-1).

These two parameters (EPA and USW) vary depending on the basic definition of the terrace orientation of each plane, i.e. whether a terrace is {111}-, {110}- or {100}-oriented, as it was discussed in the previous chapter.

For instance, in the vicinity of a {111} plane, terraces are considered to be {111}-oriented and the Effective Plane Advancement may be determined as follows, (Figure 4-2):

$$EPA_{\{111\}}(\theta) = USW_{\{111\}} \cdot \sin\theta \tag{4.1}$$

where $USW_{\{111\}}$ is a unit step width, representing how far the edge of the step will advance on {111}-oriented terrace if one chain/row is removed, and it equals to:

$$USW_{\{111\}} = \frac{5.43}{2 \cdot \sin(54.74^\circ)} \cong 3.325\,\text{Å} \tag{4.2}$$

θ is the angle of the plane with respect to {111}-oriented terrace.

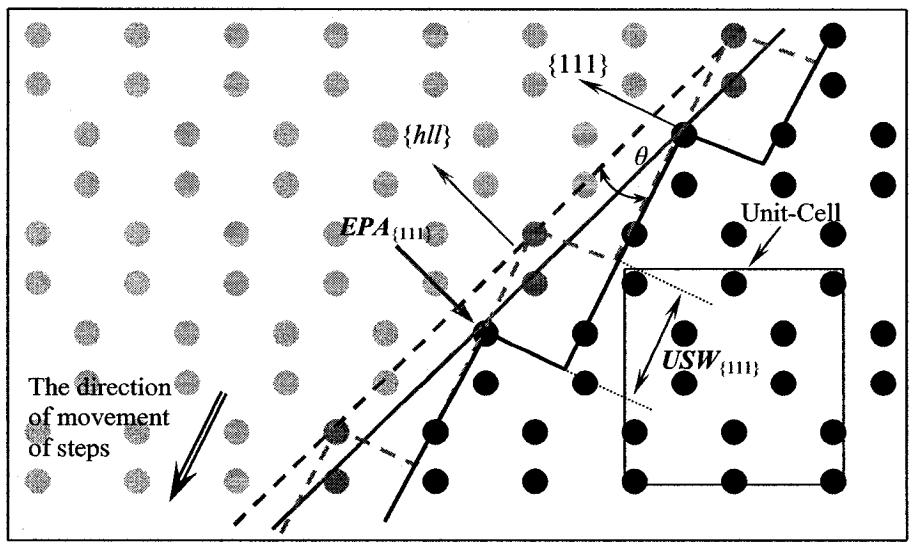

Figure 4-2: Effective plane advancement of K-based plane with {111}-oriented terraces when all the step-edges move simultaneously by one USW in the direction of movement of steps.

Etch rates of facets appearing in wagon-wheel under-etch experiment were measured. The results summarised in graphs, see Figure 4-3.

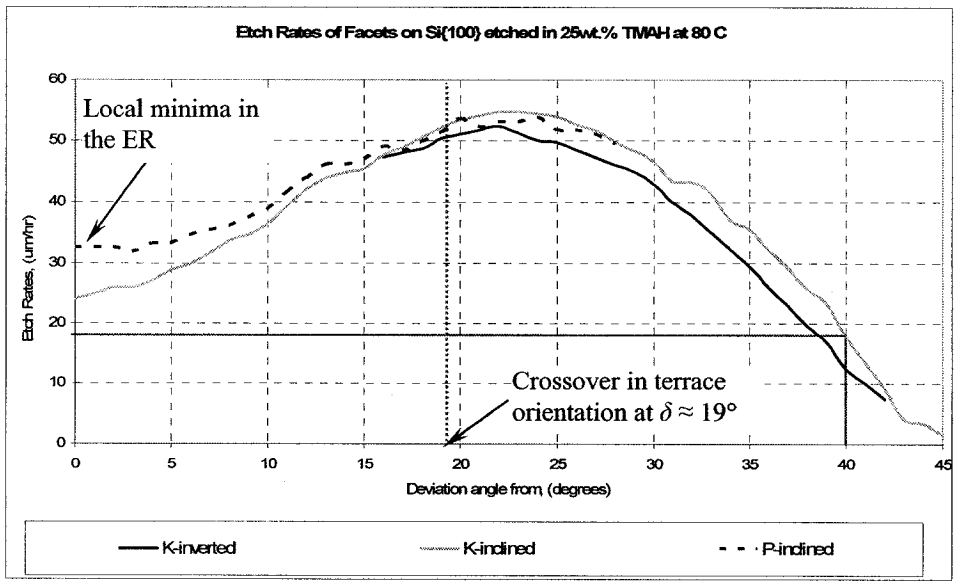

Figure 4-3: Etch rates of facets on sidewalls of spokes experimentally determined from Si{100} sample etched in 25% TMAH at 80°C.

The connection of EPA to the etch rate of a plane can be seen in the Example 4-1:

Example 4-1: In wagon-wheel under-etch experiment on Si{100} etched in 25wt.% TMAH, K-based inclined facet appears on the sidewall of a spoke at $\delta = 40°$. Inclination angle of this K-inclined facet, $\alpha \approx 56.7°$, MI - (1,19,1), angle with {111}-oriented terrace $\theta = 4.86°$. And its EPA = 0.281Å.

The etch rate, ER, of this facet obtained from the experimental data is 17.89 μm/h (Figure 4-3). In order to sustain this etch rate, $\cong 6.3 \times 10^5$ of K-rows per hour would have to be removed simultaneously from the step-edges of this plane, (Figure 4-4).

The value from the Example 4-1, expressed in K-rows per hour, is in fact the equivalent frequency of removal of K-rows from each step-edge. The general expression for removal frequency (FR) of chains/rows may be presented as follows:

$$removal\ \ frequency, FR(\theta) = \frac{ER(\theta)}{EPA(\theta)}, \tag{4.3}$$

where $ER(\theta)$ stands for the etch rate of the plane, and

EPA (θ) – the effective plane advancement.

Calculations of removal frequency for both families of planes with {111}-oriented terraces were completed. The results based on the experimental data for Si{100} etched in 25wt.% TMAH are summarized in Figure 4-4.

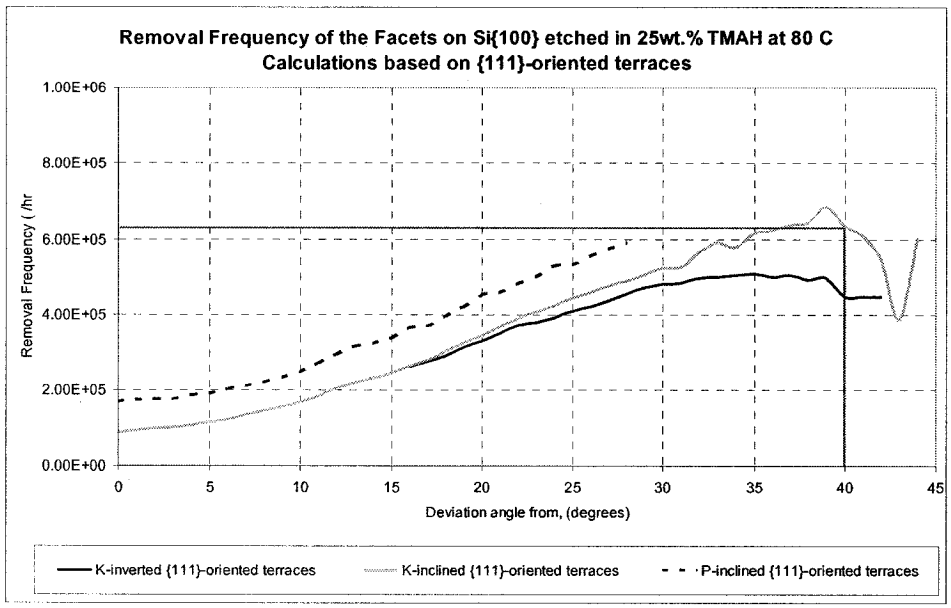

Figure 4-4: Graphic representation of summarized calculations for Removal Frequencies of all planes detected on sidewalls of spokes in the wagon-wheel under-etch experiment on Si{100} etched in 25wt.% TMAH for {111}-oriented terraces.

However, according to the analysis of step based planes discussed earlier, (see Chapter 3), planes in the vicinity of {100} and {110} basic orientations should have {100}- and {110}-oriented terraces respectively.

Thus, respective calculations were done (below) for surfaces with {100}- and {110}-oriented terraces.

4.3. Frequency of Removal of Chain/Row from the Step Edge for the Data from Canonical Curves

To generalise these calculations, Etch Rate data from canonical curves is used. Figure 4-5 illustrates the experimental data from wagon-wheel under-etch experiment summarised in

the form of canonical curves, i.e. in the form of etch rates of surfaces rotated from basic {111} oriented plane. Crossovers in terrace orientation are indicated for P-based at θ_P = 21.62°, and for K-based planes θ_K = 29.05°.

The frequency of removal of chain/row from the step edge was determined with the consideration of this crossover. In other words, planes rotated from the {110} up to approximately 14° were treated as surfaces with {110}-oriented terraces and PBC-s at the step-edges, and planes rotated from the {100} plane up to approximately 26° - as surfaces with {100}-oriented terraces and K-rows at the step-edges[14].

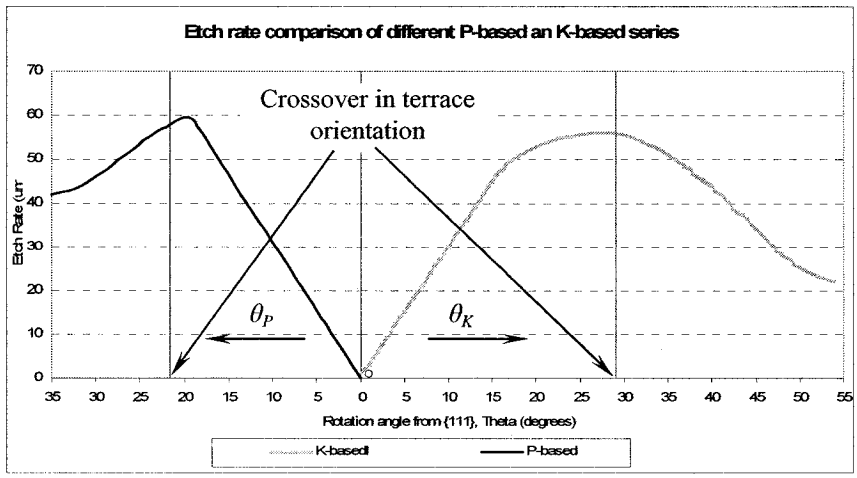

Figure 4-5: Experimental etch rate data presented in a form of canonical curves, i.e. in form of etch rates of surfaces rotated from {111} plane.

Respective Unit-Step Widths were determined[15] as well as Effective Plane Advancement, specific for the surfaces with {100}- and {110}-oriented terraces. Based on this information, direct calculations for the frequency of removal of chain/row from the step edges were conducted with the consideration of different terrace orientation. However, the mathematical calculation showed the physical impossibility of such direct

[14] See Chapter 3 for details.
[15] For detailed calculations see Appendix II

computation as calculated frequencies in the vicinity of basic {100} and {110} surfaces were approaching infinity[16].

The relationship between the etch rate (ER(θ)) and the frequency of removal of chains/rows (FR(θ)) from the step-edges may be expressed as follows:

$$ER(\theta) = FR(\theta) \cdot EPA(\theta), \tag{4.4}$$

And, since the ER of basic {100} and {110} planes is substantially greater that zero, this mathematical model needs to be adjusted.

In order to correct this problem, phenomenon of infinite FR, as we approach basic {110} and {100} planes, the "non-zero" etch rates of these planes need to be taken to consideration.

It is fair to assume that the basic {100} and {110} surfaces may be regarded as locally "flat", [21], and their $EPA_K(54.74°)$ and $EPA_P(35.26°)$, respectively, may be reasoned as an advancement of the plane in the direction perpendicular to its surface if one layer of atoms was simultaneously removed from its surface.

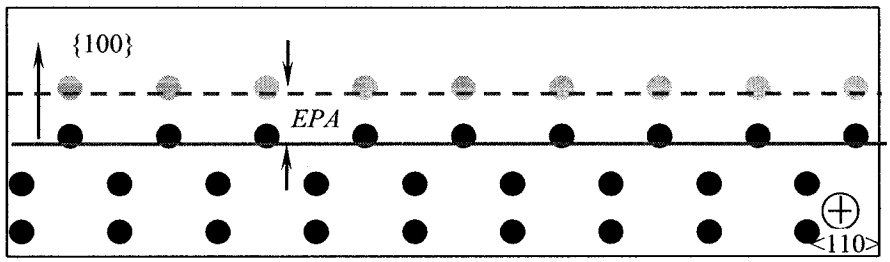

Figure 4-6: Schematic representation of a basic {100} surface.

The $EPA_K(54.74°)$ can be calculated as ¼ of a side of the unit-cell cube[17], (Figure 4-6).

$$EPA_K(54.74°) = \frac{5.43}{4} = 1.3575\,\text{Å} \tag{4.5}$$

[16] Summary of these calculations are illustrated in the Appendix II

[17] Please note that this calculation is different from that of the step height for K-based plane with {100} oriented terraces, see Figure 3-5, where the step height was calculated till the next K-row of the same configuration was present, i.e. equals to the ½ of the lattice constant.

Similarly, for Effective Plane Advancement of a basic {110} plane the following can be worked out – from Figure 4-7 it can be seen that the $EPA_P(35.26°)$ is a ¼ of a side diagonal of a unit-cell cube.

$$EPA_P(35.26°) = \frac{5.43 \cdot \sqrt{2}}{4} = 1.919794911\,\text{Å} \tag{4.6}$$

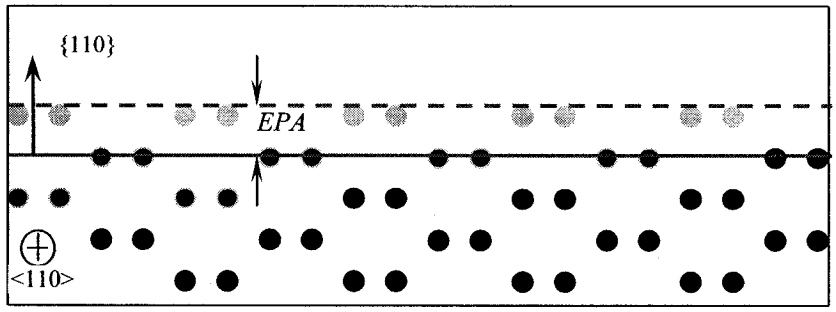

Figure 4-7: Schematic representation of a basic {110} surface.

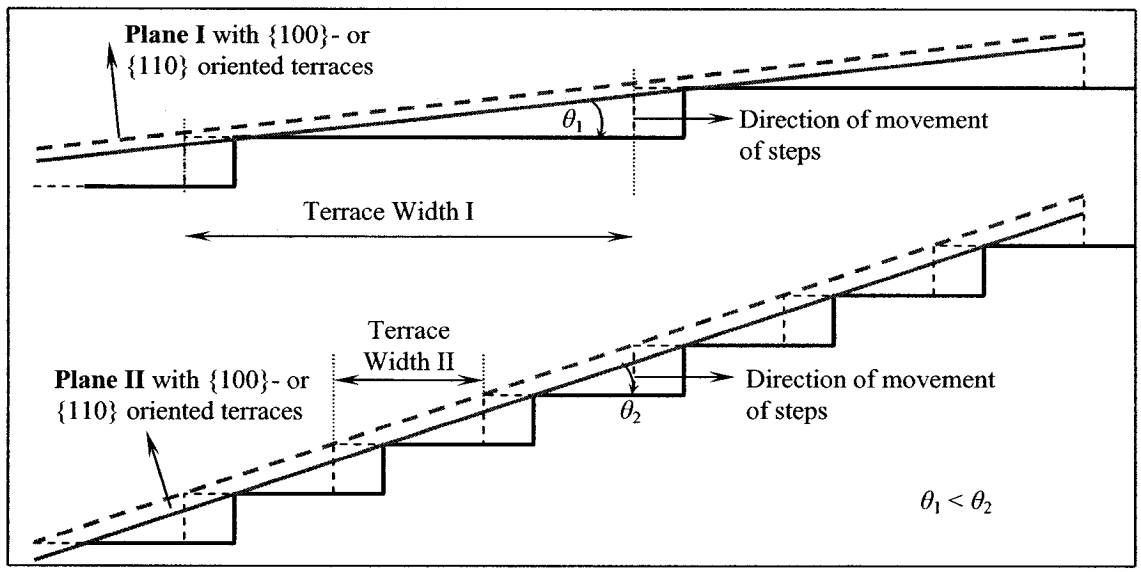

Figure 4-8: Schematic representation of Effective Plane Advancement of two planes with different terrace widths due only to the simultaneous removal of chain/rows from step-edges.

Now, with this as a foundation, one can reconsider the components which contribute to the etch rates in the vicinity of {100} and {110} planes (when the terraces are assumed to be {100} and {110} planes), taking into consideration that the ER of these surfaces is not zero – contrary to the assumption (approximation) which was used for {111}-oriented terraces.

Assuming, for the moment that the etch rate of {100}- and {110}-oriented terraces are "zero" and the only factor that contributes to the EPA is the simultaneous removal of chain/row from each step-edge, see Figure 4-8, showing two examples of θ.

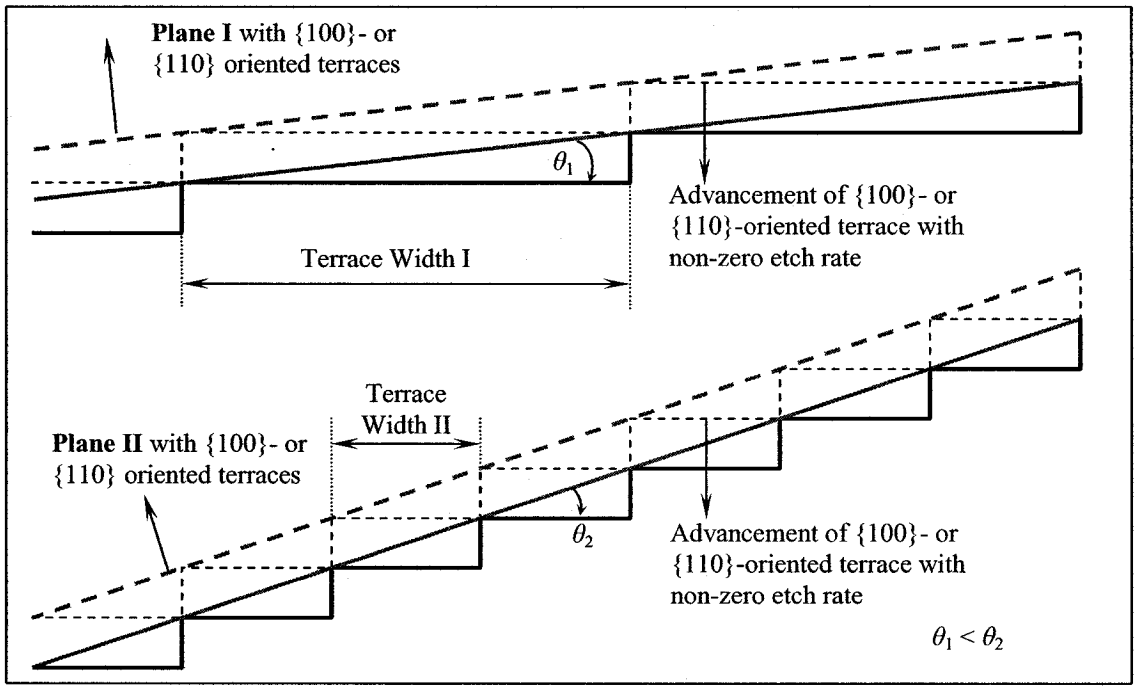

Figure 4-9: Schematic representation of Effective Plane Advancement of two planes with different terrace widths due only to the non-zero etch rate of {100}- or {110}-oriented terrace.

On the other hand, consider the other limiting case when we disregard the effect of removal of chain/row from the step-edges and assign the $EPA(\theta)$ only to the advancement of {100}- and {110}-oriented terraces with non-zero etch rates. Figure 4-9 schematically illustrates two different cases of θ.

For the **plane I** with larger terrace widths, the probability of creation of a defect in the flat plane (i.e. removal of one atom from the surface) is more likely than the probability of creation of a defect on **plane II** which has smaller terrace widths. (See Figure 4-9). The $EPA(\theta)$ due to non-zero etch rate of {100}- and {110}-oriented terraces becomes more dominant when the plane approaches {100} or {110} surface, respectively. Since

the terrace widths are many times smaller near the crossovers, this model hypothesises that the probability of creation of a defect in the terrace becomes insignificant.

With the above assumptions and constraints, the next section studies the separation of $ER(\theta)$ into two components, for surfaces with {100}- and {110}-oriented terraces.

4.4. Separation of Etch Rates of Planes with {100}- and {110}-oriented Terraces into Two Components

While it is not possible to determine, from the etch rates themselves which fractions of the etch rates are due to {100} or {110} plane advancement vs. pure chain/row removal, three different separation strategies are examined:

1. Assume that the influence of non-zero etch rate of {100}- and {110}-oriented terraces decreases linearly and reaches zero at the crossovers, and calculate what must be the chain/row removal frequencies.
2. Assume that the etch rate due to chain/row removal from the step-edges of the planes with {100}- and {110}-oriented terraces is such that it increases linearly to the crossover and calculate what must be the variation with θ of the non-zero etch rate of {100}- and {110}-oriented terraces.
3. Assume that there is a transition zone near the crossover, and that the etch rate due to chain/row removal increases linearly to the edge of that transition zone.

As a basis for these calculations, experimental etch rates summarised in canonical curves are used, (see Figure 4-5).

The canonical etch rate of P-based planes (see left side of Figure 4-5) will be separated into:

- etch rate due to removal of PBC-s from step-edges on {111}-oriented terraces (for $\theta_P < 22^\circ$)
- etch rate due to removal of PBC-s from step-edges on {110}-oriented terraces (for $\theta_P > 22^\circ$)
- etch rate due to etching of the basic {110}-oriented terrace (for $\theta_P > 22^\circ$).

The canonical etch rates of K-based planes (see right side of Figure 4-5) will be separated into:

- etch rate due to removal of K-rows from step-edges on {111}-oriented terraces (for $\theta_K < 29^\circ$)
- etch rate due to removal of K-rows from step-edges on {100}-oriented terraces (for $\theta_K > 29^\circ$)
- etch rate due to etching of the basic {100}-oriented terrace (for $\theta_K > 29^\circ$).

Note, that the etch rate of basic {111}-oriented terraces is considered to be comparatively negligible for this analysis.

4.4.1. Equation of the Line Approximation for the ER component due to "non-zero" Etch Rate of {100}- and {110}-oriented Terraces

As it was illustrated, first strategy is to use a linear approximation of a component based on the influence of "non-zero" ER-s of {100}- and {110}-oriented terraces. In order to derive this equation the following may be considered: for P-based surfaces rotated towards basic {110} plane, the terrace width is increasing eventually becoming {110}-oriented surface with the respective {110} plane etch rate. When P-based surface rotates towards the area of a crossover in terrace orientation, the {110}-oriented terrace width is

going to decrease till its width will approach the width of a P-based plane with {111}-oriented terrace[18]. At this point it is fair to assume that the etch rate of the {110}-oriented terrace is negligible (mathematically expressed as "zero"). With this in mind, the following equations can be generated:

$$ER(\theta_P)_{\substack{due\ to\ "non-zero"\ ER \\ of\ \{110\}-oriented\ terrace}} = 42 - m_{\{110\}}\left(\theta_P + 35.26^\circ\right), \tag{4.7}$$

where 42 μm/hr is the ideal etch rate of {110}-oriented surface located 35.26° from the basic {111} orientation,(Figure 4-5),

$m_{\{110\}}$ – is the slope of straight line determined as: $m_{\{110\}} = \dfrac{ER_1 - ER_2}{\theta_1 - \theta_2} \approx -3.078$

θ_P – is the angle between P-based plane and {111} oriented basic surface.

$$ER(\theta_K)_{\substack{due\ to\ "non-zero"\ ER \\ of\ \{100\}-oriented\ terrace}} = 22.1 + m_{\{100\}}\left(\theta_K - 54.74^\circ\right), \tag{4.8}$$

where 22.1 μm/hr is the ideal etch rate of {100}-oriented surface located 54.74° from the basic {111} orientation, (Figure 4-5),

$m_{\{100\}}$ – is the slope of straight line determined as: $m_{\{100\}} = \dfrac{ER_1 - ER_2}{\theta_1 - \theta_2} \approx 0.86$

θ_K – is the angle between K-based plane and {111} oriented basic surface.

And now, the ER determined by the removal of the chains/rows from the step-edges may be expressed for K-based and P-based surfaces respectively as follows:

$$ER(\theta_P)_{\substack{PBC\ removal \\ on\ P-based\ planes}} = ER(\theta_P)_{CC-P} - ER(\theta_P)_{\substack{due\ to "non-zero"\ ER \\ of\ \{110\}-oriented\ terrace}} \tag{4.9}$$

$$ER(\theta_K)_{\substack{K-row\ removal \\ on\ K-based\ planes}} = ER(\theta_K)_{CC-K} - ER(\theta_K)_{\substack{due\ to "non-zero"\ ER \\ of\ \{100\}-oriented\ terrace}} \tag{4.10}$$

[18] Please see more on the crossover and the terrace widths at the crossover in terrace orientation in Chapter 3.

where $ER(\theta_P)_{CC\text{-}P}$ and $ER(\theta_K)_{CC\text{-}K}$ are the etch rates taken from Canonical Curves of Figure 4-5 for P-based and K-based planes, respectively..

As it can be seen from Figure 4-10 the line approximation gives reasonable values for the etch rate of planes with with {100}- and {110}-oriented terraces compared to {111} terrace orientations. Solid Black and solid Grey lines of Figure 4-10 represent the etch rate component due the "zipping" of PBC-s and K-rows from the step-edges alone, with the assumption of "zero" etch rate of {110}- and {100}-oriented terraces, respectively.

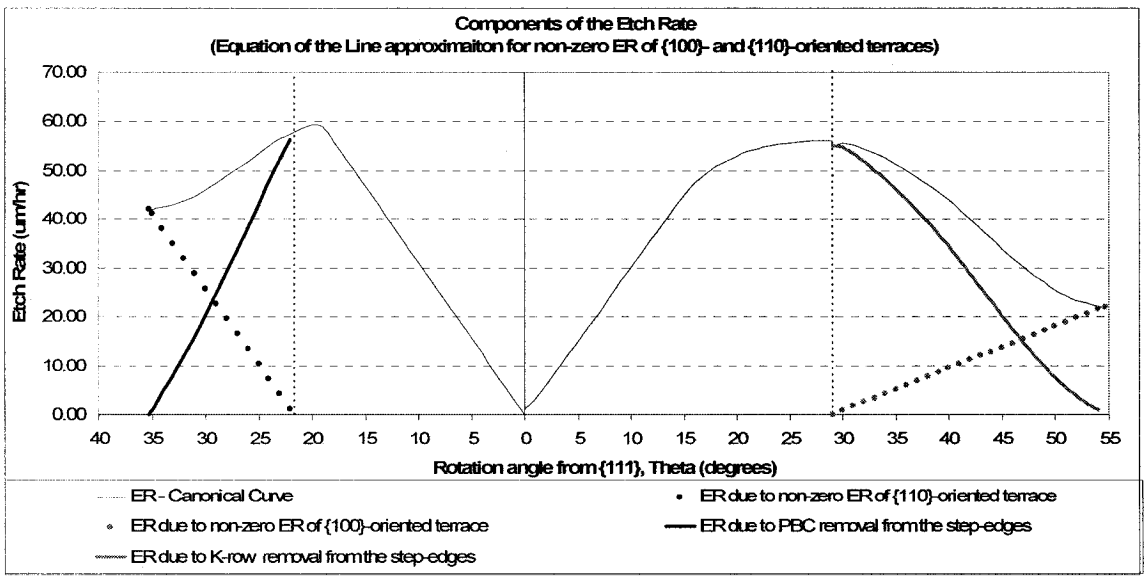

Figure 4-10: The Canonical Curve representing etch rates and their components based on the Equation of the Line for "non-zero" terrace ER

Using the equation (4.3), for the expression of frequency of removal of chains/rows, the FR for two families of planes in vicinity of basic {110} and {100} surfaces can be inferred, see Figure 4-11.

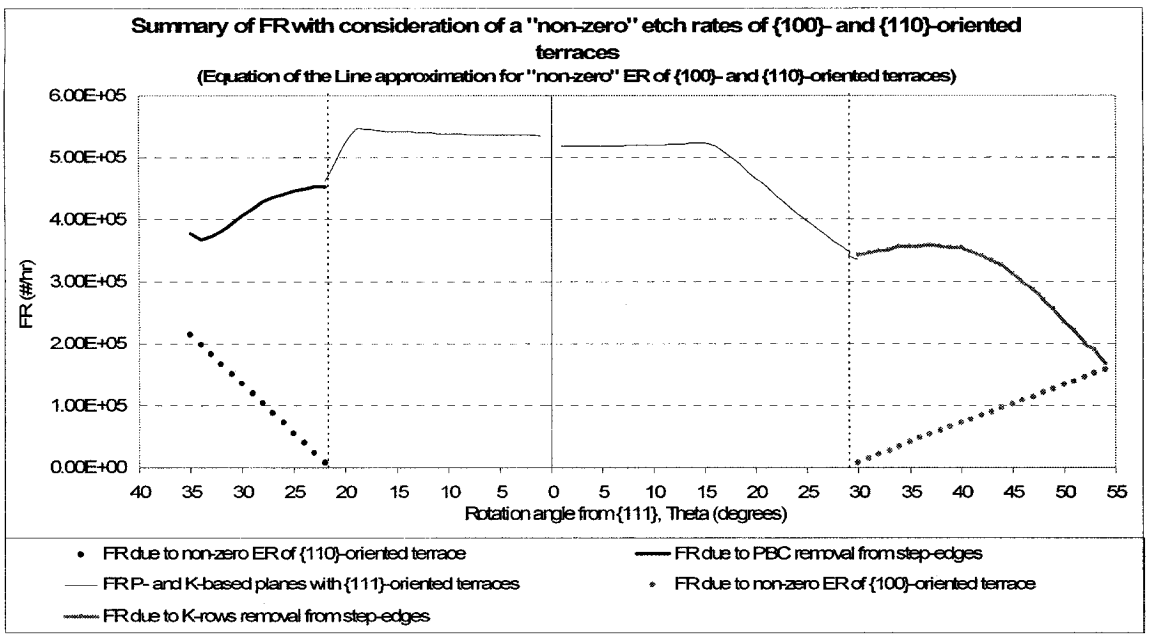

Figure 4-11: Summary of the calculations for the FR of surfaces with {111}-oriented terraces and components of FR on P- and K-based surfaces with {110}- and {100}- oriented terraces based on the Equation of the Line approximation for "non-zero" terrace ER – data from Canonical Curves.

Figure 4-11 summarizes calculations presented by equation (4.3) using earlier determined components from (4.11)-(4.14) for P-and K-based surfaces with {100}-, {110}-, and {111}-oriented terraces[19].

4.4.2. Equation of the Line Approximation for the ER Component Due to Chain/Row Removal from the Step-Edges

What happens if we were to assume similar linear approximation for the component of ER due to the chain/row removal from the Step-Edges (SE)?

It is reasonable to suggest that the chain/row influence is most significant where the number of step-edges per unit area of the surface is the largest, i.e. near the crossover

[19] Note that the FR component due to the "non-zero" ER of {100}- and {110}-oriented terraces has a different EPA term calculated from the removal of one layer of atoms from all terraces of the plane simultaneously, i.e. terrace advancement 1.3575Å and 1.92Å for K- and P-based planes, respectively. This value of EPA can be determined as:

$$EPA(\theta)_{\substack{due\ to\ "non-zero"\ ER \\ of\ \{100\}-\ and\ \{110\}-oriented\ terraces}} = EPA(\theta)_{\{100\}\ or\ \{110\}} \cdot \cos(\theta)$$

with the minimum terrace width $TW_{\min}$. This becomes negligent end eventually disappears as the terrace width approaches its maximum, i.e. at basic {100} and {110} surfaces. The equation of the line can be assembled in following manner:

$$ER(\theta_P)_{\substack{due\ to\ PBC \\ removal\ from\ SE}} = m_{\{110\}}(\theta_P + 35.26^\circ), \tag{4.11}$$

where $m_{\{110\}}$ – is the slope of straight line determined as: $m_{\{110\}} = \dfrac{ER_1 - ER_2}{\theta_1 - \theta_2} \approx 4.23$

35.26° is the location of a basic {110} surface from the {111} orientation where ER component due to the PBC removal from the step-edges is zero, and

θ_P – is the angle between P-based plane and {111} oriented basic surface.

$$ER(\theta_K)_{\substack{due\ to\ K-row \\ removal\ from\ SE}} = m_{\{100\}}(\theta_K - 54.74^\circ), \tag{4.12}$$

where $m_{\{100\}}$ – is the slope of straight line determined as: $m_{\{100\}} = \dfrac{ER_1 - ER_2}{\theta_1 - \theta_2} \approx -2.14$

54.74° is the location of a basic {100} surface from {111} orientation where ER component due to the K-rows removal from the step-edges is zero, and

θ_K – is the angle between P-based plane and {111} oriented surface.

Second component of a general ER, component due to non-zero etch rates of {100}- and {110}-oriented terraces may be written as:

$$ER(\theta_P)_{\substack{due\ to\ "non-zero"\ ER \\ of\ \{110\}-oriented\ terrace}} = ER(\theta_P)_{CC-P} - ER(\theta_P)_{\substack{PBC\ removal\ from\ SE \\ on\ P-based\ planes}} \tag{4.13}$$

$$ER(\theta_P)_{\substack{due\ to\ "non-zero"\ ER \\ of\ \{100\}-oriented\ terrace}} = ER(\theta_P)_{CC-K} - ER(\theta_P)_{\substack{K-row\ removal\ from\ SE \\ on\ K-based\ planes}} \tag{4.14}$$

where $ER(\theta_P)_{CC\text{-}P}$ and $ER(\theta_K)_{CC\text{-}K}$ are the etch rates taken from Canonical Curves for P-based and K-based planes, respectively.

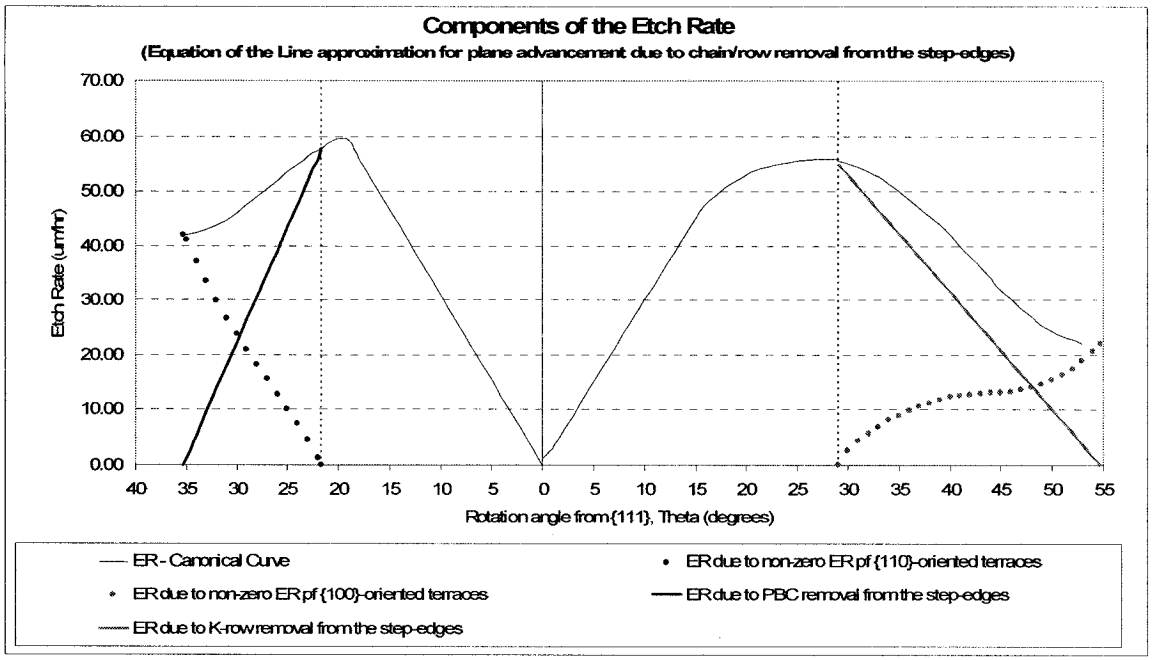

Figure 4-12: The Canonical Curve representing etch rates and their components based on the Equation of the Line for chain/row removal from the Step-Edges.

Figure 4-12 shows a break down of the etch rates into two components. The solid Black and Solid Grey lines of this graph represent a linear approximation of ER component due to the chain/row removal from the step-edges. It is worth to note that the portion of the ER due to the {110}- and {100}-oriented terrace advancement is substantially deviates from linear. This deviation may be difficult to explain from the physical point of view. However, with the help of the equation (4.3), the frequency of removal for two families of planes in vicinity of basic {100} and {110} surfaces is summarised in graphs of Figure 4-13.

Comparing Figure 4-11 and Figure 4-13 the difference in mathematical modelling demonstrates the difficulty in isolating components determining whether the removal frequency is or is not constant at large angles of rotation away from basic {111} surface.

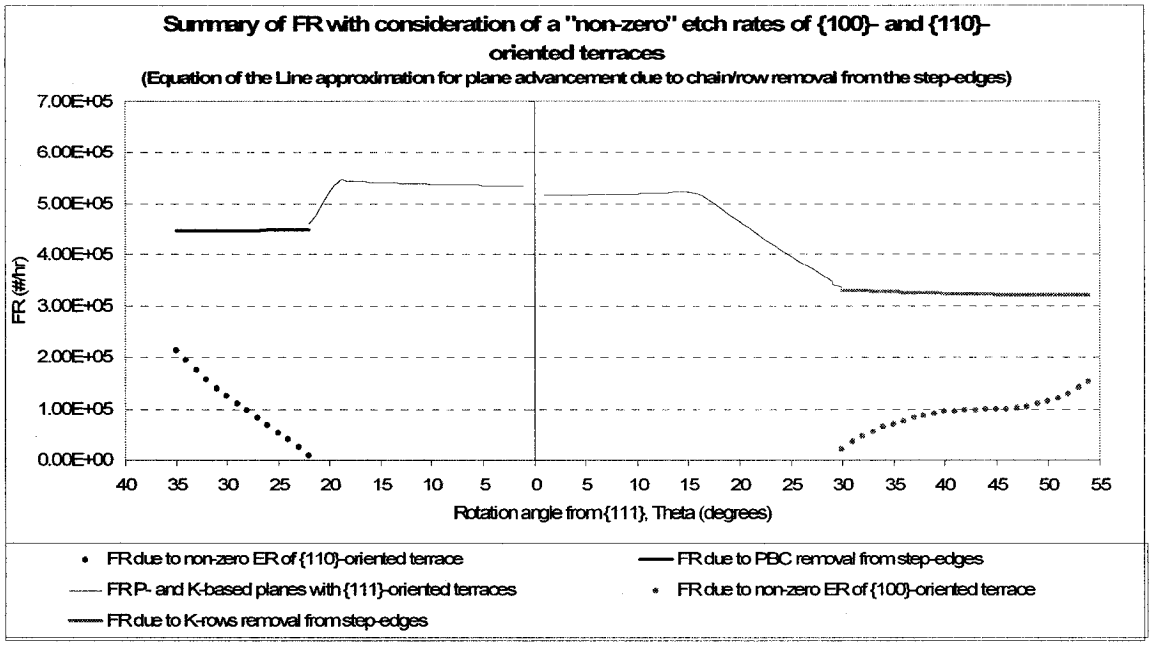

Figure 4-13: Summary of the calculations for the FR of surfaces with {111}-oriented terraces and components for P- and K-based surfaces with {110}- and {100}- oriented terraces based on the Equation of the Line for chain/row removal from the Step-Edges – data from Canonical Curves.

4.4.3. Equation of the Line Approximation for the ER component Due to Chain/Row Removal from the Step-Edges with the TRANSITION ZONE

Now, from the analysis of Figure 4-12 the following observation may be made: the linear approximation of the component of the ER responsible for the chain/row removal from the SE might be more reasonable if a Transition Zone were introduced.

As a simplification, the Transition Zone here is the area where P-based planes with {110}-oriented terraces and K-based planes with {100}-oriented terraces have the same geometry as the respective planes with {111}-oriented terraces.

It may be noted from the canonical curves that the etch rates of P-based planes with {111}-oriented terraces rotated away from {111} plane (left side in Figure 4-14) follow linear progression till $\theta_P \approx 18°$ (the inflection point on this part of canonical curve). At this point the terrace width of P-based plane with {111}-oriented terraces is

$TW_{\{111\}} \cong 9.64$ Å, see Figure 4-14. Similar reasoning applied to K-based plane with {111}-oriented terraces rotated to the right from {111} plane in Figure 4-14. This plane will stop its linear progression at $\theta_K \approx 16°$ (the inflection point of right part of canonical curve) with the terrace width $TW_{\{111\}} \cong 10.93$ Å.

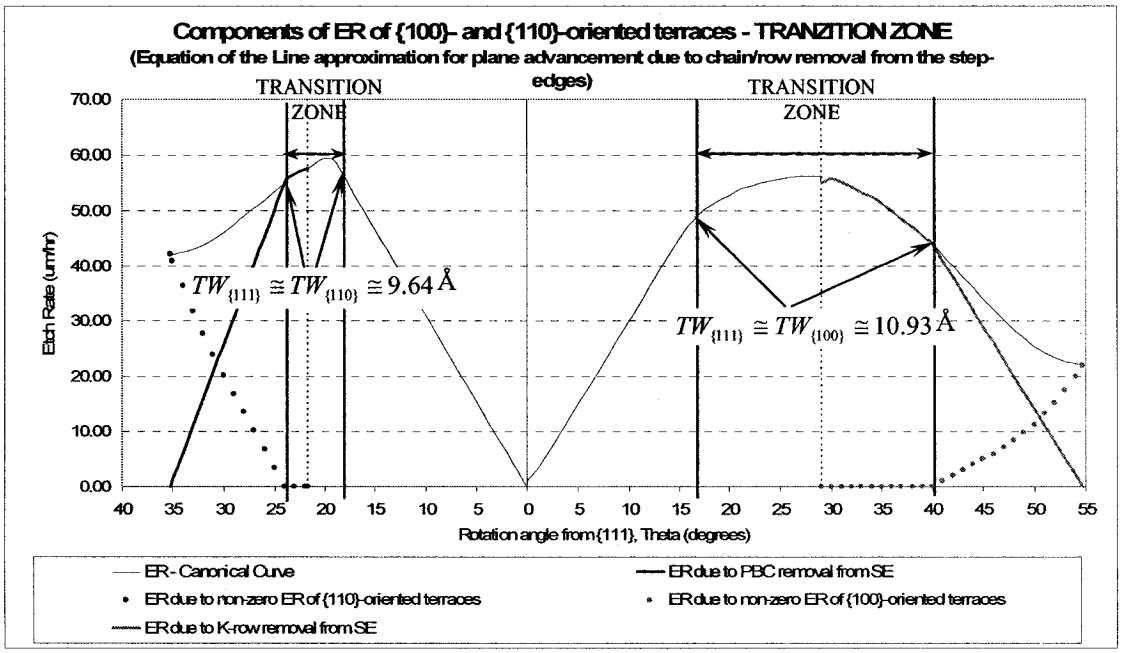

Figure 4-14: The Canonical Curve representing etch rates and their components based on the Equation of the Line for chain/row removal from the Step-Edges and the Transition Zone.

Thus, choosing the P-based plane with {110}-oriented terraces and K-based plane with {100}-oriented terraces with the same terrace width as respective surfaces with {111}-oriented terraces, the Transition Zone may be defined.

According to this argument, the Transition Zone for P-based planes will be in the region of $24° \leq \theta_P \leq 18°$, and the Transition Zone for K-based planes - $16° \leq \theta_K \leq 40°$.

Using a discussion similar to that of the previous section the following equations can be derived:

$$ER(\theta_P)_{\substack{PBC\ removal\ from\ SE \\ TRANSITION\ ZONE}} = 55 + m_{\{110\}}(\theta_P + 24°), \tag{4.15}$$

where $m_{\{110\}}$ – is the slope of straight line determined as: $m_{\{110\}} = \frac{ER_1 - ER_2}{\theta_1 - \theta_2} \approx 4.88$

θ_P = 24° is the location of a P-based surface after the crossover, with approximately the same terrace width as that of the plane with {111}-orientated terrace where ER stops being linear, and

55 μm/h – is the ER of a P-based plane from Canonical Curve at $\theta_P = 24°$.

$$ER(\theta_K)_{\substack{K-row\ removal\ from\ SE \\ TRANSITION\ ZONE}} = 44 + m_{\{100\}}(\theta_K - 40^\circ), \quad \textbf{(4.16)}$$

where $m_{\{100\}}$ – is the slope of straight line determined as: $m_{\{100\}} = \frac{ER_1 - ER_2}{\theta_1 - \theta_2} \approx -2.99$

θ_K = 40° is the location of a K-based surface after the crossover, with approximately the same terrace width as that of the plane with {111}-orientated terrace where ER stops being linear, and

44 μm/h – the ER of a K-based plane from Canonical Curve at $\theta_K = 40°$.

In the areas, defined on the graph of Figure 4-14 Transition Zone, the ER component due to the chain/row removal from the step-edges follows the ER of a Canonical Curve, similar to that of the planes with {111}-oriented terraces. The ER component due to the non-zero ER of {100}- and {110}-oriented terraces is considered to be equal to "zero" in this area.

The respective components of FR may be summarized and presented graphically in Figure 4-15.

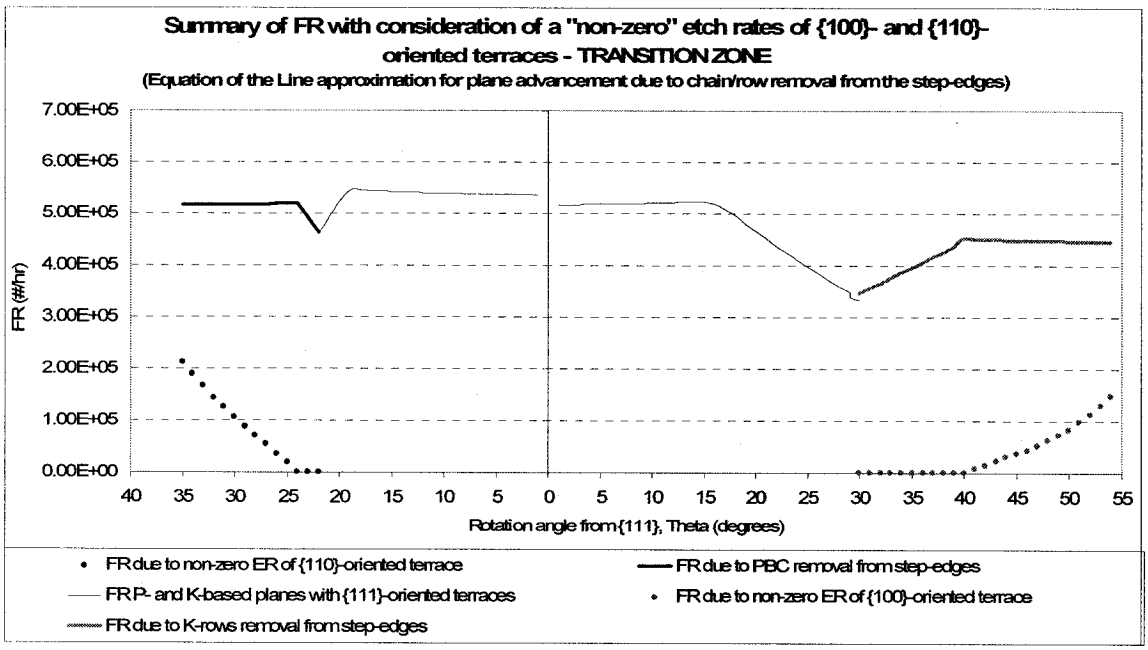

Figure 4-15: Summary of the calculations for the FR of surfaces with {111}-oriented terraces and components for P- and K-based surfaces with {110}- and {100}- oriented terraces based on the Equation of the Line for chain/row removal from the Step-Edges and the Transition Zone.

As it can be noted from the illustration of Figure 4-15, the FR component due to the chain/row removal from the Step-Edges of planes with {100}- and {110}-oriented terraces are close to those of the planes with {111}-oriented terraces. This result suggests that this approximation may have reasonable explanation of the etching process from the Frequency of Removal point of view.

However correct this model of approximation may be, it seems to be the most reflective of the etch rate mechanisms of planes with {100}- and {110}-oriented terraces. Hence, this approximation was used for the experimental data collected from the under-etch wagon-wheel experiment on Si{100} and Si{110}, details of these calculations are summarized in Appendix II.

4.5. Summary

This chapter addresses the idea of frequency of removal of chain/row from the step edges as a connection between the plane geometry and its respective etch rate.

Terrace orientation, {111}, {110}, or {100}, plays an important role in the determination of removal frequencies.

The basis for these calculations was the generally accepted step-based model of planes with {111}-oriented terraces. However, following the discussion of Chapter 3, K-based and P-based planes with {100}- and {110}-oriented terraces, respectively, were considered in the frequency of removal (FR) of chain/row from the step-edge calculations.

First, mathematical model for planes with {100}- and {110}-oriented terraces suggested that the etch rates of these terraces (i.e. "non-zero" etch rates of {100}- and {110}-oriented terraces) can not be neglected for this model to reflect the physics of the etching process. Thus, three different separation strategies are examined:

1. Assumption that the influence of non-zero etch rate of {100}- and {110}-oriented terraces decreases linearly and reaches zero at the crossovers, and calculate what must be the chain/row removal frequencies.
2. Assumption that the etch rate due to chain/row removal from the step-edges of the planes with {100}- and {110}-oriented terraces is such that it increases linearly to the crossover and calculate what must be the variation with θ of the non-zero etch rate of {100}- and {110}-oriented terraces.

3. Assumption that there is a transition zone near the crossover, and that the etch rate due to chain/row removal increases linearly to the edge of that transition zone.

As a basis for these calculations, experimental etch rates summarised in canonical curves are used, (see Figure 4-5). The etch rate of basic {111}-oriented terraces is considered to be comparatively negligible for this analysis.

General observation of the last, third, approximation, where so-called Transition Zone concept was used, FR calculations for planes with {100}- and {100}-oriented terraces suggested the results more consistent when compared to FR of planes with {111}-oriented terraces (Figure 4-15).

Further explorations of different approximations to this mathematical model might provide yet better reflection of physical processes in anisotropic etch of step-based surfaces. However, for the purpose of this study, Equation of the line approximation for chain/row removal from the step-edges with the consideration of a Transition Zone provides satisfactory results, that are used in following chapters.

4.6. Contributions

Chapter 4 provides a connection between etch rates of anisotropically etched surfaces in concave structures and their geometry. This connection was expressed in terms of frequency of removal (FR) of chain/row from the step-edges. Removal frequency is not entirely new concept, but it had to be augmented in order to accommodate rather original view on geometry of step-based surfaces.

- Removal frequency was calculated not only for surfaces with {111}-oriented terraces but also with consideration of P-based and K-based planes with {110}- and {100}-oriented terraces, respectively.
- A mathematical model was introduced, were FR for planes with {110}- and {100}-oriented terraces should be viewed as composed of two components: one accounting for "non-zero" etch rates of {100}- and {110}-oriented terraces, and another for chain/row removal from step edges.
- It was suggested, for better reflection of actual physics of the etching process, that these two components should be used for modelling etch rates. The etch rate component of a plane with {100}- or {110}-oriented terrace, accounting for chain/row removal from a step, should be equivalent to the etching process of the surfaces with {111}-oriented terraces of which etch rates may be considered negligible.
- Three different approximations of original mathematical model are analysed.
- One of these approximations, i.e. equation of the line approximation for chain/row removal from the step-edges with the consideration of a Transition Zone is considered most reflective of physical process.
- The canonical graphs of frequency of removal vs. theta, for both P-based and K-based planes, are used in subsequent chapters.

5. Step-Edge Velocity

5.1. Background Information

As it was stated earlier, (Chapters 2–4), the basic step-based model of any plane with $\{hll\}$ or $\{hhl\}$ Miller Indices can be represented schematically as shown in Figure 5-1.

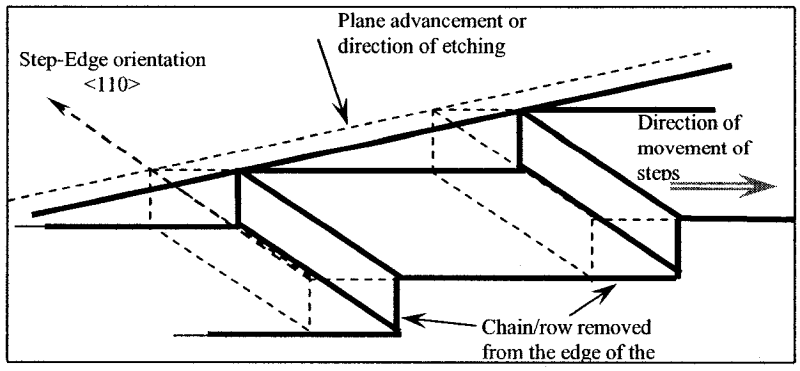

Figure 5-1: Schematic representation of the plane advancement due to the removal of chain/rows from edges of steps in the step-based plane model.

It also was pointed out that in the wagon-wheel under-etch experiment, these types of planes appear on sidewalls of spokes in the combination with other surfaces of similar structure, see Figure 5-2.

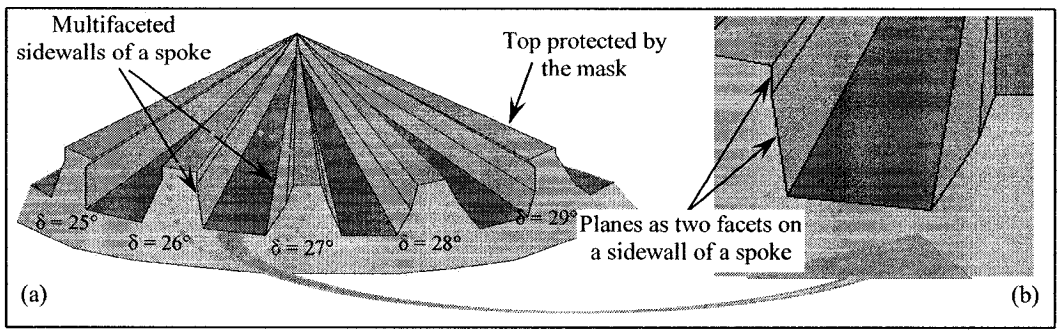

Figure 5-2: (a) Schematic representation of a segment of a sample used in under-etch wagon-wheel experiment and (b) close view on a cross-section of one of the spokes with the sidewalls composed of two facets.

Closer view at surfaces/facets on one side-wall of a spoke shows that the steps on each of the adjacent facets may move in the same or opposite direction, Figure 5-3.

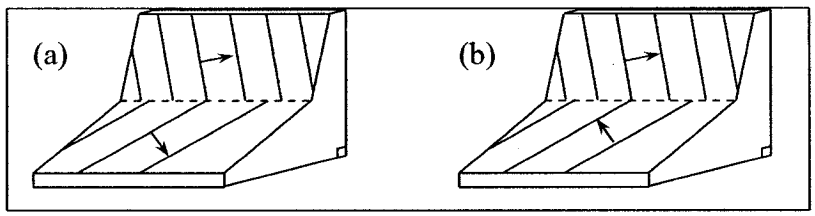

Figure 5-3: Schematic diagram of a combination of two adjacent facets on sidewall of a spoke in wagon-wheel under-etch experiment with the step-edges moving (a) in the same and (b) in the opposite directions.

In the previous work conducted in Concordia Research Microfabrication Laboratory by Z. Elalamy *et al* [9], all possible combinations of respective step movement on adjacent facets were identified and summarized.

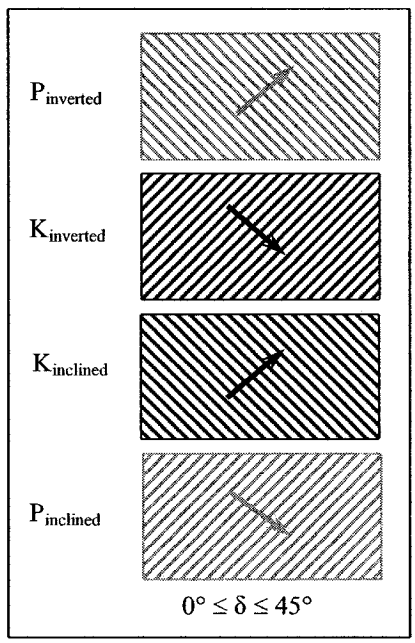

Figure 5-4: Orientation and direction of propagation of steps on Si{100}, Figure from [9].

It was discovered that for concave profiles in Si{100} wafer, all sidewall facets have step-based structures with the step-edges (SE) moving in the same direction (Figure 5-4). Facets in this figure are presented in the order as they were located in the examination of experimental data, with inverted planes appearing as the top most facets.

Similar analysis of the concave spokes anisotropically etched in Si{110} wafer, shown larger variety of facets as well as their combinations, (Figure 5-5).

Analysis of the relative movement of the step-edges of the bordering facets may explain some of the phenomena that were met in the experimental data. Especially, one of the most puzzling - different etch rates of the planes with the same Miller Indices and, consequently, same crystallographic profiles.

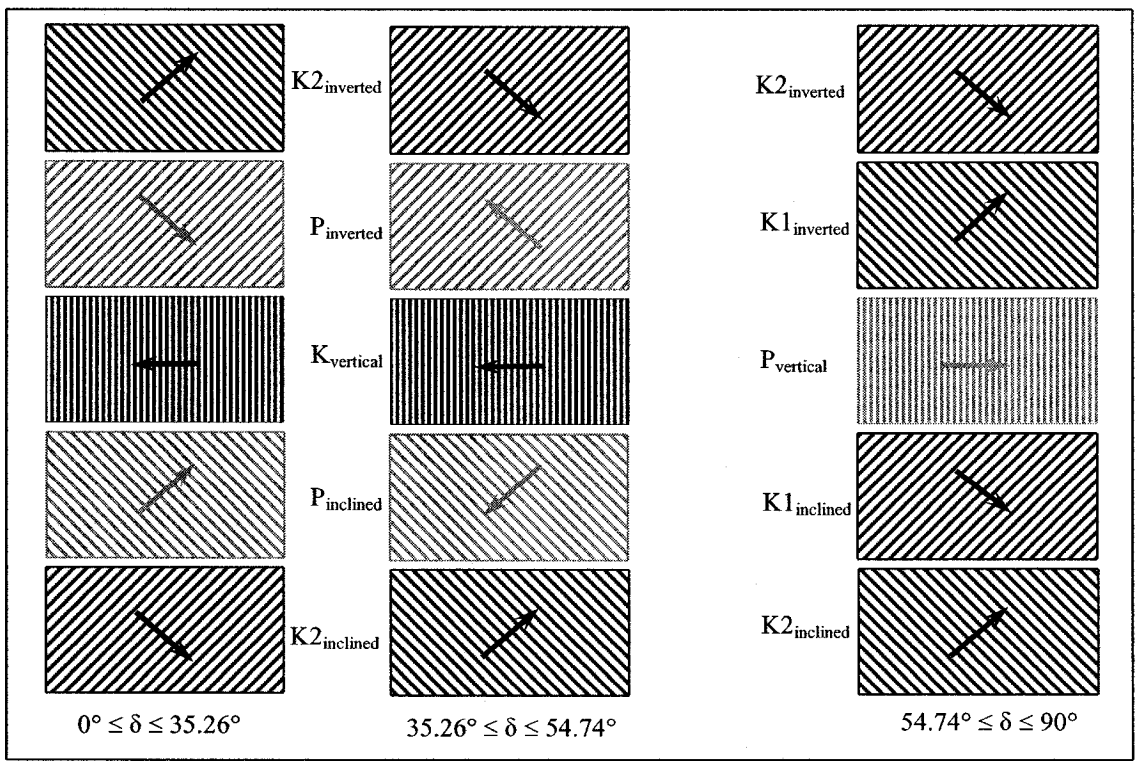

Figure 5-5: Orientation and direction of propagation of steps on Si{110}, Figure from [9].

It was discussed that the surfaces in concave structures must not be analysed alone but in combination with their respective neighbours, [9], [34]-[35]. Effect of the boundary between adjacent facets in concave structures was studied. The results, to a certain extent, proved that the etch rates variations may be at least partly explained by the influence of neighbouring planes, [9], [33]-[35], [42]. However, so far the boundary effect, i.e. influence of the etch rate of a facet on its neighbour's ER, was limited to the analysis of the boundary (detailed explanation is pending in following chapter). More dynamic

approach to these interactions with the consideration of the step-edge velocities on the adjacent facets is considered in this portion of my work.

5.2. Definitions of Basic Parameters

Since much of the upcoming analysis is novel to the field of anisotropic etching new terminology is introduced. Definitions of these terms are presented with the help of a simplified schematic representation of two adjacent facets, each composed of step-based surface as seen in Figure 5-6.

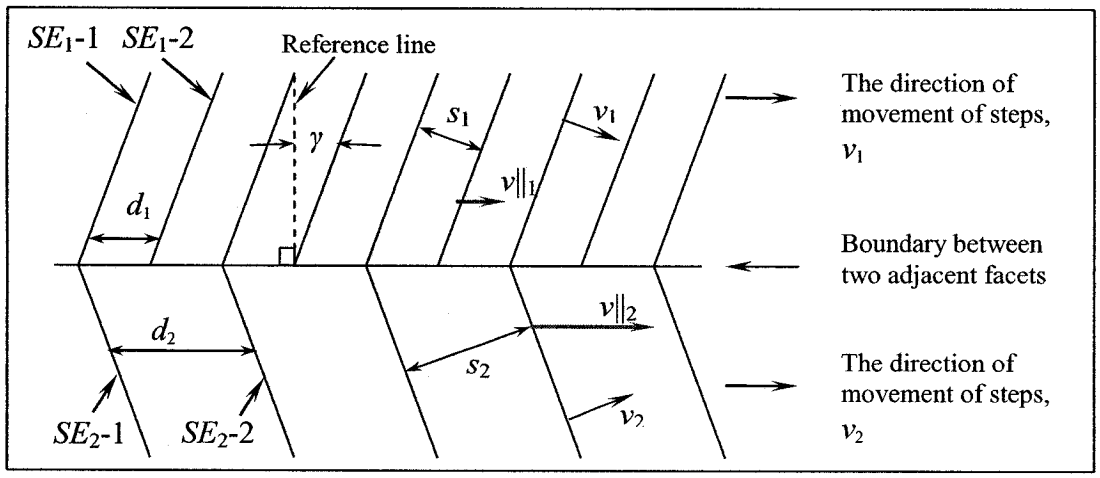

Figure 5-6: Schematic representation of two adjacent facets that might appear on a side wall of a spoke in wagon-wheel under-etch experiment with the step spacing indicating a one-to-two correspondence.

From Figure 5-6 the following symbols are defined:

SE - a step-edge, indicating the location and orientation of K-row or PBC on the edge of the step on K- or P-based plane, respectively,

SE_1 - a step-edge on the first or top-most out of two adjacent facets,

SE_1-1 - "first" step-edge on the first/top-most facet

s_1, s_2 - a step-spacing on the first and second facet, respectively, (Å)

d_1 - a distance travelled by the SE on the plane with defined etch rate, (Å)

γ - an angle that the PBC-s or K-rows at step-edges make with a reference line - line perpendicular to the boundary between two facets, (degrees)

v_1, v_2 - absolute step-edge (SE) velocity (on the first, top most, and second facet, respectively) defined as a normal to the edge of a step, (μm/h)

$v\|_1$ - relative step-edge velocity, or step-edge (SE) velocity on the first facet with respect to the boundary between two adjacent facets, (μm/h)

Step-edge velocity is a parameter that defines how fast step-edges of a step-based plane will have to advance in the "direction of movement of steps" in order to support the experimentally measured etch rate of the given plane.

Relative Step-Edge velocity is a velocity projected onto the boundary between two adjacent facets. (Parameter used for a comparison of the SE-velocities of two neighbouring facets)

Step spacing correspondence indicates how many steps, or distances between step-edges (SE), of one plane may fit within the distance between two SE of adjacent plane.

For example one-to-two correspondence of steps designates precisely two step-spacings of one facet per one step-spacing of an adjacent plane.

5.3. Determination of Step-Edge Velocity

Assuming that the etch rates (ER) of all planes appearing on sidewalls of spokes are known, the velocities of step movement for each of these surfaces can be determined.

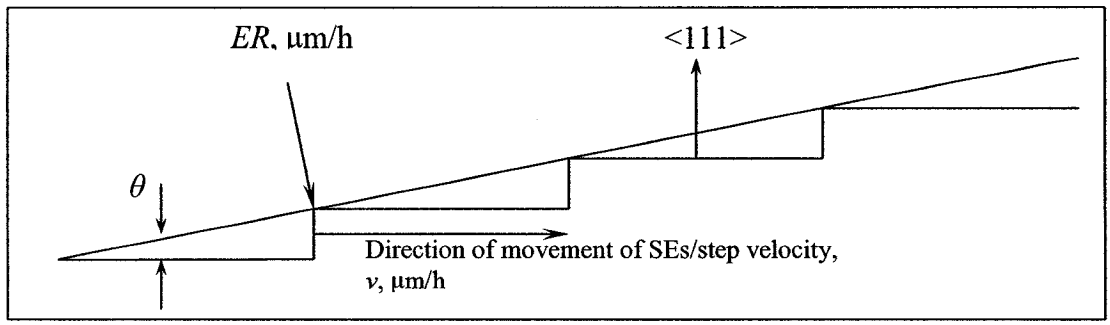

Figure 5-7: Schematic representation of a cross section of a plane with {111} oriented terraces.

From the geometry of the basic step-based model of planes with {111} oriented terraces, (Figure 5-7), the following can be written:

$$v = \frac{ER(\theta)}{\sin\theta} \tag{5.1}$$

where v is the step velocity in the direction perpendicular to the edge of the step, (SE).

In order to be able to compare the step velocities of two adjacent facets, the component of step velocity parallel to the boundary between two neighbouring facets can be found by:

$$v\|_1 = \frac{v_1}{\cos\gamma} \tag{5.2}$$

Say, in the combination of two adjacent facets, the speed of the SE's on the upper facet, in terms of the velocities with respect to the facets boundary, is $v\|_1$ and the on the lower facet $v\|_2$.

The speed of movement of the step-edges of the bottom facet with respect to the top one then can be expressed as

$$\Delta v\| = v\|_2 - v\|_1 \tag{5.3}$$

5.4. Step-Edge Velocity for Canonical Curves

Step velocities calculated for Canonical Curves etch-rate data using Equation (5.1) will closely resemble the shape of the curve for removal frequency from the previous section, see Figure 4.15. The difference is only in units, given the slight difference of mathematical derivation for respective value. The step-edge velocity is determined by equation (5.1), $v = \frac{ER(\theta)}{\sin\theta}$,

and the removal frequency (FR) by equation (4.3)

$$FR(\theta) = \frac{ER(\theta)}{EPA(\theta)} = \frac{ER(\theta)}{USW_{\{111\}} \cdot \sin\theta},$$

where $USW_{\{111\}}$ is a constant for given family of planes with {111}-oriented terraces.

The above analysis applies when the etch rate (ER) is dominated by step movement, and the etch rate of the "flat" plane (in this case {111}-oriented terrace), is negligible. However, taking to consideration other "flat" planes in the silicon system, {100} and {110}[20] (with "non-zero" etch rates), the analysis of step movements on these planes can be interpreted as follows.

Considering "non-zero" ER-s of the {100}- and {110}-oriented terraces, these velocities may be separated into two components, (see Chapter 5):

1. The step-edge velocity influenced by the removal of the chain/row from the edge of the step, (similarly to the basic step model with {111}-oriented terraces with negligible etch rates).
2. The step-edge velocity influenced by the advancement of the terrace due to its non-zero etch rate.

[20] The possibility of {100} and {110} planes to be considered "flat" under certain circumstances was discussed in great detail in Chapter 3

The mechanism of these components is schematically shown in Figure 5-8.

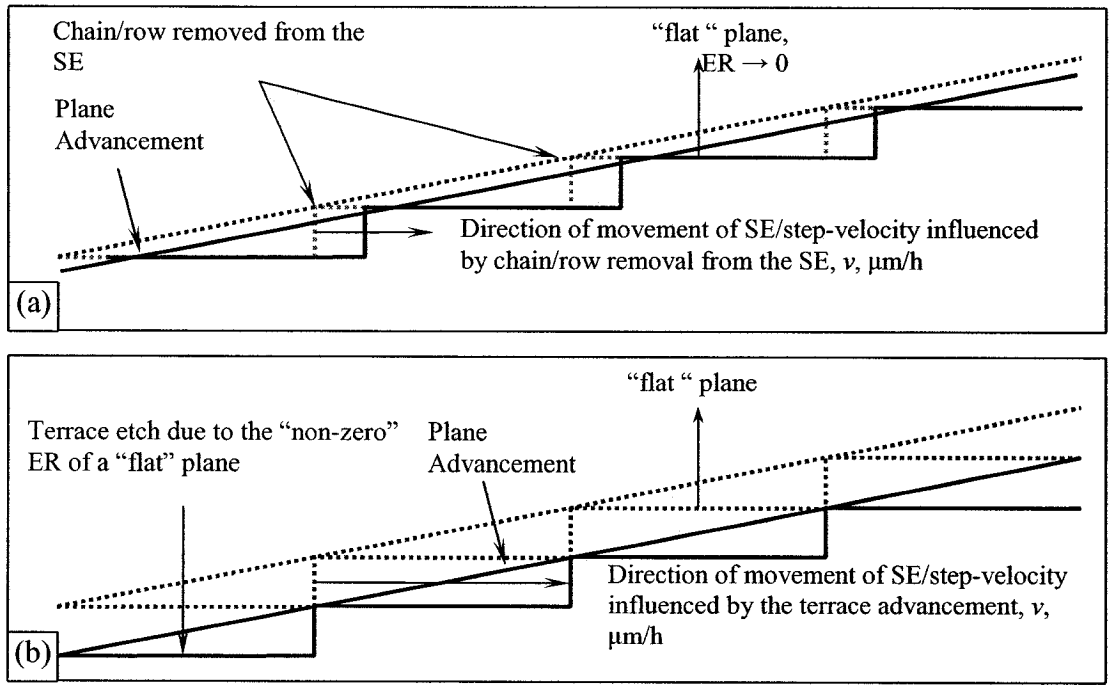

Figure 5-8: Schematic representation of the etching mechanism of the planes taking to consideration two cases (a) plane advancement with removal of the chains/rows from the step-edges only, and (b) plane advancement due to the etch of the {100}- and {110}-oriented terraces.

Three different approximations were analysed (see Chapter 4). However, one proved to have more accurate reflection of the etch mechanism on planes with {100}- and {110}-oriented terraces compared to those with {111}-oriented terraces. Therefore, the approximation of the Equation of the Line for chain/row removal from Step-Edges with the Transition Zone is used in this study. The etch rate components were determined in Chapter 5 and results are used here.

Step-edge velocity component, in this case absolute velocity, influenced by the terrace advancement ("non-zero" ER for {100}- and {110}-oriented terraces), may be written as (Figure 5-8(b)):

$$v_{\substack{due\ to "non-zero"\ ER \\ of\ \{110\}-oriented\ terrace}} = \frac{ER_{\{110\}-oriented\ terrace}}{\sin(\xi)}, \qquad (5.4)$$

where $ER_{\{110\}\text{-}oriented\ terrace}$ is Canonical Curve etch rate component due to "non-zero" {110}-oriented terrace etch rate,

ξ – is angle between {110} oriented terrace and P-based plane,

$$v_{\substack{due\ to\ PBC\ removal \\ from\ the\ SE}} = \frac{ER_{PBC\ removal\ from\ the\ SE}}{\sin(\xi)}, \tag{5.5}$$

where $ER_{PBC\ removal\ from\ the\ SE}$ is Canonical Curve etch rate component due to PBC removal from the Step-Edges (SE), (Figure 5-8(a)).

Similar equations may be derived for K-based planes with {100}-oriented terraces. Summary of these calculations are presented in Figure 5-9.

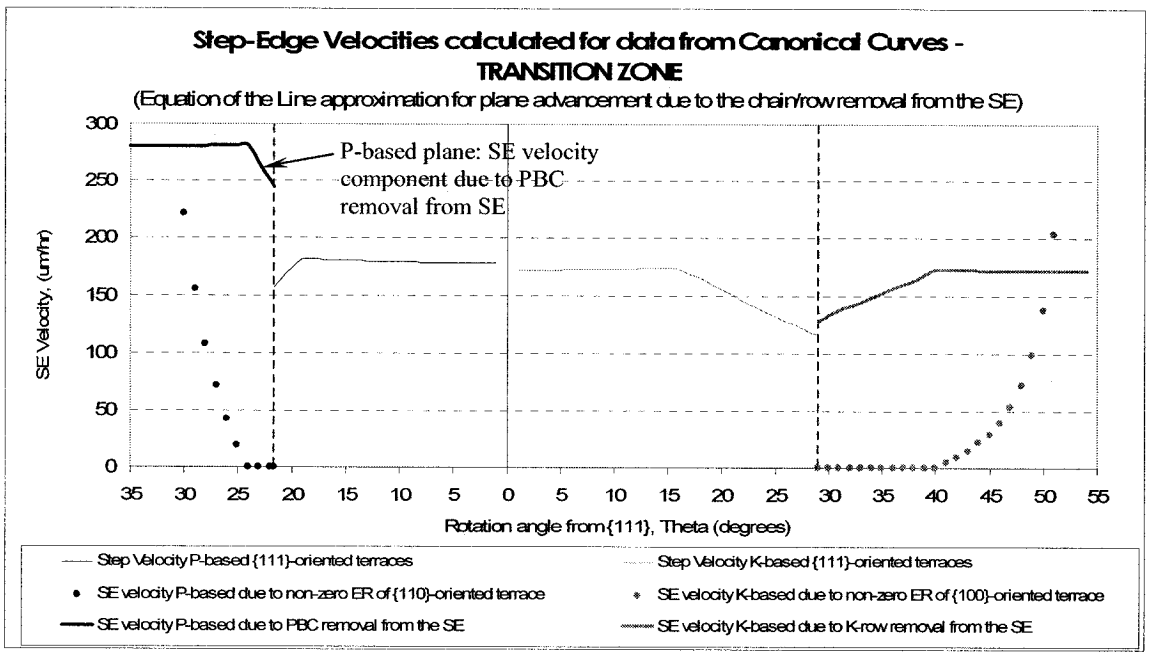

Figure 5-9: Summary of the Step-Edge Velocities for Canonical Etch Rates with the decomposition into two components for planes with {100}- and {110}-oriented terraces.

As it can be seen in Figure 5-9, there is a large difference in the SE-Velocities of P-based plane component due to PBC removal from the SE compared to the similar component of K-base plane and step-edge velocities of planes with {111}-oriented terraces. This difference may be explained with the following discussion.

The Step-Edge advancement happens when a chain/row (PBC in this case) is removed from the Step-Edge, see Figure 5-8 (a). Once the event of PBC removal takes place, the SE will advance a distance of one Unit-Step Width (USW). This distance was determined (see Chapter 4) for planes with {111}-, {110}-, and {100}-oriented terraces and their values presented below:

$$USW_{\{111\}} = \frac{5.43}{2 \cdot \sin(54.74^\circ)} \cong 3.325\,\text{Å} \tag{5.6}$$

$$USW_{\{110\}} = a = 5.43\,\text{Å} \tag{5.7}$$

$$USW_{\{100\}} = \frac{5.43\sqrt{2}}{2} = 3.83969\,\text{Å} \tag{5.8}$$

From this values, it is easy to deduce, that the removal of one PBC will move the SE almost twice (1.67, precisely) as far on P-based plane with {110}-oriented terrace compared to the P-based plane with {111}-oriented terrace (Unit-Step Width values of 5.43 Å and 3.325 Å, respectively). And compared to the SE velocity component due to K-row removal from the SE on K-based plane with {100}-oriented terraces the removal of one PBC will move the SE almost 1.5 times (1.41, precisely) as far. Thus, it may be said that to support the experimentally measured etch rates, the step-edges on P-based surfaces with {110}-oriented terraces move approximately 1.5 times faster than SE-s on K-based plane with {100}-oriented terraces and both families of planes with {111}-oriented terraces.

However, the removal frequencies for the same surfaces, i.e. for two families of planes with {111}-, {110}-, and {100}-oriented terraces, appear to be approximately the same. The key to this difference in graph's appearances (SE velocity compared to FR) is the

difference in actual meaning these two parameters. FR represents a number of chain/rows removed from the step-edges that would accommodate for the surfaces' etch rate. This number, eventually translated into the effective plane advancements as chain/rows are removed simultaneously from the SE-s of given surface. And mathematically it is accounted for in equation (4.3) by "$1/USW$" term.

5.5. Comparison of the Step-Edge Velocity with Respect to a Boundary between Two Adjacent Facets

5.5.1. Si{100}

In the following portion of this work, the data collected from under-etch experiments on Si{100} wafer is analysed with the view of the relative Step-Edge velocity – velocity with respect to a boundary between two facets ($v\|\|_1$ compared to $v\|\|_2$, see Figure 5-6).

It is known that on Si{100} wafer, for the basic step model with {111}-oriented terraces, all steps on the adjacent facets move in the same direction, (see Figure 5-4).

However, for planes with {100}- and {110}-oriented terraces this relative direction does not change due to the fact that the crossover in the terrace orientation in the sidewall facets for Si{100} occurs at approximately same deviation angle $\delta \approx 19^{\circ}$, [19]. And from this point the change in the direction of the movement of steps happens on all adjacent facets keeping their relative movement in the same direction.

Now, the interesting part in this discussion will come with the comparison of the movement of the step edges for this case.

Simple calculations using Equation (5.1) provide step velocities for the planes with {111}-oriented terraces, where the ER of the terrace is assumed to be negligible as well as two components of the surfaces with {100}- and {110}-oriented terraces.

Figure 5-10 summarizes the values of Absolute Step-Edge Velocities calculated as a velocity of the Step movement in the direction normal to its edge.

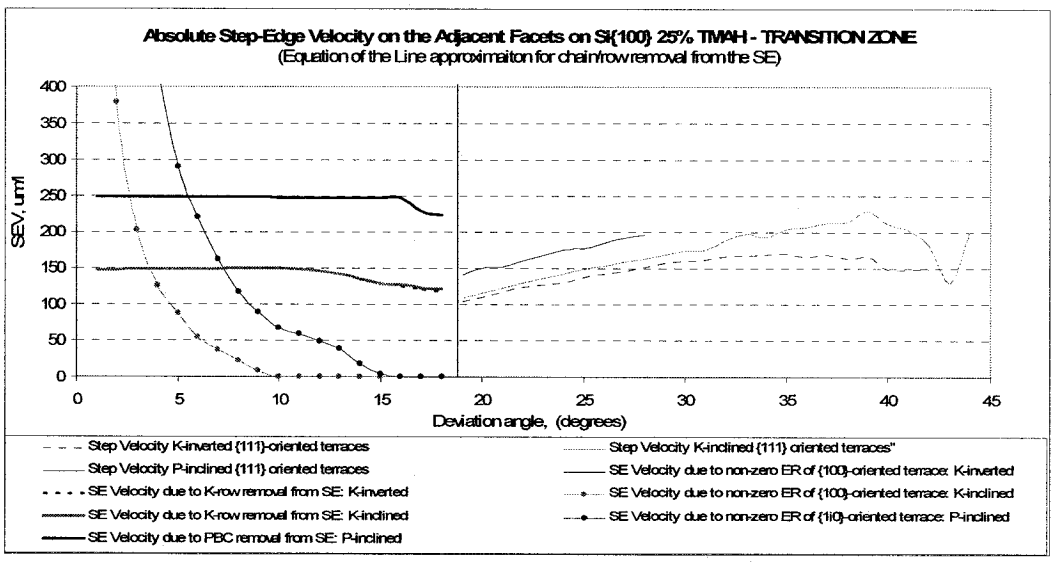

Figure 5-10: Absolute Step-Edge velocity calculated using Equation (6.1) for the experimental etch rate date measured on Si{100} etched in 25% TMAH.

It may be observed that the component of the Step-Edge Velocity due to "non-zero" {100}- and {110}-oriented terraces, approaches infinity as the surfaces move closer to their basic {100} and {110} orientations, respectively as a deviation angle $\delta \rightarrow 0°$. This is an outcome of an application of this mathematical model. However, this type of calculation does not allow the comparison of the events happening on the adjacent facets. Thus, in order to compare the velocities of step-edges on adjacent facets the Relative Step-Edge Velocity is introduced.

Relative Step-Edge Velocity the step-edge velocity projected onto a boundary between two adjacent facets: $v\|$[21]. Taking to consideration the angle of the step-edges with respect to the facets boundary, γ, (Figure 5-11), Relative Step-Edge velocities can be determined.

---

[21] $v\|_1 = \frac{v_1}{\cos\gamma}$, where γ is an angle of a chain/row on a SE with respect to the normal to a boundary between two adjacent facets.

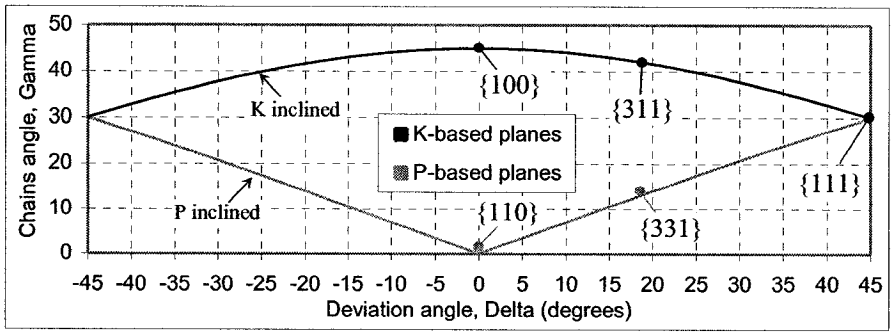

Figure 5-11: Angle of a PBC/K-row located at the Step-Edge with respect to the normal to a boundary between two adjacent facets (γ) vs. deviation angle (δ) for all possible facets on Si{100}, Figure from [9].

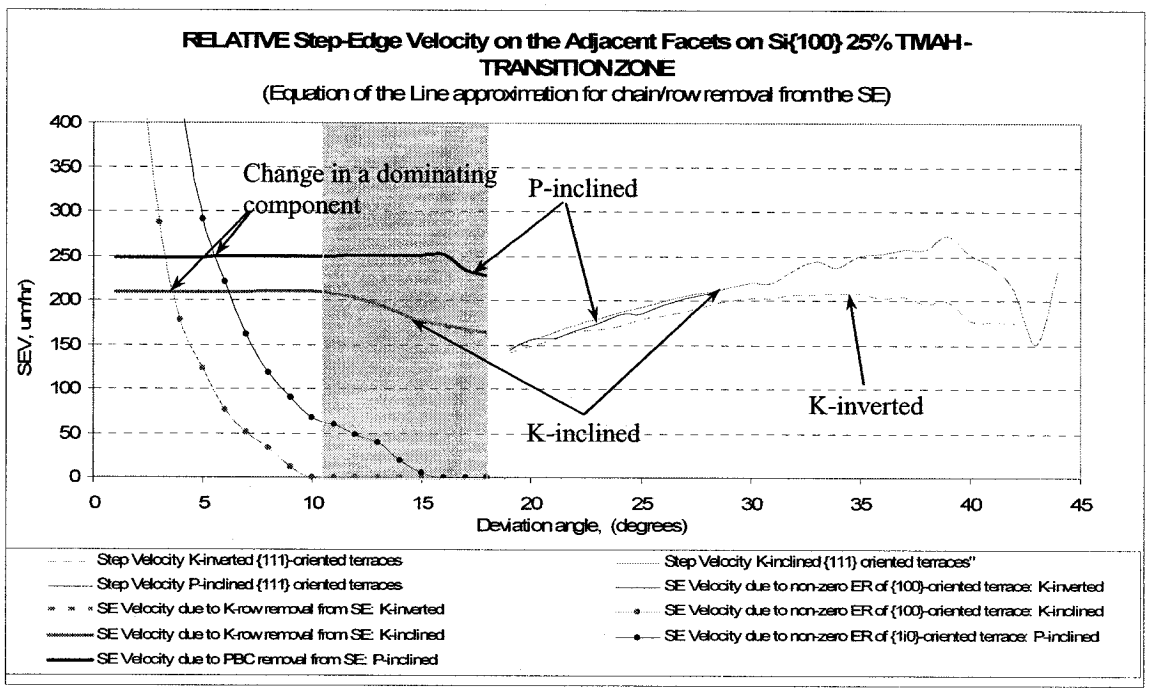

Figure 5-12: Summary of Relative Step-Edge velocity for the experimental etch rate date measured on Si{100} etched in 25% TMAH

The relative velocities are summarised in the graph of Figure 5-12.

From a basic analysis of this figure, it may be observed that the velocities the Step-Edges are approximately in the same range, depending on the accuracy of applied mathematical model. However, there the step-edges on P-based facet with {110}-oriented terraces may advance faster than the Step-Edges on K-based based facet with {100}-oriented terraces. The area that may be brought to the attention is a portion of the graph in Figure 5-12 between deviation angles $\sim 3^\circ \leq \delta \leq 6^\circ$. This part of the graph is noteworthy since the

Step-Edge velocities of P- and K-based facets undergo a change in the dominating influence on the etch rates, i.e. change in the dominance of the influence from the {100} or {110} terrace advancement to the row/chain removal from the step-edges.

In other words, it can be said, that for the deviation angles $\delta < 3°$ the SE velocities are mainly due to the "non-zero" Etch Rates of {100}- and/or {110}-oriented terraces.

For deviation angles $\delta > 6°$ the SE velocities can be approximated to the velocities on the surfaces described by the basic step-based model with negligible (or zero) terrace ER and are more influenced by the removal of the chains/rows from the edges of the steps.

5.5.2. Si{110}

Similar analysis was done using the data collected from the under-etch experiment on Si{110} wafer.

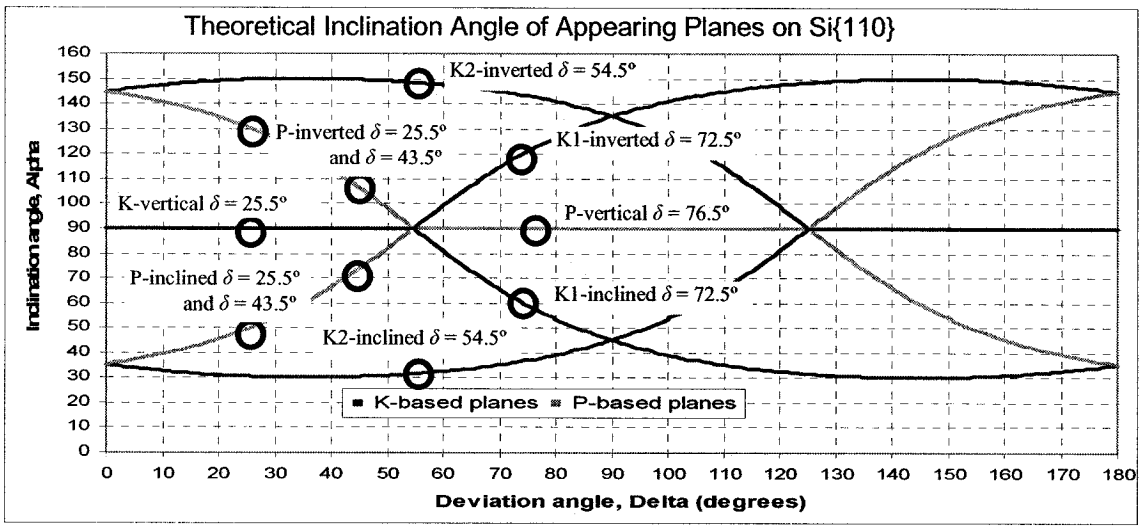

Figure 5-13: Theoretical inclination angle of planes that may appear on the sidewalls of spokes in the under-etch wagon-wheel experiment. Dark circles indicate the location of crossovers in terrace orientation for all facets theoretically detected on sidewalls of spokes in wagon-wheel under-etch experiment.

It is shown below, that the relative movement of Step-Edges on adjacent facets for the surfaces present on Si{110} is far more complex, with the possibility of the steps moving

in the opposite direction. Relative direction of steps on the adjacent facets for the basic step model with {111}-oriented terraces is presented in Figure 5-5.

However, the experimental results indicated the presence only of some surfaces appearing on side-walls of spokes (compared to all possible facets shown in Figure 5-13), and the number of the surfaces with the cross-over present, will be limited to those, obtained experimentally[22]. The corrections were done to "relative step movement" summary with the consideration of crossovers shown in Figure 5-13.

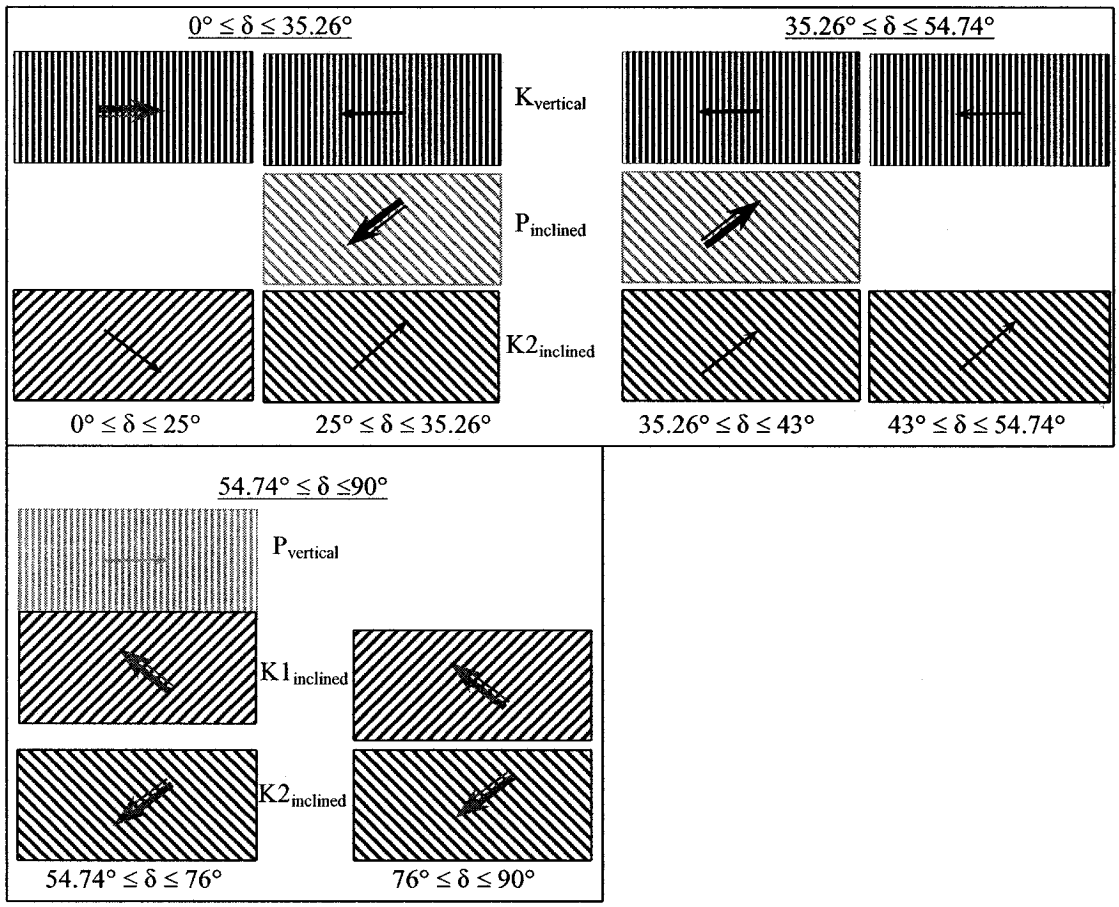

Figure 5-14: Orientation and direction of propagation of steps on Si{110} with the consideration of crossovers in the terrace orientation for the facets detected in the under-etch experiment (25% TMAH, at 80°C). Large arrows indicate the direction of movement of steps on the surfaces with {100}- or {110}-oriented terraces.

[22] For detailed discussion see Chapter 4.

Accounting for crossovers in terrace orientation and the presence of surfaces with {100}- and {110}-oriented terraces, all possible combination in terrace orientations are illustrated in Figure 5-14. Large arrows indicate a change in the direction of movement of steps due to their change in terrace orientations.

It can be seen that in some circumstances, Si{110} wafer offers a number of cases with the steps moving in opposite direction with respect to each other. Therefore, a study of all possible cases offered by this data is conducted below.

As a first attempt to make sense of this data, simple calculations using Equation (5.1) was done to determine "absolute" Step-Edge Velocities of all facets present in this experiment. The results are summarized in graph of Figure 5-15.

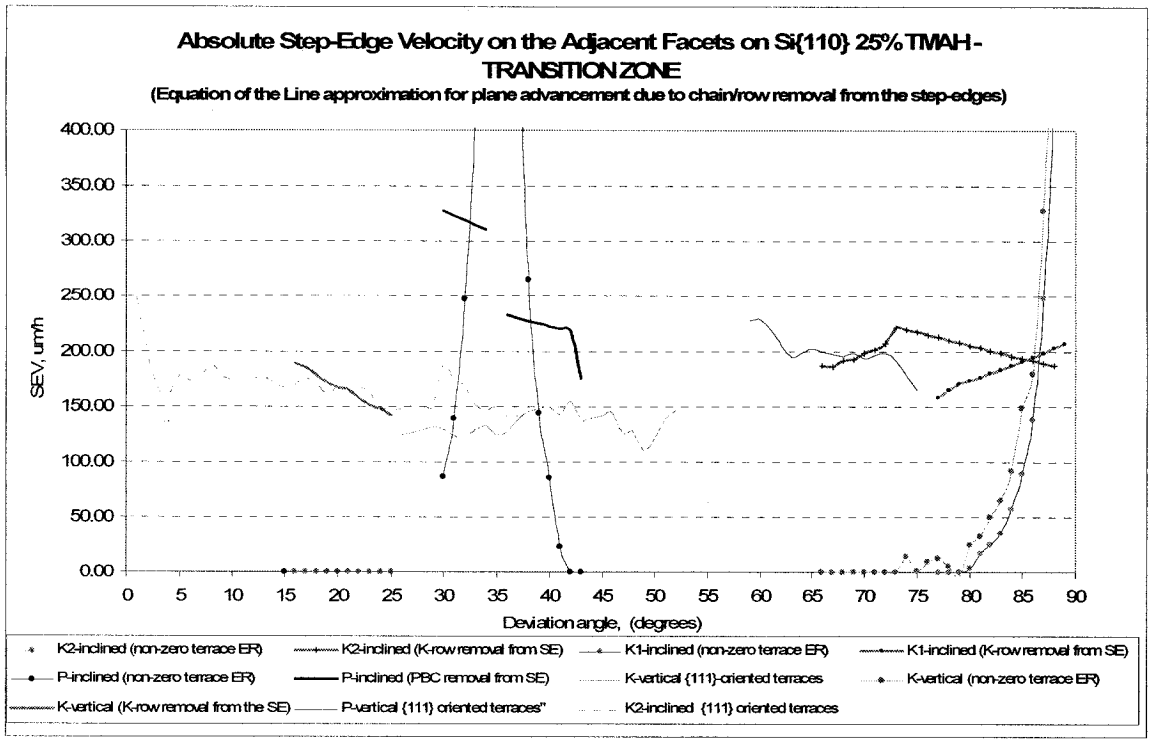

Figure 5-15: Absolute Step-Edge velocity calculated using Equation (5.1) for the experimental etch rate date measured on Si{110} etched in 25% TMAH.

The absolute Step-Edge Velocity gives an indication as to which SE-s move faster as a general rule. However, this graph of absolute Step-Edge Velocity does not indicate the

relative directions of motion of the steps. Therefore, the "Relative Step-Edge Velocity" of adjacent facets, $v||$, is calculated.

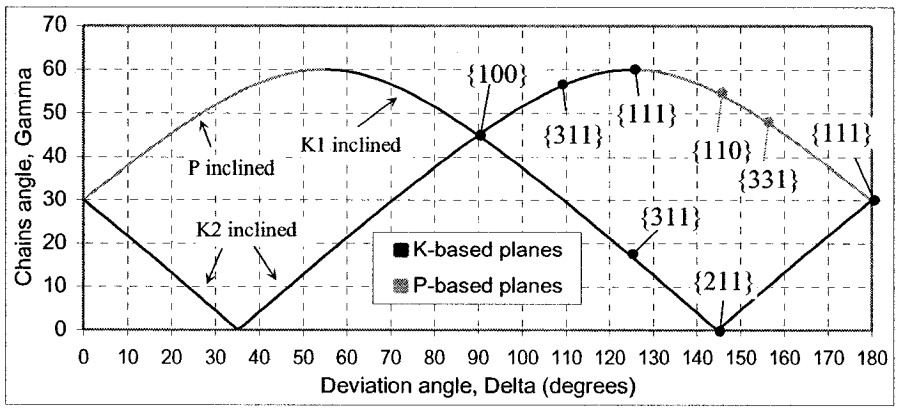

Figure 5-16: Angle of a PBC/K-row located at the Step-Edge with respect to the normal to a boundary between two adjacent facets (γ) vs. deviation angle (δ) for all non-vertical facets on Si{110}, Figure from [9].

Using Equation (5.2), where γ-angles respective to each facet on sidewalls of spokes in under-etch experiment on Si{110} are depicted in Figure 5-16, Relative Step-Edge Velocity was determined.

In order to depict the complexity of the problem at hand the relative direction of movement of steps needs to be considered, especially in the areas where steps move in opposite directions. To visualise this process, the direction of movement of steps from left to right, as seen in Figure 5-14, is considered a positive one and the movement of steps oppose to it – negative. Using this information new illustration of the step movements is made.

From a general inspection of Figure 5-17 it is apparent in which areas the steps, or step-edges, on adjacent facets move in opposite directions on adjacent facets, (see shaded areas in Figure 5-17).

Following areas of interest on this figure are identified:

- areas with the SE-s moving in opposite directions

- $25° \leq \delta \leq 43°$
- $66° \leq \delta \leq 76°$

- areas with the dominating "non-zero" terrace ER component:
  - $33° \leq \delta \leq 38°$ - on P-inclined
  - $85° \leq \delta \leq 90°$ - on K2-inclined and K1-inclined.

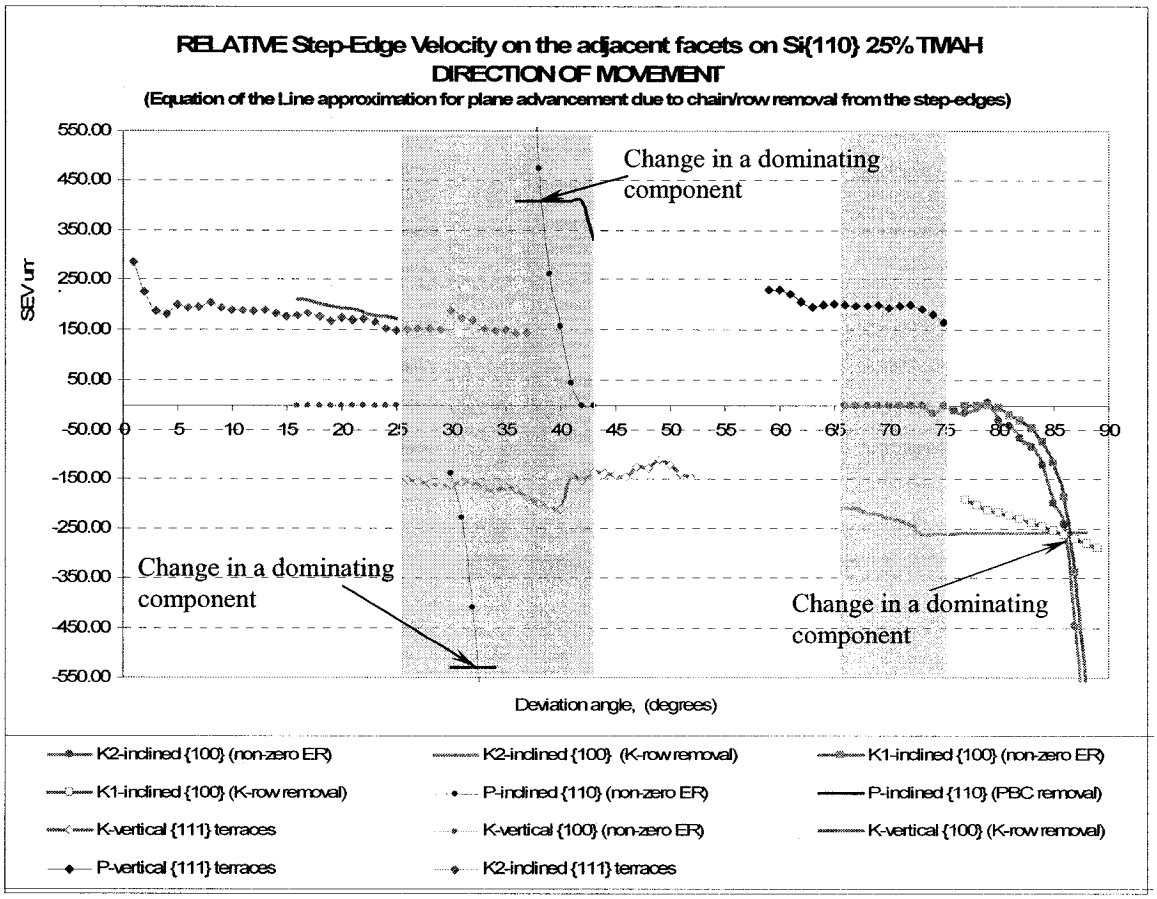

Figure 5-17: Relative Step-Edge velocity calculated for the experimental etch rate date measured on Si{110} etched in 25% TMAH presented with consideration of the relative direction of movement of steps. Shaded regions indicate the areas in which steps on adjacent facets move in opposite direction.

5.6. Summary

This chapter introduces and develops a concept of step-edge velocity. Based on the etch rate data, collected in the wagon-wheel experiment for Si{100} and Si{110} samples, these velocities were calculated as a step-edge advancement in the direction perpendicular to the front of a step-edge – absolute step-edge velocity, (Figure 5-10 and Figure 5-15). These velocities were translated into the values relative to a boundary between two adjacent facets, thus enabling a possibility of comparison of these velocities as well as consideration of their relative movement (same or opposite direction), see Figure 5-12 and Figure 5-17. All velocities (absolute as well as relative) were determined with the consideration of the respective terrace orientation and with the use of Equation of the Line Approximation for the chain/row removal from the step-edges and with the consideration of a Transition Zone[23].

With the assumption that the used mathematical model is acceptable for the purpose of this study, regions with the dominating influence of "non-zero" terrace etch rates for {100}- and {110}-oriented terraces were identified.

5.7. Contributions

Contributions, based on the ER data collected by Z. Elalamy[24], [9], are in the interpretation of this data.

- Translation of the etch rates of facets in under-etch experiment, using Equation of the Line Approximation for the chain/row removal from the step-edges and with the consideration of a Transition Zone, into two components, where applicable.

[23] Detailed explanation of this approximation was done in Chapter 4.
[24] Large amount of the etch rate data was done with my help (actual etching process observation, measurements of the under-etch rates, analysis of some of the collected data).

- Introduction of a concept of Absolute Step-Edge Velocity and Relative Step-Edge Velocity.
- Analysis of the relative step-edge velocities for the data from Si{100} and Si{110}.
- Identification, based on the assumption of applicability of used mathematical model, of certain areas of interest for the SE velocities such as:
    - Areas with different dominating components (i.e. dominating component due to "non-zero" ER of {100}- or {110}-oriented terraces, or due to chain/row removal from the step-edges)
    - Areas on which step-edges of neighbouring facets move in opposite directions.

6. Atomic Level Analysis of Step-based Silicon Surfaces

All discussions in this work so far approached the relationship between the geometry of step-based surfaces and their etch rates. This, rather general, approach provides a reasonable explanation of some of the anomalies present in the anisotropic etching of concave structures. However, this analysis would not be complete without consideration of actual atomic structure of studied surfaces and their interaction with the neighbouring surfaces on atomic level.

6.1. Background Information

The analysis of the step-based surfaces on atomic level is not entirely novel approach. Studies were conducted in order to provide an explanation of the etching mechanism of the surfaces in wet anisotropic etchant, [7], [9], [21], [25], [29], [30]-[31], [33]-[34], [36]-[38],[43]-[47]. In order to help a better understanding of anisotropic etching process and as an ultimate goal of this type of study, variety of computer simulations were attempted, [7], [43]-[47]. One of works in building an anisotropic etch simulator of concave structures, was done by M. A. Gosalvez *et al.*, [43]. The results, based on detailed analysis of the atomic structure of silicon surfaces exposed to the etchant and the effect of "first" and "second" neighbours (atoms), proved to be very accurate.

The experimental data was obtained from a wagon-wheel under-etch experiment on Si{100} wafers using 10wt.% KOH solution at 75°C.

General summary of these results, i.e. experimental versus simulation, are shown in Figure 6-1. The investigation of the end portion of spokes in the wagon well (not shown in the image above) was conducted and may be announced as very accurate, Figure 6-2.

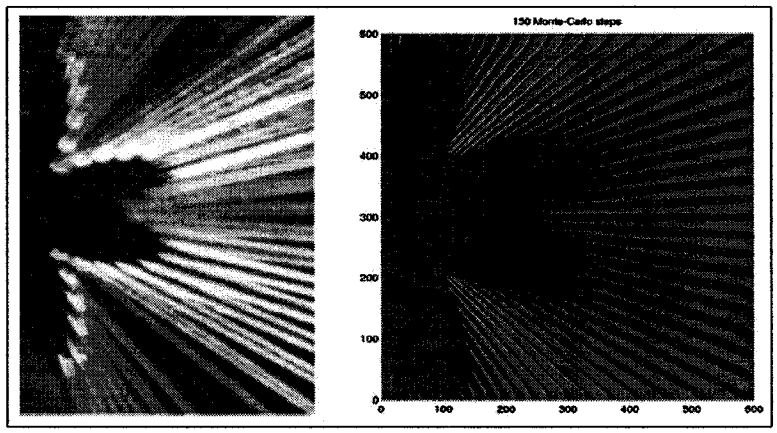

Figure 6-1: Comparison between experiment (left) and simulation for a mask consisting of half of a wagon wheel. The angular distance between two spokes is 5° for the experiment and 3° for the simulation. The planar size of the simulated system is 600 x 600 unit cells (about 0.35 μm x 0.35 μm) and the diameter of the full experimental wagon wheel is 20 mm, of which only a region of about 10mm x 7mm us shown, Figure from [43].

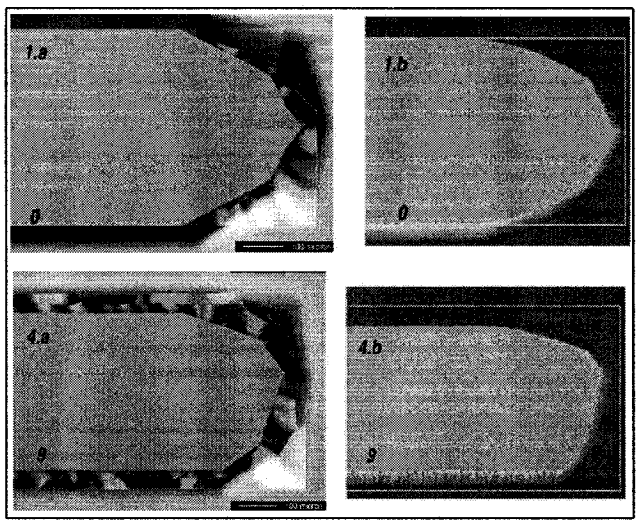

Figure 6-2: Comparison of experimental (left) and simulation results. Under-etching below one end of the oxide islands is shown for the orientations indicated by the lower-left number (degrees) on each frame. The shiny features around the polygonal forms in the experimental frames (left) are due to the wavy shape acquired by the part of the oxide mask which is no longer supported by the silicon crystal. The thin line describing a rectangular contour in the simulation frames (right) represents the extent of the oxide mask (i.e. rectangular islands below which under-etching occurs, Figure from [43].

However, the main portion of this investigation was predominantly concentrated on the convex corners of the wagon-wheel.

Another comment is that as accurate as this investigation is, it is limited to the very small dimensions: 0.35 μm x 0.35 μm sized simulation of the mask versus 20 mm diameter of actual sample[25] (Figure 6-1).

Another group of researchers from China conducted a study of an atomic structure of three basic surfaces, {100}, {110}, and {111} with the view of the mechanism of silicon anisotropic etching in KOH, [44]. This study analysed the actual chemical process and its connection to the atomic structure of each of three basic planes and their activation energies. This model was suggested as a basis for an application in simulation of anisotropic etching of silicon.

A.J. Nijdam *et al.* , [7], in his extensive work analysed the anomalies of anisotropically etched {111} and {100} surface of silicon. Monte-Carlo simulation based on the atomic structure of these surfaces was introduced.

T. Kakinaga, N. Baba, O. Tabata, et *al.*, [45], proposed yet another simulation method based on the atomic structure of basic surfaces of silicon crystal. As a basis for this model, a unit-cell cube was taken as a basic entity, Figure 6-3.

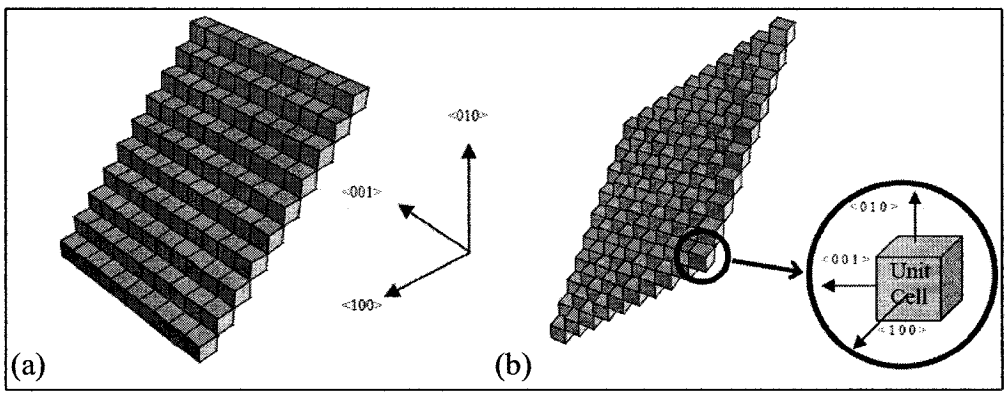

Figure 6-3: The initial surface of (a) (110) plane and (b) (111) plane, Figure from [45].

[25] Obviously this limitation is going to fade away with the progress in computer technology, since the size of simulation in this case is greatly depends on it, (IS)

The atomic structure of each of these three basic surfaces was studied, and probability of removal and influence of dangling bonds of the surface atoms were analyzed.

Analysis of H-terminated surfaces in vicinity of {111}-oriented plane, pre-cut to $\{1\bar{1}2\}$ and $\{\bar{1}\bar{1}2\}$ orientations, etched in 0.02% IPA-doped NH_4F with kinetic Monte Carlo simulations was performed by Hines *et al.*, [30], [36].

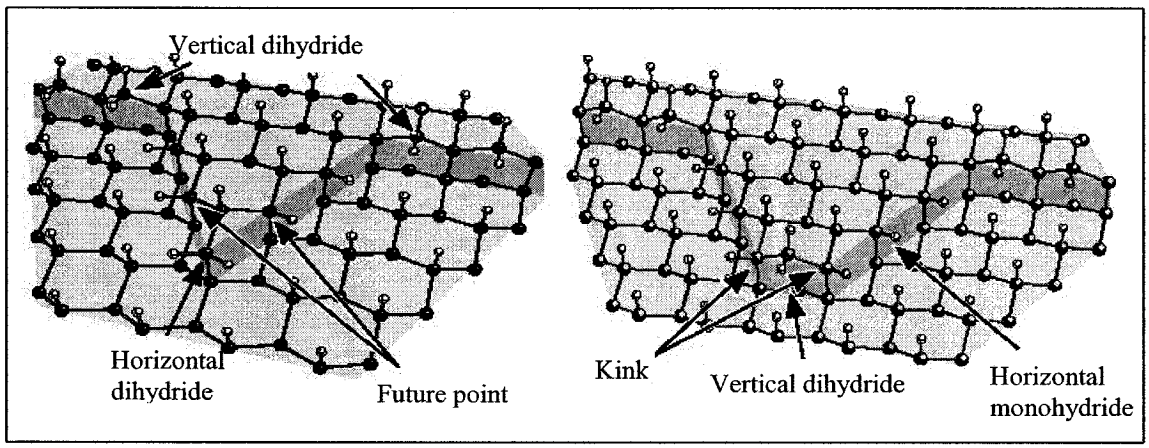

Figure 6-4: Specific sites identified on H-terminated vicinal-{111} Si planes during an anisotropic etch, [30], [36].

Figure 6-4 shows possible atom configurations that differ according to the number of dangling bonds facing the etchant and the orientation of dangling bonds. It is generally believed, [30], [36], and [7], [43]-[45], that silicon atom with larger number of dangling bonds is easier remove from the surface, i.e. etch. Furthermore, dangling bonds are subject to further possible interactions as in the case of vertical dihydrides, located on ledges (step-edges) with vertical monohydrides, basis of the {111}-oriented terraces, Figure 6-4.

P. Jacob *et al.*, [37], develop an atomic reconstruction of K-based surfaces proving that the only certain type of the atoms is located at the step-edge.

A. A. Baski *et al.*, [38], study surfaces in the vicinity of {100} and {111} basic orientations concentrating on the surface reconstruction on the atomic level.

There is yet large list of the researchers and research groups that study the atomic structure of silicon crystal and specifically its surface. However, all of them even though prove the importance, if not necessity, of such analysis, did not concentrate on the surface morphology of the adjacent facets on the sidewalls of concave structures.

This type of analysis follows.

6.2. Angle of Interactions between Chains/Rows on the Step-Edges of Adjacent Facets

It has been argued throughout this work, that there is a possibility of two adjacent facets on the sidewall of a concave structure (spoke) to interact at the boundary (step-edge alignment). It was also stated (see Chapter 2) that the etching of each facet is due to the advancement of the steps along "flat" terraces. However, the advancement of the step-edges was assigned to the "zipping" of respective PBC or K-row at the edge of these steps. Thus the orientation of this PBC or K-row can be considered of essential significance.

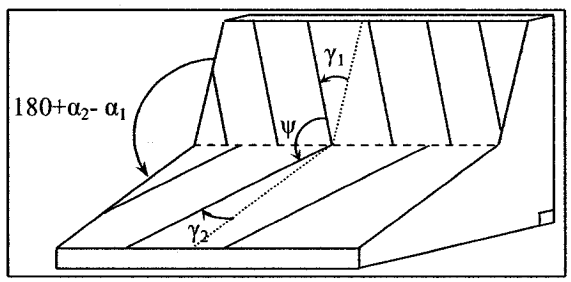

Figure 6-5: Schematic representation of the angles defining the orientation of PBCs and K-rows on adjacent facets, [9].

Two parameters that help to characterize this chain/row orientation need to be defined:

γ - the orientation of a chain/row with respect to a normal to a boundary between two adjacent facets, already was in use (Chapter 5) and

ψ - the angle of interaction between chains/rows of adjacent facets, Figure 6-5.

The first of the defined angles, γ, was calculated for all facets on sidewalls of spokes by Z. Elalamy, [9], and summarised for both Si{100} and Si{110} in graphs of Figure 6-6 and Figure 6-7.

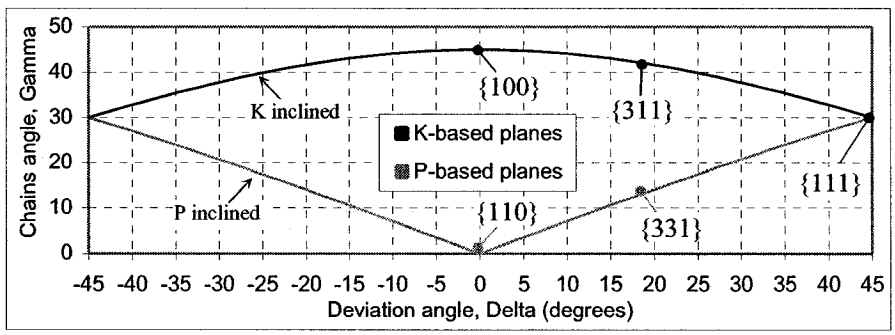

Figure 6-6: Chain/row angle (γ) versus mask edge deviation angle (δ) for Si{100}, [9].

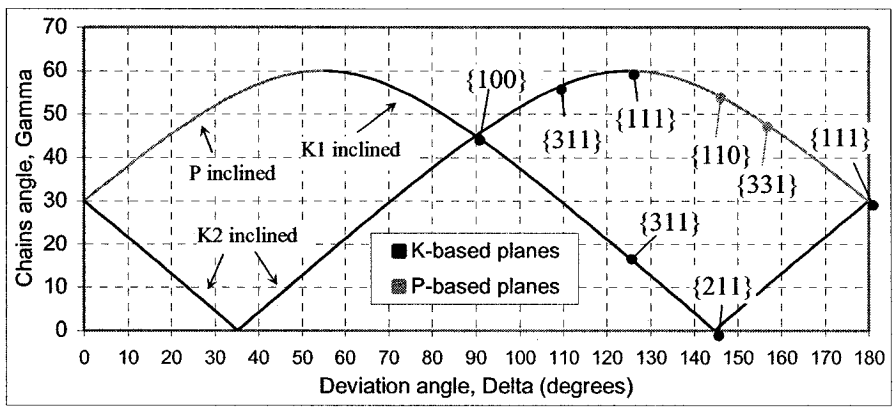

Figure 6-7 : Chain/row angle (γ) versus mask edge deviation angle (δ) for non vertical planes on Si{110}, [9].

The second angle, ψ, as it was discovered by Z. Elalamy, [9], has only three specific values of 60°, 90°, and 120° for different combinations of chains/rows[26].

The definition of this angle provides an interesting phenomena in case of interaction of bottom surface of a spoke in Si{100} with the bottom most facets on the sidewall of this spoke, Figure 6-8. Due to specifics of {100}-oriented surface – orientation of rows changes as atomic monolayers are being etched away – the angle between possible

[26] Because chains are aligned with a <110>-family direction, the angles of interaction (ψ) between chains must all be 60°, 90°, or 120°, [9].

interacting rows on K-inclined facet and rows on {100}-oriented bottom surface are going to alternate between 60 and 120 degrees as illustrated in Figure 6-8(a).

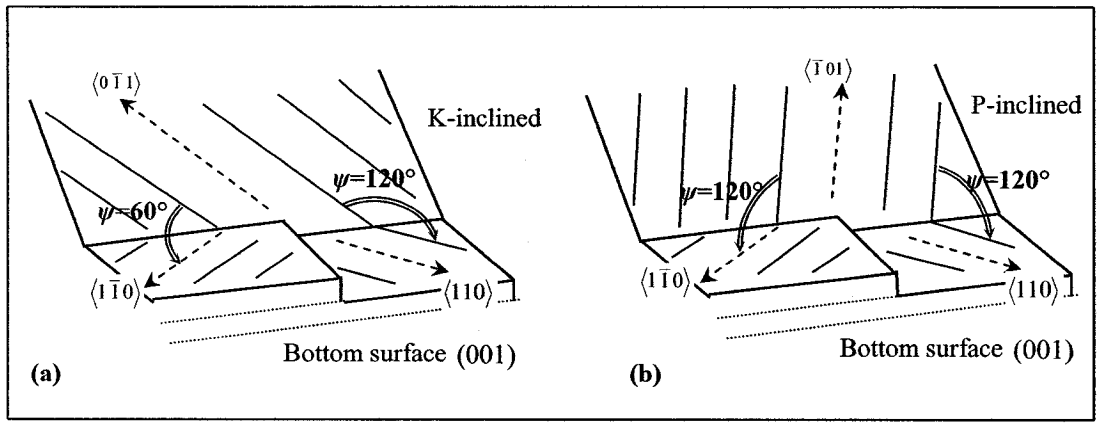

Figure 6-8 : Schematic representation of interaction angles ψ between the bottom surface and: (a) the K-inclined and (b) the P-inclined facets on Si{100}. The variations in ψ angles are due to the fact that K-rows on the bottom surface of Si{100} are alternatively oriented in the $<1\bar{1}0>$ direction and in the $<110>$ direction, as atomic mono-layers are etched, Figure from [9]

However, in case of interaction of P-inclined facet with the bottom {100}-oriented surface, angle ψ does not change, even though the orientation of K-rows on {100} bottom surface alternates its orientation between $<1\bar{1}0>$ to $<110>$, Figure 6-8(b).

These variations in the angle of interaction may be related to different roughness profiles of etched planes.

Continuing the discussion on the angles between interacting chains/rows, it is reasonable to assume that based on two families of planes, K-based and P-based, a maximum of three original combinations are possible for each of these angles (60°, 90°, and 120°), i.e. PBC/PBC, PBC/K-row, and K-row/K-row, making the total count of these combinations nine. However, only seven of said combinations were detected in concave structures of wagon-wheel under-etch experiment, Figure 6-9. As it can be seen in this figure, an additional notation is introduced. For example, K-P-90° means that a K-row of one, K-based, facet interacting with a PBC of another, P-based, facet makes an angle ψ of 90°.

The variety of these combinations suggests that there might be different types of interaction between chains/rows based on these combinations.

The detailed analysis of frequent combinations was conducted and summarized in the following sections.

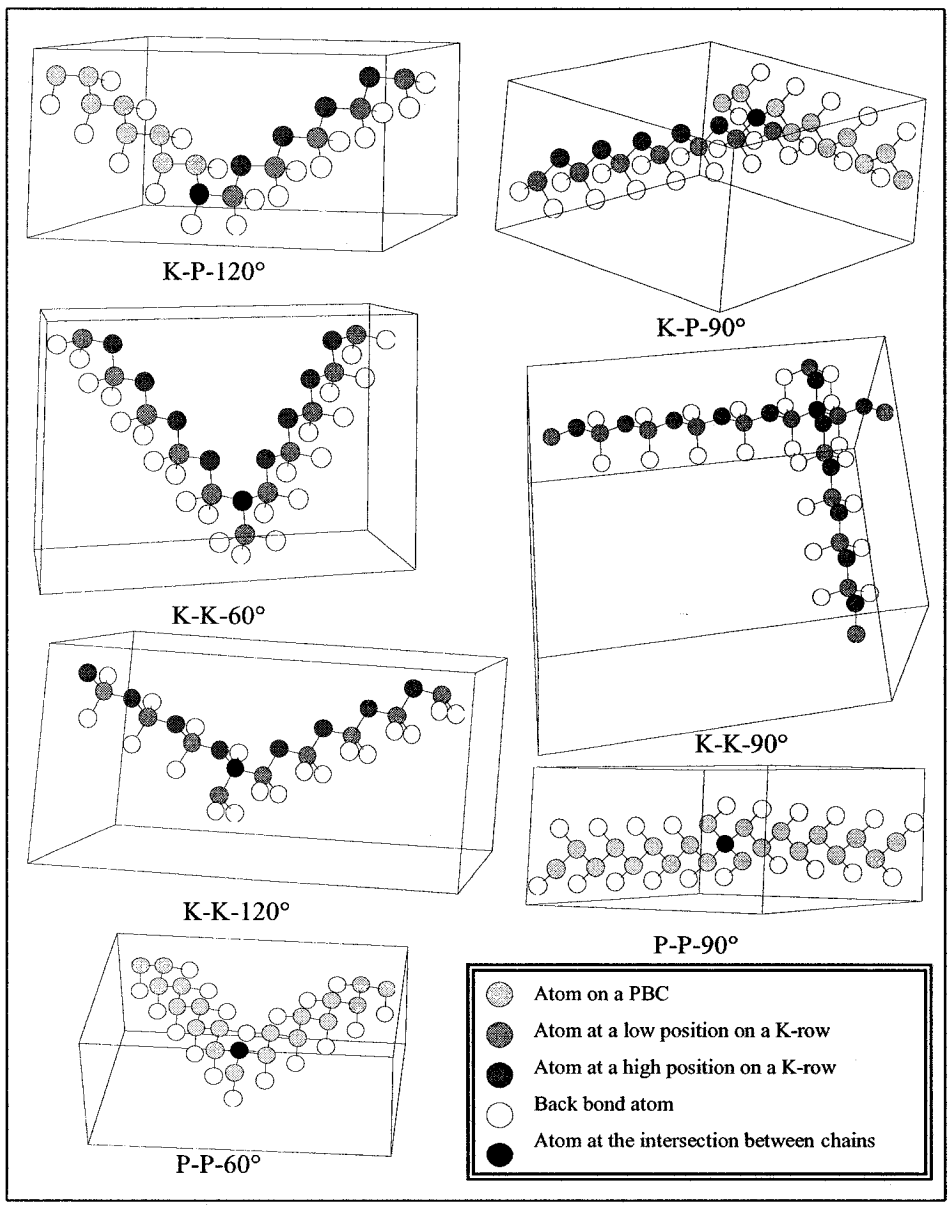

Figure 6-9: The seven possible connections between Chains (PBCs or K-rows), Figure from [9].

6.3. Step Spacing Correspondence

One of the parameters that appeared in above analysis is worth mentioning – step spacing correspondence. This parameter, relative to the geometric features of studied surfaces, may help in better understanding of the interactions between adjacent facets.

6.3.1. Si{100}

Step spacing for all facets, appearing on Si{100} wafer in under-etch wagon-wheel experiment, was determined earlier in this work[27].

Step spacing can be translated into a comparable value, d_1 or d_2, representing step spacing with respect to the boundary between two adjacent facets of the first (in this context top facet out of two adjacent) and second neighbouring facets .

The distance d_1 can be determined from calculations on the step spacing, conducted previously, and the angle γ.

$$d_1 = \frac{s_1}{\cos\gamma} \tag{6.1}$$

where s_1 is the calculated step spacing.

Ratio between two values of d for any combination of two neighbouring facets is interpreted as a step spacing correspondence.

As it can be seen from the data summarized in Table 6-1, all steps for the adjacent facets, ideally, are aligned, i.e. have one-to-one correspondence.

If these steps, or rather step-edges were moving with the same velocity, it may be argued that the resulting profiles should be rather smooth.

---

[27] Chapter 4.

Table 6-1: Summary of step spacing correspondence for all combinations of adjacent facets that may, theoretically, appear on sidewalls of spokes in under-etch wagon-wheel experiment on Si{100}.

δ	Step Spacing, s_1 (Å)				γ, (degrees) K-based planes	γ, (degrees) P-based planes	Step Spacing relative to the boundary between two facets, d_1, d_2, (Å)		Step Spacing Correspondence
	K-inverted	K-inclined	P-inverted	P-inclined			K-inc K-inv	P-inc P-inv	K-inv - P-inv K-inv - P-inc K-inc - P-inv K-inc - P-inc
0					45	0			
1	110.018482	110.018482	155.554093	155.554093	44.99127	0.707089	155.5659	155.5659	1
2	55.0427332	55.0427332	77.7711265	77.7711265	44.96511	1.41407	77.79482	77.79482	1
3	36.7323435	36.7323435	51.8408457	51.8408457	44.92153	2.120835	51.87638	51.87638	1
4	27.5882648	27.5882648	38.8737427	38.8737427	44.8606	2.827277	38.92112	38.92112	1
5	22.1106786	22.1106786	31.0919182	31.0919182	44.78238	3.533287	31.15113	31.15113	1
6	18.4663047	18.4663047	25.9027408	25.9027408	44.68698	4.238756	25.97379	25.97379	1
7	15.8694454	15.8694454	22.1950841	22.1950841	44.5745	4.943575	22.27796	22.27796	1
8	13.9272469	13.9272469	19.4133865	19.4133865	44.44508	5.647633	19.50808	19.50808	1
9	12.4214526	12.4214526	17.2490038	17.2490038	44.29887	6.350819	17.35551	17.35551	1
10	11.2211048	11.2211048	15.5167505	15.5167505	44.13603	7.053022	15.63506	15.63506	1
11	10.2428635	10.2428635	14.0987825	14.0987825	43.95675	7.754129	14.22889	14.22889	1
12	9.43116605	9.43116605	12.9165378	12.9165378	43.76124	8.454025	13.05843	13.05843	1
13	8.74754362	8.74754362	11.9156284	11.9156284	43.54971	9.152596	12.06929	12.06929	1
14	8.1645164	8.1645164	11.0572066	11.0572066	43.32239	9.849724	11.22263	11.22263	1
15	7.66193089	7.66193089	10.3127849	10.3127849	43.07952	10.54529	10.48995	10.48995	1
16	7.22467048	7.22467048	9.66099837	9.66099837	42.82135	11.23918	9.849899	9.849899	1
17	6.84117424	6.84117424	9.08551003	9.08551003	42.54815	11.93126	9.286124	9.286124	1
18	6.50244936	6.50244936	8.57361405	8.57361405	42.2602	12.62142	8.785925	8.785925	1
Crossover in terrace orientation									
19	6.51334946	6.51334946	8.52351002	8.52351002	41.95776	13.30952	8.758765	8.758765	1
20	6.78959456	6.78959456	8.81554765	8.81554765	41.64114	13.99545	9.085244	9.085244	1
21	7.09076972	7.09076972	9.13187276	9.13187276	41.31063	14.67906	9.43999	9.43999	1
22	7.42005486	7.42005486	9.4756662	9.4756662	40.96653	15.36023	9.82668	9.82668	1
23	7.78120873	7.78120873	9.85068797	9.85068797	40.60913	16.03882	10.24966	10.24966	1
24	8.17870689	8.17870689	10.2614152	10.2614152	40.23876	16.7147	10.7141	10.7141	1
25	8.61792101	8.61792101	10.7132213	10.7132213	39.85571	17.38772	11.22621	11.22621	1
26	9.10535487	9.10535487	11.2126121	11.2126121	39.4603	18.05774	11.79351	11.79351	1
27	9.64895889	9.64895889	11.7675402	11.7675402	39.05283	18.72461	12.42517	12.42517	1
28	10.2585558	10.2585558	12.3878306	12.3878306	38.63363	19.38818	13.13256	13.13256	1
29	10.9464257	10.9464257	13.0857659	13.0857659	38.203	20.0483	13.92986	13.92986	1
30	11.7281256	11.7281256	13.8769054	13.8769054	37.76124	20.70481	14.83504	14.83504	1
31	12.6236595	12.6236595	14.7812555	14.7812555	37.30867	21.35755	15.8712	15.8712	1
32	13.6591887	13.6591887	15.8249804	15.8249804	36.84559	22.00636	17.06856	17.06856	1
33	14.8695983	14.8695983	17.0429671	17.0429671	36.3723	22.65106	18.46741	18.46741	1
34	16.3024616	16.3024616	18.4827916	18.4827916	35.88909	23.29149	20.12269	20.12269	1
35	18.0243847	18.0243847	20.2110622	20.2110622	35.39626	23.92746	22.11132	22.11132	1
36	20.1315805	20.1315805	22.3239938	22.3239938	34.8941	24.5588	24.5444	24.5444	1
37	22.7683726	22.7683726	24.9659122	24.9659122	34.38289	25.18532	27.58859	27.58859	1
38	26.1615605	26.1615605	28.3636187	28.3636187	33.86291	25.80683	31.50579	31.50579	1
39	30.689149	30.689149	32.8951198	32.8951198	33.33444	26.42313	36.73248	36.73248	1
40	37.0315541	37.0315541	39.240833	39.240833	32.79775	27.03402	44.05435	44.05435	1
41	46.5496166	46.5496166	48.7616002	48.7616002	32.2531	27.6393	55.04277	55.04277	1
42	62.418643	62.418643	64.6327293	64.6327293	31.70075	28.23876	73.36428	73.36428	1
43	94.1645705	94.1645705	96.3801581	96.3801581	31.14095	28.83217	110.0185	110.0185	1
44	189.417119	189.417119	191.633607	191.633607	30.57395	29.41933	220.0035	220.0035	1
45					30	30	0	0	

However, it was shown in the number of works (Refs. [9],[31],[33]-[35]) that the etch rates of the planes with the same crystal structure, i.e. planes with the same Miller Indices

and step spacing, were different. This was and still is (to certain extend) considered one of the mysteries of etching mechanism.

So, the alignment distance, *d*, described by equation (6.1) for the experimental data obtained in under-etch wagon-wheel experiment was summarized in graph of Figure 6-10.

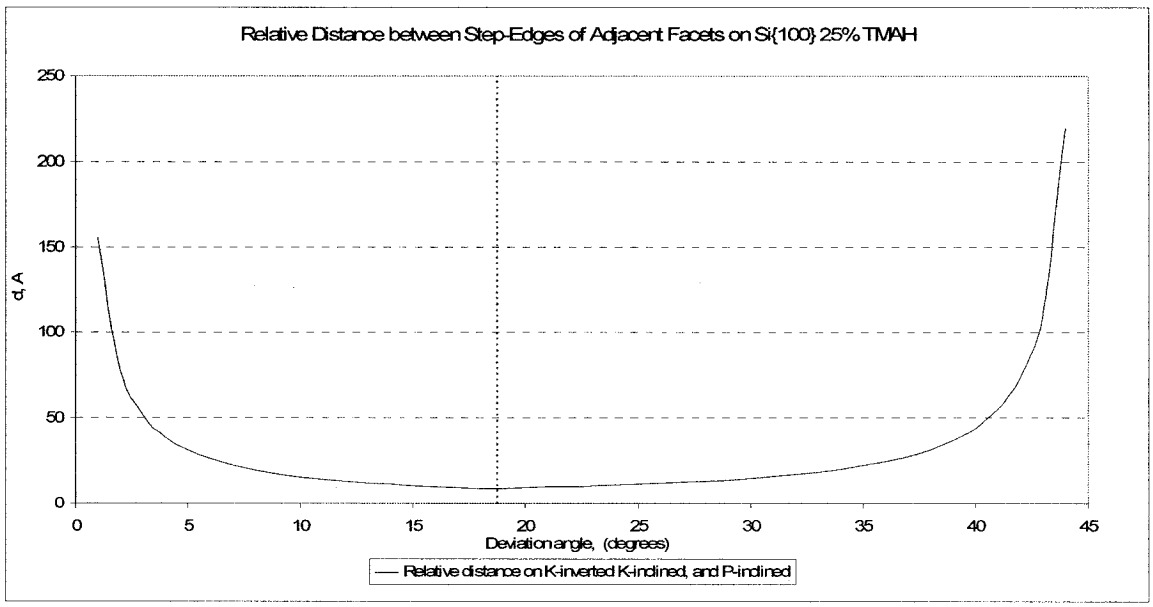

Figure 6-10: Relative distance between the step-edges on adjacent facets with the consideration of respective terrace orientation on Si{100} etched at 25% TMAH.

6.3.2. Si{110}

Step spacing for all facets, appearing on Si{110} wafer in under-etch wagon-wheel experiment, was also determined. Accordingly, the step-spacing correspondence of all possible combinations based on theoretical data (see Figure 5.5 from Chapter 5) was calculated and its values are summarised in Table 6-2.

Table 6-2: Summary of step spacing correspondence for all possible combinations of adjacent facets that may, theoretically, appear on sidewalls of spokes in under-etch wagon-wheel experiment on Si{110}.

δ	Possible combinations between two adjacent facets					
	K1-inc - K2-inc K1-inv - K2-inc K2-inv - K1-inc K2-inv - K1-inv	K2-inc - P-inc K2-inc - P-inv K2-inv - P-inc K2-inv - P-inv	K-vert - K2-inc K2-inv - K-vert	P-vert - K2 - inc K2-inv - P-vert	P-vert - K1-inc K1-inv - P-vert	K-vert - P-inc K-vert - P-inv
1		0.350084178	0.700168356			2
2		0.417450646	0.834901291			2
3		0.447781955	0.895563909			2
4		0.465919519	0.931839038			2
5		0.47847091	0.956941821			2
6		1	2			2
7		1	2			2
8		1	2			2
9		1	2			2
10		1	2			2
11		1	2			2
12		1	2			2
13		1	2			2
14		1	2			2
15		1	2			2
16		1	2			2
17		1	2			2
18		1	2			2
19		1	2			2
20		1	2			2
21		1	2			2
22		1	2			2
23		1	2			2
24		1	2			2
25		1	2			2
26		1.111645319	1.8995675			2.111645319
27		1.289406861	1.775550395			2.289406861
28		1.51572824	1.659748874			2.51572824
29		1.813865469	1.551308803			2.813865469
30		2.224744871	1.449489743			3.224744871
31		2.827681522	1.353646616			3.827681522
32		3.799178533	1.263214795			4.799178533
33		5.627528011	1.177697916			6.627528011
34		10.34577347	1.096657829			11.34577347
35			1.01970628			
36		18.6908827	0.946497979			17.6908827
37		8.111930666	0.876724785			7.111930666
38		5.266229362	0.810110815			4.266229362
39		3.943346834	0.746408307			2.943346834
40		3.178579867	0.685394094			2.178579867
41		2.680006691	0.626866603			1.680006691
42		2.329065683	0.570643281			1.329065683

43		2.06850206	0.516558374			1.06850206
44		2.153033236	0.464461014			1
45		2.414213562	0.414213562			1
46		2.734555378	0.365690162			1
47		3.137004119	0.318775482			1
48		3.658131366	0.273363611			1
49		4.360013382	0.229357094			1
50		5.357159734	0.186666079			1
51		6.886693667	0.145207562			1
52		9.532458724	0.104904729			1
53		15.22386133	0.065686358			1
54		36.3817654	0.027486297			1
55	53.0667328					
56	15.04376131			20.69154694	0.727048652	
57	8.09056714			11.25505602	0.71883846	
58	5.40579583			7.598357067	0.711442721	
59	3.986415342			5.655363044	0.704891147	
60	3.111141019			4.449489743	0.699212988	
61	2.519229543			3.627730938	0.694436711	
62	2.093492488			3.031456479	0.690589656	
63	1.773444256			2.578813723	0.687697696	
64	1.524699164			2.223290638	0.685784908	
65	1.32625751			1.93650065	0.684873259	
66	1.164563925			1.700137172	0.684982332	
67	1.030472685			1.501864151	0.686129091	
68	0.917585895			1.333065479	0.6883277	
69	0.821290816			1.187541065	0.691589403	
70	0.738175713			1.060715443	0.695922472	
71	0.665661287			0.949138329	0.701332216	
72	0.601760268			0.850158755	0.707821057	
73	0.608247394			0.761706244	0.798532766	
74	0.621679584			0.682140151	0.911366357	
75	0.636223396			0.610143601	1.042743701	
76	0.651900624			0.544647359	1.196922399	
77	0.668731581			0.5	1.337463161	
78	0.686735262			0.5	1.373470523	
79	0.705929513			0.5	1.411859027	
80	0.726331203			0.5	1.452662406	
81	0.747956372			0.5	1.495912743	
82	0.770820375			0.5	1.54164075	
83	0.794937989			0.5	1.589875979	
84	0.820323494			0.5	1.640646988	
85	0.846990709			0.5	1.693981418	
86	0.874952994			0.5	1.749905989	
87	0.904223205			0.5	1.80844641	
88	0.934813595			0.5	1.86962719	
89	0.966735672			0.5	1.933471344	
90						

Note that calculations of step correspondence are done with the consideration of the terrace orientation based on the location of an individual plane with respect to each of three basic surfaces: {100}, {110}, and {111}.

However, as it was shown earlier, only selected facets were detected on sidewalls of spokes in wagon-wheel under-etch experiment, Figure 6-11.

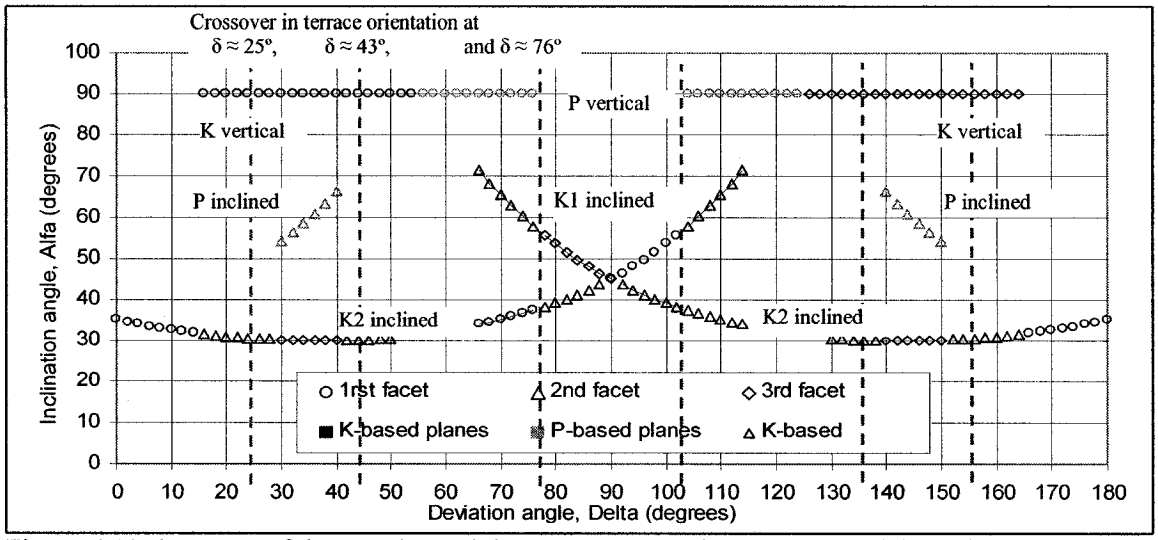

Figure 6-11: Summary of the experimental data representing relative position of the inclination angles of the facets on the side-walls of a spoke with respect to the deviation angle on Si{110} etched in 25% TMAH with the indication of the crossover in the terrace orientation, (Figure from [9]).

The relative step correspondence for our experimental data can be studied on the following intervals, as reflected in Figure 5.21:

- **$0° \leq \delta \leq 25°$:**
  - $0° \leq \delta \leq 15°$ - K2-inclined appears alone, (e.g. see Figure 6-12)

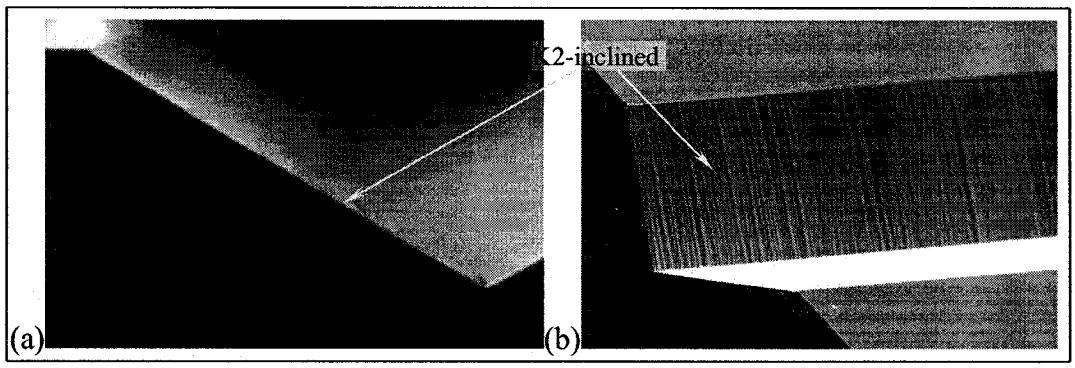

Figure 6-12: SEM images of the sidewall of a spoke on Si{110} etched in 25% TMAH at 80°C at $\delta \approx 12°$ after 1hour 30 minutes etching time (only K2-inclined facet is present) (a) cross-section view and (b) view of a sidewall, [9].

  - $15° \leq \delta \leq 25°$ K-vertical with {100}-oriented terrace – K2-inclined {111}-oriented terrace - **2:1 correspondence**

- **$25° \leq \delta \leq 35.26°$:**

Three facets were detected on this interval: K-vertical, P-inclined and K2-inclined. However, at certain deviation angles, e.g. $\delta = 26°$, only two of these facets can be found, (Figure 6-13).

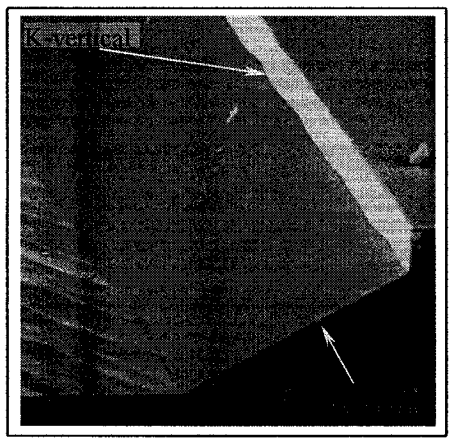

Figure 6-13: SEM images of the sidewall of a spoke on Si{110} etched in 25% TMAH at 80°C at $\delta \approx 26°$ after 1hour 30 minutes etching time (K-vertical and K2-inclined facets are present) view of a sidewall.

- $30° \leq \delta \leq 35.26°$ - K-vertical {111} oriented terrace – P-inclined {110} oriented terrace - **2:1 correspondence**
- Other two combinations possible on this interval with the specifics of the terrace orientations presented in the Table 6-3.

Table 6-3: Summary of step spacing correspondence between two adjacent facets appearance of which based on the experimental data ($30° \leq \delta \leq 35.26°$).

δ	P-inclined {110} oriented terrace – K2-inclined {111} oriented terrace	K-vertical {111} oriented terrace – K2-inclined {111} oriented terrace
26		1 : 1.8995675
27		1 : 1.775550395
28		1 : 1.659748874
29		1 : 1.551308803
30	2.224744871 : 1	
31	2.827681522 : 1	
32	3.799178533 : 1	
33	5.627528011 : 1	
34	10.34577347 : 1	
35	P-inclined → {110}	

- **$35.26° \leq \delta \leq 43°$:**

On this interval, three facets were identified in the under-etch experiment: K-vertical, P-inclined and K2-inclined, (Figure 6-14).

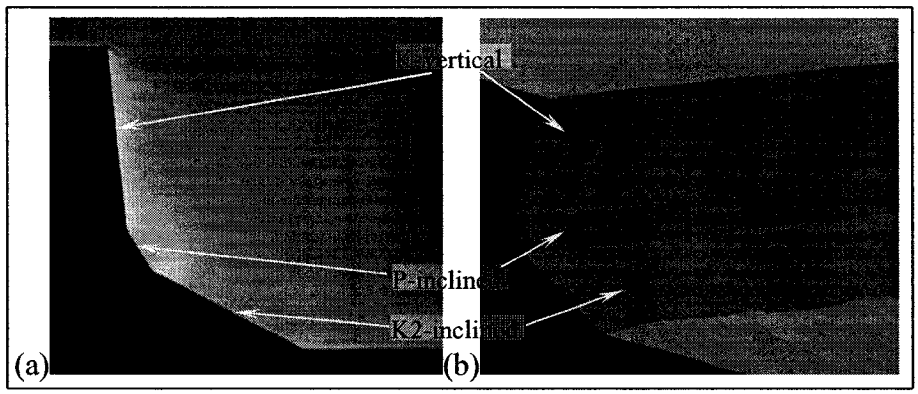

Figure 6-14: SEM images of the sidewall of a spoke on Si{110} etched in 25% TMAH at 80°C at $\delta \approx 39°$ after 1hour 30 minutes etching time (K-vertical, P-inclined and K2-inclined facets are present) (a) cross-section view and (b) view of a sidewall, [9].

Step spacing correspondence for all possible combinations on this interval is presented in Table 6-4.

Table 6-4: Summary of step spacing correspondence between two adjacent facets, appearance of which based on the experimental data ($35.26° \leq \delta \leq 43°$).

δ	P-inclined {110} oriented terrace – K2-inclined {111} oriented terrace	K-vertical {111} oriented terrace – P-inclined {110} oriented terrace
36	18.6908827 : 1	1 : 17.6908827
37	8.111930666 : 1	1 : 7.111930666
38		1 : 4.266229362
39		1 : 2.943346834
40		1 : 2.178579867
41		1 : 1.680006691
42		1 : 1.329065683
43		1 : 1.06850206

- **$43° \leq \delta \leq 54.74°$:**

Two facets were detected: K-vertical and K2-inclined, Figure 6-15.

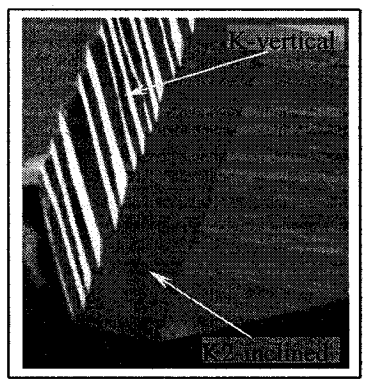

Figure 6-15: SEM images of the sidewall of a spoke on Si{110} etched in 25% TMAH at 80°C at $\delta \approx 44°$ after 1hour 30 minutes etching time (K-vertical and K2-inclined facets are present) view of a sidewall.

Step spacing correspondence between K-vertical and K2-inclined facets on this interval is presented in Table 6-5.

Table 6-5: Summary of step spacing correspondence between two adjacent facets, appearance of which based on the experimental data ($43° \leq \delta \leq 54.74°$).

δ	K-vertical {111}-oriented terrace – K2-inclined {111}-oriented terrace
44	1 : 0.464461014
45	1 : 0.414213562
46	1 : 0.365690162
47	1 : 0.318775482
48	1 : 0.273363611
49	1 : 0.229357094
50	1 : 0.186666079
51	1 : 0.145207562
52	1 : 0.104904729
53	1 : 0.065686358
54	1:0.027486297

- **$54.74° \leq \delta \leq 76°$:**

Three facets were identified on this interval: P-vertical, K1-inclined and K2-inclined, Figure 5-21, Figure 6-11, and Figure 6-16.

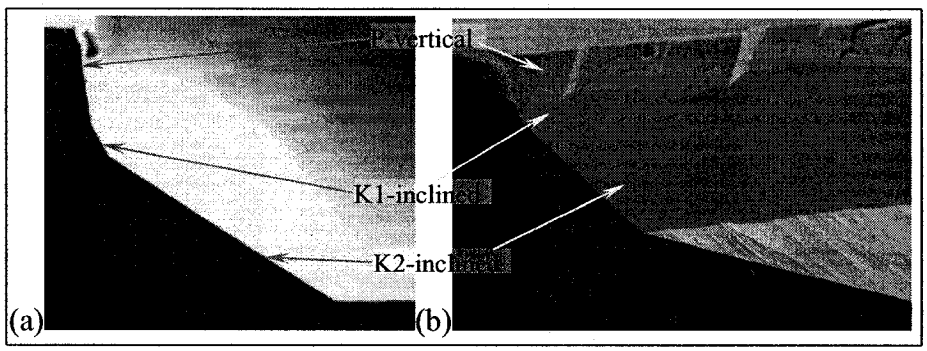

Figure 6-16: SEM images of the sidewall of a spoke on Si{110} etched in 25% TMAH at 80°C at $\delta \approx 69°$ after 1hour 30 minutes etching time (P-vertical, K1-inclined and K2-inclined facets are present) (a) cross-section view and (b) view of a sidewall, [9].

- Step spacing correspondence was determined and its summary for all possible combinations on this interval are presented in the Table 6-6 below.

Table 6-6: Summary of step spacing correspondence between two adjacent facets, appearance of which based on the experimental data ($54.74° \leq \delta \leq 76°$).

δ	P-vertical {111}-oriented terrace – K2-inclined {100}-oriented terrace	P-vertical {111}-oriented terrace – K1-inclined {111}/{100}-oriented terrace[28]	K1-inclined {111}/{100}-oriented terrace – K2-inclined {100}-oriented terrace
55			53.0667328 : 1
56	20.69154694 : 1	1 : 0.727048652	15.04376131 : 1
57	11.25505602 : 1	1 : 0.71883846	8.09056714 : 1
58	7.598357067 : 1	1 : 0.711442721	5.40579583 : 1
59	5.655363044 : 1	1 : 0.704891147	3.986415342 : 1
60	4.449489743 : 1	1 : 0.699212988	3.111141019 : 1
61	3.627730938 : 1	1 : 0.694436711	2.519229543 : 1
62	3.031456479 : 1	1 : 0.690589656	2.093492488 : 1
63	2.578813723 : 1	1 : 0.687697696	1.773444256 : 1
64	2.223290638 : 1	1 : 0.685784908	1.524699164 : 1
65	1.93650065 : 1	1 : 0.684873259	1.32625751 : 1
66	1.700137172 : 1	1 : 0.684982332	1.164563925 : 1
67	1.501864151 : 1	1 : 0.686129091	1.030472685 : 1
68	1.333065479 : 1	1 : 0.6883277	0.917585895 : 1
69	1.187541065 : 1	1 : 0.691589403	0.821290816 : 1
70	1.060715443 : 1	1 : 0.695922472	0.738175713 : 1
71	0.949138329 : 1	1 : 0.701332216	0.665661287 : 1
72	0.850158755 : 1	1 : 0.707821057	0.601760268 : 1
Crossover in terrace orientation for K1-inclined facet			
73	0.761706244 : 1	1 : 0.798532766	0.608247394 : 1
74	0.682140151 : 1	1 : 0.911366357	0.621679584 : 1
75	0.610143601 : 1	1 : 1.042743701	0.636223396 : 1
76	0.544647359 : 1	1 : 1.196922399	0.651900624 : 1

- **$76° \leq \delta \leq 90°$:**

  Two facets were detected in this area – K1-inclined and K2-inclined (Figure 5-21, Figure 6-11, and Figure 6-17).

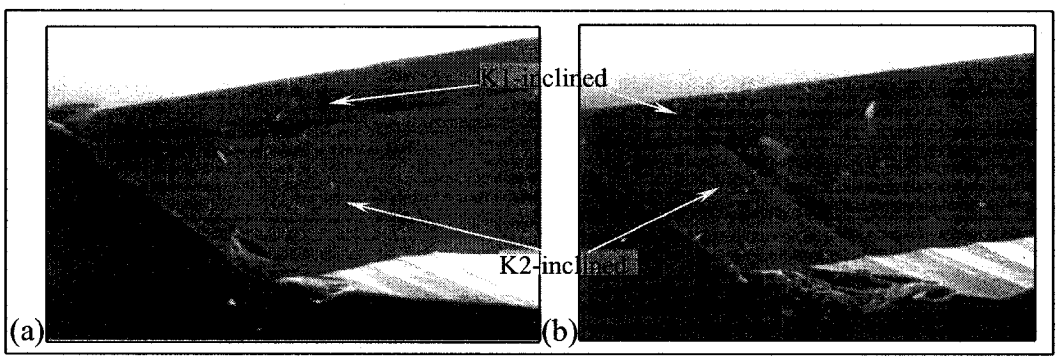

Figure 6-17: SEM images of the sidewall of a spoke on Si{110} etched in 25% TMAH at 80°C after 1hour 30 minutes etching time (K1-inclined and K2-inclined facets are present) (a) $\delta \approx 76°$ and (b) $\delta \approx 78°$.

  - The step correspondence between K1-inclined and K2-inclined facets is summarised in Table 6-7 below:

[28] Shaded cells in this table represent step-spacing correspondence involving K1-inclined facet with {111}-oriented terraces.

Table 6-7: Summary of step spacing correspondence between two adjacent facets, appearance of which based on the experimental data ($76° \leq \delta \leq 90°$).

δ	K1-inclined with {100}-oriented terraces – K2-inclined with {100}- oriented terraces
77	1 : 0.668731581
78	1 : 0.686735262
79	1 : 0.705929513
80	1 : 0.726331203
81	1 : 0.747956372
82	1 : 0.770820375
83	1 : 0.794937989
84	1 : 0.820323494
85	1 : 0.846990709
86	1 : 0.874952994
87	1 : 0.904223205
88	1 : 0.934813595
89	1 : 0.966735672

Now, that the step spacing correspondence is derived, as additional information, the relative distance, *d*, described by equation (6.1) can be summarised for the experimental data obtained in under-etch wagon-wheel experiment, see Figure 6-18.

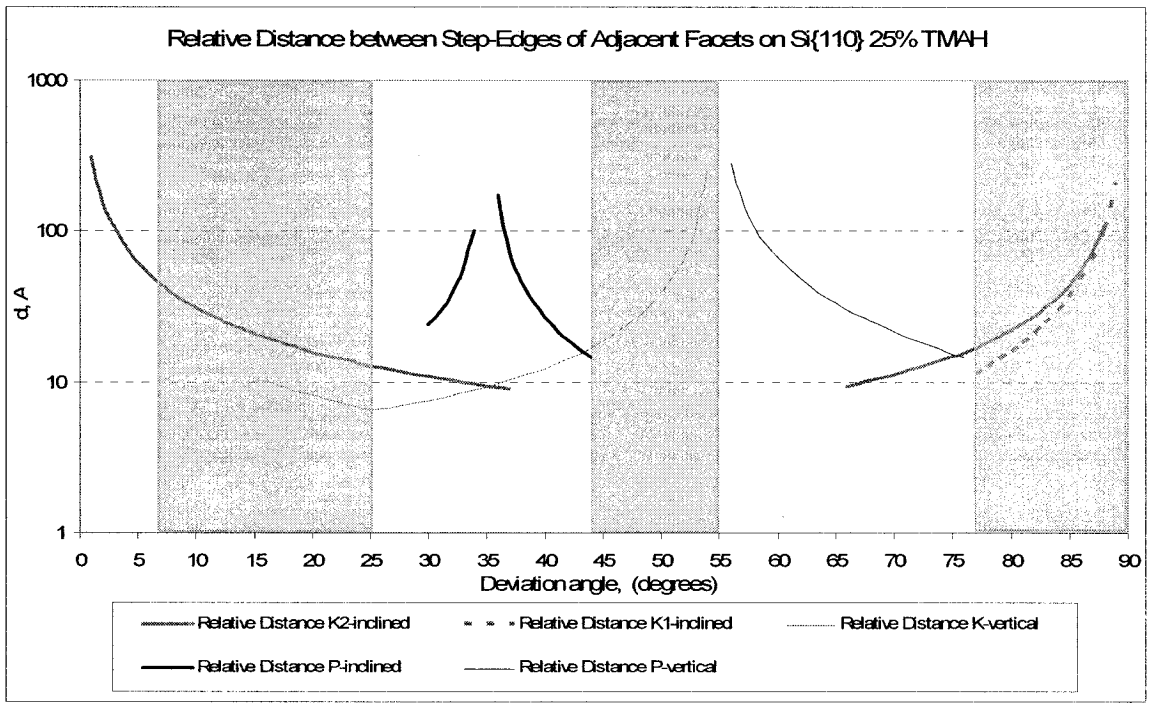

Figure 6-18: Relative distance between the step-edges on adjacent facets with the consideration of terrace orientation on Si{110} etched at 25% TMAH at T = 80°C. Shaded regions represent areas with 1:1, 1:2 and 2:1 step-spacing correspondents.

As it can be seen from Figure 6-18, areas, where step-spacing correspondence is 1:1 or 1:2 (shaded regions in this figure), are signified by a minimal number of facets present

(one, or maximum of two out of five possible facets determined theoretically as illustrated in Figure 3.16)

6.4. K-P-120°, [42]

Reference [42] examines the K-P-120° combination - a case frequently found in under etch experiments, where the zipping chains on adjacent facets are of different types.

The notation K-P-120° stands for an interacting K-row and PBC, located on two adjacent facets and ψ = 120° as the angle between two chains. In its abstract form, the K-P-120° case is illustrated in Figure 6-19.

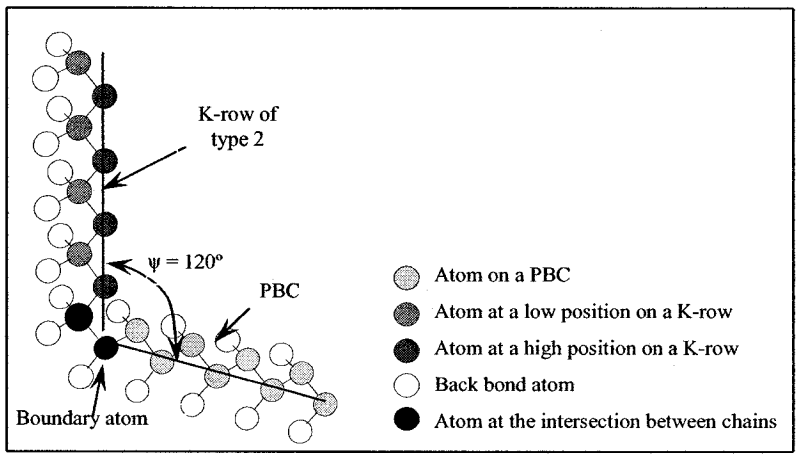

Figure 6-19: Abstract crystal model of the K-P-120° configuration. The K-row and PBC intersect at two boundary atoms, at an angle of 120 degrees.

One very interesting case can be found on Si{110}, etched in 25 wt% TMAH, at the deviation angle δ = 37°, Figure 6-20.

The SEM picture (Figure 6-20(a)) presents a plan view of the sidewall of a spoke that is composed of three facets: the topmost facet is vertical, K-based, with inclination angle α = 90°, referred to as "K-vertical", second from the top facet is P-based, with inclination angle $\alpha \cong 62°$ (theoretically 62.18°), referred to as "P-inclined", and the lower facet is another K-based facet, inclined at $\alpha \cong 30°$, (theoretically 30.01°), referred to as "K2-inclined" or "K2".

The roughness on each facet is aligned with the orientation of the PBC-s and K-rows on the relevant facets. Even though these roughness patterns (in air) are more macroscopic than the few-angstrom-high crystallographic steps, the fact that they are parallel with the crystallographic step edges is consistent with the fundamental assumption of step-based etching in liquid anisotropic etchant.

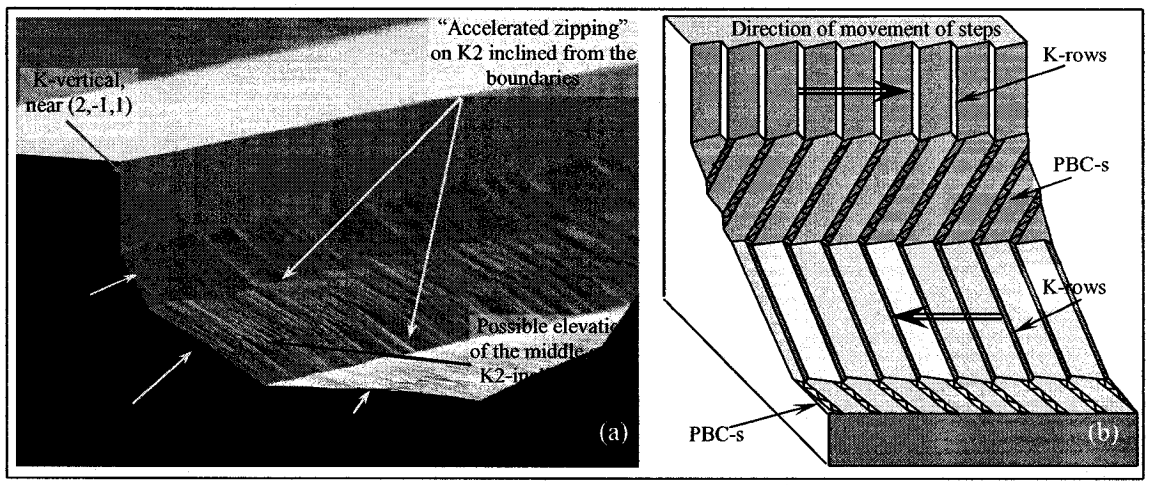

Figure 6-20: (a) SEM picture of a sidewall of a spoke at $\delta = 37°$ on Si{110} etched in 25wt.% TMAH for 3 hours and (b) a schematic representation of the step-based etching surfaces showing relative movement of steps at $\delta = 35.3°$.

Figure 6-20(b) schematically represents the orientation of the crystallographic steps on each of the facets. An interesting property of these facets is that, in the ideal case, the steps are continuous from the top edge of the top most facet across all three facets to the bottom surface of the cavity. The steps alternate in type (in order, from the mask material: kinks, to PBC's, to kinks, to PBC's on the bottom surface of the cavity), each transition being in the K-P-120° configuration, providing opportunity for study of propagation of zipping of different-type-steps across facet boundaries.

Accurate calculations of Miller Indices at $\delta = 37°$ show that the K2-inclined facet in Figure 6-20 is of a MI family very close that of the K-vertical facet, i.e. $(94,\overline{50},50)$ for K2-inclined and (50,50,97) for K-vertical, approximated as $(2\bar{1}1)$ and (112), respectively.

Based on this similarity of the Miller Indices, these two facets could (ideally) have effectively the same crystal features. However, the roughness patterns on these two K-based facets are very different: fairly regular and aligned vertically – as rows of kinks – on K-vertical, and quite unusual on K2-inclined, Figure 6-20(a). On K2-inclined there appear to be two sources of roughness – striations appear to extend from both upper and lower facet boundaries toward the center of the facet. The region in the middle of K2-inclined may be raised slightly (as it appears in the SEM Figure 6-20(a)). In other words, this roughness pattern seems to be consistent with the K2-inclined facet being etched by zipping of chains from each of the facet edges, boundaries with P-based facets (P-inclined and P-bottom). If this "accelerated" zipping process were predominant in the etching of K2 facet, zipping events would be uncorrelated, and would reach the middle of the K2 facet at random times, potentially leading to the disordered roughness pattern seen in the middle of this facet.

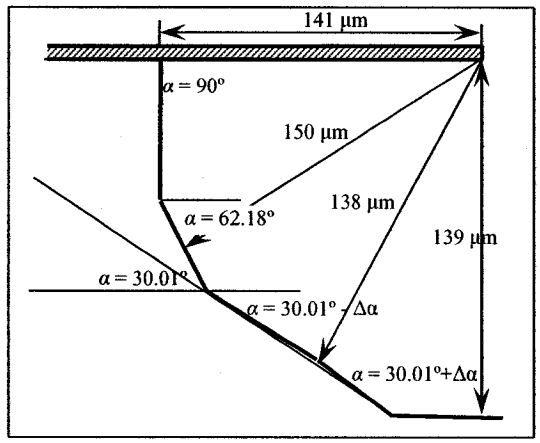

Figure 6-21: Schematic cross-sectional view of the sidewall of a spoke at $\delta = 37°$ on Si{110} etched in 25wt.% TMAH for 3 hours, showing the position of the original mask edge (which was removed prior to the SEM), and estimated etch rates of the various surfaces.

To analyze this case further, relative etch rates of all facets are taken to consideration. Figure 6-21 demonstrates the etch of each of the three facets and bottom surface. The two P-based surfaces, with very similar crystallographic features, are etching at roughly the

same rate (with P-inclined etching slightly faster), and the two K-based surfaces, with very close crystallographic features, are etching at approximately the same rate.

This simplified case, very close to the real case shown in Figure 6-20, was analyzed using an idealized crystallographic representation of the three facet surfaces and the bottom surface of the cavity at $\delta = 35.3°$.

The K-vertical facet and K2-inclined facets are from the same K-based Miller Index family, {211}, with {111}-oriented terraces, and the P-inclined and the bottom surface are from the same P-based Miller Index family, {110}, and the steps are all (in the ideal), continuous across all four surfaces, Figure 6-22.

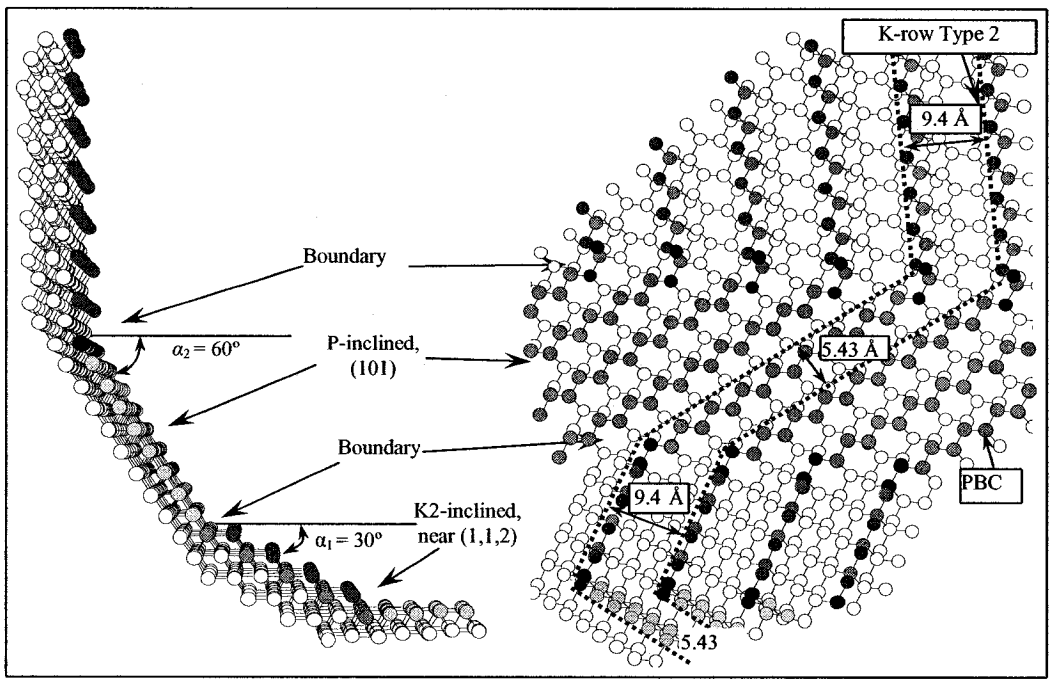

Figure 6-22: Idealized crystallographic reconstruction of the sidewall of the spoke on Si{110} at $\delta = 35.3°$ (a) cross-sectional view, showing the three sidewall facets and cavity-bottom {110} surface; (b) front view, showing the steps on each of the three sidewall facets and cavity bottom, continuous at all facet boundaries.

On K-based facets, the dark-grey and light-grey atoms differentiate between the atoms that are most-directly exposed to the etchant on the K-based step-edge and those that are one atom removed from the edge, respectively. On P-based facets, the grey colours

indicate the atoms on the periodic bond chains (directly exposed to the etchant), Figure 6-22.

On the K-vertical and K2-inclined facets, the step spacing (distance between the two step-edges, similar to the width of the {111}-oriented terraces) slightly deviates from 9.4 Å. Calculation of the EPA gives the following results: 1.11Å for {211} and 1.92Å for {110}, and from the etch rates evident in the Figure 6-21 the frequency of removal of steps on each of the four surfaces in the structure can be determined.

In order to achieve the idealised structure shown in Figure 6-22, with the etch rates shown in Figure 6-21, the step removal rates on the four surfaces are, approximately[29]:

K-vertical, {211} plane with {111}-oriented terraces	$3.74\times10^{5}h^{-1}$
P-inclined, approximated to {110} basic plane	$2.6\times10^{5}h^{-1}$ [30]
K2-inclined, {211} plane with {111}-oriented terraces	$4.49\times10^{5}h^{-1}$
P-bottom, {110} basic plane	$2.41\times10^{5}h^{-1}$ [31]

Note at this deviation angle (δ = 35.3°), steps on each facet correspond approximately one-to-one with the steps on all neighbouring facets, including the bottom of the cavity. But from the comparison of the etch rates of adjacent facets, schematically shown in Figure 6-21, it is clear that the etching of the facets must not propagate through all facet boundaries. Substantially more rows of kinks are removed on the K-based facets that PBC's on P-based facets. Therefore, it is clear that not all zipping events on rows of kinks have propagated through the P-inclined facet, or onto the P-based bottom surface of the cavity. Note if we consider the P-based planes to be ideal {110} planes, there are no steps moving. If we consider them to be tightly-spaced P-steps on minimal (degenerate) {111}

[29] Detailed calculations of step removal rates or, frequency of removal, are presented in Appendix II.
[30] These removal rates account for all PBC-s removed on the P-based surfaces, as if they are on {111} terraces.
[31] Difference in the Frequency of Removal of PBC's on basic {110} oriented surfaces are due to known phenomenon observed in wet anisotropic etch experiment – planes with the same Miller Indices, i.e. same atomic structure of the surface, exposed to the etchant have different etch rates.

terraces, then they can be considered to move in either direction, and can be consistent with each of the real step movements on the adjacent K-based facets, going opposite directions.

A slightly different situation, at the actual $\delta \approx 37°$, as illustrated in SEM picture of Figure 6-20(a), needs to be addressed[32]. At this deviation angle, the P-inclined facet has MI about $(15,\bar{1},15)$, ~2.7° rotated from the (101) plane, represented by a surface with {110}-oriented terraces.

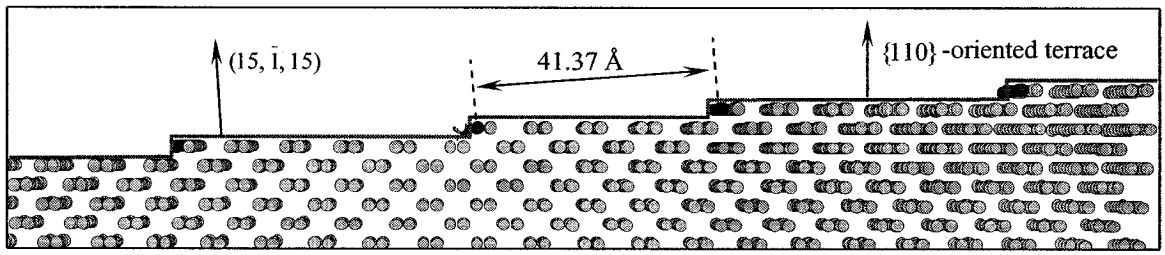

Figure 6-23: Crystallographic reconstruction of P-inclined plane with MI $(15,\bar{1},15)$ appearing on sidewalls of a spoke[33] on Si{110} wafer etched in 25% TMAH at 80°C at $\delta \approx 37°$.

The average spacing between PBC's on the step-edges of {110}-oriented terraces on this P-based surface is 41.37 Å. (The spacing of PBC's on each {110}-oriented terrace is 5.43 Å, PBC spacing calculated for an ideal {110} surface).

In this case the frequency of removal of PBC-s from the step-edges was determined using an approximation method of etch rates separation into two components (equation of the line approximation for chain/row removal from the step-edges with a transition zone[34]). Thus, the component of FR due to PBC removal from SE, for P-inclined facet detected

---

[32] Note also that Figure 6-20(a) is nominally $\delta \approx 37°$, but there could be some error in the deviation angle value and it could be in the range of 35 - 36°.

[33] Please note, that the actual plane reconstructed in this figure has MI {10, 1, 10}. The reason for such inconsistency in the fact that the reconstruction of actual {15, 1, 15} surface was impossible due to the limitations of a software used for reconstruction. However, the only difference would be in the terrace width as it appears in this figure: much larger for {15, 1, 15} plane. There would be no difference in terrace orientation.

[34] See Chapter 5.

on sidewall of a spoke at $\delta \approx 37°$, is estimated approximately $4.2 \times 10^5 h^{-1}$. This value is comparable to the FR of K-based facets in this configuration. However, another parameter needs to be taken into consideration – the Step-Edge Velocity. The values of relative SE velocities of the surfaces in question are as follows:

K-vertical, {211} plane with {111}-oriented terraces: $-188 \mu m/h$

P-inclined, $(15,\bar{1},15)$ plane with {110}-oriented terraces: $407 \mu m/h$

K2-inclined, {211} plane with {111}-oriented terraces: $142 \mu m/h$[35]

Note that the minus sign for the SE velocity of K-vertical facet indicates that this facet is moving in the direction opposite to P-inclined and K2-inclined (steps on P-inclined and K2-inclined facets move in the same direction). It is also evident that the SE velocity of P-inclined facet is roughly (more than) double of SE velocities on K-based surfaces.

Table 6-8: Summary of the specifics for sidewall facets detected at deviation angle $\delta \approx 37°$ on Si{110}.

	K-vertical {111}-oriented terrace	P-inclined {110}-oriented terrace	K2-inclined {111}-oriented terrace
Inclination angle, α	90°	62.18°	30.01°
MI	{1.88, 1, 1}	{15.22, 1, 15.22}	{1, 1, 2.06}
MI approximation	{211}	{166}	{112}
Step-spacing, Å	10.29	41.37	9.02
FR component due to chain/row removal from the step-edges, h^{-1}	4.15×10^5	4.24×10^5	4.28×10^5
Step-spacing correspondence with adjacent facet	1 : 1		
Relative Step-Edge Velocity, *μm/h*	-188	+407	+142[36]
Angle of a plane with respect to {111} surface	$\theta_K = 17.74°$	$\theta_P = 32.61°$	$\theta_K = 20.34°$
Angle of a plane with respect to basic {100} or {110} surface	~37°	~2.7°	~34.4°
Canonical Etch Rates, *μm/h*	~50.8	43.75	52.9
Experimental Etch Rates, *μm/h*	42	36.2	49.5

All parameters relevant to the studied case of K-P-120° combination found on Si{110} at deviation angle $\delta \approx 37°$ are summarised in the Table 6-9.

[35] The difference in the magnitude of the step-edge velocity of planes with the same Miller Indices, is assigned to the etch rate phenomena – different etch rates for planes with the same crystal structure exposed to the etchant.

[36] The "+" or "-" indicate a relative direction of movement of steps. Different signs indicate steps movement in opposite directions.

This information may be interpreted in the following way:

- K-vertical and P-inclined – step-edges move in opposite directions with the step-edge velocity on P-inclined approximately twice of that on K-vertical. The absence of any significant features at the boundary between these two facets (Figure 6-20(a)) may be considered as an indication of none or insignificant interaction.
- P-inclined and K2-inclined – step edges move in the same direction with the step-edge velocity of P-inclined almost three times larger than the velocity of step-edges on K2-inclined. The step-spacing correspondence for the step edges on these two facets is (ideally) approximately 1:8. Roughly one out of eight K-rows on the K2-inclined facet interacts with a PBC on a step-edge on the P-inclined facet, leaving seven other K-rows to have possible interaction with PBC's on {110}-oriented terrace. Due to the fact that the etch rate of {110}-oriented terraces is not negligible, the probability of nucleation of a defect on a PBC on this terrace is large, followed by zipping of this PBC towards an interacting K-row on the K2-inclined facet. This may be a cause of the roughness profiles, evident from Figure 6-20(a).

With this in mind, one can examine more closely the atomic configurations at ideal K-P-120° facet boundaries, to determine whether the bonding configurations would favour zipping from K-based to P-based surfaces, or P-based to K-based surfaces.

For the analysis in this work, it is assumed that etching process of a PBC or K-row begins by the removal of one atom, and then continues by rapid propagation (zipping) to adjacent atoms in both directions, Figure 6-24(a) and (b).

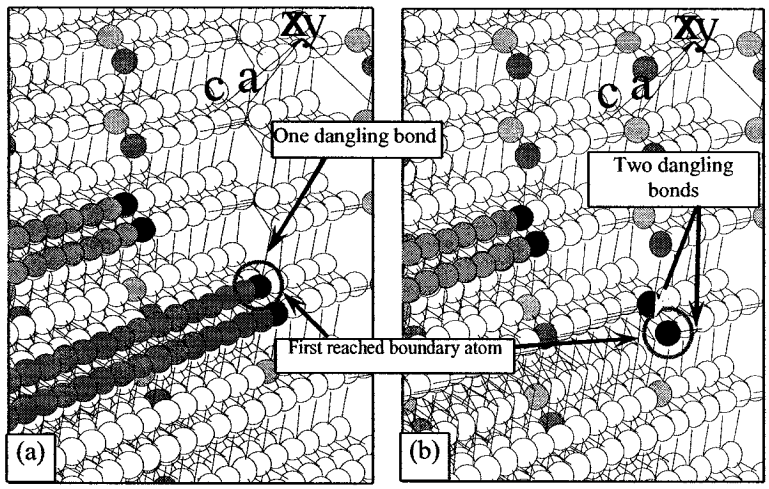

Figure 6-24: Crystallographic reconstruction of a sidewall of the spoke on Si{110} at $\delta = 35.3°$ (a) the result of a zipping process: a K-row has been removed, not including boundary atoms shared with the intersecting PBC; and (b) the result of a zipping process, where a PBC has been removed, not including boundary atoms shared with the intersecting K-row. In each of (a) and (b), another intersecting pair of K-row and PBC is shown for comparison with the zipping chains.

The black-coloured atoms (see Figure 6-22 and Figure 6-24(a), (b)) represent the atoms common to both intersecting chains. These are defined to be the "boundary atoms", shared by both intersecting chains, whose bonding configuration changes when one of the chains disappears without yet removing any atoms on the other chain. The black-colored boundary atoms are indicated in pairs, because the first-reached shared atom is different depending on the direction of zipping (zipping from the P-based chain vs. zipping from the K-based chain).

Suppose that "zipping" begins in the K-vertical facet, not at the facet boundary, and propagates toward a facet-boundary (black) atom. Once the process reaches the boundary atom, what is the likelihood to continue zipping across the boundary to the connecting P-based chain of the adjacent facet? Figure 6-24(a) shows the resulting structure after the K-based chain has been removed. In this case, the first-reached boundary atom has one dangling bond, two bonds to other atoms in the connecting PBC including one bond to the other black-colored atom, and one bond to an atom which has no dangling bonds.

This is the same as any typical atom in a PBC. Therefore, it is not likely that zipping from a K-based chain to a P-based chain will be automatic.

Now, suppose that "zipping" begins in the P-inclined facet, not at the facet boundary, and propagates toward a facet-boundary (black) atom. Once the process reaches the boundary atom, what is the likelihood to continue zipping across the boundary to the connecting K-based chain of the adjacent facet? Figure 6-24(b) shows the resulting structure after the P-based chain has been removed. In this case, (assuming that the row of kinks is of the type shown in Figure 2-7(b), the first-reached boundary atom is not the same as that reached in Figure 6-24(a). It is the other (lower-right) black-colored boundary atom in Figure 6-24(b). After removal of the P-based chain, the first-reached boundary atom has two dangling bonds and two bonds to light-grey-colored atoms in the connecting K-row. Neither of these light-grey-colored atoms has dangling bonds.

While (in the idealized silicon lattice), this is the same as any other atom in a K-row, it may be important that this is at the end of a K-row. Note that the under etch experimental data indicates that K-rows must zip. In order to zip freely, this configuration at the end of a K-row must be relatively weakly bound. The mechanism of zipping may involve surface reconstruction. If there is surface reconstruction on such K-rows, then the reconstruction is likely to be different here at the end of the row in proximity of the adjacent P-based facet. Therefore, one may hypothesize that zipping from a P-based chain to a K-based chain may be more likely than from K-based to P-based. The same arguments may be applied for the boundary between P-inclined and K2-inclined facets, and between the P-bottom and K2-inclined facets, since the geometry of the boundary atoms is the same. The observed roughness patterns (Figure 6-20(a))

support the hypothesis that zipping from P-based to K-based facets may be favored. For this example, (Figure 6-20 - Figure 6-24) this notion is also consistent with the calculated relationships between step removal frequencies on the different exposed surfaces. Substantially more K-based steps are removed than are P-based steps, consistent with steps on K-based surfaces removed both by processes initiated on the K-based surfaces and by propagation from adjacent facets.

Summarizing the above stated, the K-P-120° step-interaction configuration at a boundary between facets on under-etched surfaces for a particular case of under etching of Si{110}, three factors support the hypothesis that zipping is more favored from P-based steps to K-based steps than from K-based steps to P-based steps.

1) Roughness patterns on one of the K-based facets are consistent with step-based zipping independently from each of the two facet boundaries;
2) Analysis of the configuration of boundary atoms for the K-P-120° intersection in the ideal crystal lattice suggests less-stable boundary atoms when zipping from the P-based side.

Another case of K-P-120° is illustrated in SEM picture of Figure 6-25(b)-(d) may be found at deviation angle $\delta \approx 9°$ on Si{100}. This case (Figure 6-25(b)) illustrates two K-P-120° interactions:

- between K-based inclined facet with Miller Indices of approximately {161} (precise {1, 6.314, 1}) with {100}-oriented terraces and P-based inclined facet with {166} Miller Indices (precise {1, 6.314, 6.314}) and {110}-oriented terraces,
  between P-inclined facet and {100}-oriented bottom surface.

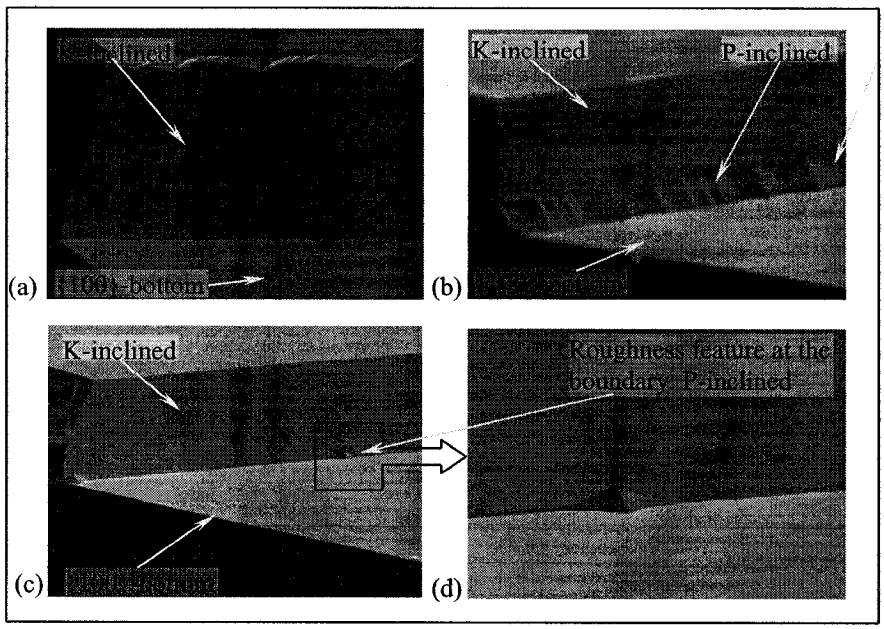

Figure 6-25: SEM picture of sidewalls of spokes on Si{100} etched in 25% TMAH for 5 hours (a) at $\delta \approx 37°$, where K-inclined facet is interacting with the bottom {100}-oriented surface after 5 hours etching time, (b) at $\delta \approx 9°$, where P-inclined facet interacts with the bottom {100}-oriented surface after 50 minutes etching time, (c) at $\delta \approx 9°$, after 5 hours etching time where P-inclined facet disappears, leaving roughness-like features at the boundary between K-inclined and the bottom{100}-oriented surface, and (d) close up of a roughness feature (P-inclined facet) at the boundary between K-inclined and bottom {100}-oriented surface at $\delta \approx 9°$.

All relevant parameters are summarised in the Table 6-9.

Table 6-9: Summary of the specifics for K-inclined and P-inclined planes located on sidewall of spoke at deviation angle $\delta \approx 9°$ on Si{100}

	K-inclined, {100}-oriented terrace	P-inclined, {110}-oriented terrace
Inclination angle, α	81.11°	45.35°
MI	{1, 6.314, 1}	{1, 6.314, 6.314}
MI approximation	{161}	{166}
Step-spacing, Å	12.4	17.14
FR component due to chain/row removal from the step-edges, h^{-1}	3.91×10^5	4.56×10^5
Step-spacing correspondence with adjacent facet	1 : 1	
Relative Step-Edge Velocity, *μm/h*	+209.73	+249.41
Angle of a plane with respect to {111} surface	$\theta_K = 42.11°$	$\theta_P = 28.87°$
Angle of a plane with respect to basic {100} or {110} surface	~12.63°	~6.39°
Canonical Etch Rates, *μm/h*	40	47.5
Experimental Etch Rates, *μm/h*	34.58	37.49

It was shown earlier (see Chapter 5) that the steps on both types of facets on Si{100} wafer move in the same direction for all deviation angles with almost the same step-edge velocity, see Table 6-9. Based on removal frequency component due to chain/row

removal from the step-edges, there are more steps removed from P-inclined facets compared to K-inclined, see shaded cell in Table 6-9 (above).

From the inspection of roughness features on K- and P-inclined adjacent facets (see Figure 6-25(b)) there is no direct evidence of their interaction. However, after long etching time (5 hours) the P-inclined facets nearly disappears, (Figure 6-25(c) and (d)), which may be assigned to its higher etch rate, (see Table 6-9).

The roughness features on K-inclined and P-inclined facets are also may be compared to the roughness features on the same set of adjacent surfaces but at different deviation angle, $\delta \approx 5°$, Figure 6-26(a)-(d).

Details of all parameters for K- and P-inclined facets at this deviation angle are summarized in Table 6-10.

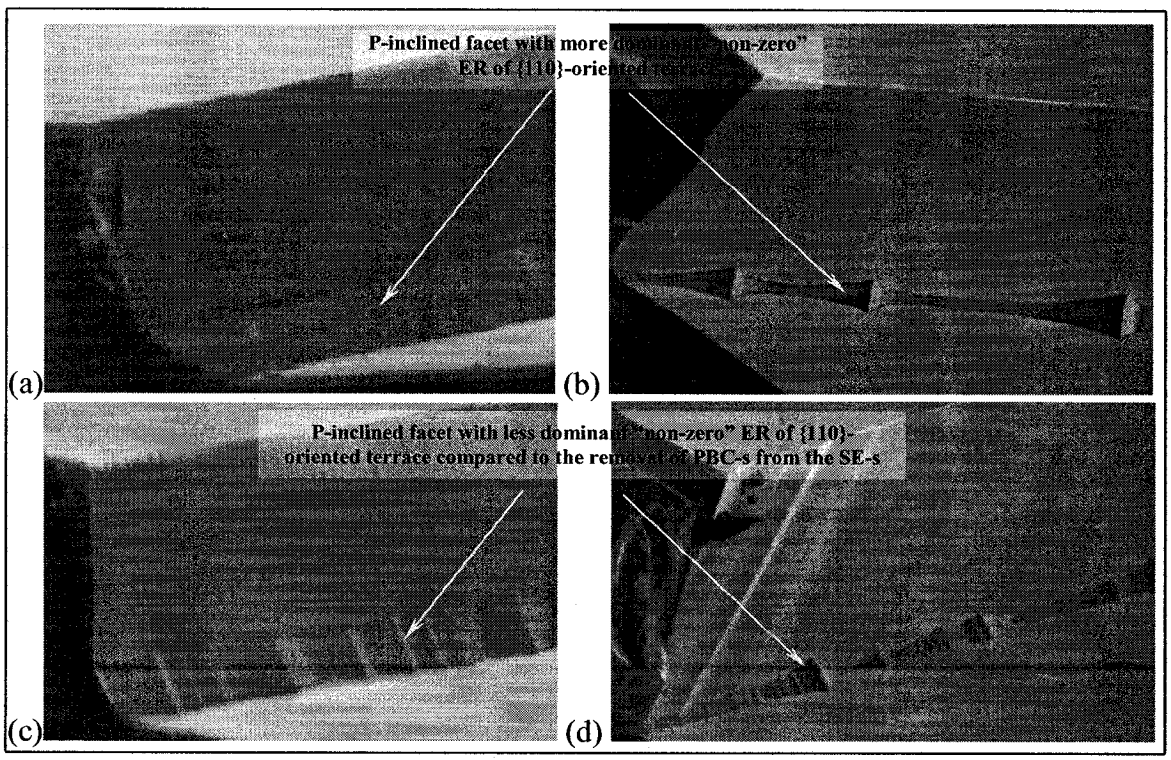

Figure 6-26: SEM images of the sidewall of the spoke (a) at $\delta \approx 5.1°$ for 50 minutes etching time, (b) $\delta \approx 5.5°$ for 3 hours etching time presenting the P-inclined facet in the area of possible dominating influence of "non-zero" ER of {110}-oriented terrace, and (c) at $\delta \approx 9.1°$ for 50 minutes etching time, and (d) $\delta \approx 9.5°$ for 3 hours etching time presenting the P-inclined facet in the area of dominant influence of removal of PBC-s from the step-edge, [9].

Analyzing the morphology of P-inclined facet at these two deviation angles, Figure 6-26, a distinct difference in the roughness profiles may be observed. Referring to the approximation model (Chapters 4 and 5), these differences may be interpreted in the following way: for a plane in the vicinity of a basic surface, {110} in case of P-inclined, non-zero etch rate of {110}-oriented terrace has a larger influence on the plane advancement, compared to PBC's removal from step-edges, see P-inclined facet at $\delta \approx 5°$ ~3.54° rotated from {110} shown in Figure 6-26(a) and (b) – terrace width ~31Å. As a plane (P-based in this case) rotates further away from {110} surface, {110}-oriented terraces reduce in size (terrace width ~17 Å), and their non-zero etch rate will become less dominant compared to the PBC removal from the step-edge, see P-inclined facet at $\delta \approx 9°$, ~6.39° rotated from {110} shown in Figure 6-26(c) and (d).

Table 6-10: Summary of the specifics for K-inclined and P-inclined planes located on sidewall of spoke at deviation angle $\delta \approx 5°$ on Si{100}

	K-inclined, {100}-oriented terrace	P-inclined, {110}-oriented terrace
Inclination angle, α	85.02°	45.11°
MI	{1, 11.43, 1}	{1, 11.43, 11.43}
MI approximation	{1, 11, 1}	{1, 11, 11}
Step-spacing, Å	22.11	31.09
FR component due to chain/row removal from the step-edges, h^{-1}	3.87×10^5	4.57×10^5
Step-spacing correspondence with adjacent facet	1 : 1	
Relative Step-Edge Velocity, *μm/h*	+209.13	+248.699
Angle of a plane with respect to {111} surface	$\theta_K = 47.68°$	$\theta_P = 31.72°$
Angle of a plane with respect to basic {100} or {110} surface	~7.05°	~3.54°
Canonical Etch Rates, *μm/h*	28.5	43.75
Experimental Etch Rates, *μm/h*	28.89	33.23

This difference in dominating component may be responsible for the roughness profiles of P-inclined facets illustrated in Figure 6-26.

Similar discussion applies to K-based inclined surface adjacent to P-inclined. However, there is no significant difference in the surface morphology for K-inclined plane at $\delta \approx 5^{\circ}$ compared to K-inclined at $\delta \approx 9^{\circ}$ can be observed from the SEM pictures of Figure 6-26. If earlier discussion of the dominating component were applied in this case[37] the following may be stated: K-inclined surfaces rotated further away from basic {100}-oriented plane (~7.07° at $\delta \approx 5^{\circ}$ and ~12.63° at $\delta \approx 9^{\circ}$) which is almost double of the angle of rotation of P-inclined surface from basic {110}-oriented plane (~3.54° at $\delta \approx 5^{\circ}$ and ~6.39° at $\delta \approx 9^{\circ}$). This fact may be interpreted that at the smaller deviation angle studied here, $\delta \approx 5^{\circ}$, K-inclined facet already reached the area, (due to its geometric position within the crystal) where the influence of "non-zero" ER of {100}-oriented terraces becomes less influential on overall etch rate of this surface. Thus, keeping applied mathematical model in mind, it may be said that in these two cases (illustrated in Figure 6-26 and Table 6-9 and Table 6-10) ER of K-inclined facet influenced mostly by the K-row removal from the step-edges, and to a lesser degree by a "non-zero" ER of {100}-oriented terrace, see Figure 5.12.

.

[37] Dominating component due to the "non-zero" etch rates of {100}- or {110}-oriented terraces in the vicinity of these basic (i.e. {100} and/or {110} surfaces) used in mathematical model in Chapter 5 and related to the physics of the etching process here.

6.5. K-K-90°, [33]

Similar analysis was done for another chain/row combination - K-K-90°, where two rows of kinks on adjacent facets intersect at 90°, Figure 6-27. Reference [33] examines this case.

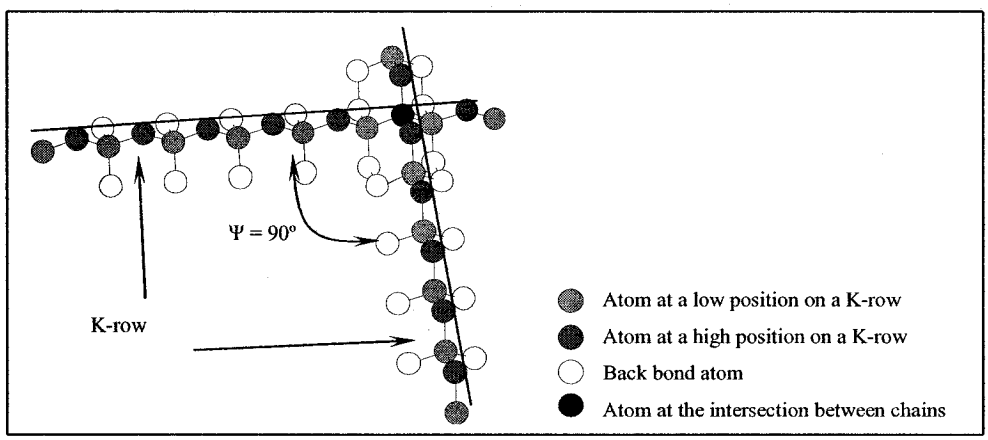

Figure 6-27: Abstract crystal model of the K-K-90° configuration. The K-rows intersect at a boundary atom, at an angle of 90°.

Note that in K-K-90°, the two zipping chains on adjacent facets are of the same type. At any given time during etching, one of the K-rows is "lower" and the other is "higher". However, if one of the intersecting K-rows is removed by "zipping" then the other (previously "lower") K-row on the other facet, would then be "higher".

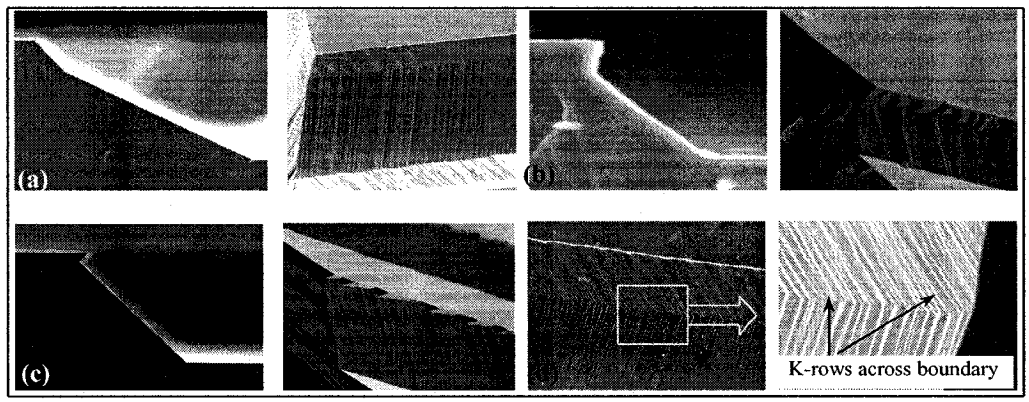

Figure 6-28: SEM of under-etched surfaces at (a) $\delta \approx 70°$ on Si{110}, etched in 25% TMAH, etching time = 5 hours, (b) $\delta \approx 26°$ on Si{100}, etched in 19% TMAH, etching time 25 minutes,(c) $\delta \approx 37°$ on Si{100}, etched in 25% TMAH, etching time 5 hours, and (d) $\delta \approx 84°$ on Si{110}, etched for 5 hours in 25% TMAH, showing the orientation of K-rows and their possible interaction

K-K-90° configuration appears in several conditions during under-etch experiments on both Si{110} and Si{100}.

Several cases of such interacting facets are found experimentally. Even though the basic configuration of step intersection on the adjacent facets involves the same K-K-90° configuration, there are dramatic differences in the morphology of the etched facets, Figure 6-28. While in at least one case it appears (from the roughness patterns) that the zipping of steps propagates across the facet junction, (Figure 6-28(d)), in other cases such zipping seems unlikely. One case of K-K-90° below, located on sidewalls of a spoke located at deviation angle $\delta \approx 70°$ on Si{110} is discussed in greater detail.

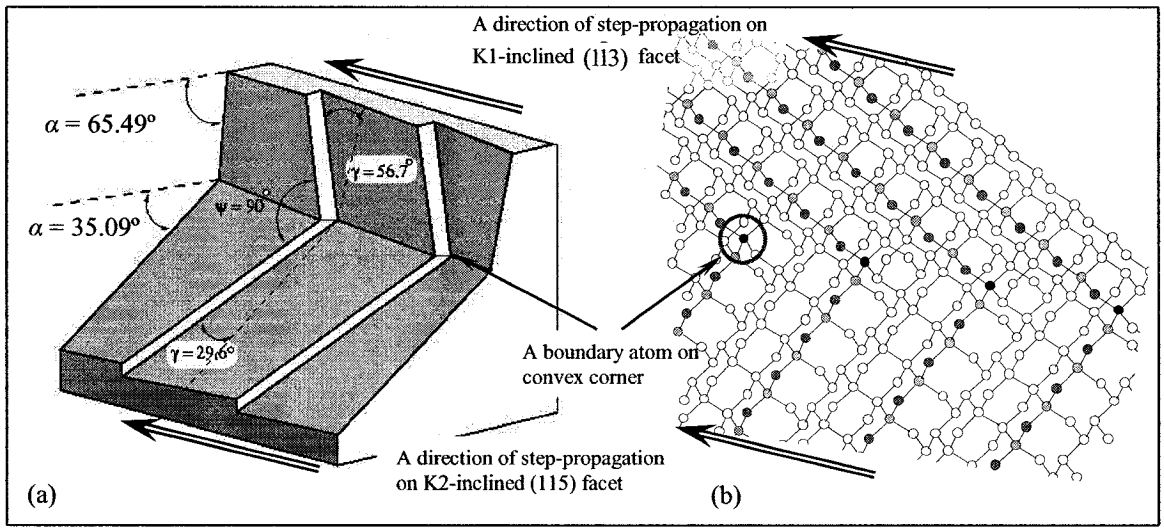

Figure 6-29: Schematic representations of K-K-90° on a sidewall of under etched spokes: (a) two inclined ($\alpha < 90°$) facets, for Si{110}, 25% TMAH, $\delta \approx 70°$, (K1-inclined with MI approximately (1$\bar{1}$3) and for K2-inclined with MI – approximately (115)), and (b) crystallographic reconstruction of K-K-90° combination of two inclined K-based facets, front view.

Figure 6-29(b) shows crystallographic construction of the case schematically depicted in Figure 6-29(a), allowing analysis of the process of removal (zipping) of a row of atoms, in order to inspect what might happen at the boundary between two facets.

Suppose that "zipping" starts from the upper end of a K-row on the K1-inclined facet in Figure 6-29(b), and propagates down toward the boundary atom, removing both the

topmost (dark grey coloured) and next-level (light grey coloured) atoms. As the process reaches the boundary atom (black coloured one), what is the likelihood of the zipping to continue propagating across the boundary to the intersecting chain on the adjacent facet? In this case, once the process reaches the boundary atom (black atom in Figure 6-29(b)) this atom will have 1 dangling bond, and 3 bonds to atoms which have fewer than 2 dangling bonds. This would suggest that zipping should not propagate from the K1-inclined to the K2-inclined facet in this case.

Now, suppose that zipping starts from the bottom of the etched cavity, at the bottom end of the K-row of the K2-inclined facet, and propagates in the direction of the boundary between the facets. If one analyses the boundary atom in Figure 6-29(b), after the entire chain on the inclined facet has been removed, the boundary atom (part of both intersecting chains), has 2 back bonds and 2 dangling bonds, similar to the bonding configuration of any other atom on a K-row. While one may hypothesize that this probability of propagation is greater than when the zipping starts from the other (top, K1-inclined) facet (described above), it is still not clear why zipping should propagate across the junction.

If zipping began at the convex boundary, then the removal of the two K-rows would start simultaneously and continue in both directions: up to the mask-edge on the inverted facet and down to the bottom surface on the inclined facet.

K1-inclined, MI $(1\bar{1}3)$ (precise $(1, \bar{1}, 1.256)$), facet has the angle with the respective $\{111\}$ surface, $\theta_K = 25.78°$ and K2-inclined, MI (115) (precise $(1, 1, 1.488)$), facet has $\theta_K = 38.59°$.

All relevant parameters (from the basic surface geometry and related calculations (using the mathematical model approximation) are summarised in the **Error! Reference source not found..**

Table 6-11: Summary of the specifics for K1-inclined and K2-inclined planes located on sidewall of spoke at deviation angle $\delta \approx 70°$ on Si{110}

	K1-inclined	K2-inclined
Inclination angle, α	65.49°	35.09°
MI	{1, 1, 1.256}	{1, 1, 1.448}
MI approximation	{113}	{115}
Step-spacing, Å	7.21	9.76
FR component due to chain/row removal from the step-edges, h^{-1}	2.99×10^5	5.2×10^5
Step-spacing correspondence with adjacent facet	1.355 : 1	
Relative Step-Edge Velocity, *μm/h*	124.25	-228.41
Angle of a plane with respect to {111} surface	$\theta_K = 25.78°$	$\theta_K = 38.59°$
Angle of a plane with respect to basic {100} or {110} surface	~28.95°	~16.14°
Canonical Etch Rates, *μm/h*	56	45.5
Experimental Etch Rates, *μm/h*	43.22	55.24

As it was discussed earlier, the crossover in the terrace orientation appears at $\theta_K = 29.05°$, and, therefore, K1-inclined facet, located very close to the terrace crossover, but located on the side from the crossover with dominating {111} terrace orientations, crystallographic construction of this surface is illustrated in Figure 6-30(a). K2-inclined facet is located on "the other side" of a crossover in terrace orientation, where terraces in the surface step-based structure are {100}-oriented, crystallographic construction of (115) plane is illustrated in Figure 6-30(b).

This geometry will reflect on calculations of step spacing and removal frequency.

With the consideration of respective terrace orientations step spacing on K1-inclined, $(1\bar{1}3)$, plane with {111}-oriented terraces equals ~7.21 Å, and on K2-inclined, (115) plane with {100}-oriented terraces is ~9.76 Å.

Calculation of the EPA gives the following results: 1.45Å for($1\bar{1}3$) 2.39 Å or and for (115) planes with {111}- or {100}-oriented terraces, respectively.

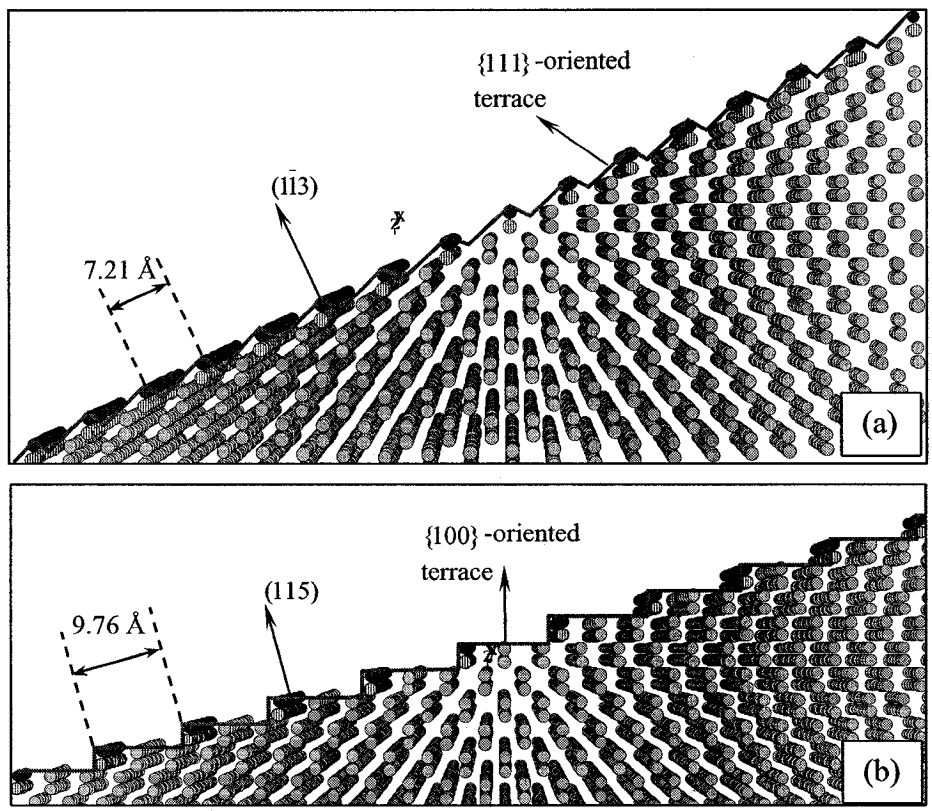

Figure 6-30: Crystallographic construction of planes appearing on sidewalls of a spoke on Si{110} wafer etched in 25% TMAH at 80°C at $\delta \approx 70°$. (a) Construction of a specific ($1\bar{1}3$) surface with {111}-oriented terraces and (b) construction of specific (115) surface with {100}-oriented terraces.

From the experimental data, the etch rates of K1-inclined and K2-inclined facets are 43.22 μm/h and 55.24 μm/h, respectively, Figure 6-31.

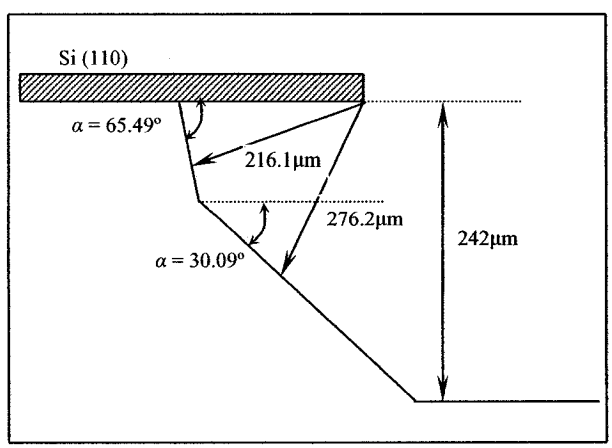

Figure 6-31: Schematic cross-sectional view of the sidewall of a spoke at $\delta \approx 70°$ on Si{110} etched in 25wt.% TMAH for 5 hours, showing the position of the original mask edge and estimated etch rates of the various surfaces.

It can be observed, that according to the calculations, almost twice as many K-rows are removed from K2-inclined facet compared to K1-inclined, and the step-edge velocity on K2-inclined is almost double of that on K1-inclined with the steps moving in opposite directions (see shaded cells in **Error! Reference source not found.**).

However, the roughness features that are observed on SEM in Figure 6-28(a), with the presented magnification, do not seem to indicate any influence of the etch of one facet on another, as might be seen in Figure 6-28(d), (visible continuation of K-rows from one facet to another).

It might be said that these two facets etch independently without any significant influence of the interactions between these two facets, in part, due to their atomic structure, (Figure 6-29(b)).

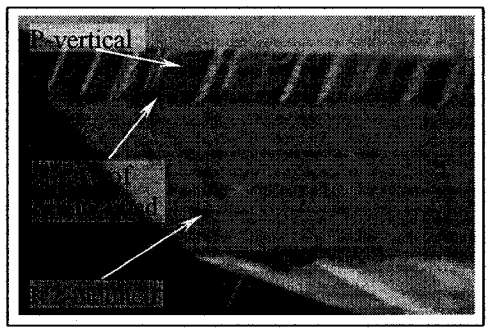

Figure 6-32: SEM images of the sidewall of a spoke at $\delta \approx 70°$ after 10 minutes etching time (P-vertical, trace of K1-inclined and K2-inclined facets present) on Si{110} etched in 25% TMAH at 80°C, [9].

Another interesting observation of this case is the progression of the facet developments with time.

At the beginning of the etching, after 10 minutes, three facets can be identified: P-vertical, K2-inclined and a trace of K1-inclined, see Figure 6-32. However, the presence of K1-inclined facet is not obvious and its detection is, to large degree obstructed by the macro-features of P-vertical facet.

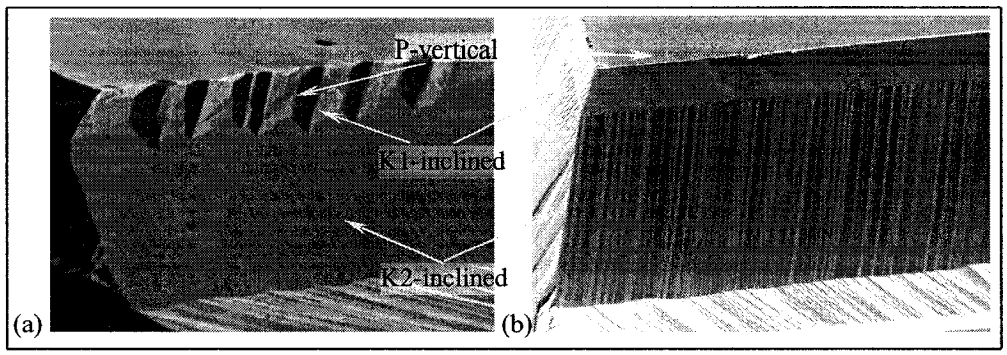

Figure 6-33: SEM images of the sidewall of a spoke at (a) $\delta \approx 70°$ after 50 minutes etching time (P-vertical, K1-inclined and K2-inclined facets present) and (b) $\delta \approx 70°$ after 5 hours etching time (P-vertical K1-inclined and K2-inclined facets present) on Si{110} etched in 25% TMAH at 80°C, [9].

It may be argued that the presence of K1-inclined facet can be explained by the relative movement of P-vertical and K2-inclined facets. It (K1-inclined facet) seem to appear almost immediately after a formation of the spoke (see Figure 6-32), then, after 50 minutes etching time, develops to larger dimensions, (Figure 6-33(a)), and, eventually, becomes clearly pronounced after a sufficient etching time, whereas P-vertical facet almost completely disappears, see Figure 6-33(b),

6.6. Other Interesting Observations

From general observation of a variety of SEM pictures, few surfaces with significant roughness profiles may by selected.

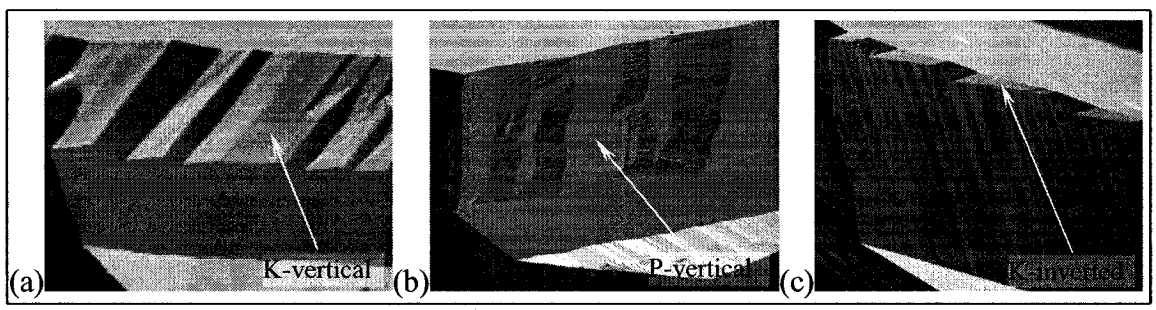

Figure 6-34: SEM images of the sidewall of a spoke etched in 25% TMAH at 80°C for 3 hours on (a) Si{110} at $\delta \approx 39°$ with macro-roughness profile on K-vertical, (b) Si{110} at $\delta \approx 63°$ with macro-roughness profile on P-vertical, and (c) Si{100} at $\delta \approx 37°$ with macro-roughness profile on K-inverted.

Figure 6-34 illustrates three cases with rather distinct macro-roughness profiles on K-vertical, P-vertical and K-inverted facets detected on sidewalls of spokes at deviation

angles $\delta \approx 39°$, $\delta \approx 63°$ on Si{110}, and $\delta \approx 37°$ Si{100}, respectively. The similarity in these plane's morphology may be identified as a splitting of an original surface into two, creating a "saw-tooth" profile. These facets, originally, were representing planes with the following Miller Indices: K-vertical - {1.75, 1, 1}(can be approximated to {2,1,1}), P-vertical – {1, 1.387, 1.387} (approximated to {7,9,9}), and K-inverted – {1.327, 1, 1}(can be approximated to {13,10,10}). A crystallographic reconstruction of these surfaces (or rather, to simplify the reconstruction, their approximations) was done with the view of identification of their common trends. The specifics for each of analysed surfaces are summarised in the Table 6-12.

Table 6-12: Summary of the specifics of three planes with similar roughness profiles

	Si {110}		Si{100}
	K-vertical	**P-vertical**	**K-inverted**
Deviation angle, δ	39°	63°	37°
Location	Top-most facet		
MI	{1.75, 1, 1}	{1, 1.387, 1.387}	{1.327, 1, 1}
MI approximation	{2,1,1}	{7,9,9}	{13,10,10}
Terrace orientation	{111}-oriented terraces		
Step-spacing, Å	11.56	21.81	22.78
Step-spacing correspondence with adjacent facet	~1.34 : 1	~2.58 : 1	1 : 1
Step-Edge Velocity, *μm/h*	206.04	194.79	203.58
Step-Edge Velocity and the direction of adjacent facet, *μm/h*	~ -142	~ -208	+257.72
Angle of a plane with respect to {111} surface	$\theta_K = 15.74°$	$\theta_P = 8.26°$	$\theta_K = 7.91°$
Canonical Etch Rates, *μm/h*	50.8	24.88	24
Experimental Etch Rates, *μm/h*	40	28	27

Surfaces, properties of which are listed in Table 6-12 above, may be found at the following angles of rotation, θ, from basic {111} plane: K-vertical, at $\theta_K = 15.74°$, P-vertical at $\theta_P = 8.26°$, and K-inverted at $\theta_K = 7.91°$, see Figure 6-35.

It is interesting to note, that all three surfaces are located on linear portion of the canonical etch rate curve, and two of these surfaces, P-vertical and K-inverted, have the same etch rates, see Table 6-12 and Figure 6-35.

All three surfaces have very close, if not the same, relative step-edge velocity.

Crystallographic construction of these surfaces is presented in Figure 6-36.

The common for all three plane is the fact that they all have {111}-oriented terraces. However, the step-spacing on this surfaces is quite different, ranging from 11.56 Å on K-vertical (approximated to {2,1,1}), through 21.81 Å on P-vertical (approximated to {7,9,9}), to 22.77 Å on K-inverted (for simplicity of construction approximated to {13,10,10}).

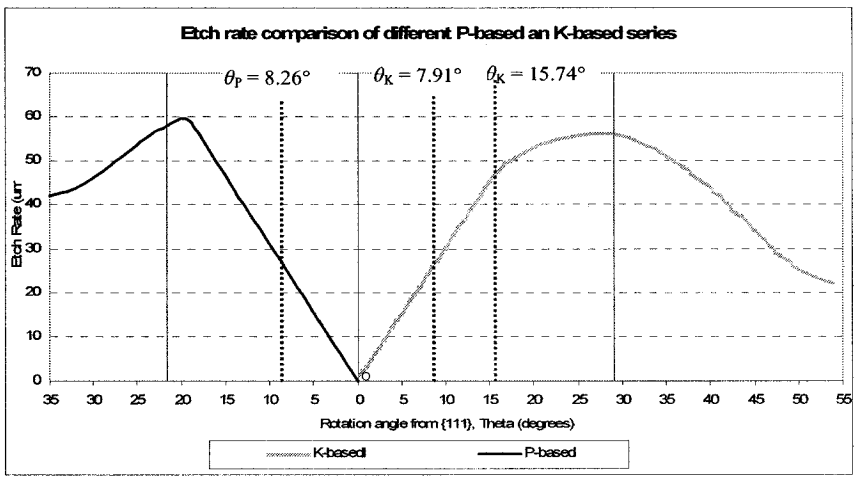

Figure 6-35: Experimental etch rate data presented in a form of canonical curves, i.e. in form of etch rates of surfaces rotated from {111} plane.

From the collected information, it may be said that a number of factors may lead to a creation of "saw-tooth" profile of a facet. It seems to be, predominantly, the top-most surface with {111}-oriented terraces, not vicinal to basic, {111}, orientation, $\theta > 5°$.

These surfaces seem to have similar step-edge velocity (~200 *μm/h*) and are in combination with facets whose steps move in opposite direction (in case of K-vertical and P-vertical facets on Si{110}) or in the same direction but with larger velocity (in case of K-inverted on Si{100}).

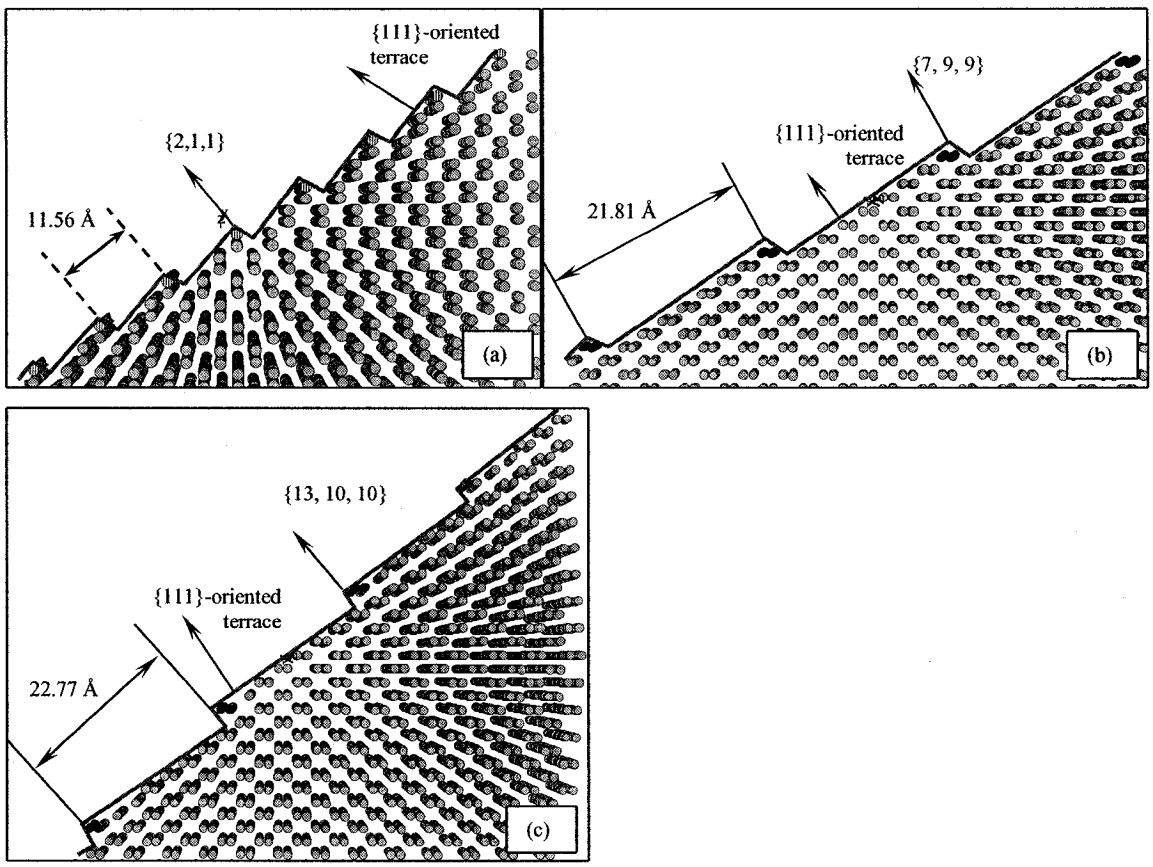

Figure 6-36: Crystallographic construction of planes appearing on sidewalls of spokes etched in 25% TMAH at 80°C on (a) Si{110} at $\delta \approx 39°$ of K-vertical with approximated {2,1,1} Miller Indices, (b) Si{110} at $\delta \approx 63°$ of P-vertical with approximated {7,9,9} Miller Indices and (c) Si{100} of K-inverted with approximated {13, 10, 10} Miller Indices.

6.7. Summary

This chapter introduces a detailed analysis of surfaces in concave structures on atomic level. From the previous research it was shown that based on angles between interacting chains/rows for two families of planes, K-based and P-based, maximum of three original combinations are possible for each of these angles (60°, 90°, and 120°), i.e. PBC/PBC, PBC/K-row, and K-row/K-row, making the total count of these combinations nine. However, only seven of said combinations were detected in concave structures of wagon-wheel under-etch experiment.

Using this information atomic level analysis was conducted for two of the most frequent combinations: K-P-120° and K-K-90°.

Based on this analysis it was shown (on the example of K-P-120° combination) that zipping is more favoured from P-based steps to K-based steps than from K-based steps to P-based steps.

- Roughness patterns on one of the K-based facets are consistent with step-based zipping independently from each of the two facet boundaries;
- Analysis of the configuration of boundary atoms for the K-P-120° intersection in the ideal crystal lattice suggests less-stable boundary atoms when zipping from the P-based side.

Outcome of the analysis of K-K-90° did not support the likelihood of K-row propagation across the boundary from one K-based facet to another.

Next, the step-spacing correspondence of steps on adjacent facets was introduced and exact values were summarized in Table 6-1 and Table 6-2. Due to the complexity of the combinations of adjacent facets detected on Si{110}, the analysis of step-spacing correspondence was done in greater detail.

In addition the analysis of three cases of the facets with "saw-tooth" profile was conducted with the view of tracing common trends that lead to such surface roughness. Outcome of this analysis is not entirely conclusive; however, it was observed that at least in these three cases, "saw-tooth" profile appeared on surfaces with following similarities[38]:

- Surfaces that appear as a top-most facets

[38] Please note that this analysis applies for the experimental data obtained from the under-etch wagon-wheel experiment on samples etched in 25% TMAH.

- Surfaces with{111}-oriented terraces, not vicinal to basic, {111}, orientation, with $\theta > 5°$.
- These surfaces with similar step-edge velocity (~200 $\mu m/h$)
- Surfaces in combination with facets whose steps move in opposite or in the same direction but with larger velocity.

6.8. Contributions

My contribution in this portion of work is in introduction of an atomic level analysis of the interactions between adjacent facets.

- Step-spacing correspondence was calculated for all surfaces detected on sidewalls of spokes in under-etch wagon-wheel experiment with the consideration of crossovers in terrace orientation.
- Certain areas with more significant step-spacing correspondence were indicated (1:1 and 1:2)
- Analysis of two most frequent cases K-P-120° and K-K-90° was conducted and showed certain tendencies in the interaction between the facets containing such combinations:
    - On the example of K-P-120° combination it was shown that zipping is more favoured from P-based steps to K-based steps than from K-based steps to P-based steps.
    - Roughness patterns on one of the K-based facets are consistent with step-based zipping independently from each of the two facet boundaries;

- Analysis of the configuration of boundary atoms for the K-P-120° intersection in the ideal crystal lattice suggests less-stable boundary atoms when zipping from the P-based side.
- Outcome of the analysis of K-K-90° did not support the likelihood of K-row propagation across the boundary from one K-based facet to another.

- Analysis of three cases of the facets with "saw-tooth" profile showed a possibility of common trends based on crystallographic construction of these surfaces, their relative location with respect to other facets, step-edge velocity, etc.

7. Etch Rate Control: Introduction of the Light Illumination to Wagon-Wheel Under-Etch Experiment

7.1. Introduction

Up to now, wet anisotropic etching of silicon has been used primarily to create micro-structures, with dimensions of several microns or greater. The accuracy of anisotropic etch techniques, used in the development of these devices were satisfactory. However, with the development of nanotechnology, new challenges arise. E.g., investigations of the creation of porous silicon by L. Pavesi *et al* show that silicon, formed into low dimensions, can be turned into an active photonic material, [49]-[50]. However, construction of ordered structures of such dimensions proves to be quite challenging, especially when it comes to a precision control of the etch rates. The limitation in control of the etch technique is due to lack of an efficient predictive model of the development of concave structures as well as adequate simulation tools.

7.1.1. Etch Stop Techniques

Different methods were used to control the etch rate of silicon in an anisotropic etchant. Etchant concentration and temperature, as two of the most important factors in silicon anisotropic etching, were investigated with the view of their affect on silicon etching rates and surface roughness for all crystal orientations. In depth study of these effects was conducted by two research teams – Tabata *et al*, [48], and Sato *et al*, [51].

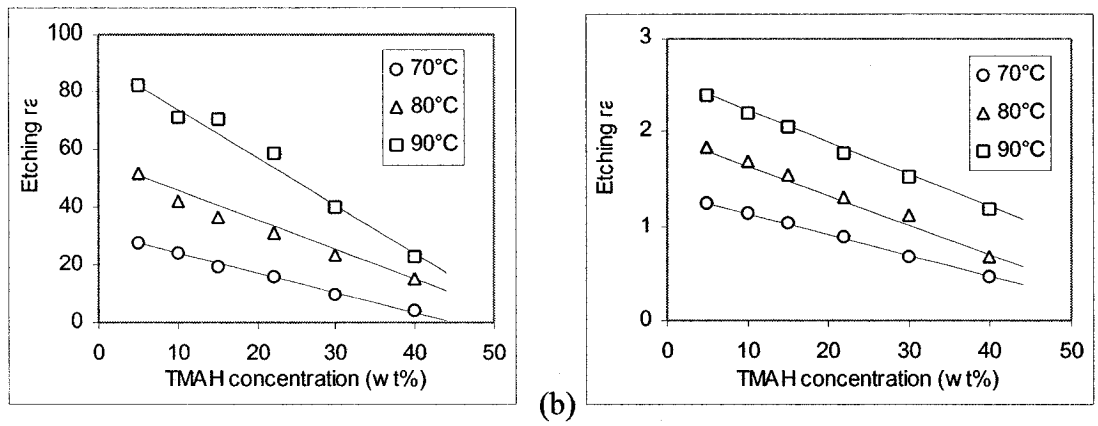

Figure 7-1 : Dependencies of (a) {100}-oriented surface and (b) {111}-oriented surface etching rates on temperature and concentration of TMAH, Figure from [48].

As can be seen from Figure 7-1, summarizing the results of the experimental work by Tabata *et al*, the general dependence of the etch rate of two basic orientations in silicon crystal ({100} and {111}) is greatly dependent on the temperature, increasing with increasing temperature. Regarding anisotropic etchant concentration, etch rates showed steady increase as the concentration of TMAH was reduced, [48].

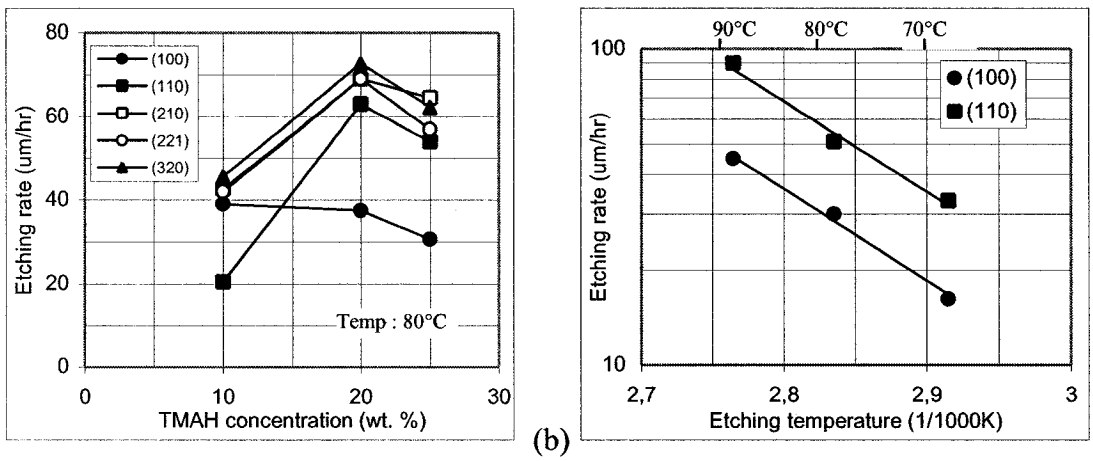

Figure 7-2: Dependence of the etch rates of (a) various silicon crystal orientations on TMAH concentration and (b) {100}-oriented surface and {110}-oriented surface on temperature of TMAH, Figure from [51].

Figure 7-2 shows results of experimental work by Sato *et al*, [51]. As it can be seen in Figure 7-2(a) as TMAH concentration varies from 10wt% to 25wt% most of analysed orientations indicated the maximum at 20wt% with one exception. Si{100} has a steady increase in the etch rate with the decrease of TMAH concentration with the maximum at

approximately 2-5wt%, [51]. Results similar to those of Tabata *et al* showed steady reduction in etch rate with decrease of the temperature (see Arrhenius plots of Figure 7-2(b)). The {100}/{111} etch rate ratio, however is also decreases with decrease of the temperature and increasing concentration, thus affecting actual anisotropy of the etching process. These results, i.e. change in the anisotropy ratio, could also be found in the reports of Schnakenberg *et al*, [15].

Work on etch rate dependence was also conducted in our research group by S. Naseh, [39], A. Pandy, [31], and Z. Elalamy, [9].

Changes in etchant concentration as well as in temperature may provide control over the ER-s of the surfaces in concave structures. However, such experiments were not as yet satisfactory due to variable surface roughness, [9], [31].

Another potential method to regulate etch rates is an introduction of additives in order to modify TMAH etching characteristics. Two outcomes of additives introduction are the adjustment of the anisotropic properties of TMAH (limitation of undercut, change in side-walls morphology, i.e. reduction of facets quantity) and improvement of the surface roughness, especially for low TMAH concentrations.

From comparison of the anisotropy profiles of two etchants, TMAH and KOH, it was implied that not only hydroxide ions but also cations have an influence on the anisotropic etching mechanism. Thus, the addition of potassium ions to TMAH using K_2CO_3 was suggested. Tabata et *al*, [52]-[53], confirmed the effect K_2CO_3 on the TMAH anisotropy as well as on SiO_2 selectivity. The experiment was conducted with a use of a hemispherical single crystal silicon (similar to that used by Sato et *al*) etched in 20wt%

TMAH at 80°C with the addition of 0.5g/L K_2CO_3 is 0.5 g/L, (amount that shown most influence in TMAH properties at given concentration).

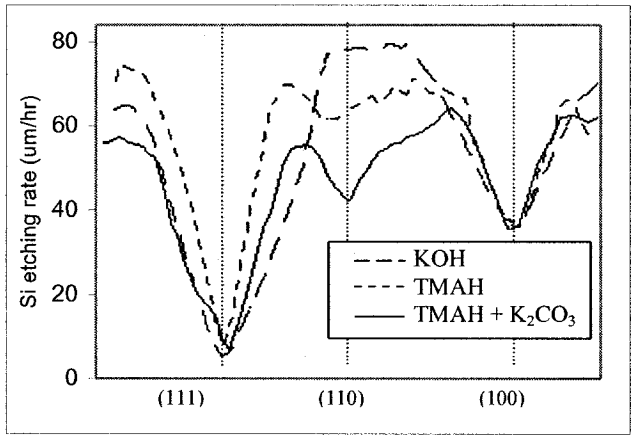

Figure 7-3: Etching rate distribution along a line from the (111) to (110) and from (110) to the (100) plane, showing the effects of adding 0.5g/L K_2CO_3 in TMAH 20wt.% 80°C, Figure from [48].

As it can be seen from Figure 7-3, introduction of the additive considerably changes the anisotropy profile. However, it also introduces change to the environment, i.e. properties of the etchant, which, consequently, can not be used for other applications.

Very interesting results were achieved with the use of electrochemical etch-stop techniques. Some of these techniques accomplished by heavy p-type (Boron) doping of the area of interest, another involve the use of electrodes and the applied potential.

The heavy boron doping etch stop effect (doping levels grater than $2\text{-}3\times10^{19}cm^{-3}$) was first observed during etching in EDP (1969) and KOH, [9], [54]-[55]. Silicon etch rate was measured depending on the boron doping concentration. It was shown that for the extreme coping levels, ($\geq10^{20}cm^{-3}$) the etch rate was reduced by a factor of more than 40, see Figure 7-4.

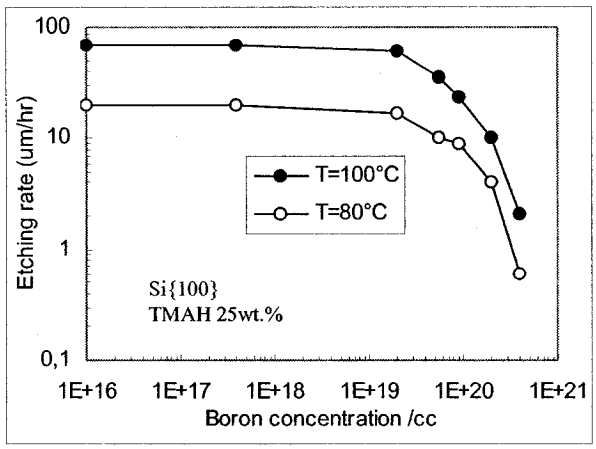

Figure 7-4: Si{100} etching rate in TMAH 25wt.% vs. boron concentration, Figure from [55].

Seidel et al, [11], provides a well-designed model and explanation of this etch stop technique.

At high level of doping concentration, p-type in this case, the Fermi energy level falls below the top of the valence band, Figure 7-5(b), compared to that of lightly doped p-type silicon, Figure 7-5(a).

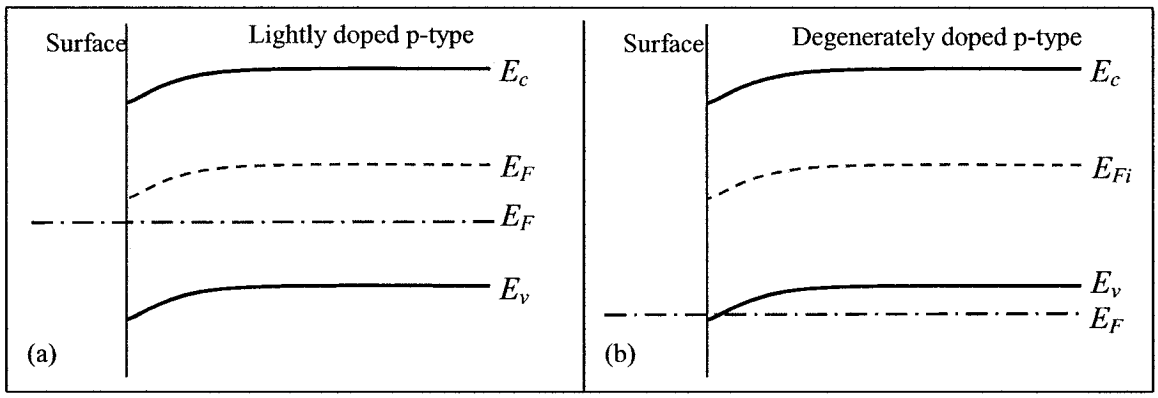

Figure 7-5: Energy band diagram of (a) lightly doped p-type silicon (b) degenerately doped p-type silicon.

As silicon at the surface dissolves, resulting electrons are injected into the conduction band by the oxidation step, Equation (7.1).

- the oxidation step, [11]:

$$Si + 4OH^- \rightarrow Si(OH)_4 + 4e^-_{cond.\ band} \qquad \textbf{(7.1)}$$

- the reduction step

$$4H_2O + 4e^-_{cond.\ band} \rightarrow 4OH^- + 2H_2 \quad (7.2)$$

However, due to the narrowing of the potential for degenerately doped silicon, the narrow space charge region at the surface can not confine the injected electrons, which in turn will tunnel through the surface charge layer and will recombine (with large degree of probability) with many available holes. As a consequence, these electrons are no longer available for the reaction with water molecules in the overall reaction, Equation (7.2). This results in the reduction of the formation of new hydroxide ions in the proximity of negatively charged surface, necessary to the etching mechanism, [11].

A major disadvantage of this method is in its incompatibility with the standard CMOS technology and, consequently, limiting its applications.

7.1.2. Electrochemical Etch Stop Technique

More and more attention is being given to the electrochemical etching and, in the context of this work, electrochemical etch stop.

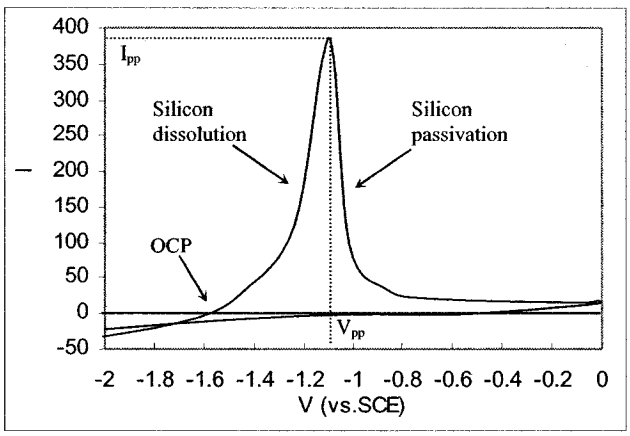

Figure 7-6: A cyclic voltammogram of p-type Si in 25wt.% TMAH at 80°C, using an SCE[39] as reference, [56].

A simplified description of this technique may be narrowed down to silicon electrode placed in an etching solution and the voltage applied between the silicon and another

[39] SCE – saturated calomel electrodes.

electrode in the same solution. As a result of this potential difference, current will flow between electrodes. Figure 7-6 illustrates a "voltammogram" of p-type silicon electrochemically etched in 25et% TMAH at 80°C, [56]. Please note that the value of current is greatly dependent on the area of electrodes.

Two important values of potential difference may be indicated, Figure 7-6. The first is the open circuit potential (OCP), signifying "zero" current and results in the chemical etch of silicon with the ER dependent only on temperature and the etchant composition. The second is the passivation potential (V_{pp}), after which current begins to drop due to the growth of an oxide layer on silicon surface. Return to the negative potential will not have significant difference on the current, since the oxide layer grown on silicon obstructs the access of the etchant to silicon surface and the silicon dioxide itself has a very low etch rate, Figure 7-6.

The energy band diagram at the silicon-etchant interface and the chemical reactions associated with different applied voltages may provide better explanation of the etch-stop mechanism.

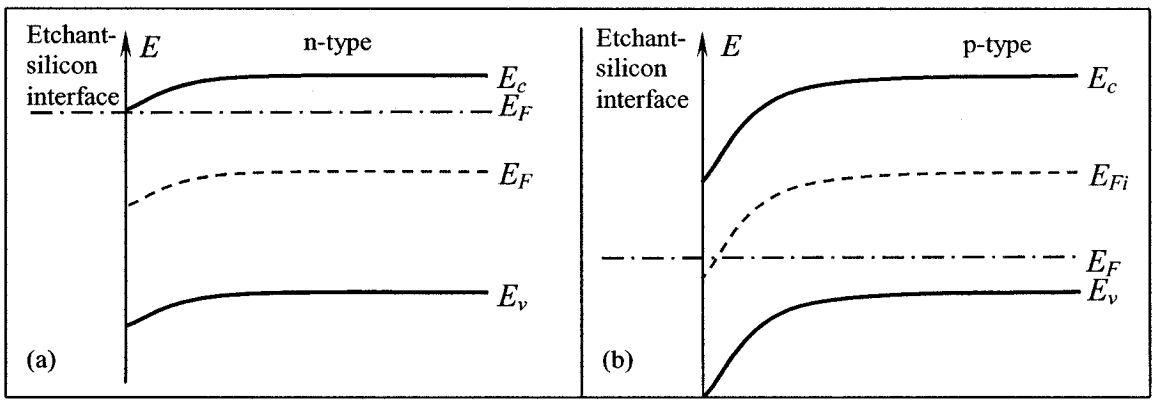

Figure 7-7: Energy band diagram without applied voltage, i.e. at OCP of (a) n-type silicon and (b) p-type silicon in etchant.

Figure 7-7 illustrates a simplified version of n- and p-type silicon immersed in the etchant in the state of open circuit potential (OPC). At this point, the whole system may be considered at thermal equilibrium. The energy bands bend downward, [11], for both types of silicon, with larger bending for p-type silicon due to the greater initial difference between Fermi levels of electrolyte and silicon, [57].

The reaction of silicon etching can be further expanded from Equation (7.1) to

$$Si(OH)_4 \rightarrow SiO_2(OH)_2 + 2H^+ \qquad (7.3)$$

If the potential of the silicon sample is increased (made more positive) with respect to the solution, there is an increase in hole concentration at the surface with the potential difference that equals to the passivation potential, V_{pp}, water molecules with electrolyte, see Figure 7-8.

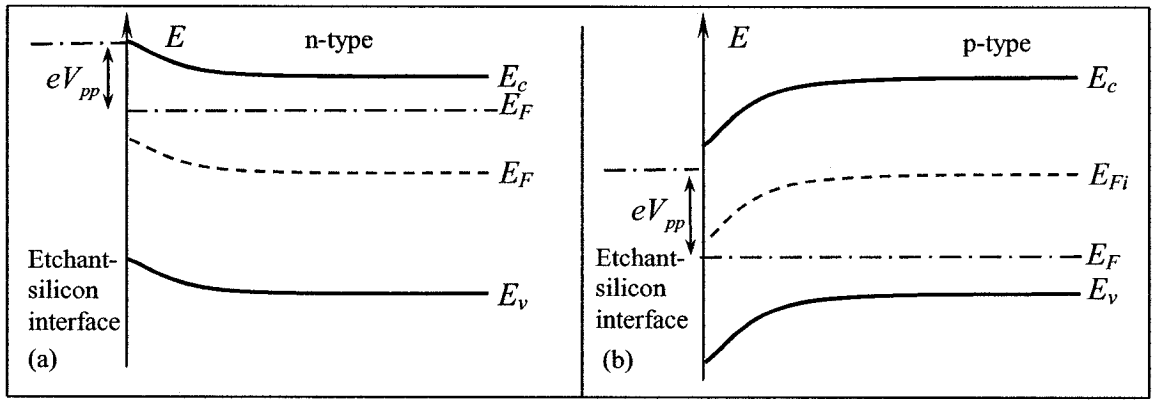

Figure 7-8: Energy band diagram of (a) n-type silicon and (b) p-type silicon in etchant with the applied potential corresponding to V_{pp}.

The resulting hydroxyl ions will be attracted to the surface of silicon.

$$\mathbf{Si^{2+} + 2(OH^-) \rightarrow Si(OH)_2} \qquad (7.4)$$

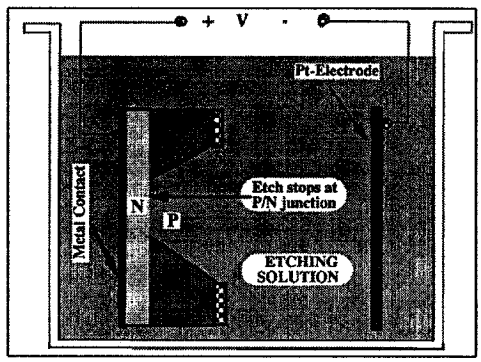

Figure 7-9: A schematic representation of pn-junction electrochemical etch-stop technique, Figure from [58].

The hydrogen gas is liberated from $Si(OH)_2$ that results in SiO_2 formation at the surface. This type of passivation is often used to remove one type of doped silicon while passivating another. This method is also known as a pn-junction etch stop technique, Figure 7-9.

7.1.3. Etch Stop Using Light Illumination

Novel approach to the control of the etch rates was taken by E. M. Conway *et al.* in University of Limerick, [59]. The study by this group concentrated on the electrochemical reaction at Si/TMAH interface in the dark conditions and under the white light illumination. It was shown that for p-type {100}-oriented silicon surfaces in alkaline systems (e.g. KOH) the white light shifts V_{pp} to more positive potentials, relative to its values in the dark conditions. For n-type silicon, shift of V_{pp} into more negative potential values relative to its values in the dark was observed, [60]. It was concluded, that the white light can act as an etch stop for n-type silicon, where in dark conditions the etching was expected. E. M. Conway *et al.*, [59], used this information to apply to the samples of {100}-oriented p- and n-type silicon, and {111}-oriented p-type silicon, electrochemically etched in 5wt% TMAH at constant temperature of 52°C.

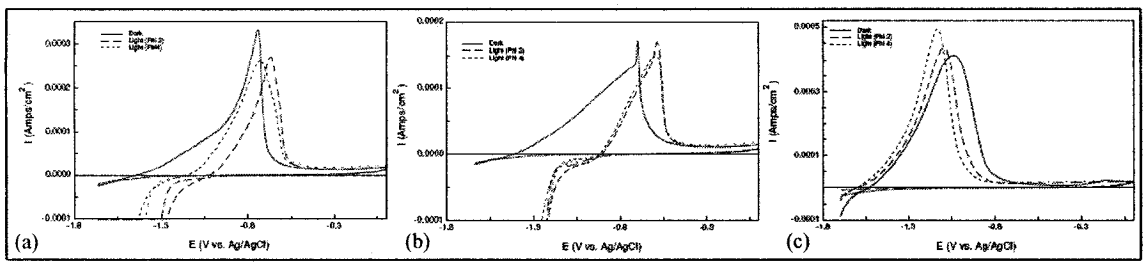

Figure 7-10: Voltammograms under distinct levels of illumination (dark conditions – solid curve) of (a) p-type {100}-oriented, (b) p-type {111}-oriented, and (c) n-type, {100}-oriented silicon samples, figure from [59].

According to the results illustrated in Figure 7-10, open circuit potential (OCP) of the p-type silicon samples of both {100} and {111} orientation shifted to more positive (anodic) values under the white light illumination. Only slight shift of OCP into more negative (cathodic) values was observed for n-type {100}–oriented illuminated samples. Similar shift (anodic for p-type and cathodic for n-type) was detected for V_{pp}, (Figure 7-10). Summarised results of this work showed the following:

- White light has an enhancing kinetic effect on the Hydrogen evolution reaction and the oxidation reaction, Equations (7.1) – (7.3).
- Cathodic photocurrents observed in p-type silicon samples were linearly dependent on light intensity.
- "For n-type silicon, the etch rate is expected not to alter under white light conditions since n-type silicon is under accumulations at OCP", [59].

Based on this information and summarised conclusions light effect on the etch rates of anisotropically etched concave structures in wagon-wheel experiment is considered as least invasive way of the etch control.

It is important to acknowledge, that the experiments done in our laboratory supply the data for a study of etch rates of structures far more complex than a plain surface of certain orientation. The wagon-wheel under-etch experiment provides the formation of

planes in such combination that due to their mutual etch rate dependence[40], [9], [33], [35], slight change in the etching conditions may have notable influence on the resulting etch rates of these surfaces. As the change in the etching conditions the white light illumination of the etched pattern is introduced. The following is the description of the wagon-wheel under-etch experiment that was conducted on Si{100} and Si{110} samples etched in 25% TMAH at 80°C with the light illumination.

7.2. Experiment Description

Subsequent to the necessity of the illumination of the etched surface, the customary oil bath employed in previous experimentation could not be used. Therefore, a new experimental setup had to be introduced.

The conditions necessary for this test are:

→ Uniform illumination of the etched surface

→ Controllability of the light intensity

→ Control of temperature

→ Stirring

The experimental setup combining these conditions presented in Figure 7-11.

The hot plate used Corning® Hotware with variable temperature (25 - 480°C) and variable stirring (60 – 1100 RPM).

The light source used is Fiber Optic Illuminator (150W) with a goose-neck adaptor and variable light intensity controller (0-100%)

[40] See more on boundary between two adjacent facets in Chapter 6.

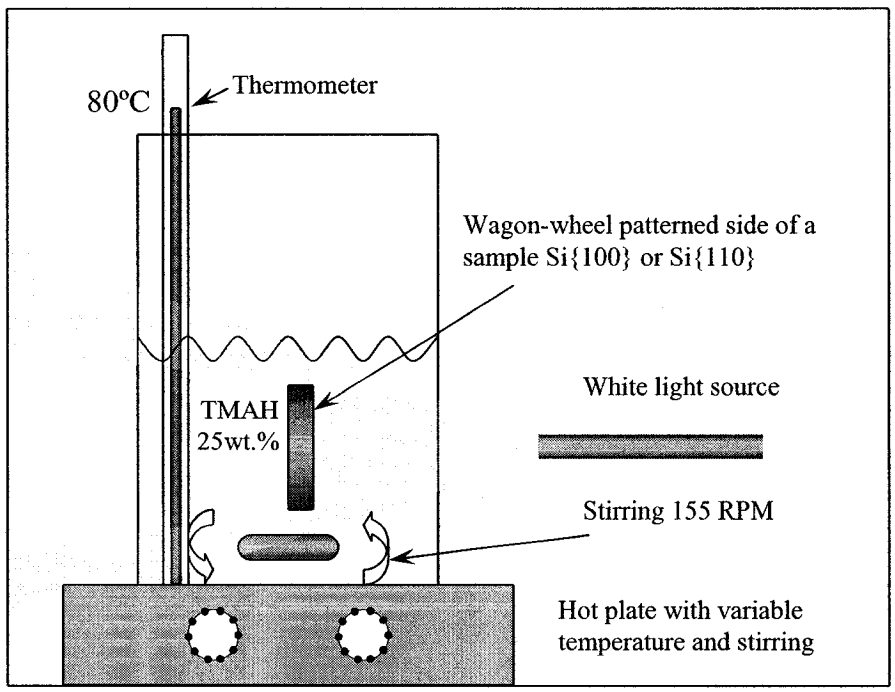

Figure 7-11: Schematic representation of the experimental setup.

One of the main concerns in this setup is an adequate temperature control. The oil bath, used in previous experimentation, [9], provided very stable temperature conditions. In the hot plate setup of Figure 7-11 the temperature variations were within ±0.5 and up to ±4°C. Therefore, the analysis needed to be set in such way that it would compensate for these deviations.

As a result, the purpose of the experimentation was more to the point of showing the comparison of the data collected from the illuminated samples (in the following text referred to as "light" samples) within certain range of the temperatures to the samples etched within the similar temperature window in the light isolated conditions, or so called "dark" samples.

The "light" conditions were created, therefore, as shown in Figure 7-11.

The "dark" conditions were imposed by the positioning a "black box"[41] over the whole setup as to isolate any light accessing the patterned surface of a sample.

7.3. Sample Preparation

Samples for the experiment were prepared primarily from the p-type silicon wafers of Si{100} and Si{110} with low doping concentration of ~10^{15}cm^{-3}.

Additional samples were done for p-type silicon with the resistivity of 7-10 Ω-cm and for the n-type silicon with the resistivity 50Ω-cm .

Oxidized samples (oxide thickness of approximately 0.75 – 1.0 μm) were patterned using the same wagon-wheel mask used in the previous experiments, Figure 7-12, through the typical CMOS photolithography process.

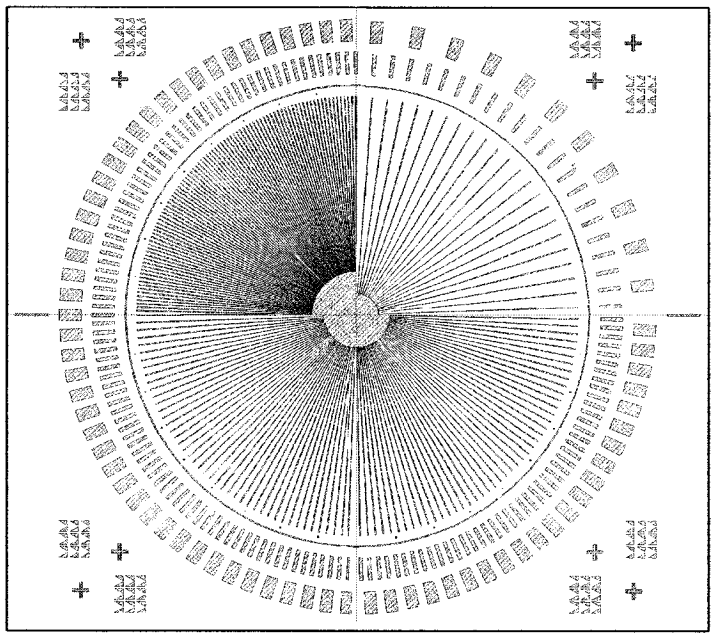

Figure 7-12: Mask for the pattern transferred on Si{100} wafer, figure from [9].

Patterned samples were cleaned in HF solutions (1:50 with DI water) to remove any possible native oxide from the exposed silicon and then immersed in the beaker

[41] Literally black box.

containing TMAH 25wt% heated to the desired temperature and positioned in the "dark" or "light" conditions following the above description.

After one hour of the etching time (60 min time limit was kept for all experiments to simplify the etch rate calculations) the samples were removed from the solution and the under-etch rate was measured using an optical microscope.

7.4. Preliminary results on p-type Si{100} and Si{110} Samples with White Light Illumination

The wagon-wheel under-etch experiment under white light illumination was repeated with the same (or near the same) conditions a number of times. The example of measurements of the results of one of these experiments with calculated under-etch rates (UER) on Si{100} samples are summarised in graphs of Figure 7-13.

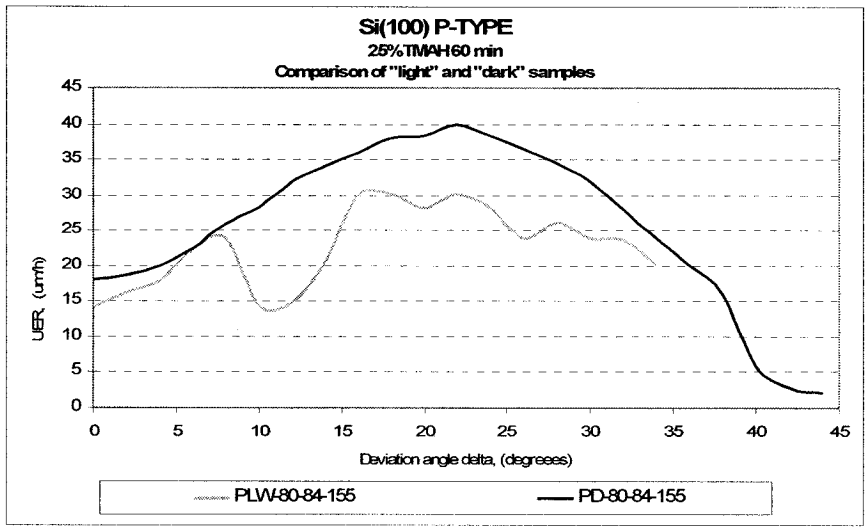

Figure 7-13: UER comparison of Si{100} samples etched in "dark" and "light" conditions in TMAH 25% at the temperature ≈ 80°C.

The translation of the legend in Figure 7-13 provides the following information:

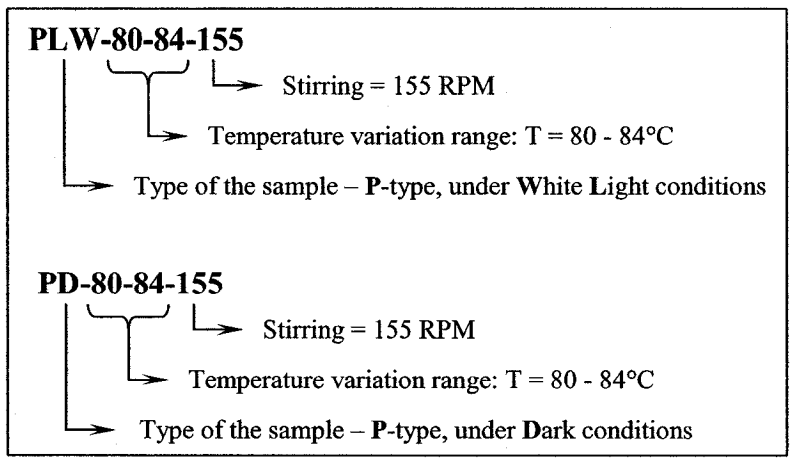

The majority of measurements resulting from the illumination of samples with the white light provided very inconsistent results (light grey curve in Figure 7-13). These variations in the under-etch rate data may be tentatively explained by imprecision of experimental measurements as well as to the fact that the white light is a combination of the range of the wavelengths and thus may have complex effect on the respective etch rates of different surfaces.

Similar experimentation was done on Si{110} samples. The example of measurements of the under-etch distance (UED) and the calculations of the resulting under-etch rates (UER) on Si{110}samples are presented in the graph of Figure 7-14 .

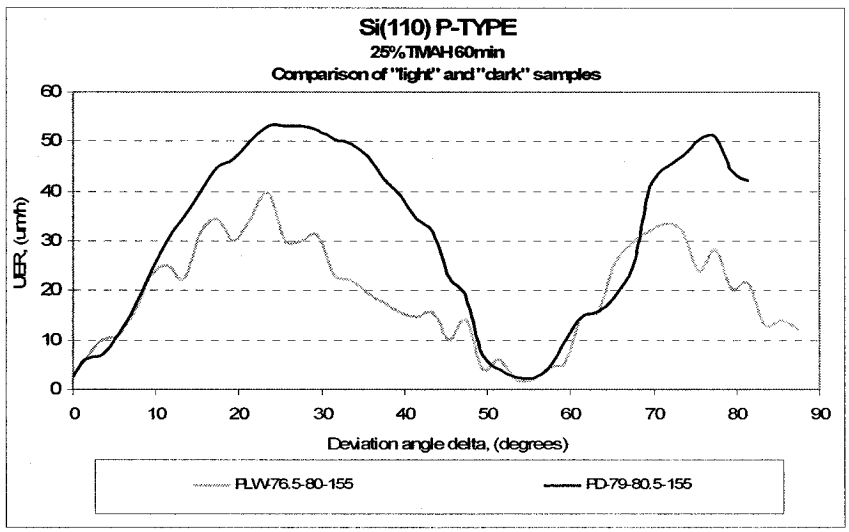

Figure 7-14: UER comparison of Si{110} samples etched in "dark" and "light" conditions.

Similar conclusion can be made in the case of Si{110} samples illuminated with the white light. Analysis of a large number of experimental trials with the white light illumination illustrated a consistent under-etch rate reduction of illuminated samples. However, due to the large deviations in the measured under-etch rates of "light" samples, no conclusive statement can be made at this point.

Thus, new set of experiments was done to identify, how much influence different range of wavelengths might have had on these under-etch rates.

7.5. Preliminary Results on p-type Si{100} and Si{110} Samples Illuminated with Mercury Vapor Light Source

To identify wavelength range a set of experiments for Si{100} and Si{110} samples under the light with selected range of wavelengths was performed. For this experiment a Mercury Vapor Light Source, model OS-9286A, was used. The specifications of available wavelengths and a power distribution with respect to the wavelengths are shown in Figure 7-15.

Colour	Frequency, Hz	Wavelength, nm
Yellow	5.18672×10^{14}	578
Green	5.48996×10^{14}	546.074
Blue	6.87658×10^{14}	435.835
Violet	7.40868×10^{14}	404.656
UV	8.20264×10^{14}	365.483

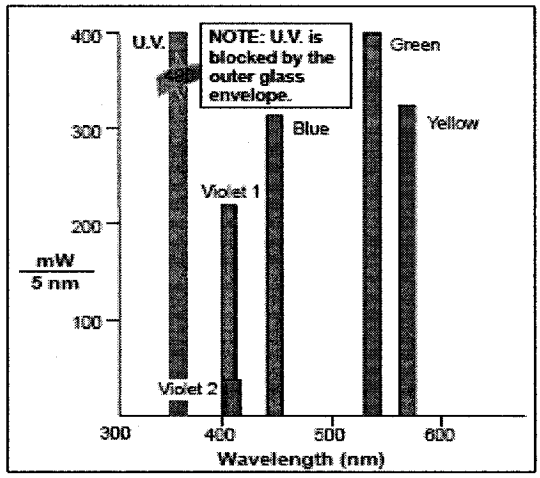

Figure 7-15: The specification for the Mercury lamp used in this light illumination experiment with selected range of wavelengths. Note that UV is blocked by the outer glass envelope.

The results of optical measurements translated into the under-etch rates are summarised in graphs of Figure 7-16 and Figure 7-17.

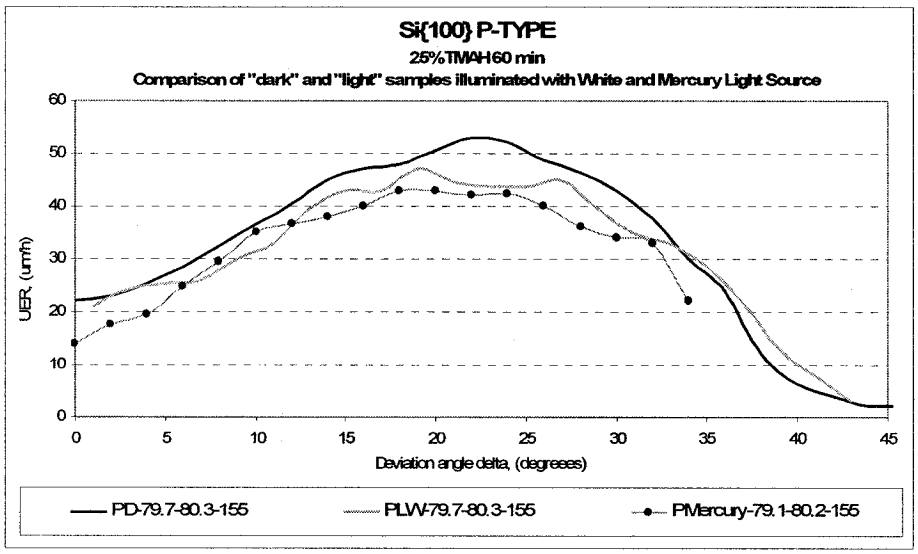

Figure 7-16: UER comparison of Si{100} samples etched in "dark" and "light" conditions under the White and Mercury Light Source Illumination.

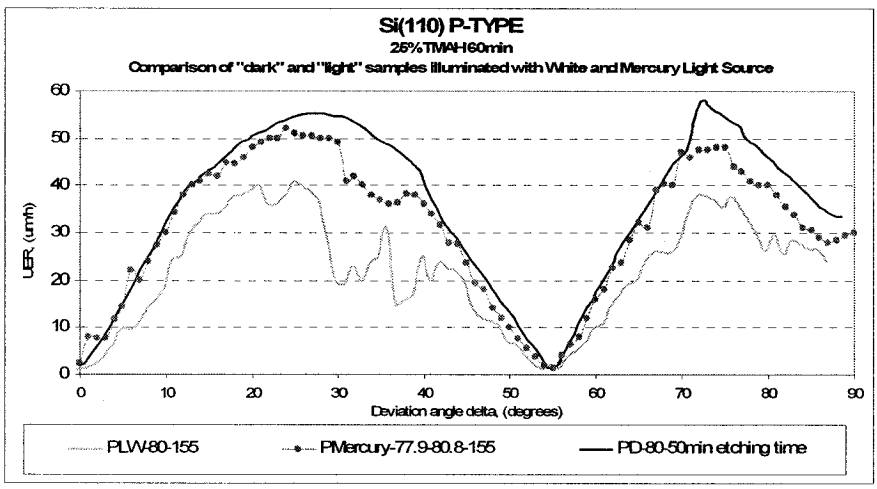

Figure 7-17: UER comparison of Si{110} samples etched in "dark" and "light" conditions under the White and Mercury Light Source Illumination.

Under-etch results of Figure 7-16 and Figure 7-17 shows, to some extent, better outline of under-etch rates under the light illumination from the Mercury Light Source (dotted line on the graphs of Figure 7-16 and Figure 7-17), compared to the samples illuminated with the white light (light grey line of Figure 7-16 and Figure 7-17). However, it seems

reasonable to assume that an individual wavelength, λ, may provide yet better results with different degree of influence on the under-etch rates, and, consequently, etch rates.
To limit the number of experiments, preliminary calculations were conducted in order to determine some basis for the wavelengths to use.

7.6. Activation Energy Estimation

It may be suggested that the light effect on under-etch/etch rates of surfaces in concave structures may be due to the influence of photon energies on the activation energy of bonds in silicon lattice.

Silicon atoms, as any other atom, may be described as a number of electrons (14) orbiting around a nucleus. Four of these electrons are located in lower energy (valence) orbit of the atom. In the crystal lattice, each atom shares electrons with four other atoms in tetrahedron structure (see Chapter 2), thus forming four covalent bonds. These electrons are restricted to orbits with certain energies, i.e. allowed energy levels. It is known that two electrons do not exist in the same space at the same time. So, when two atoms of the same type bond, valence orbits adjust in such way that there is slight difference between their energy levels[42]. More atoms combined together, as in bulk silicon, larger variety of valence energy levels will create an energy band, composed of energy levels that ever so slightly differ from each other.

Electrons can not exist at any other state in-between these levels/bands. But they may jump from one allowed energy level to another consequently changing the balance or the strength of a bond between any two atoms. Specific amount of energy is absorbed

[42] Pauli Exclusion Principle: when we bring together two atoms that, individually, have electrons in the same energy level, the energy levels tend to separate very minimally so as to obey this law of quantum mechanics, [61].

or emitted when such jump happens. The amount of energy ΔE is restricted to the values of the allowed energy levels. For example, for an electron to move from the level with the energy E_1 to the level with the energy E_2, where $E_2 > E_1$, ΔE needed for this electron can be simple defined as: $\Delta E = E_2 - E_1$.

An electron can gain energy needed to change its position within the allowed energy levels by absorbing light, [43]. This brings us to the purpose of this discussion.

As it was showed earlier, study of physics and chemistry of anisotropic etching of bulk silicon was done in various laboratories and provided reasonable if not complete explanations to the mechanics of the etching process, [12], [13].

Basic idea is that the OH groups from an anisotropic etchant attach themselves to the silicon dangling bond located at the surface. As a result, the rest of the bonds of the surface atom weaken, thus facilitating the removal of this atom.

This part of my work should demonstrate the link between the activation energies of Si-Si bonding on specified planes and their connection to the influence of the light with specified photon energies and their respective wavelengths.

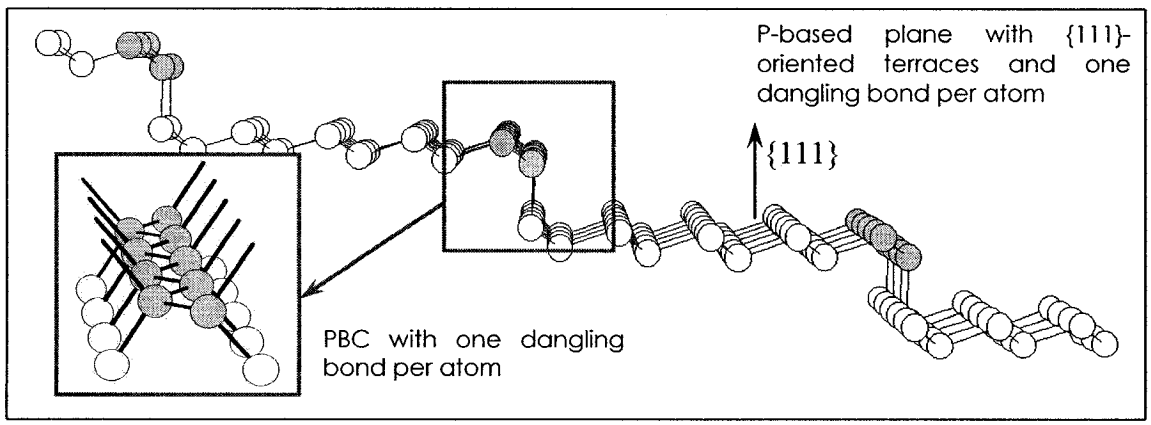

Figure 7-18: Crystallographic reconstruction of P-based plane with {111} oriented terrace and PBC at the step-edge.

In earlier chapters (Chapter 2) it was shown that P-based surfaces are the planes with the step based profiles, in which the step edges are Periodic Bond Chains (PBC-s). These

type of planes may be found in silicon crystal between {110} and {111} basic orientations, Figure 7-18.

For planes in vicinity of {111} orientation, the step terraces are {111} oriented, see Figure 7-18. Each atom on these terraces will have one dangling bond, exposed to the etchant and three, so called "back bonds", are connected to silicon atoms in bulk.

The step edges, defined as Periodic Bond Chains (PBC), on another hand have slightly different profiles. The structure of atoms at the Step-Edge in P-type planes is approaching one of the {110} oriented surface, where each atom has one dangling bond (similar to surface atoms in {111} planes) one back bond, and two bonds on the Step-Edge.

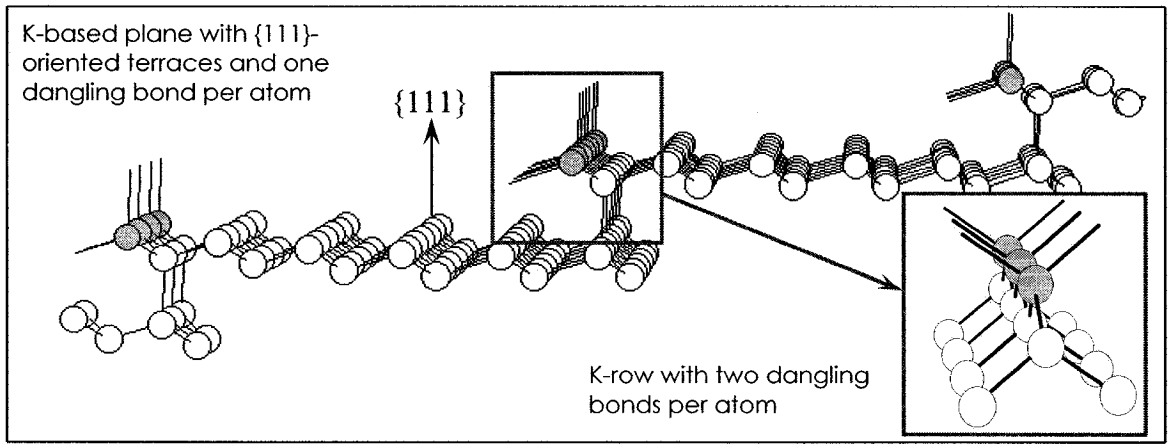

Figure 7-19: Crystallographic reconstruction of K-based plane with {111} oriented terrace and K-row at the step-edge.

Step-edges of K-based planes, Figure 7-19, has different structures as being composed of K-rows in such configuration that each atom has two dangling bonds and two back bonds.

Due to these slight differences in the bonding of atoms on the face of a terrace compared to the atoms at the edge of a step, different activation energies may be assigned to the bonding of these atoms.

M. Elwenspoek, [10], in his work, determined an activation energy for the step velocity on Si(111) to be 0.6 eV, referring to the surface roughness and dislocations in otherwise atomically flat {111} oriented surface. The Si{111} etch rate was identified to have an activation energy of 0.7 eV, [44]. It was stated in this work that the further determination of activation energies of different planes should be done experimentally.

Photon energy dependence on the wavelength is expressed as:

$$E_a = \frac{hc}{\lambda} \tag{7.5}$$

where E_a - the photon energy, eV

h – a Planck's Constant, 4.135 x 10^{-15} eV-s

c – the speed of light in vacuum, 2.998 x 10^{10} cm/s

Rearranging the Equation (7.5) we can get

$$\lambda = \frac{hc}{E_a} \tag{7.6}$$

For the activation energy 0.7 eV of the etch rate of the "flat" {111} surface, the wave length may be determined to be 1770.96 nm.

This puts the wavelength that might affect the etch rate of {111} oriented surface in the range of the IR light, i.e. being affected mostly by the heat.

However, in this work, an implication is being made to the fact that the light with shorter wavelengths, having larger energies, may have more influence on the resulting etch rates of illuminated samples. Three values for the wavelengths were chosen: ~700 nm, ~500 nm, and 400 nm.

Based on this suggestion a set of experiments was done using filtered light in the range of Red, Green and Blue wavelengths spectrum.

7.7. Experiments on p-type Si{100} and Si{110} Samples Illuminated with Filtered Light

In order to obtain the necessary wavelengths, three Optical Cast Plastic Color Filters were used – Red, Green, and Blue. The transmission graph of these filters is presented in Figure 7-20.

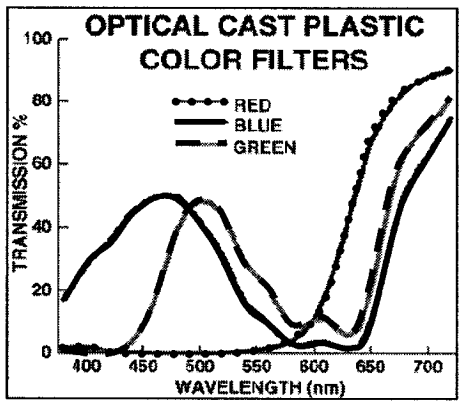

Figure 7-20: Optical Cast Plastic Color Filters transmission graph, [62].

Thermoset ADC (CD-39®) Optical filters used in the experiment are 1.5 mm thick, with refractive index of 1.501 at the room temperature and maximum continuous working temperature of 100°C.

Some alterations were done to the experimental setup of Figure 7-11 and schematically illustrated in Figure 7-21.

Given the fact that the precise temperature control proved to be somewhat challenging, both samples were positioned in the same etching environment with the only difference that one of these samples were facing incident filtered light, and another was facing away from it, see Figure 7-21. It is understandable that so-called "dark" sample in this arrangement is not going to be in the ideal dark conditions, however, for the purpose of

this experiment this arrangement proved to be sufficient to show a difference in the resulting under-etch/etch rates.

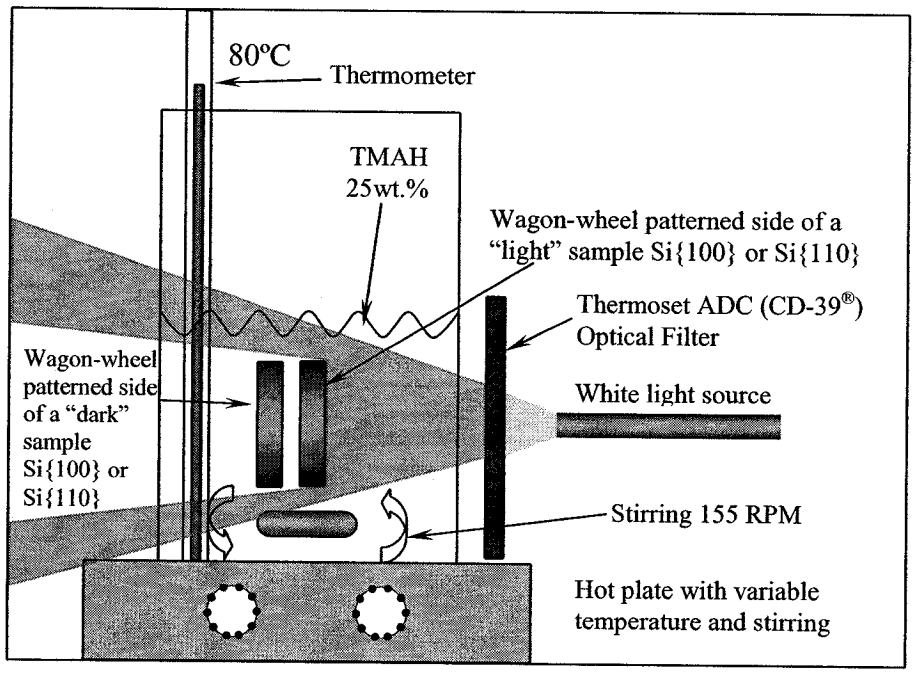

Figure 7-21: Schematic representation of the experimental setup for the comparison of a "light" sample illuminated with the filtered light and a "dark" sample in relatively dark conditions.

Presented below are the results of the experimental measurements translated into the under-etch rates for the samples etched in the same etching conditions but with one being under direct illumination – "light" sample and another – facing away form the light source – "dark" sample.

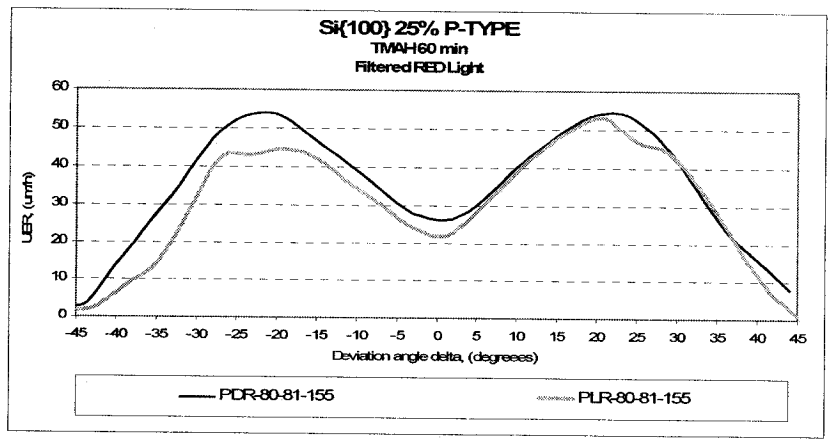

Figure 7-22: UER comparison of Si{100} samples etched in "dark" and "light" conditions illuminated with Filtered RED Light.

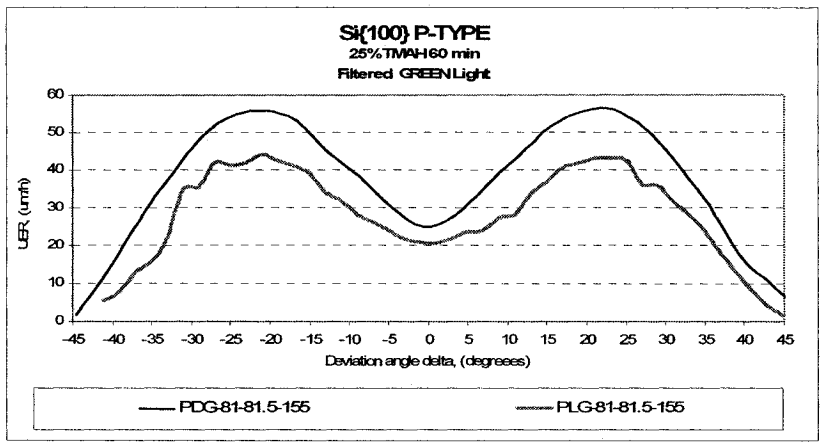

Figure 7-23: UER comparison of Si{100} samples etched in "dark" and "light" conditions illuminated with Filtered GREEN Light.

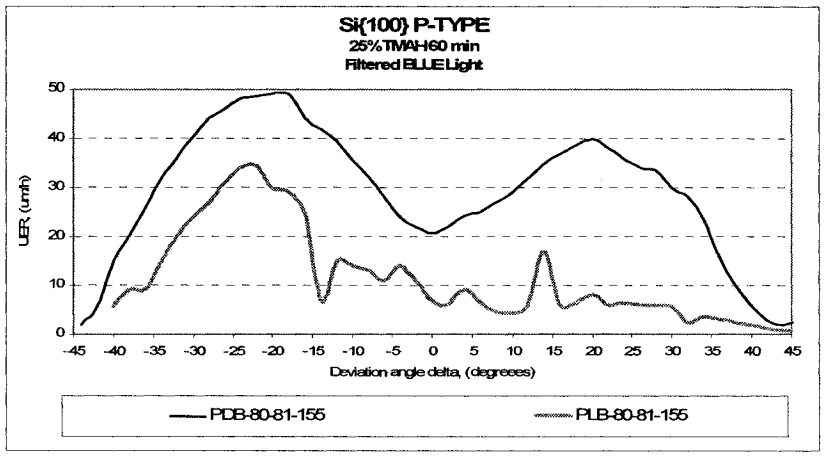

Figure 7-24: UER comparison of Si{100} samples etched in "dark" and "light" conditions illuminated with Filtered BLUE Light.

From the basic inspection of these under-etch curves, following statements may be made:

- Even though, some "noise" in the measurement curve is still present, these results proved to be consistent with the statement that the light illumination of the p-type Boron doped silicon samples predominantly slows the under-etch rates of samples in question Figure 7-22, Figure 7-23, and Figure 7-24.
- It may be observed, that there is increase of influence on the under-etch rates of illuminated samples with the decrease of the wavelength from Red light through Green and to Blue, Figure 7-22, Figure 7-23, and Figure 7-24.

- Graphs of Figure 7-22 and Figure 7-24 shows some asymmetry, which is the result of a relative sample position with respect to stirring (see Figure 7-21) that in some cases (unfortunate positioning of a sample) may result in such profiles.

In view of this work, of most interest is the light influence on particular etch rates of exposed surfaces.

7.8. Preliminary Facet Description for p-type Si{100} Samples Illuminated with Filtered Green and Red Light

The measurements of effective inclination angles[43] (see Figure 7-25) were conducted for Si{100} p-type samples illuminated with Green and Red Filtered Light. (Sample with Blue Light Illumination were not considered due to the data deviations, Figure 7-24).

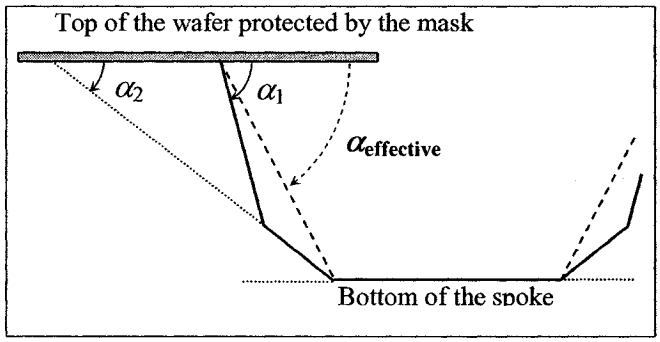

Figure 7-25: Schematic cross-section of an under-etched spoke with the indication of inclination angles α of the side-wall facets.

Preliminary calculations were done with the assumption that the same facets appear on sidewalls of spokes as in case of samples etched in "dark" conditions; see Figure 7-26(a). This assumption referred to as preliminary due to the fact that all information used for the etch rate determination is based on the optical microscope measurements alone, thus providing only partial information of sidewalls profiles. However, even based on this

[43] Effective inclination angle is the angle between an imaginary line connecting the top of a spokes' sidewall and its bottom with the top surface of the wafer.

limited information, tentative calculations may be done (with some degree of accuracy) in order to determine appearing facets and their etch rates.

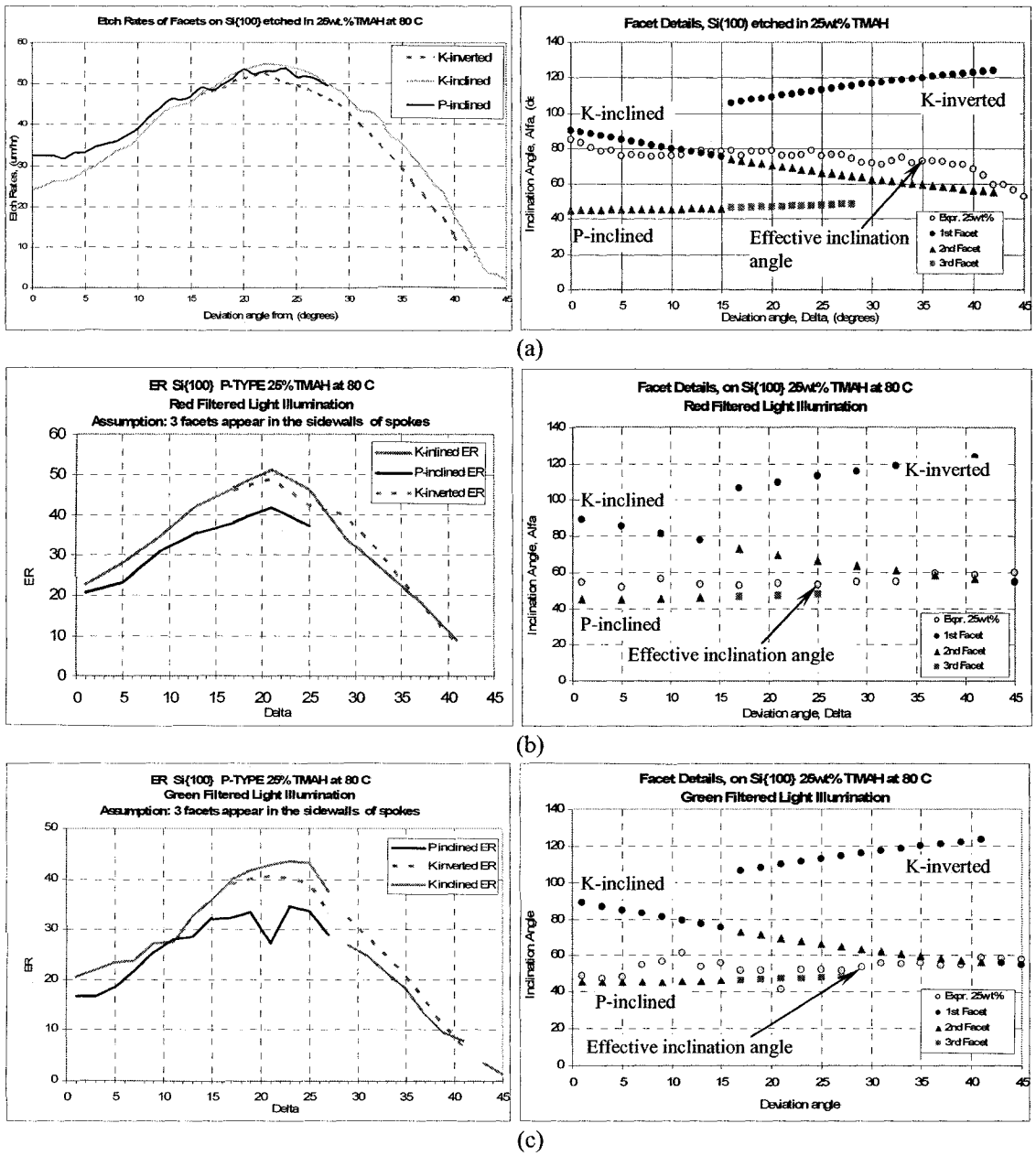

Figure 7-26: Preliminary etch rates of facets appearing on sidewalls of spokes based on the assumption that the same three facets (K-inverted, K-inclined and P-inclined) are present on the illuminated samples as on the sample etched in dark conditions. (a) ER data for Si{100} sample etched in "dark" conditions and details of facets detected on sidewalls of spokes on Si{100} etched in "dark" conditions, (b) ER data for Si{100} sample etched under Red Filtered light illumination, and (c) ER data for Si{100} sample etched under Green Filtered light illumination.

For Si{100} samples, illuminated with Red and Green Filtered Light, the calculations of the etch rates with the assumption of the presence of three types of facets (K-inverted, K-inclined and P-inclined) are summarised in graphs of Figure 7-26(b) and (c).

Based on the assumption that the same facets appear on sidewalls of spokes etched under filtered light illumination it is reasonable to accept a general tendency of a P-inclined facet (black solid line on graphs of Figure 7-26(b) and (c)) to have a larger etch rate reduction compared to the K-based surfaces (Grey lines on graphs of Figure 7-26(b) and (c)). Assuming that these preliminary calculations are correct, there is a clear etch rate reduction. The approximate values of calculated etch rates are summarised in Table 7-1 for three facets possibly appearing in sidewalls of spokes at the point of maximum ER-s ($\delta \approx 21°$):

Table 7-1: Comparison of the etch rates at the point of maximum etch rates ($\delta \approx 21°$) on Si{100} samples etched in 25% TMAH at 80°C under "dark" conditions, and illuminated with Red Filtered Light and Green Filtered Light:

	Dark Conditions	Red Filtered Light Illumination	Green Filtered Light Illumination
K-inverted	≈ 50 μm/h	≈ 50 μm/h	≈ 40 μm/h
K-inclined	≈ 55 μm/h	≈ 48 μm/h	≈ 45 μm/h
P-inclined	≈ 52 μm/h	≈ 42 μm/h	≈ 30 μm/h

From this information, it may be concluded, that the light influence on the etch rates of p-type samples is dependent on the wavelength – smaller the wavelength, larger the influence, with the general tendency of affecting P-based facets more compared to K-based surfaces.

7.9. Experiments on n-type Si{100} Samples Illuminated with Filtered Light

It was argued in the work by E. M. Conway *et al*, [59], that the n-type semiconductor is not affected to the same extend by the white light illumination. This concept was analysed in the view of my work. N-type samples, Phosphorous doped, were exposed to

white and filtered light in the same arrangement as illustrated in Figure 7-21. Optical measurements of under-etch distances and resulting calculations of under-etch rates for Si{100} were summarised in the graphs of Figure 7-27 to Figure 7-30 presented below.

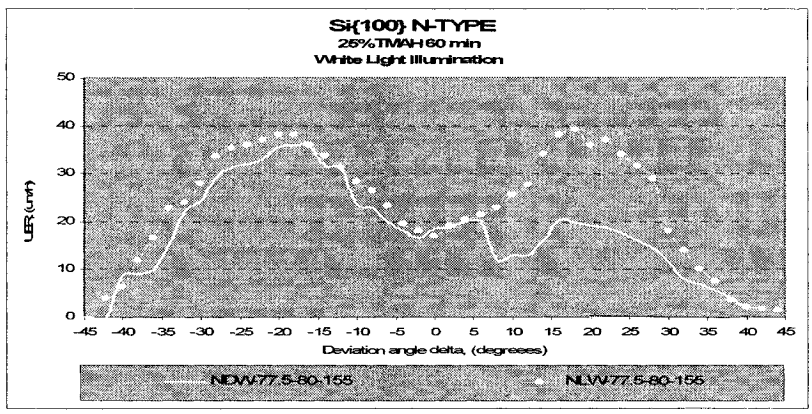

Figure 7-27: UER comparison of n-type Si{100} samples etched in "dark" and "light" conditions illuminated with White Light.

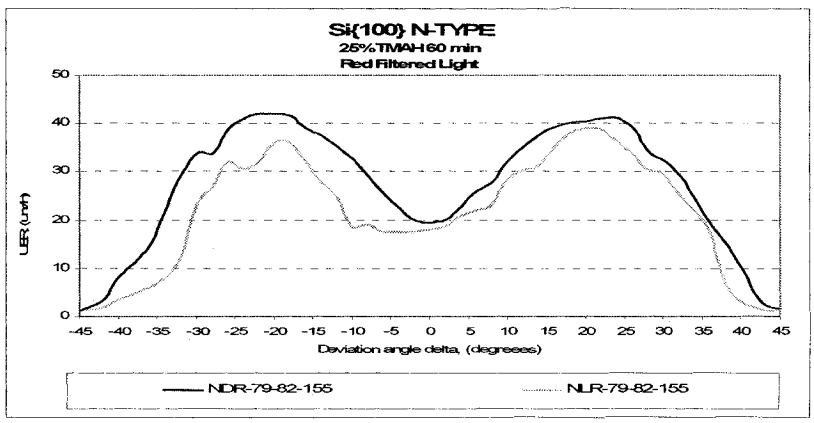

Figure 7-28: UER comparison of n-type Si{100} samples etched in "dark" and "light" conditions illuminated with Red Filtered Light.

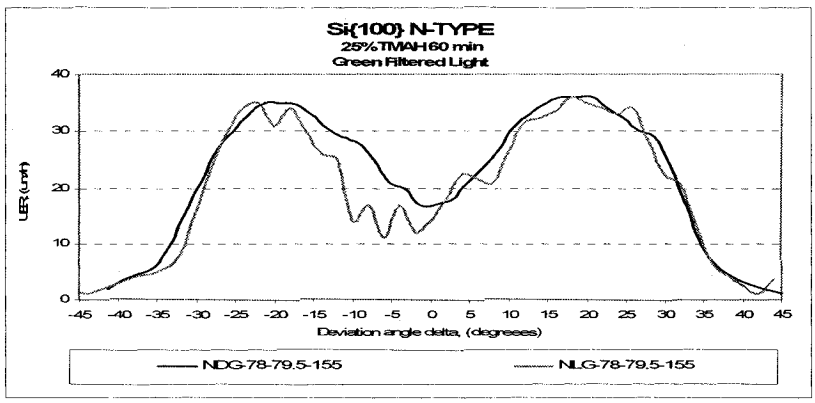

Figure 7-29: UER comparison of n-type Si{100} samples etched in "dark" and "light" conditions illuminated with Green Filtered Light.

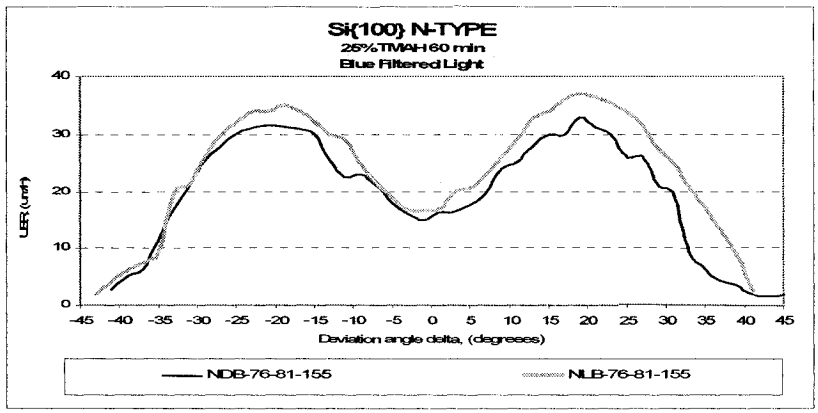

Figure 7-30: UER comparison of n-type Si{100} samples etched in "dark" and "light" conditions illuminated with Blue Filtered Light.

After general inspection of the under-etch curves of the n-type Si{100} samples illuminated with white and filtered light following may be said:

- Comparison of the under-etch rates of illuminated n-type samples to those, that were under "dark" conditions, does not show the same consistency as it were in case of p-type samples. In some occasions, illuminated samples showed decrease in the under-etch rates (illuminated with the red filtered light), Figure 7-28, in other – increase in the under-etch rate (white light illumination, and blue filtered light), Figure 7-27 and Figure 7-30, or no consistent change at all (Green filtered light), Figure 7-29.
- Thus, no significant statement can be made at this point. Further analysis is needed.

Number of follow up experiments were done on n-type Si{100} samples. And in each case there was no general trend as to the light effect on the etch rate process.

7.10. Elaboration on the p- and n-type Silicon

The surface of any material may be considered as a defect, especially for the materials with the ordered crystal structure. Silicon crystal with its diamond crystal lattice presents

a great example. On the surface, periodic crystal structure is no longer followed. Surface atoms have unsatisfied, or "dangling", bonds that in the bulk are connected to other atoms in tetrahedron structure, [63].

The discussion of the properties of intrinsic silicon could be useful, but for the purpose of this work, lightly doped samples of n-type and p-type silicon are considered, (doping concentration of approximately $10^{15}cm^{-3}$). The reason behind this choice of doped material is the fact that doped silicon used in majority of applications, and thus this consideration may be of most use.

7.10.1. N-type Silicon

First, let's consider n-type silicon material, lightly doped with Phosphorus[44] to $10^{15}cm^{-3}$. Phosphorus dissolves in silicon substitutionally, [64]. Schematic representation of this interaction is illustrated in Figure 7-31(a) and (b).

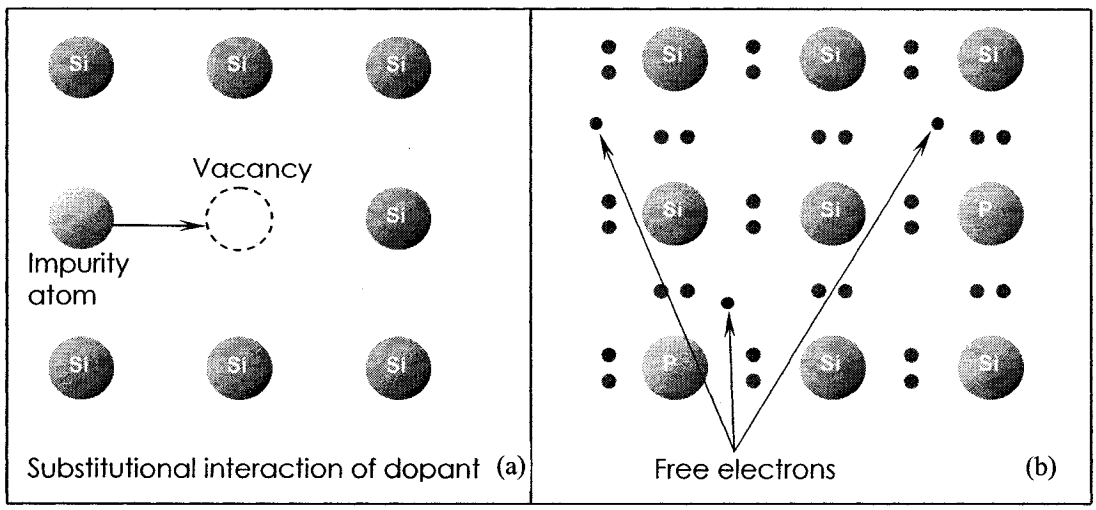

Figure 7-31: A schematic representation of (a) a substitutional interaction of dopant and (b) a view of silicon lattice doped with Phosphorus with free electrons.

[44] Phosphorus is an element of group V from periodic table.

A crystal structure of doped silicon is somewhat altered, but this modification of lattice for presented doping concentration is negligible (1 Phosphorous atom per approximately 50 million silicon atoms, considering a uniform doping).

At the surface of the n-type silicon periodic structure no longer exists. Number of unfilled states are present.

When surface is "brought into a contact with bulk" free electrons are rushed to the surface to fill free surface states thus depleting of free electrons a region adjacent to the surface. As a result, a depletion region is formed between the surface and the bulk of n-type silicon crystal.

Equilibrium is reached as soon as it makes no difference if one more electron is in the bulk or on the surface, Figure 7-32.

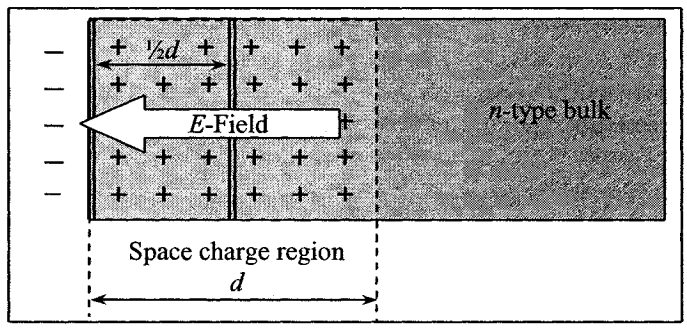

Figure 7-32: Schematic representation of the space charge region appearing in the region adjacent to the surface.

$$W = d = \left\{\frac{2\varepsilon_0\varepsilon_r U}{eN_d}\right\}^{1/2} = \left\{\frac{2\varepsilon_0\varepsilon_r V_{bi}}{eN_d}\right\}^{1/2} \tag{7.7}$$

where e is the electron charge (1.60218×10^{-19}C, value from [65]) and

U is the potential difference of the extreme values of the built-in potential, V_{bi}, which is the difference of the Fermi energies expressed as potential

ε_0 is the permittivity of free space, (8.85×10^{-14}F/cm^2)

ε_r is the dielectric constant, (11.7 for Si), [66].

Densities of electrons may be approximated to the doping concentration of the given type of semiconductor (Si).

Space charge region determination for Si in our case can be narrowed down to the one-dimensional problem.

7.10.2. P-type Silicon

P-type silicon material, lightly doped with Boron[45] to $10^{15}cm^{-3}$. Similarly to Phosphorus, Boron dissolves in silicon substitutionally, [64]. Schematic representation of this interaction is illustrated in Figure 7-31(a) and Figure 7-33.

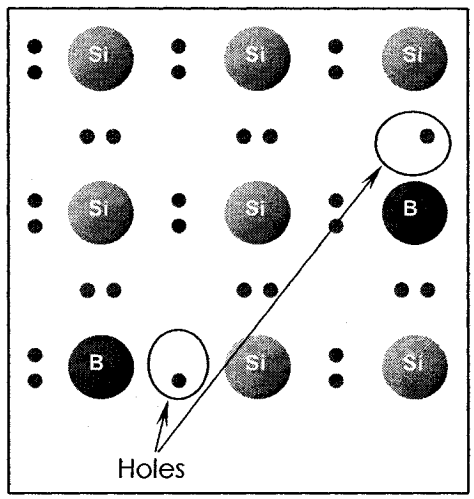

Figure 7-33: A schematic representation of a view of silicon lattice doped with Boron.

As for n-type silicon crystal structure of boron doped one is somewhat altered, but for uniform doping these modification of a crystal lattice may be neglected. However, it is of use to go through the same analysis as in case of an n-type material.

At the surface of the p-type silicon periodic structure no longer exists, hence additional (free) surface states that will attract "free" electrons from the bulk.

When surface is "brought into a contact with bulk" free electrons are rushed to the surface to fill free surface states thus depleting of free electrons a region adjacent to the

[45] Boron is an element of group III from periodic table.

surface. Though, given the fact that we are dealing with a p-type material, slightly different result will occur.

The free electrons in the bulk will move to occupy vacant surface states, thus making surface negatively charged. However, some of the electrons will recombine with holes available due to the acceptor doping.

The region depleted of free electrons, i.e. region just below the surface may be treated as a region with an accumulation of additional positive charges. The approximate schematics of this process may be illustrated as seen in Figure 7-34.

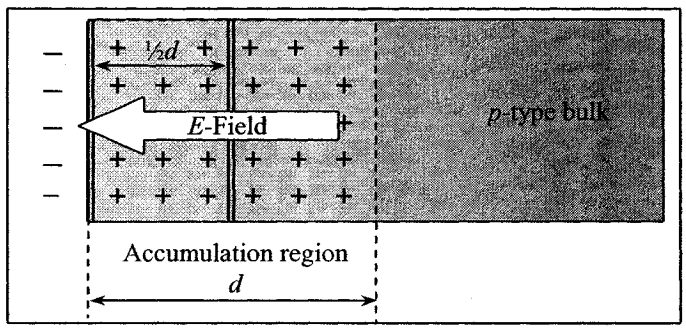

Figure 7-34: Schematic representation of the space charge region appearing in the region adjacent to the surface.

This discussion leads to the same expression for the width of a depletion region as in case of n-type silicon:

$$W = d = \left\{ \frac{2\varepsilon_0 \varepsilon_r V_{bi}}{eN_a} \right\}^{1/2}$$

7.10.3. Comparison of the depletion/accumulation regions on p-type and n-type silicon samples

However for silicon samples immersed in the TMAH (the etchant at OCP is considered at "negative" potential, [11]), p-type silicon will have a depletion region and n-type-silicon,

small depletion or accumulation region (depending on TMAH being more or less negative than the n-type silicon).

With the introduction of visible light, which is absorbed by silicon sample of either type close to the surface, additional number of electron-hole pairs is introduced.

Due to the presence of an electric field existing in the space charge region of p-type silicon, electrons will be swept towards the surface where they may take part in "so-called" reduction step (see equation (7.2)) required for the generation of new hydroxide ions at silicon surface, [11]. However, if the number of additional "free" electrons is large, they will accumulate at the surface of semiconductor, thus creating negative charge similar to that of a capacitance plate. This being the case, negatively charged surface may repel OH^- ions (see equation (7.1)), thus slowing the actual etch rate of a p-type silicon sample.

In case of n-type silicon, introduction of light has similar effect, creating additional electron-hole pairs. However, based on the relative TMAH potential (more negative than n-type silicon or less negative), free electrons may move either towards the surface (accumulation region in n-type silicon) or towards the bulk silicon (depletion region in n-type silicon due to more negative TMAH potential). If the homogeneity of the TMAH concentration as well as incident light can not be maintained across the whole n-type silicon surface, it might be reasonable to assume that there will be different depletion/accumulation regions across the n-type sample. This may explain the fact that there is no consistent light effect on the under-etch/etch rates of n-type silicon sample.

7.11. Summary

In this chapter a less exploited method of the etch rate control – light illumination - was introduced. Experimental setup was designed with the view of etching a silicon sample in TMAH in reasonably controlled temperature conditions with the addition of a light illumination.

Number of experiments was done with the use of a white light and the outcome proved to be inconsistent. Even though, the illuminated samples showed a notable decrease in the under-etch/etch rates, the results were unpredictable.

New experimental setup was designed for the illumination of the samples with the light in the range of predetermined wavelengths – Red, Green, and Blue Filtered Light. The results proved to be more reliable and repeatable. Samples illuminated with Filtered light showed consistent decrease of the under-etch/etch rates.

Preliminary etch rates were calculated for two samples illuminated with Red and Green Filtered Light. The tentative results indicated larger influence of the filtered light on P-based surfaces compared to K-based, Figure 7-26. However, further study in this area should be done to provide more precise results.

N-type samples were used for the same type of experiment. Illuminated samples of n-type silicon did not show the same consistency in decrease in the under-etch/etch rates. The discussion of this phenomenon was done in the attempt to explain such behaviour.

This portion of the work is in its beginning stage. Only preliminary data is available. However, the results that were achieved, may provide a sufficient background for the future research in the area of the etch rate control with the light illumination.

7.12. Contributions

This chapter addresses a less studied approach to the etch rate control – light illumination. The following work was done in order to identify light influence on the etch rate of concave structures:

- Experimental setup was develop in order to enable sample illuminations with the light
- Samples illuminated with white light were studied and the set of experiments with illumination by specified wavelengths were set.
- Preliminary explanation as to the choice of these wavelengths was done, and Red, Green and Blue filtered light were introduced to the experiment.
- Number of experiments were conducted with the use of Red, Green and Blue filtered light in order to see reproducibility of the outcome.
- Summarised graphs showed distinct reduction in the under-etch/etch rate of p-type silicon samples with the tendency of P-based surfaces to be more affected by the filtered light compared to the K-based (see Table 7-1)
- Summarised graphs of the measurements on n-type samples proved to be inconsistent. Under-etch/etch rate deviations did not show the same tendency of the reduction for the illuminated samples compared to the results on p-type silicon samples.

Tentative explanation of observed behaviour of n-type samples under the filtered light illumination was done, suggesting the reason for the lack of consistency in the under-etch/etch rates.

8. Summary and Conclusion

8.1. Overview

A main goal of this work was to build a fundamental theory of modelling and behaviour of planes exposed on the side-walls of concave structures anisotropically etched in bulk silicon crystal.

An explanation of some of the phenomena and anomalies met in the study of experimental data obtained from wagon-wheel under-etch experiments was provided.

Use of concave structures was justified and implemented for the purpose of this study in form of a wagon-wheel mask.

Thus, the final part of this work was devoted to the exploration of the etch control techniques, concentrating on one the control of the etch rates with white and filtered light illumination.

Below, summaries and contributions are listed in order of their progression through seven chapters[46].

8.2. Summary and Contributions

Chapter 1, or Introduction, established a general outline of this work, facilitating the understanding of pages to follow with the definitions of some basic terms.

Chapter 2, Geometric Properties of Step-based Planes, addressed all geometric properties of surfaces that appear as facets on sidewalls of concave structures/spokes obtained in under-etch wagon-wheel experiments.

[46] Bullets in text are indicative of specific contributions.

A large portion of these parameters was described by Z. Elalamy *et al.*,[9]. However, as a part of the research group, I contributed to a majority of this study.

- My particular share of the work included detailed calculations of Miller Indices of all planes appearing on sidewalls of spokes and the crystallographic reconstruction of said surfaces. The work in this Chapter is necessary for a fundamental understanding of silicon surface geometry and a large part of subsequent study is based on this understanding.

Chapter 3, Step Spacing Determination, details the parameters that would, contribute to the mathematical model of anisotropically etched concave structures.

- This chapter expands the general analysis of two families of planes that were typically observed in the under-etch wagon-wheel experiment. As an important parameter fundamental to subsequent discussions, step spacings on P- and K-based planes were calculated. The basis for these calculations was a traditional Step-Based Model of P- and K-based planes with terraces composed of {111}-oriented surfaces. However, this model was extended to include planes in the vicinity of two basic orientations, {100} and {110}, as being composed of steps and terraces of {100} and {110} orientation, respectively.
- The concept of "cross-over" in terrace orientation for planes rotated from {111} towards {100} or {110} oriented surfaces was introduced and analyzed.
- The notion of a crossover deviation angle at which the width of {111} terrace is equal to the width of {100}- of {110}-oriented terraces, and the determination that this crossover occurs at $\delta \approx 19^{\circ}$ for both families of planes on Si{100}, where the under-

etched facets are observed to be composed of 3 facets, and there is the potential for quasi continuous terrace edges across all three facets.

- Si{110} wafers provide larger variety of facets on sidewalls of spokes and, consequently the crossover in terrace orientation can be listed for the respective facets as follows, see Figure 3-16:

  - K2-inclined, K2-inverted - $\delta \approx 54.5°$
  - K1-inclined, K1-inverted - $\delta \approx 72.5°$
  - K-vertical - $\delta \approx 25.5°$
  - P-vertical - $\delta \approx 76.5°$
  - P-inclined, P-inverted - $\delta \approx 25.5°$ and $\delta \approx 43.5°$
  - K2-inclined, K2-inverted - $\delta \approx 25°$

- When the top-most facet in a wagon-wheel under-etch experiment is a crossover facet, this often corresponds to a local or global maximum in under-etch rate, for both Si{100} (at $\delta \approx 19°$) and Si{110} under-etch experiments, (at $\delta \approx 25°$ and $\delta \approx 76°$).

Crossovers may significantly influence the complexity of etch rate variation and facet appearance or disappearance in an under-etch experiment

Chapter 4, Removal Frequency and Etch Rates, connects the etch rate of any given facet to the actual plane geometry.

Terrace orientation, {111}, {110}, or {100}, plays an important role in the determination of removal frequencies.

The basis for these calculations was the generally accepted step-based model of planes with {111}-oriented terraces. However, following the discussion of Chapter 3, K-based

and P-based planes with {100}- and {110}-oriented terraces, respectively, were considered in the frequency of removal (FR) of chain/row from the step-edge calculations.

First, mathematical model for planes with {100}- and {110}-oriented terraces suggested that the etch rates of these terraces (i.e. "non-zero" etch rates of {100}- and {110}-oriented terraces) can not be neglected for this model to reflect the physics of the etching process. Thus, three different separation strategies are examined:

1. Assumption that the influence of non-zero etch rate of {100}- and {110}-oriented terraces decreases linearly and reaches zero at the crossovers, and calculate what must be the chain/row removal frequencies.
2. Assumption that the etch rate due to chain/row removal from the step-edges of the planes with {100}- and {110}-oriented terraces is such that it increases linearly to the crossover and calculate what must be the variation with θ of the non-zero etch rate of {100}- and {110}-oriented terraces.
3. Assumption that there is a transition zone near the crossover, and that the etch rate due to chain/row removal increases linearly to the edge of that transition zone.

As a basis for these calculations, experimental etch rates summarised in canonical curves are used, (see Figure 4-5). The etch rate of basic {111}-oriented terraces is considered to be comparatively negligible for this analysis.

General observation of the last, third, approximation, where so-called Transition Zone concept was used, FR calculations for planes with {100}- and {100}-oriented terraces

suggested the results more consistent when compared to FR of planes with {111}-oriented terraces (Figure 4-5).

Further explorations of different approximations to this mathematical model might provide yet better reflection of physical processes in anisotropic etch of step-based surfaces. However, for the purpose of this study, Equation of the line approximation for chain/row removal from the step-edges with the consideration of a Transition Zone provides satisfactory results, that are used in following chapters.

Removal frequency is not entirely new concept, but it had to be augmented in order to accommodate rather original view on geometry of step-based surfaces.

- Removal frequency was calculated not only for surfaces with {111}-oriented terraces but also with consideration of P-based and K-based planes with {110}- and {100}-oriented terraces, respectively.
- A mathematical model was introduced, were FR for planes with {110}- and {100}-oriented terraces should be viewed as composed of two components: one accounting for "non-zero" etch rates of {100}- and {110}-oriented terraces, and another for chain/row removal from step edges.
- It was suggested, for better reflection of actual physics of the etching process, that these two components should be used for modelling etch rates. The etch rate component of a plane with {100}- or {110}-oriented terrace, accounting for chain/row removal from a step, should be equivalent to the etching process of the surfaces with {111}-oriented terraces of which etch rates may be considered negligible.
- Three different approximations of original mathematical model are analysed.

- One of these approximations, i.e. equation of the line approximation for chain/row removal from the step-edges with the consideration of a Transition Zone is considered most reflective of physical process.

The canonical graphs of frequency of removal vs. theta, for both P-based and K-based planes, are used in subsequent chapters.

Chapter 5, Step-Edge Velocity, introduces and develops a concept of step-edge velocity. Based on the etch rate data, collected in the wagon-wheel experiment for Si{100} and Si{110} samples, these velocities were calculated as a step-edge advancement in the direction perpendicular to the front of a step-edge – absolute step-edge velocity. These velocities were translated into the values relative to a boundary between two adjacent facets, thus enabling a possibility of comparison of these velocities as well as consideration of their relative movement (same or opposite direction). All velocities (absolute as well as relative) were determined with the consideration of the respective terrace orientation and with the use of Equation of the Line Approximation for the chain/row removal from the step-edges and with the consideration of a Transition Zone.

With the assumption that the used mathematical model is acceptable for the purpose of this study, regions with the dominating influence of "non-zero" terrace etch rates for {100}- and {110}-oriented terraces were identified.

Contributions, based on the ER data collected by Z. Elalamy, [9], are in the interpretation of this data.

- Translation of the etch rates of facets in under-etch experiment, using Equation of the Line Approximation for the chain/row removal from the step-edges and with the consideration of a Transition Zone, into two components, where applicable.
- Introduction of a concept of Absolute Step-Edge Velocity and Relative Step-Edge Velocity.
- Analysis of the relative step-edge velocities for the data from Si{100} and Si{110}.
- Identification, based on the assumption of applicability of used mathematical model, of certain areas of interest for the SE velocities such as:
    - Areas with different dominating components (i.e. dominating component due to "non-zero" ER of {100}- or {110}-oriented terraces, or due to chain/row removal from the step-edges)
    - Areas on which step-edges of neighbouring facets move in opposite directions.

Chapter 6, Atomic Level Analysis of Step-based Silicon Surfaces, introduces a detailed analysis of surfaces in concave structures on atomic level. From the previous research it was shown that based on angles between interacting chains/rows for two families of planes, K-based and P-based, maximum of three original combinations are possible for each of these angles (60°, 90°, and 120°), i.e. PBC/PBC, PBC/K-row, and K-row/K-row, making the total count of these combinations nine. However, only seven of said combinations were detected in concave structures of wagon-wheel under-etch experiment.

Using this information atomic level analysis was conducted for two of the most frequent combinations: K-P-120° and K-K-90°.

Based on this analysis it was shown (on the example of K-P-120° combination) that zipping is more favoured from P-based steps to K-based steps than from K-based steps to P-based steps.

(i) Roughness patterns on one of the K-based facets are consistent with step-based zipping independently from each of the two facet boundaries;

(ii) Analysis of the configuration of boundary atoms for the K-P-120° intersection in the ideal crystal lattice suggests less-stable boundary atoms when zipping from the P-based side.

Outcome of the analysis of K-K-90° did not support the likelihood of K-row propagation across the boundary from one K-based facet to another.

Next, the step-spacing correspondence of steps on adjacent facets was introduced and exact values were summarized in Table 6-1 and Table 6-2. Due to the complexity of the combinations of adjacent facets detected on Si{110}, the analysis of step-spacing correspondence was done in greater detail.

In addition the analysis of three cases of the facets with "saw-tooth" profile was conducted with the view of tracing common trends that lead to such surface roughness. Outcome of this analysis is not entirely conclusive; however, it was observed that at least in these three cases, "saw-tooth" profile appeared on surfaces with following similarities:

(i) Surfaces that appear as a top-most facets

(ii) Surfaces with{111}-oriented terraces, not vicinal to basic, {111}, orientation, with $\theta > 5°$.

(iii)These surfaces with similar step-edge velocity (~200 $\mu m/h$)

My contribution in this portion of work is in introduction of an atomic level analysis of the interactions between adjacent facets.

- Step-spacing correspondence was calculated for all surfaces detected on sidewalls of spokes in under-etch wagon-wheel experiment with the consideration of crossovers in terrace orientation.
- Areas with more significant step-spacing correspondence were indicated (1:1 and 1:2)
- Analysis of two most frequent cases K-P-120° and K-K-90° was conducted and showed certain tendencies in the interaction between the facets containing such combinations:
  - On the example of K-P-120° combination it was shown that zipping is more favoured from P-based steps to K-based steps than from K-based steps to P-based steps.
  - Roughness patterns on one of the K-based facets are consistent with step-based zipping independently from each of the two facet boundaries;
  - Analysis of the configuration of boundary atoms for the K-P-120° intersection in the ideal crystal lattice suggests less-stable boundary atoms when zipping from the P-based side.
  - Outcome of the analysis of K-K-90° did not support the likelihood of K-row propagation across the boundary from one K-based facet to another.
- Analysis of three cases of the facets with "saw-tooth" profile showed a possibility of common trends based on crystallographic construction of these surfaces, their relative location with respect to other facets, step-edge velocity, etc

Chapter 7, Etch Rate Control: Introduction of the Light Illumination to Wagon-Wheel Under-Etch Experiment, a less exploited method of the etch rate control – light illumination - was introduced. Experimental setup was designed with the view of etching a silicon sample in TMAH in reasonably controlled temperature conditions with the addition of a light illumination.

Number of experiments was done with the use of a white light and the outcome proved to be inconsistent. Even though, the illuminated samples showed a notable decrease in the under-etch/etch rates, the results were unpredictable.

New experimental setup was designed for the illumination of the samples with the light in the range of predetermined wavelengths – Red, Green, and Blue Filtered Light. The results proved to be more reliable and repeatable. Samples illuminated with Filtered light showed consistent decrease of the under-etch/etch rates.

Preliminary etch rates were calculated for two samples illuminated with Red and Green Filtered Light. The tentative results indicated larger influence of the filtered light on P-based surfaces compared to K-based. However, further study in this area should be done to provide more precise results.

N-type samples were used for the same type of experiment. Illuminated samples of n-type silicon did not show the same consistency in decrease in the under-etch/etch rates. The discussion of this phenomenon was done in the attempt to explain such behaviour.

This portion of the work is in its beginning stage. Only preliminary data is available. However, the results that were achieved, may provide a sufficient background for the future research in the area of the etch rate control with the light illumination.

The following work was done in order to identify light influence on the etch rate of concave structures:

- Experimental setup was develop in order to enable sample illuminations with the light
- Samples illuminated with white light were studied and the set of experiments with illumination by specified wavelengths were set.
- Preliminary explanation as to the choice of these wavelengths was done, and Red, Green and Blue filtered light were introduced to the experiment.
- Number of experiments were conducted with the use of Red, Green and Blue filtered light in order to see reproducibility of the outcome.
- Summarised graphs showed distinct reduction in the under-etch/etch rate of p-type silicon samples with the tendency of P-based surfaces to be more affected by the filtered light compared to the K-based
- Summarised graphs of the measurements on n-type samples proved to be inconsistent. Under-etch/etch rate deviations did not show the same tendency of the reduction for the illuminated samples compared to the results on p-type silicon samples
- Tentative explanation of observed behaviour of n-type samples under the filtered light illumination was done, suggesting the reason for the lack of consistency in the under-etch/etch rates.

8.3. Future Work

Some portions of this work may provide a good background for further advanced study in the area of wet-chemical anisotropic etching of concave structures on silicon.

The development of a mathematical model that considers terrace orientations of step-based surfaces with non-negligible etch rates, may be developed further, providing better definition of a Transition Zone (see Chapter 4).

Step-edge velocities, following enhanced model (if such model is developed) will provide better description of the etching process.

All of these factors will serve as a background for more precise analysis of the facets and their interactions on atomic level.

Addressing the last portion of this study, further work needs to be done in order to determine with precision the specific wavelengths and their influence on the etch rate reduction of p-type silicon samples. There is a reasonable indication of P-based surfaces being more affected by the light (or, perhaps, only light with the specific energy) compared to the K-based planes. This direction of future study may provide exceptional control of the predetermined structures in anisotropic etchant.

Behaviour of the n-type silicon samples needs to be studied further. The preliminary experiments, conducted in this work on n-type silicon wafers, might not be reflective of the actual effect of the light on the etch rates of these samples.

Thus, the final part of my work, introduced the light illumination as a tool that might be applied to control the etch rates of silicon surfaces in concave structures.

9. References

[1] M. Lannoo, Nanotechnology and Semiconducting Materials, Materials: Science and Engineering, Max Planck Multimedia, p. 63-66, 2005

[2] T. Sargent, The dance of molecules: How nanotechnology is changing our lives, Viking Canada, Penguin Books, Ltd., 2005

[3] www.icknowledge.com/glossary/s.htmlc, 2005

[4] http://www.definethat.com, 2005

[5] http://ece-www.colorado.edu/~bart/book/book/chapter2/ch2_2.htm B.Van Zeghbroeck, 2004

[6] Dr. Kathy Rooney, Encarta Concise English Dictionary, Bloomsbury Publishing Plc., 1999-2000

[7] A.J. Nijdam, Anisotropic Wet-Chemical Etching of Silicon, Pits, Peaks, Principles, Pyramids and Particles, Ph. D. Theses, University of Twente, Enschede, the Netheralnds, 2001

[8] L. M. Landsberger, S. Naseh, M. Kahrizi, and M. Paranjape, On Hillocks Generated During Anisotropic Etching of Si in TMAH, Journal of Micromechanical Systems, Vol. 5, No. 2, 1996

[9] M.-Z. Elalamy, Modeling of Anisotroping Etching of Silicon in Tetra-Methyl Ammonium Hydroxide: Anomalies due to Facet Boundary Effects, a Thesis in the Electrical and Computer Department, Concordia University, Montreal, Canada, 2002

[10] M. Elwenspoek, The form of etch rate minima in wet chemical anisotropic etching of silicon, J. Micromech. Microeng., Vol. 6, p. 405-409, 1996

[11] H. Seidel, L. Csepregi. A. Heuberger, H. Baumgartel, Anisotropic Etching of Crystalline Silicon in Alkaline Solutions I. Orientation Dependence and Behaviour of Passivation Layers, J. Electrochem. Soc., Vol. 137, No. 11, p. 3612-3626, 1990

[12] J. van Suchtelen, K. Sato, E. van Veenendaal, A. J. Nijdam, J. G. E. Gardeniers, W. J. P. van Enckevort, M. Elwenspoek, Simulation of anisotropic wet etching using a physical model. Sensors and Actuators A, 84, 2000

[13] M. A. Gozalvez , R. M. Nieminen, Surface morphology during anisotropic wet chemical etching of crystalline silicon, New J. Phys, 2003

[14] M. Asano, T. Cho, and H. Muraoka, Application of chlorine in semiconductor technology, Electrochem. Soc. Extended Abstracts, p. 911, 1976

[15] U. Schnakenberg, W. Benecke, and P. Lange, TMAHW etchants for silicon micromachining", 6th Int. Conf. Solid-State Sensors and Actuators, Tranducers'91, p. 815-818, 1991

[16] O. Tabata, R. Asahi, H. Funabashi, and S. Sugiyama, Tec. Dig. of Int. Conf. on Solid-State Sensors and Actuators, 811, 1991

[17] J. Haneveld, H. Jansen, E. Berenschot, N. Tas, and M. Elwenspoek, Wet anisotropic etching for fluidic 1D nanochannels, Journal of Micromech. Microeng., Vol 13, p. S62 – S66, 2003

[18] L. Pavesi, Z. Gaburro, L. Dal Negro, P. Bettotti, G. Vijaya Prakash, M. Gazzanelli, C. J. Oton, Nanostructured silicon as a photonic material, Optics and Lasers in Engineering, Vol. 39, p. 345 – 368, 2003

[19] I. Stateikina, L. M. Landsberger, M. Kahrizi, N. Hoque, and V. Rossokhaty, Silicon Wet Etch Anisotropy: Analysis of the Impact of {111}, {110}, {100} Terrace Widths, Sensors and Materials, Vol. 17, No.4, p. 199-210, 2005

[20] P. Allongue, V. Kieling, H. Gerischer, Etching of silicon in NaOH solutions. Part I : in situ STM investigation of Si(111), J. Electrochem. Soc., 140, 1009-1016, 1993

[21] M. Elwenspoek, U. Lindberg, H. Kok, L. Smith, Wet chemical etching mechanism of silicon, MEMS'94, Proceedings, IEEE Workshop, p. 223-228, 1994

[22] M. Elwenspoek, The form of etch rate minima in wet chemical anisotropic etching of silicon, Journal of Micoromech. Microeng., Vol. 6, p. 405-409, 1996

[23] J. Kasparian, M. Elwenspoek, P. Allongue, Digital computation and in situ WTM approach of silicon anisotropic etching, Surface Science, Vol. 388, p. 50-62, 1997

[24] A. J. Nijdam, J. W. Berenschot, J. van Suchtelen, J. G. E. Gardeniers, and M. Elwenspoek, Velocity sources as an explanation for experimentally observed variations in Si{111} etch rates, Journal of Micromech. Microeng., Vol. 9, p. 135 – 138, 1999

[25] J. van Suchtelen, K. Sato, E. van Veenendaal, A. J. Nijdam, J. G. E. Gardeniers, W. J. P. van Enckevort, and M. Elwenspoek, Simulation of anisotropic wet-chemical etching using a physical model, Proceedings of IEEE MEMS 99, Workshop, Orlando, p. 332 – 337, 1999

[26] R. E. Oosterbroek, J. W. Berenschot, H. V. Jansen, A. J. Nijdam, G. Pandraud, A. van den Berg, and M. Elwenspoek, Journal of Microelectromechanical Systems, Vol.9, No. 3, p. 390 – 398, 2000

[27] A. J. Nijdam, J. G. E. Gardeniers, J. W. Berenschot, E. van Veenendaal, J. van Suchtelen, and M. Elwenspoek, Influence of the angle between etched (near) Si{111} surfaces and the substrate orientation of the underetch rate during anisotropic wet-chemical etching of silicon, Journal of Micromech. Microeng., Vol. 11, p. 499 – 503, 2001

[28] E. van Veenendaal, H. M. Cuppen, J. P. van Enckevort, J. van Suchtelen, A. J. Nijdam, M. Elwenspoek, and E. Vlieg, A Monte Carlo study of etching in the presence of a mask junction, Journal of Micromech. Microeng., Vol. 11, p. 409 – 415, 2001

[29] S. Tan, R. Boudreau, and M. Reed, Effects of Mask misalignment and wafer misorientation on silicon V-groove etching, Sensors and Materials, Vol. 15, No. 2, p.101 – 112, 2003

[30] M. A. Hines, Understanding the evolution of silicon surface morphology during aqueous etching, Sensors and Materials, 13 (5), p.247-258, 2001

[31] A. Pandy, Experimental Investigation of Anisotropic Etching of Silicon in TMAH, a Thesis in the Electrical and Computer Engineering Department, Concordia University, Montreal, Canada, 2002

[32] L. M. Landsberger, Microtransducer Process Technology, a Course pack for the ELEC-6251 in the Electrical and Computer Engineering Department, Concordia University, Montreal, Canada, 2000

[33] I. Stateikina, M.-Z. Elalamy, L. M. Landsberger, M. Kahrizi, Step-Based Silicon Surfaces, in Wet Anisotropic Etching, CCECE, Montreal, May 2003

[34] M.-Z. Elalamy, L. M. Landsberger, A. Pandy, M. Kahrizi, I. Stateikina, S. Michel, Anomalies in Modelling of Anisotropic Etching of Silicon, Journal of Vacuum Science and Technology, A 20(6) p.1927, 2002

[35] M.-Z. Elalamy, L. M. Landsberger, M. Kahrizi, I. Stateikina, S. Michel, Modelling of Anisotropic Etching of Silicon due to Facet Boundary Effects, Sensors and Materials, Vol.15, No.2, 2003

[36] R. A. Wind, M. A. Hines, Surf. Sci. 460, 21, 2000

[37] P. Jacob and Y. J. Chabal, Chemical Etching of Vicinal Si(111): Dependence of the Surface Structure and the Hydrogen Termination on the pH of the Etching Solutions. J. Chem. Phys. 95 (4), 1991

[38] A. A. Baski, S. C. Erwin, L. J. Whitman, The structure of Silicon Surfaces from (001) to (111). Surf. Sci. 392, 69 , 1997

[39] S. Naseh, Experimental Investigation of Anisotropic Etching of Silicon in Tetra-Methyl Ammonium Hydroxide, a Thesis in the Electrical and Computer Department, Concordia University, Montreal, Canada, 1995

[40] www.en.wikipedia.org/wiki/Vector_calculus, June, 2006

[41] N. Hoque, Analysis of Terrace Width and Etch Rate on Step Based Silicon Planes in Wet Anisotropic Etchant, a Project in the ECE Department, Concordia University, Montreal, 2003

[42] I. Stateikina, M.-Z. Elalamy, L. M. Landsberger, M. Kahrizi, Analysis of Step–Based Silicon Surfaces at Facet Boundaries during Wet Anisotropic Etching, submitted to Journal of Vacuum Science and Technology, 2003

[43] M. A. Gosalvez, R. M. Nieminen, P. Kilpinen, E. Haimi and V. Lindroos, Anisotropic wet chemical etching of crystalline silicon: atomistic Monte-Carlo simulations and experiments, Applied Surface Science, v. 178, p. 7-26, 2001

[44] Yanfeng Jiang and Quing-an Huang, A Physical Model for Silicon Anisotropic Chemical Etching, Semiconductor Science and Technology, v. 20, p. 524-531, 2005

[45] T. Kakinaga, N. Baba, O. Tabata, Y. Isono, K-Ehrmann, J.G. Korvink, Simulation of Anisotropic Chemical Etching of Single Crystalline Silicon Using a Cellular – Automata, 3rd PCWES-2002,Conference Proceedings, p. 31-36, 2002

[46] A. Horn, H. Schröder, E. Obermeier, G. Wachutka, Simulation of Orientation Dependent Etching of Silicon Using a New Step Flow Model of 3D Structuring, Preprint SFB-438-0010, Technische Universität München, Universität Ausburg, 2000

[47] M. A. Gosalvez, Atomistic Modelling of Anisotropic Etching of Crystalline Silicon, Ph. D. Theses in the Department of Engineering Physics and Mathematics, Helsinki University of Technology, Finland, 2003

[48] O. Tabata, Anisotropic etching of silicon in TMAH solutions, Sensors and Materials, Vol. 13, No. 5, p. 271-283, 2001

[49] O. Bisi, S. Ossicini, L. Pavesi, Porous Silicon: a Quantum Sponge Structure for Silicon Based Optoelectronics, Surface Science Reports, vol.38, p. 1-126, 2000

[50] L. Pavesi, Z. Gaburro, L. Dal Negro, P. Bettotti, G. Vijaya Prakash, M. Gazzanelli, C. J. Oton, Nanostructured Silicon as Photonic Material, Optics and Lasers in Engineering, vol. 39, p. 345-368, 2003

[51] M. Shikida, K. Sato, K. Tokoro, and D. Uchikawa: Comparison of Anisotropic Etching Properties between KOH and TMAH Solutions, Proc of IEEE Int. MEMS-99 Conf., p. 315-320, Orlando, 17. 21. Jan. 1999

[52] O. Tabata, Anisotropy and selectivity control of TMAH, MEMS'98, p. 229-233, 1998

[53] O. Tabata, M. Yashima, T. Yoshioka, K. Sato, Effect of potassium ion on anisotropy of TMAH, 10th Int. Conf. on Solid-State Sensors and Actuators, p. 542, 1999

[54] M. Madou, Fundamentals of Microfabrication, CRC press, ISBN: 0-8493-9451-1, 1997

[55] E. Steinsland, M. Nese, A. Hanneborg, R. W. Bernstein, F. Meringdal, H. Sandmo, and G. Kittilsland, Boron etch-stop in TMAH solutions, Sensors and Actuators, A54, p.728-732, 1996

[56] C. M. A. Ashruf, P. J. French, P. M. M. C. Bressers, P. M. Sarro, and J. J. Kelly, A new contactless electrochemical etch-stop based on a gold/silicon/TMAH galvanic cell, Sensors and Actuators, A66, p. 284-291, 1998

[57] E. H. Klaassen, Micromachined Instrumentation System, A Ph. D. Dissertation in Electrical Engineering Department, Stanford University, 1996

[58] J. J. Pak, G. W. Neudeck, A. E. Kabir, Micromechanical Sensors Using Merged Epitaxial Lateral Overgrowth of Silicon, ECE Technical Reports, Purdue University, 1993

[59] E. M. Conway, V. J. Cunnane, Electrochemical Characterization of Si in Tetra-Methyl Ammonium Hydroxide (TMAH) and TMAH:Triton-X-100 solutions under

White Light Effects, Journal of Micromechanics and Microengineering, v. 12, p.136-148, 2002

[60] C. H. Özdemir, J. G. Smith, New phenomena observed in electrochemical micromachining of silicon, Sensors and Actuators A, Vol. 34, No. 1, p. 87-93, 1992

[61] http://www.hardwareanalysis.com/content/article/1583.5/ , 2006

[62] Edmund Optics On-Line Catalogue, http://www.edmundoptics.com/onlinecatalog, 2006

[63] http://www.tf.uni-kiel.de/matwis/amat/semi_en/kap_2/backbone/r2_2_4.html, H. Föll, 2004

[64] A. A. Brown, P. J. Rosser, P. B. Moynagh, D. J. Godfrey, D. de Cogan, D. Nobili, Diffusion, Solid Solubility and Implantation of Group III and Group V Impurities, Properties of Silicon, INSPEC, The Institution of Electrical Engineers, London and New York, No. 4, p. 325-407, 1988

[65] S. M. Sze, Physics of Semiconductor Devices, 2nd edition, Bell Laboratories, Inc. Murray Hill, John Wiley & Sons, 1981

[66] Donald A. Neamen, Semiconductor Physics & Devices: Basic Principles, 2nd edition, McGraw-Hill, 1997

[67] B.J.Van Zeghbroeck http://www.ee.ui.ac.id/~astha/courses/ts/teksem/thermo.htm, 1997

[68] http://www.lyon.edu/webdata/users/shutton/phy335-fall2003/Fermilevelofsemiconductors.doc, 2003

[69] N. Sanjay Rebello, Chandramouli Ravipati, Dean A. Zollman, and Lawrence T. Escalada, Kansas State University, Physics Department, Computer Simulation of pn Junction Devices, http://perg.phys.ksu.edu/papers/sds/SDSPaper.htm, 2006

Appendix I

I. Oxidation and Photolithography

A necessary step in creation of any 3D structure as well as IC components is a patterning of silicon in such way that only predefined areas of silicon surface are exposed to further processing. This step may be achieved via oxidation and following photolithography. Oxidation is a natural process resulting in formation of silicon dioxide layer (SiO_2) on the surface of silicon crystal exposed to the oxygen (native oxide). Silicon dioxide, or oxide, is an excellent insulator (dielectric constant of 3.9 and a breakdown limit of 107 V/cm). Oxide can be used as insulator in IC and/or as a masking material for the pattern transfer on silicon surface, Figure I-1. To increase the rate of oxide growth, thermal oxidation or chemical vapor deposition is used in CMOS (Complimentary Metal Oxide Semiconductor) technology.

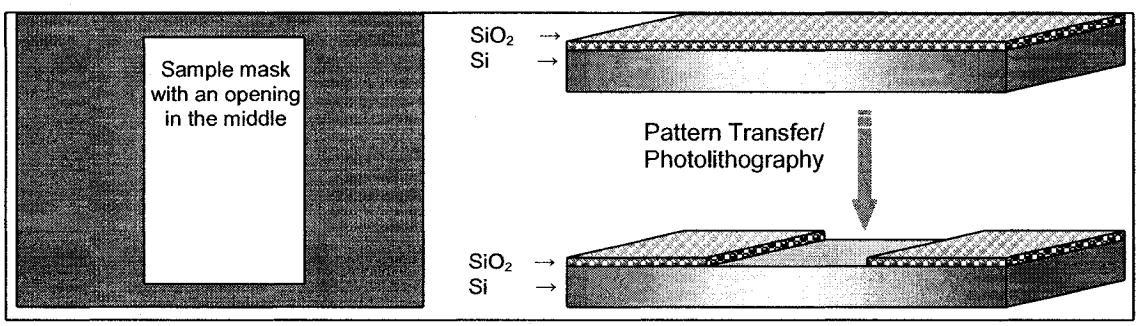

Figure I-1: Schematic representation of a simple geometric shape transfer onto the silicon surface using photolithography.

In CMOS fabrication sequence, oxidation precedes almost every step involving pattern transfer or photolithography, Figure I-1. Photolithography[47] is the process of transporting geometric shapes from a mask to the surface of a silicon wafer used for further processing.

[47] Photolithography meaning light-stone-writing (φωτο-λιθο-γραφία) from Greek

Appendix II

II. Determination of Removal Frequency

Unit-Step Width for K-based plane with {100}-oriented terraces ($USW_{\{100\}}$), can be determined as a ½ of side diagonal of a Unit-Cell Cube, Figure II-1:

$$USW_{\{100\}} = \frac{5.43\sqrt{2}}{2} = 3.83969\,\text{Å} \tag{1}$$

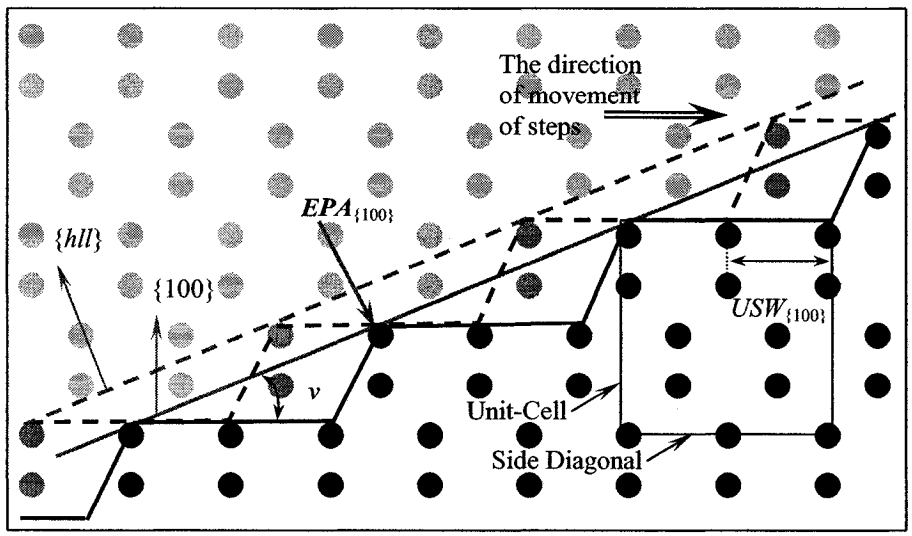

Figure II-1: Effective plane advancement of K-based plane with {100}-oriented terraces when all the step-edges move simultaneously one USW in the direction of movement of steps.

Therefore, the Effective Plane Advancement (EPA) can be determined as:

$$EPA_{\{100\}} = USW_{\{100\}} \cdot \sin\nu \tag{2}$$

Similarly, $USW_{\{110\}}$ and respective EPA for P-based planes with {110} oriented terraces can be identified as follows, see Figure II-2:

$$USW_{\{110\}} = a = 5.43\,\text{Å} \tag{3}$$

$$EPA_{\{110\}} = USW_{\{110\}} \cdot \sin\xi \tag{4}$$

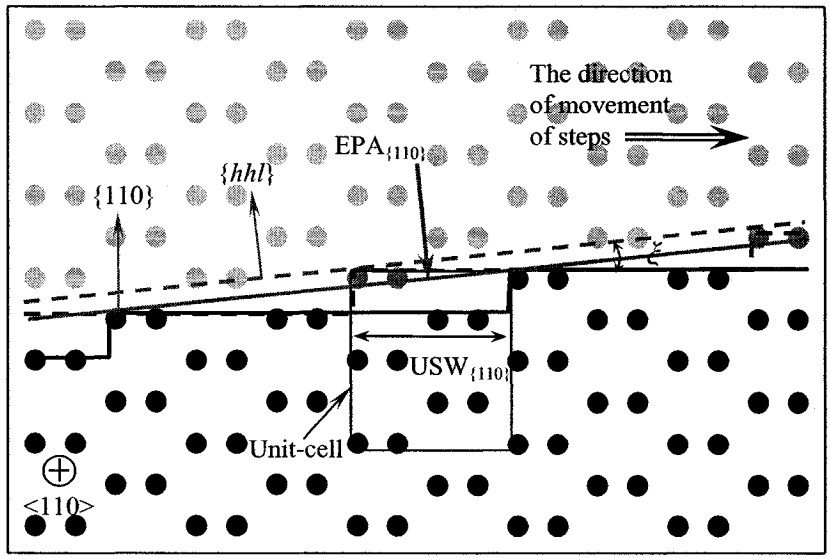

Figure II-2: Effective plane advancement of P-based plane with {110}-oriented terraces when all the step-edges move simultaneously one USW in the direction of movement of steps.

Figure II-3 summarizes the calculations of the frequency of removal of chains/rows on Si{100} etched in 25wt.% TMAH taking to consideration the crossover in terrace orientation.

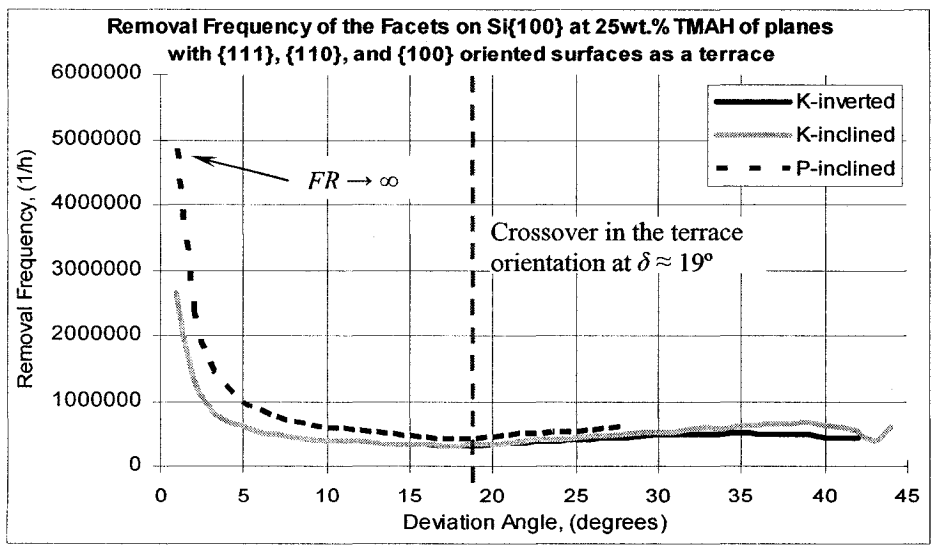

Figure II-3: Graphic representation of summarized calculations for Removal Frequencies of all planes detected on sidewalls of spokes in the wagon-wheel under-etch experiment on Si{100} etched in 25wt.% TMAH, taking to account the crossover in the terrace orientation.

Please note that crossover for K-inclined, K-inverted and P-inclined facets that were detected in the experiment in Si{100} wafer, appears approximately at the same deviation angle $\delta \approx 19^{o}$, as was discussed in Chapter 3.

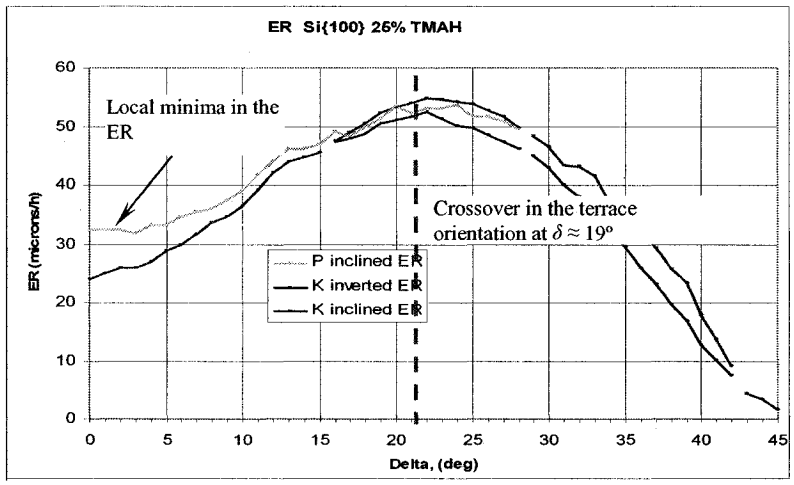

Figure II-4: Relative etch rates of facets detected in the wagon wheel under-etch experiment on Si{100} etched in 25wt.% TMAH at 80°C, experimental data.

Comparing this information to the etch rate data; it is evident that the cross-over in terrace orientation appears to be at or near the point of the maximum etch rate, Figure II-4.

It is important to remark the fact that the FR of the planes with {100}- and {110}-oriented terraces seems to be infinite as the K- and P-based planes move towards {100} and {110} basic orientations (δ = 0°). This seem to be contradictory with the basic physics of the planes etch rates, which are directly proportional to the FR, see Figure II-3 and Figure II-4. For the planes on sidewalls of spoke at deviation angle, δ, approaching zero there is a local minima in ER as these planes become {100} and {110}.

Further analysis of this phenomenon is done based on the canonical curves.

II.1. Canonical Curves

More detailed analysis of the Frequency of Removal of PBC/K-row from the step-edges and its connection to the etch rates of the respective surfaces is attempted in the following pages.

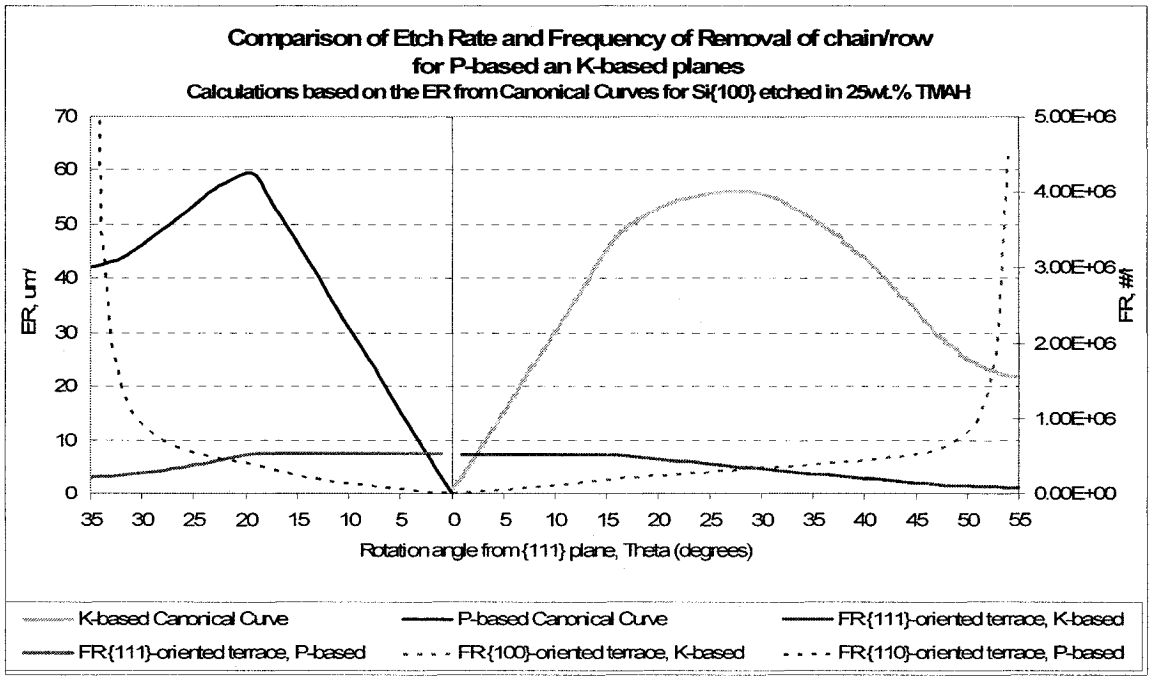

Figure II-5: The graph representing the ideal etch rates and their comparison to the respective removal frequencies calculated from the experimental data obtained from the wagon-wheel under-etch experiment on Si{100} etched at 25wt.% TMAH.

The summary of etch rates for P-based and K-based planes presented in form of Canonical Curves with FR calculated using general FR Equation (5.3) with the consideration of the crossover in terrace orientation is presented in the graph of Figure II-5. As it can be seen from this figure, calculated removal frequencies of P-based and K-based surfaces with {110} and {100} oriented terraces (dashed lines on the graph of Figure II-5) in the vicinity of basic {100} and {110} surfaces asymptotically approach infinity. This represents a physical impossibility.

II.2.Separation of Etch Rates of Planes with {100}- and {110}-oriented Terraces into Two Components

The main objective is to use certain approximation in order to separate the data from experimental etch rate curves into two components.

II.2.1. Equation of the Line Approximation for the ER component due to "non-zero" Etch Rate of {100}- and {110}-oriented Terraces

Now, this model may be used on the experimental data from wagon-wheel under-etch experiment. However, to simplify the analysis, the following approximations are used on data collected from under-etch wagon-wheel experiment on Si{100} wafer.

II.2.1.1. Si{100}

The equation of the line for surfaces detected in our experiment:

- P-based inclined plane

$$ER_{\substack{due\ to\ "non-zero"\\ ER\ of\ \{110\}-oriented\ terrace}} = m_{\{110\}}\left(\delta - 18.945^{\circ}\right), \tag{5}$$

where $m_{\{110\}}$ – is the slope of straight line determined as: $m_{\{110\}} = \dfrac{ER_1 - ER_2}{\delta_1 - \delta_2} \approx -1.717$

δ – is the deviation angle on Si{100}

$\delta = 18.945°$ – location of crossover in terrace orientation on P-inclined plane

- K-based inclined and K-based inverted plane[48]

$$ER_{\substack{due\ to\ "non-zero"\\ ER\ of\ \{100\}-oriented\ terrace}} = m_{\{100\}}\left(\delta - 18.784^{\circ}\right), \tag{6}$$

[48] K-based inclined and K-based inverted planes are the planes from the same family at specified deviation angle. These planes will have identical profiles and the only difference is in their respective etch rates.

where $m_{\{100\}}$ – is the slope of straight line determined as: $m_{\{100\}} = \dfrac{ER_1 - ER_2}{\delta_1 - \delta_2} \approx -1.278$

$\delta = 18.784°$ – location of crossover in terrace orientation on K-inclined plane.

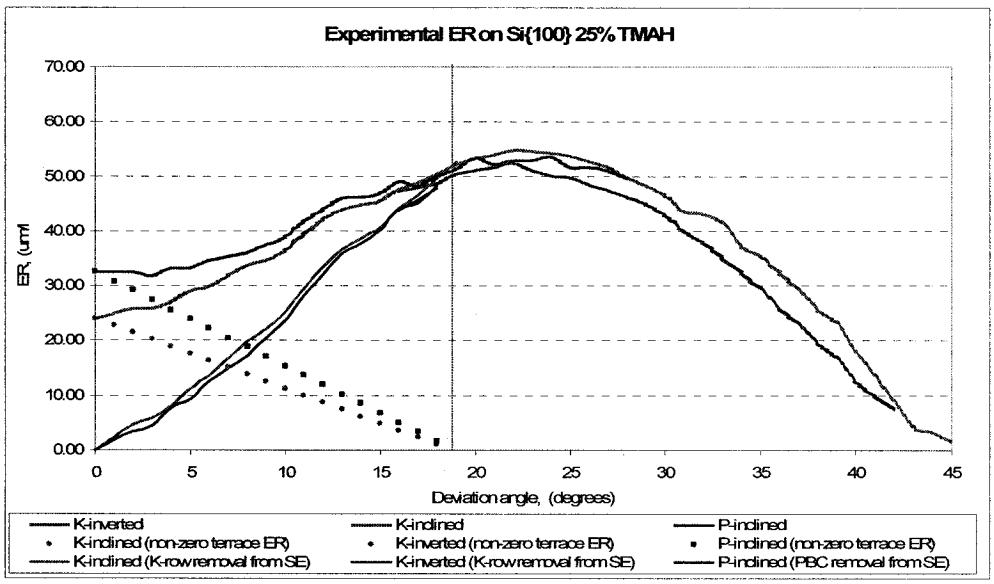

Figure II-6: Relative etch rates of facets detected in the wagon wheel under-etch experiment on Si{100} etched in 25wt.% TMAH at 80°C, experimental data with their respective components.

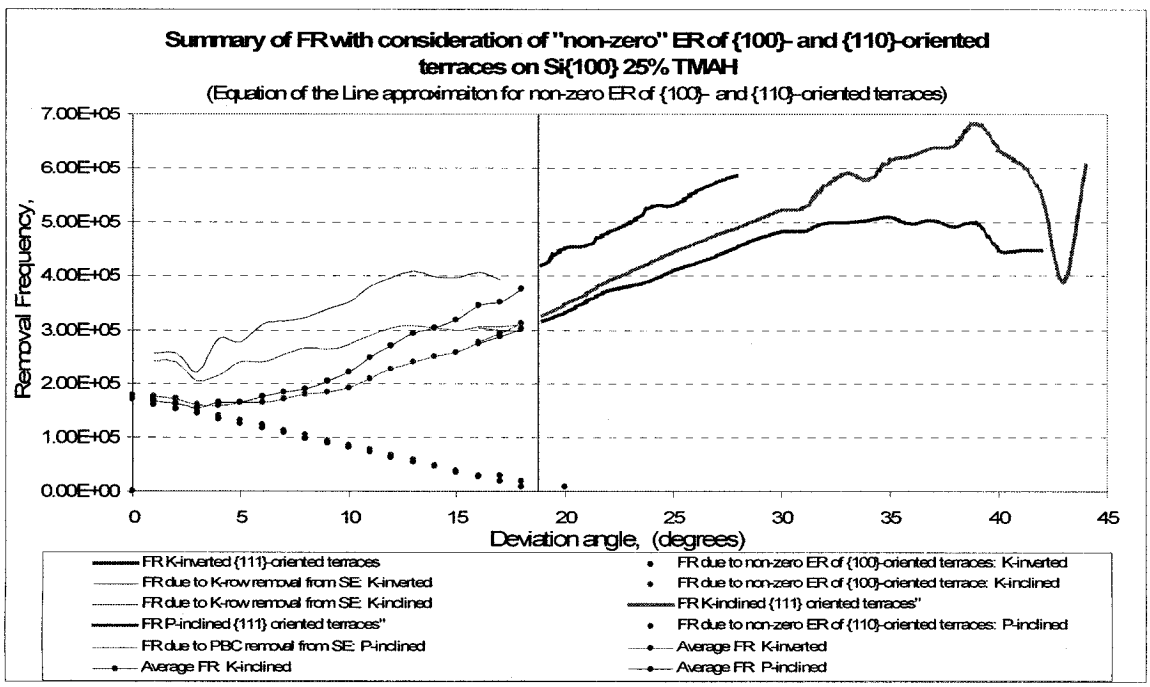

Figure II-7: Summary of the calculations for the FR of surfaces with {111}-oriented terraces and components of FR on P- and K-based surfaces with {110}- and {100}- oriented terraces based on the Equation of the Line approximation for "non-zero" terrace ER on the experimental data from Si{100} in 25wt.% TMAH at 80°C.

These calculations are summarized in graphs of Figure II-6. Respective frequencies of removal of chains/rows from step-edges are illustrated in Figure II-7.

II.2.2. Equation of the Line Approximation for the ER Component Due to Chain/Row Removal from the Step-Edges

II.2.2.1. Si{100}

Similar calculations may be done for the facets detected in under-etch experiment:

- P-based inclined plane

$$ER_{\substack{due\ to\ chain/row \\ removal\ from\ the\ SE}} = 51.37 + m_{\{110\}}\left(\delta - 18.945^{\circ}\right), \tag{7}$$

where $m_{\{110\}}$ – is the slope of straight line determined as: $m_{\{110\}} = \dfrac{ER_1 - ER_2}{\delta_1 - \delta_2} \approx 2.70$

δ – is the deviation angle on Si{100}

$\delta = 18.945°$ – location of crossover in terrace orientation on P-inclined plane

51.37 μm/h – the etch rate of the P-inclined surface at the crossover.

- K-based inclined and K-based inverted plane

$$ER_{\substack{due\ to\ chain/row \\ removal\ from\ the\ SE}} = 52.25 + m_{\{100\}}\left(\delta - 18.784^{\circ}\right), \tag{8}$$

where $m_{\{100\}}$ – is the slope of straight line determined as: $m_{\{100\}} = \dfrac{ER_1 - ER_2}{\delta_1 - \delta_2} \approx 2.75$

$\delta = 18.784°$ – location of cross-over in terrace orientation on K-inclined plane

52.25 μm/h – the etch rate of the K-inclined surface at the crossover.

- K-based inverted plane

$$ER_{\substack{due\ to\ chain/row \\ removal\ from\ the\ SE}} = 50.40 + m_{\{100\}}\left(\delta - 18.784^{\circ}\right), \tag{9}$$

where $m_{\{100\}}$ – is the slope of straight line determined as: $m_{\{100\}} = \frac{ER_1 - ER_2}{\delta_1 - \delta_2} \approx 2.65$

$\delta = 18.784°$ – location of cross-over in terrace orientation on K-inclined plane

50.40 μm/h – the etch rate of the K-inverted surface at the crossover.

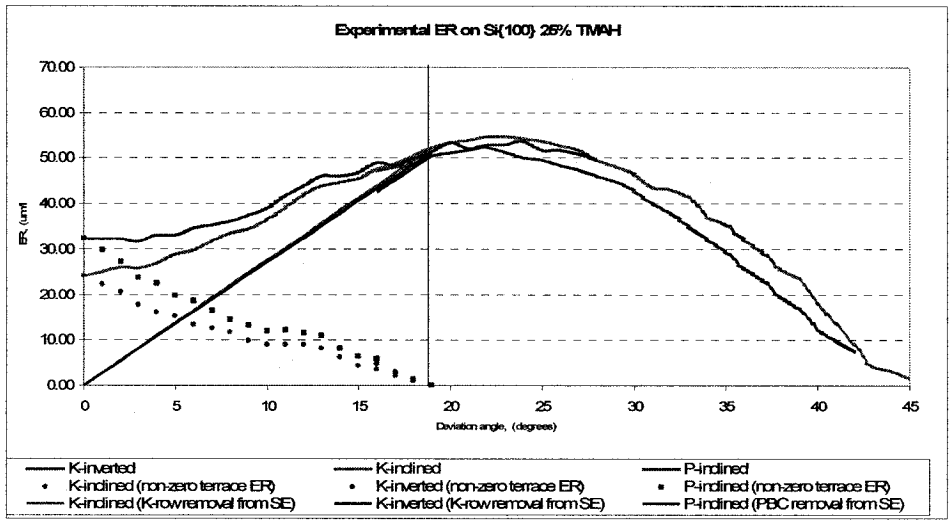

Figure II-8: Relative etch rates of facets detected in the wagon wheel under-etch experiment on Si{100} etched in 25wt.% TMAH at 80°C, experimental data with their respective components.

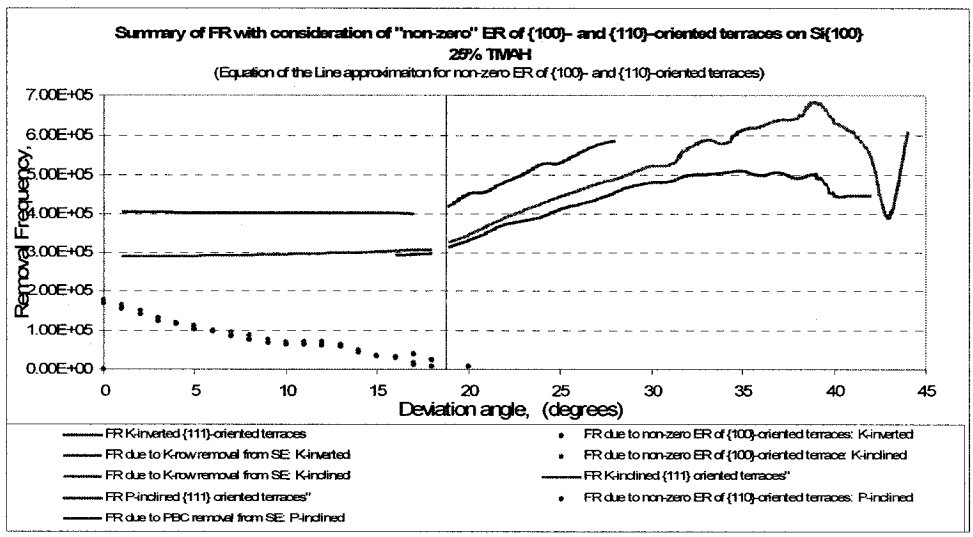

Figure II-9: Summary of the calculations for the FR of surfaces with {111}-oriented terraces and components of FR on P- and K-based surfaces with {110}- and {100}- oriented terraces based on the Equation of the Line for chain/row removal from the Step-Edges on the experimental data from Si{100} in 25wt.% TMAH at 80°C.

Due to the fact that experimental etch rates of K-inclined and K-inverted facets are involved in the equation of the line for this approximation, these two equations (8) and (9) are different.

The summary of etch rate components and relative removal frequencies are presented in graphs of Figure II-8 and Figure II-9.

II.2.2.2. Application of Etch Rate Components to the Experimental Data on Si{100}

Applying the Transition Zone Approximation to the experimental data from wagon-wheel under-etch experiment, the following can be achieved:

- For P-based inclined plane, the terrace width closest to the $TW_{\{111\}} \cong 9.64$ Å is located at $\delta = 16°$ ($TW_{\{110\}} \cong 9.468$ Å)

$$ER_{\substack{PBC\ removal\ from\ SE \\ TRANSITION\ ZONE}} = 49 + m_{\{110\}}\left(\delta - 16^{\circ}\right), \tag{10}$$

where $m_{\{110\}}$ – is the slope of straight line determined as: $m_{\{110\}} = \dfrac{ER_1 - ER_2}{\theta_1 - \theta_2} \approx 3.065$

49 μm/h – is the ER of a P-based plane (value form the experimental data) at δ = 16°.

- K-based inclined and K-based inverted plane, the terrace width closest to the $TW_{\{111\}} \cong 10.933$ Å is located at $\delta = 10°$ ($TW_{\{100\}} \cong 10.89$ Å)

$$ER_{\substack{K-row\ removal\ from\ SE \\ TRANSITION\ ZONE}} = 36.45 + m_{\{100\}}\left(\delta - 10^{\circ}\right), \tag{11}$$

where $m_{\{100\}}$ – is the slope of straight line determined as: $m_{\{100\}} = \dfrac{ER_1 - ER_2}{\delta_1 - \delta_2} \approx 3.645$

36.45 μm/h – is the ER of a K-based plane (value form the experimental data) at δ = 10°.

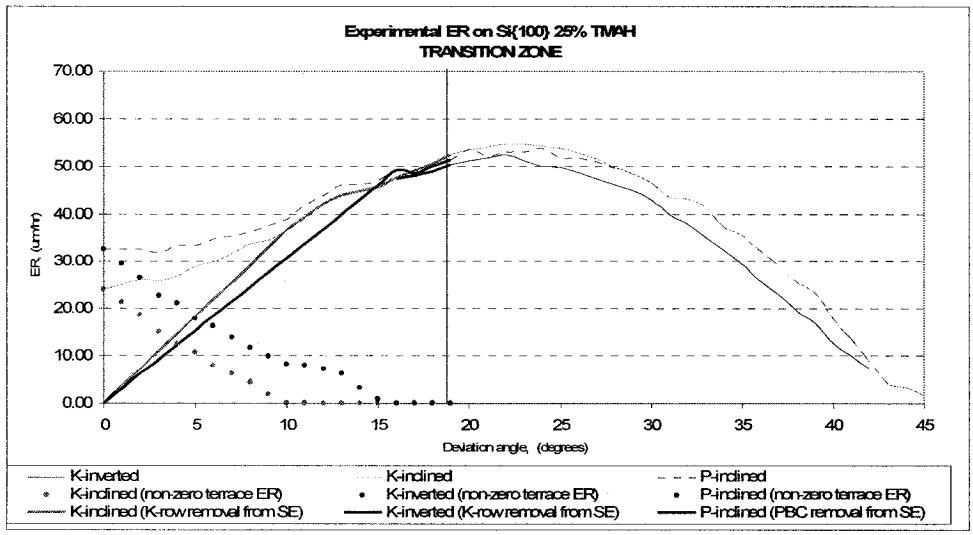

Figure II-10: Relative etch rates of facets detected in the wagon wheel under-etch experiment on Si{100} etched in 25wt.% TMAH at 80°C, experimental data with their respective components.

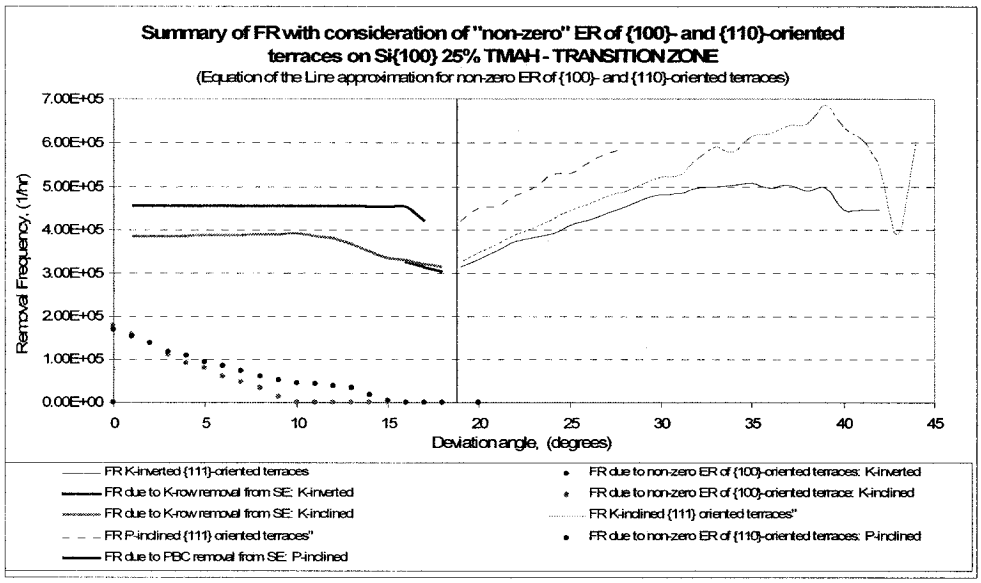

Figure II-11: Summary of the calculations for the FR of surfaces with {111}-oriented terraces and components of FR on P- and K-based surfaces with {110}- and {100}- oriented terraces based on the Equation of the Line approximation for "non-zero" terrace ER and TRANSITION ZONE on the experimental data from Si{100} in 25wt.% TMAH at 80°C.

II.2.2.3. Application of Etch Rate Components to the Experimental Data on Si{110}

Silicon wafer of {110} orientation, as it was shown earlier, provides larger variety of surfaces in the under-etch experiment, Figure II-12

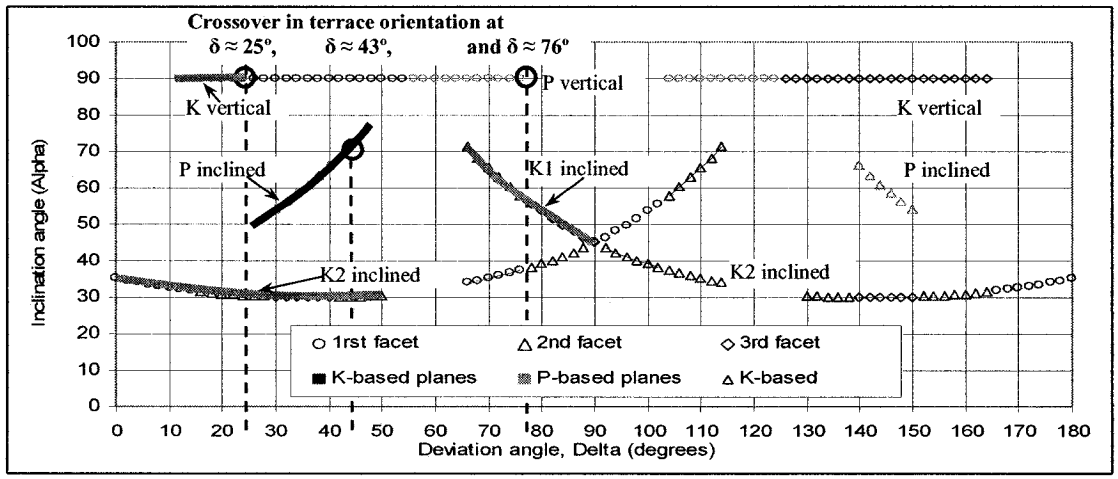

Figure II-12: Summary of the experimental data representing relative position of the inclination angles of the facets on the side-walls of a spoke with respect to the deviation angle on Si{110} etched in 25% TMAH with the indication of the crossover in the terrace orientation, (Figure from [9]).

In the area delimited by deviation angle $0° \leq \delta \leq 90°$ five different types of facets were identified: K2-inclined, K1-inclined, K-vertical, P-vertical and P-inclined, Figure II-12.

It can be seen, that in this area ($0° \leq \delta \leq 90°$) three points with the crossover in the terrace orientation are indicated. Therefore, the three of the identified surfaces, i.e. K-vertical, P-inclined and P-vertical, have crossovers at $\delta \approx 25°$ (to be exact $\delta = 25.6875°$), $\delta \approx 43°$ ($\delta = 43.522°$), and $\delta \approx 76°$, ($\delta = 76.357°$), respectively. The terrace orientation may be indicated as follows:

- $0 \leq \delta \leq 35.26°$ - K-vertical with {100}-oriented terraces on $\delta \leq 25°$ and {111}-oriented terraces on $\delta > 25°$;
- $35.26° \leq \delta \leq 54.74°$ - P-inclined with {110}-oriented terraces on ($25.5° \leq$) $\delta \leq 43°$ and {111}-oriented terraces on $\delta > 43°$;

- $54.74^{o} \leq \delta \leq 90^{o}$ - P-vertical with {111}-oriented terraces on $\delta \leq 76^{o}$ and {110}-oriented terraces on $\delta > 76^{o}$.

All areas, in which the K-based surfaces with {100}-oriented terraces and P-based surfaces with and {110}-oriented terraces are present, indicated in the Figure II-12 with solid Grey and solid Black lines, respectively.

Applying the Transition Zone Approximation to the experimental data from wagon-wheel under-etch experiment on Si{110}, the following brake down of the ER-s is done:

- For P-inclined plane, two different regions with two separate equations of the line are present: (1) – for $30° \leq \delta \leq \sim 35°$ and (2) for $\sim 35° \leq \delta \leq 44°$. Reason for such separation is in the fact that at the deviation angle $\delta \approx 35°$ (35.2643°, precisely), P-based plane through its "rotation" reaches the basic {110} orientation after which it continues as a plane with complementary Miller Indices, but not necessary identical etch rates[49].

  (1) $30° \leq \delta \leq \sim 35°$ plane with the terrace width closest to the $TW_{\{111\}} \cong 9.64$ Å is not present in the experiment but its location can be determined from the basic crystal geometry and can be found, hypothetically speaking, at $\delta = 27°$ ($TW_{\{110\}} \cong 9.716$ Å)

$$ER_{\substack{PBC\ removal\ from\ SE \\ TRANSITION\ ZONE}} = m_{\{110\}}\left(\delta - 35^{\circ}\right), \tag{12}$$

where $m_{\{110\}}$ – is the slope of straight line determined as:

$$m_{\{110\}} = \frac{ER_1 - ER_2}{\theta_1 - \theta_2} \approx -8.00$$

[49] As it was discussed earlier this is one of the most significant anomalies in a behaviour of planes with the same crystal structure in the under-etch experiment.

35° - is the deviation angle at which a basic {110} surface is located. The ER due to the PBC removal from the step-edges is considered to be "zero".

(2) $\sim 35° \leq \delta \leq 44°$ plane with the terrace width closest to the $TW_{\{111\}} \cong 9.64$ Å is located at $\delta = 42°$ ($TW_{\{110\}} \cong 9.932$ Å)

$$ER_{\substack{PBC\ removal\ from\ SE \\ TRANSITION\ ZONE}} = m_{\{110\}}\left(\delta - 35°\right), \tag{13}$$

where $m_{\{110\}}$ – is the slope of straight line determined as:

$$m_{\{110\}} = \frac{ER_1 - ER_2}{\theta_1 - \theta_2} \approx 6.156$$

- K2-inclined, the terrace width closest to the $TW_{\{111\}} \cong 10.933$ Å is located at $\delta =$ 73° ($TW_{\{100\}} \cong 10.80$ Å)

$$ER_{\substack{K-row\ removal\ from\ SE \\ TRANSITION\ ZONE}} = m_{\{100\}}\left(\delta - 90°\right), \tag{14}$$

where $m_{\{100\}}$ – is the slope of straight line determined as:

$$m_{\{100\}} = \frac{ER_1 - ER_2}{\delta_1 - \delta_2} \approx -3.183$$

90° is the deviation angle at which a basic {100} surface is located. The ER due to K-row removal from the step-edges on this plane is considered to be "zero".

- K1-inclined, the terrace width closest to the $TW_{\{111\}} \cong 10.933$ Å is located at $\delta =$ 79° ($TW_{\{100\}} \cong 11.0$ Å)

$$ER_{\substack{K-row\ removal\ from\ SE \\ TRANSITION\ ZONE}} = m_{\{100\}}\left(\delta - 90°\right), \tag{15}$$

where $m_{\{100\}}$ – is the slope of straight line determined as:

$$m_{\{100\}} = \frac{ER_1 - ER_2}{\delta_1 - \delta_2} \approx -3.7$$

90° is the deviation angle at which a basic {100} surface is located. The ER due to K-row removal from the step-edges on this plane is considered to be "zero".

- K-vertical with the terrace width close to that of $TW_{\{111\}} \cong 10.933$ Å not present in the under-etch experiment for 80°C in 25% TMAH. Whatever portion of this surface is present past a crossover at $\delta \approx 25°$ is located in so called "transition zone". Hence its breakdown just follows the experimental ER profile for the K-row removal from a SE and the Component due to "non-zero" ER of {100}-oriented terrace is, interestingly enough, "zero", see Figure II-13.

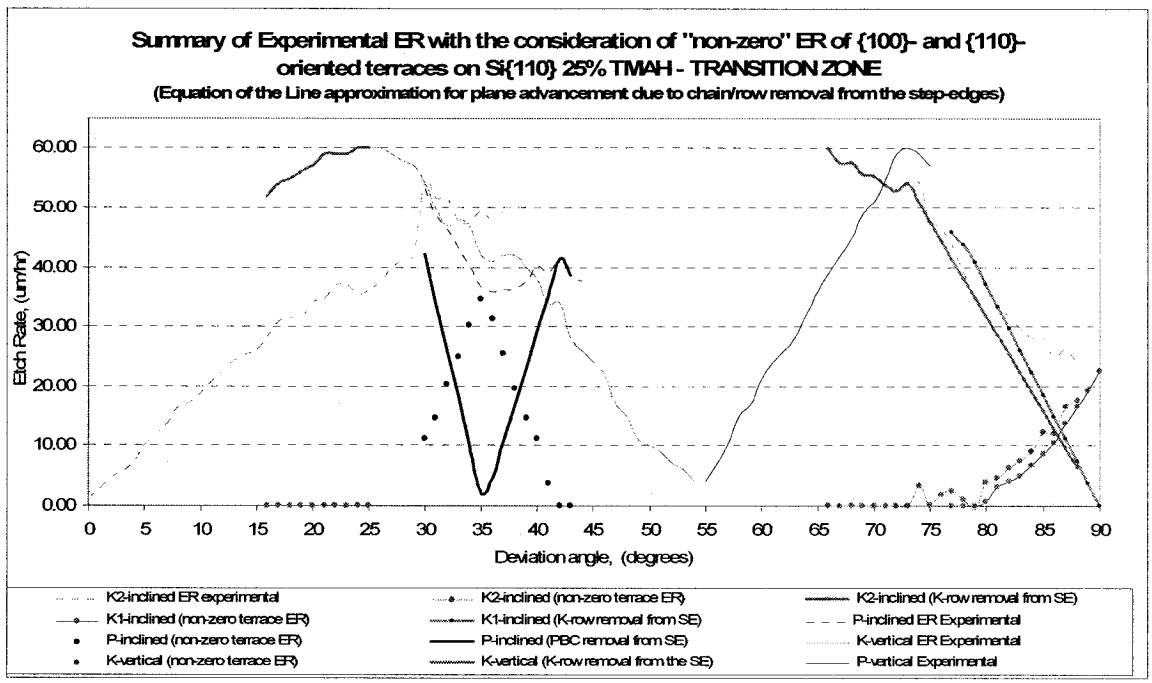

Figure II-13: Relative etch rates of facets detected in the wagon wheel under-etch experiment on Si{100} etched in 25wt.% TMAH at 80°C, experimental data with their respective components.

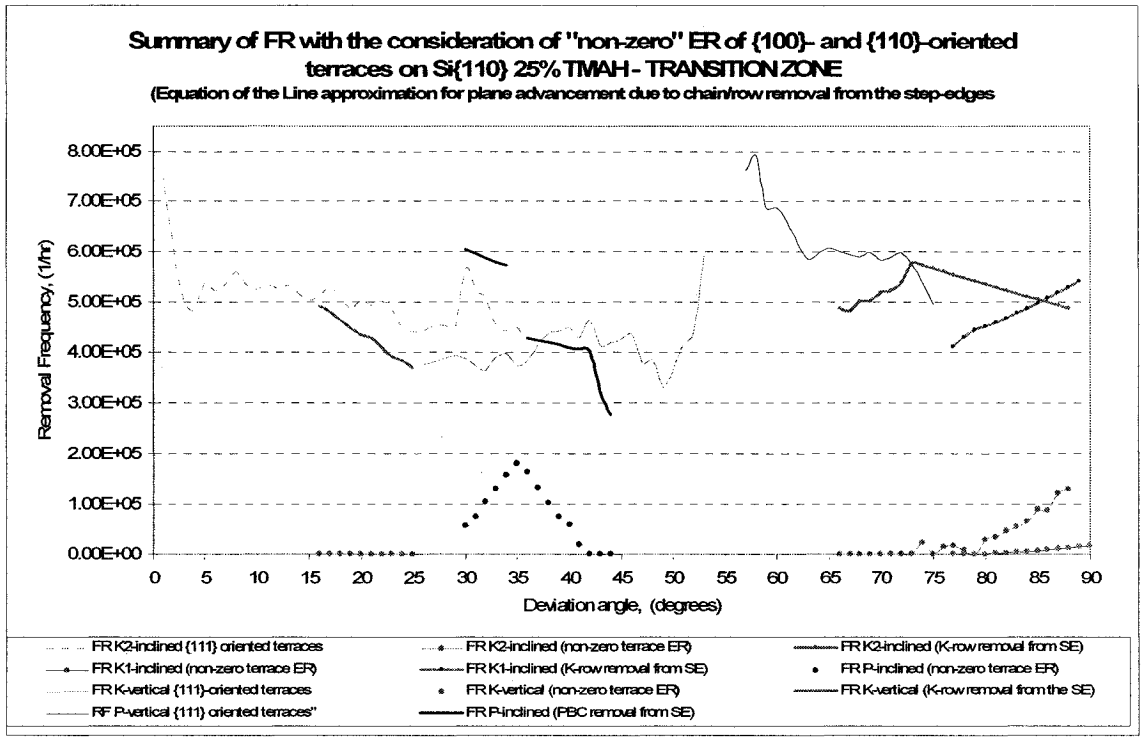

Figure II-14: Summary of the calculations for the FR of surfaces with {111}-oriented terraces and components of FR on P- and K-based surfaces with {110}- and {100}- oriented terraces based on the Equation of the Line approximation for "non-zero" terrace ER and TRANSITION ZONE on the experimental data from Si{100} in 25wt.% TMAH at 80°C.

Figure II-13 summarizes all etch rates of the facets present on Si{110} in wagon-wheel under-etch experiment and their breakdown into two components. However, due to the complexity of this summary, better reference for the following graph of the respective removal frequencies would be that of Figure II-12.

As it can be seen in Figure II-14, general summary can be made – frequencies of the removal of chains/rows from the step-edges seem to be of the same order of magnitude. Conversely, deviations in these values are obvious and their correlation may be of major interest.